Observations of the Cosmic Microwave Background : Planck and beyond

Paolo de Bernardis

Dipartimento di Fisica, Universita’ La Sapienza, Roma

Ioffe Institute – Saint Petersburg

20/March/2012

We live in an expanding universe

- All distances at cosmological scales increase with time.
- Photons travelling in the universe increase their wavelength by the same factor as all other lengths. (**redshift**, Hubble's law).

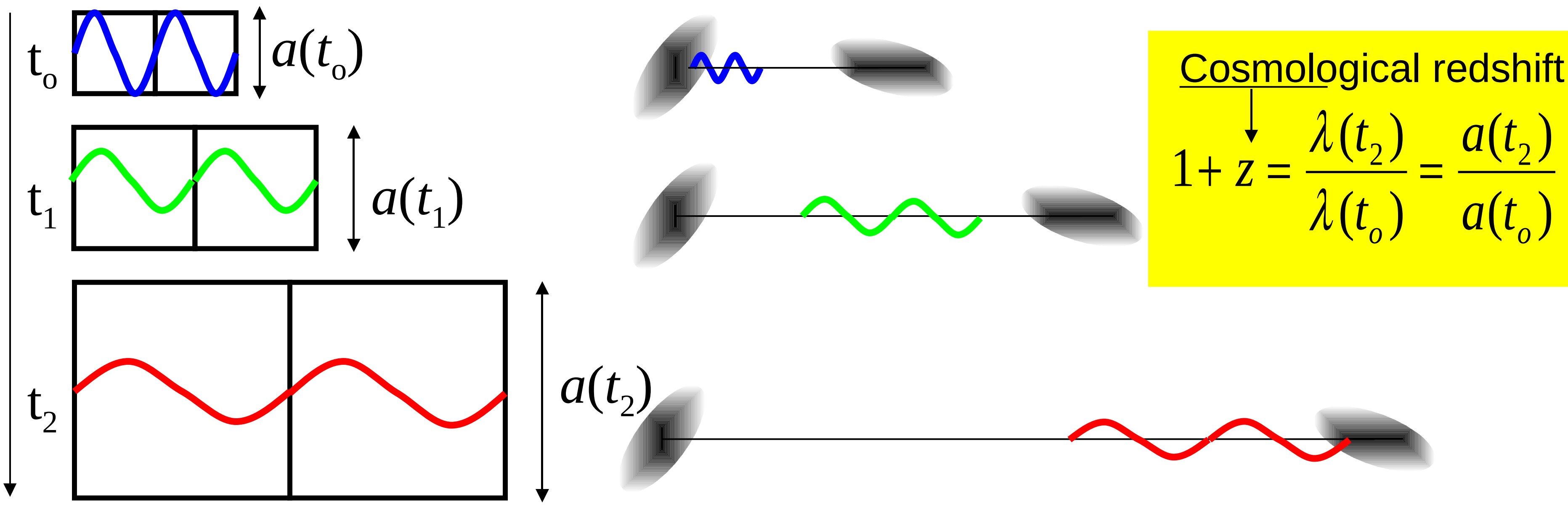

$$1 + z = \frac{\lambda(t_2)}{\lambda(t_o)} = \frac{a(t_2)}{a(t_o)}$$

- The expanding universe **cools down**.
- Looking far away we observe distant regions of the Universe as they were in early epochs. If we look far enough, we will observe the epoch when the universe was so hot to be ionized, the **primeval fireball**.
- The light present at that epoch is received today as a faind background of microwaves, the Cosmic Microwave Background **CMB** (z_{CMB}=1100).

Solar granulation

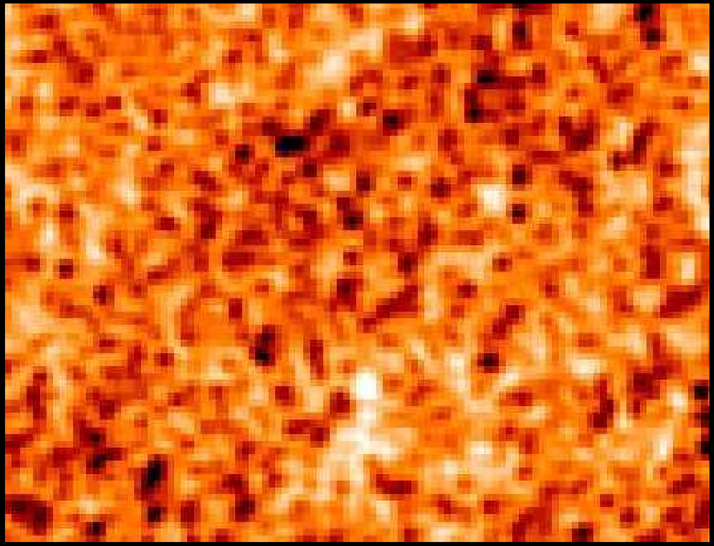

Plasma in the solar
photosphere (5700K)

8 light-minutes

Here, now

Solar granulation

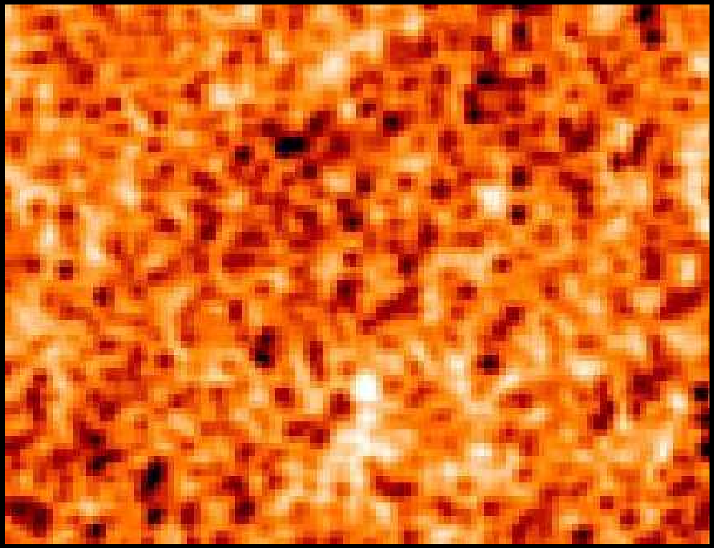

Plasma in the solar photosphere (5700K)

8 light-minutes

Here, now

Plasma in the early universe (the cosmic photosphere, 3000K)

mm-waves

light

14 billion light-years

Here, now

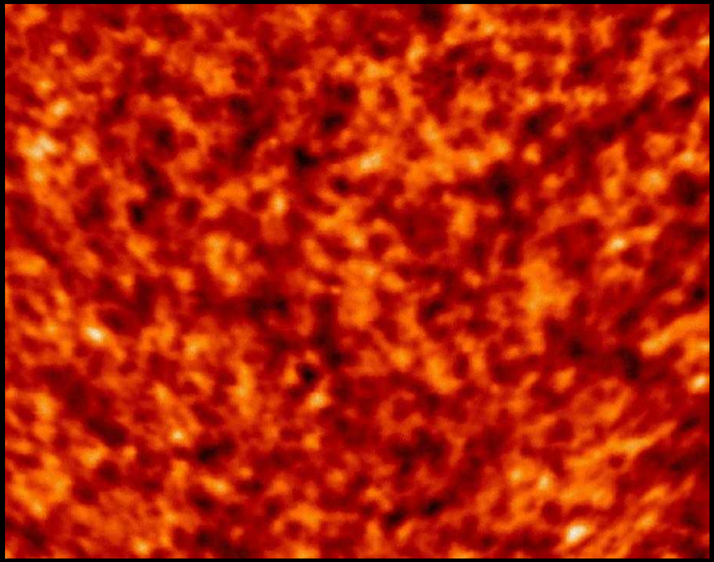

BOOMERanG map of the early universe

What is the CMB

10^{-6}s

T >1GeV

$$b+\bar{b} \rightarrow 2\gamma$$

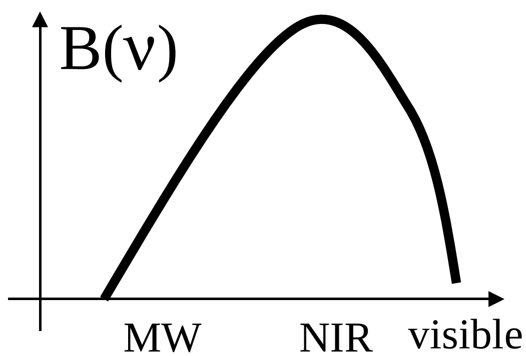

10^{13}s

T=3000K

$$1+z = \frac{\lambda_{now}}{\lambda_{em}} = \frac{r_{now}}{r_{em}}$$

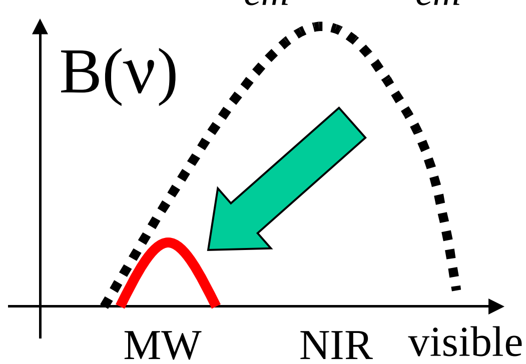

10^{17}s

T=3K

t

Today 411 γ/cm^3

According to modern cosmology:

An abundant background of photons filling the Universe.

- **Generated** in the very early universe, less than 4 μs after the Big Bang ($10^9\gamma$ for each baryon)
- **Thermalized** in the primeval fireball (in the first 380000 years after the big bang) *by repeated scattering against free electrons*
- **Redshifted** to microwave frequencies **and diluted** in the subsequent 14 Gyrs of expansion of the Universe

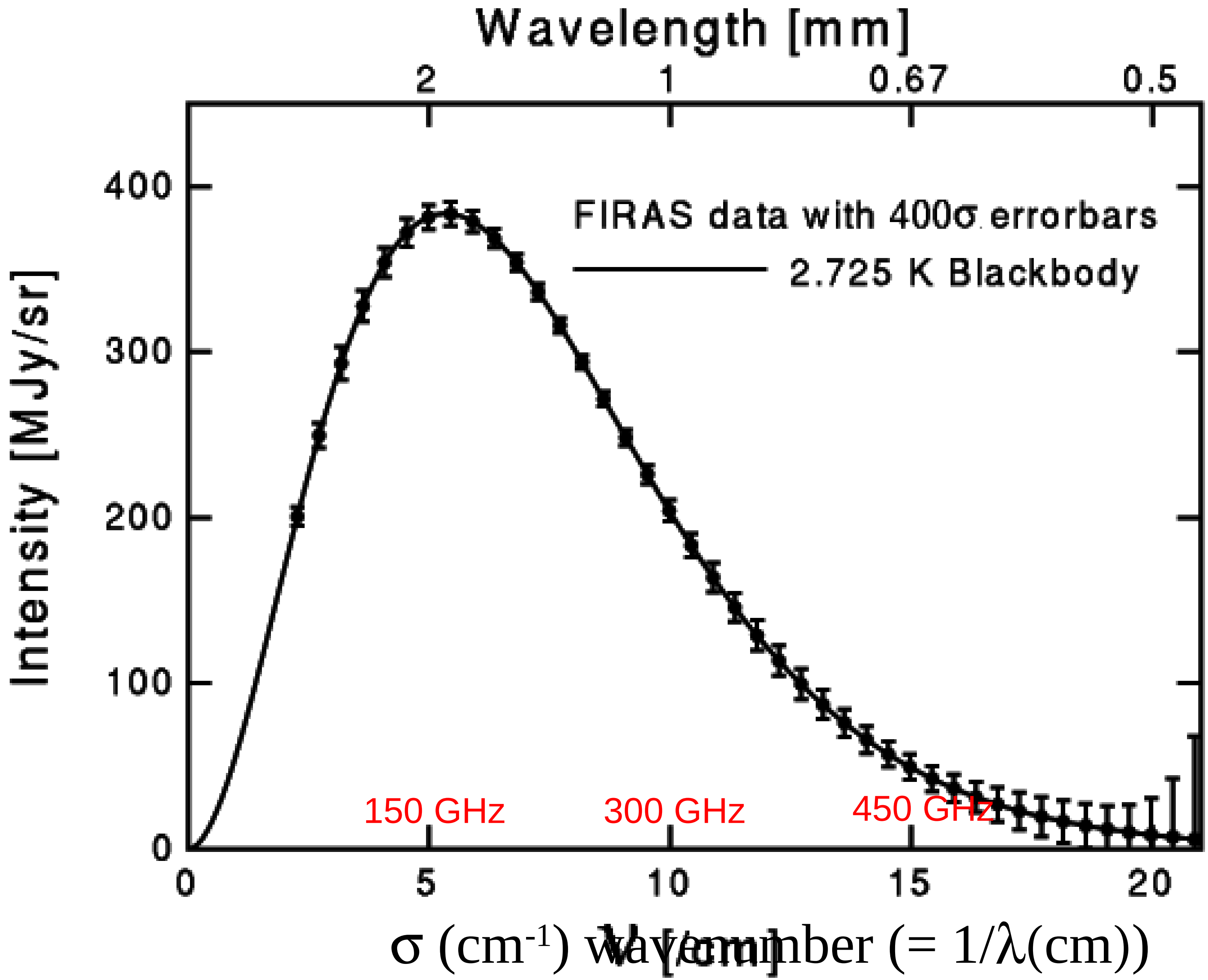
Wavelength [mm]
2
1
0.67
0.5
400
300
200
100
0
Intensity [MJy/sr]
FIRAS data with 400σ errorbars
2.725 K Blackbody
150 GHz
300 GHz
450 GHz
0
5
10
15
20
σ (cm-1) wavenumber (= 1/λ(cm))

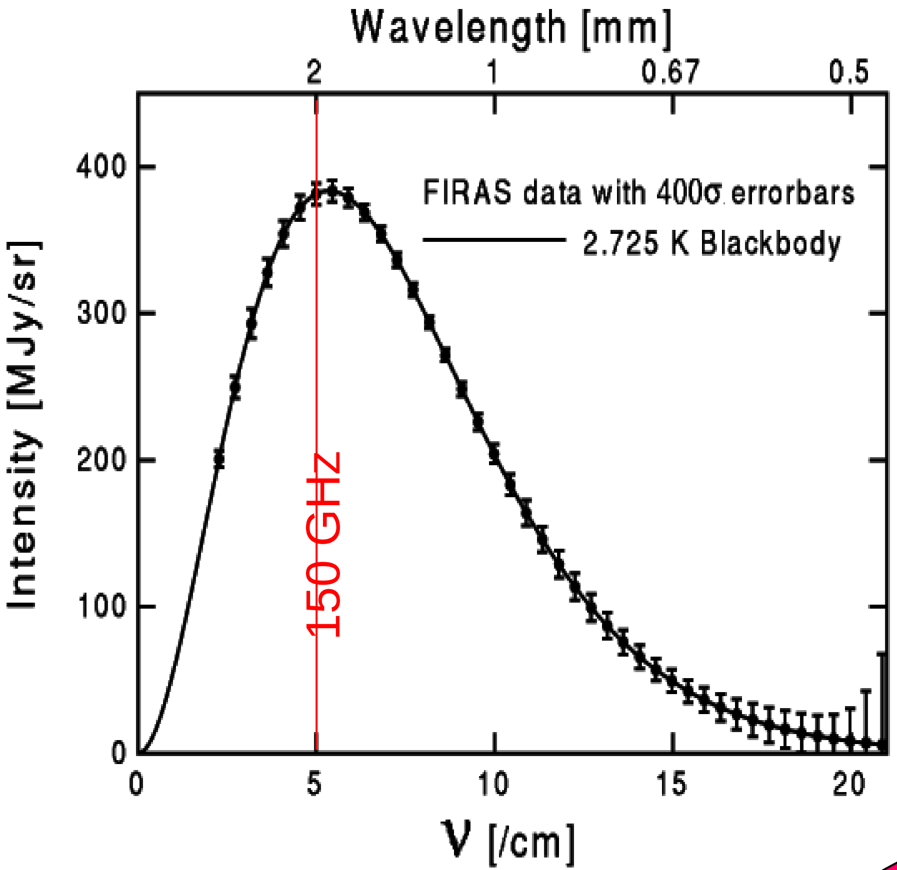

400 photons/cm^3

Thermal radiation ….

… and isotropic

Homogeneity of the early universe

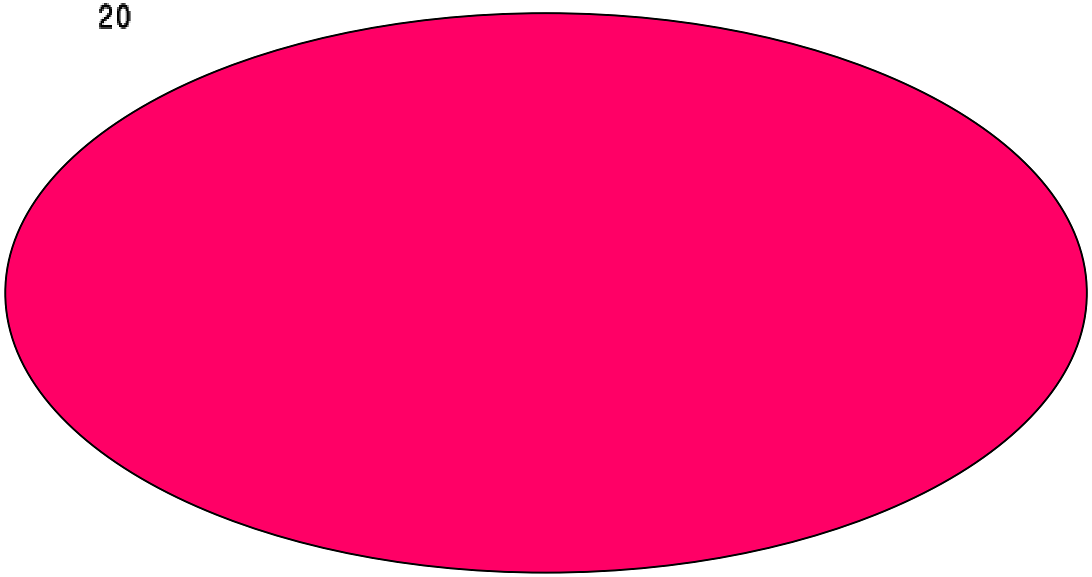

- The study of solar oscillations, evident as perturbations of the solar photosohere, allows us to infer the interior structure of the sun, well behind the photosphere.

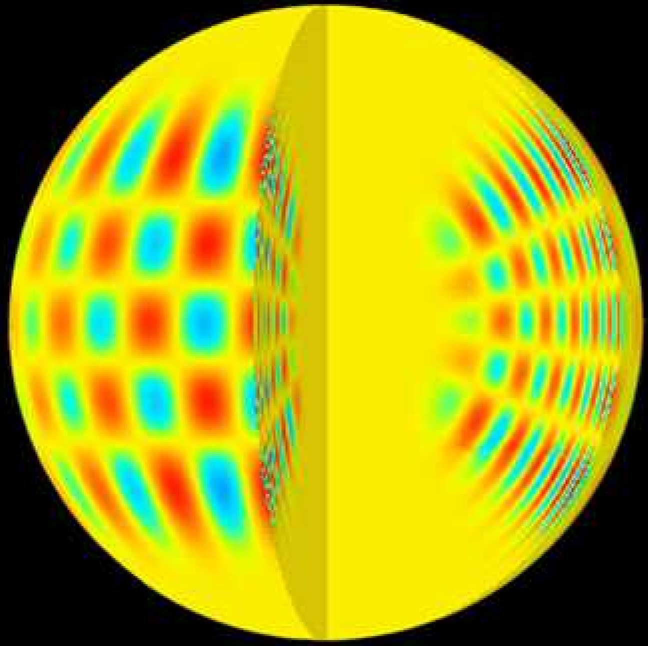

- The study of CMB anisotropy allows us to study the universe well behind (well before) the cosmic photosphere (the recombination epoch)

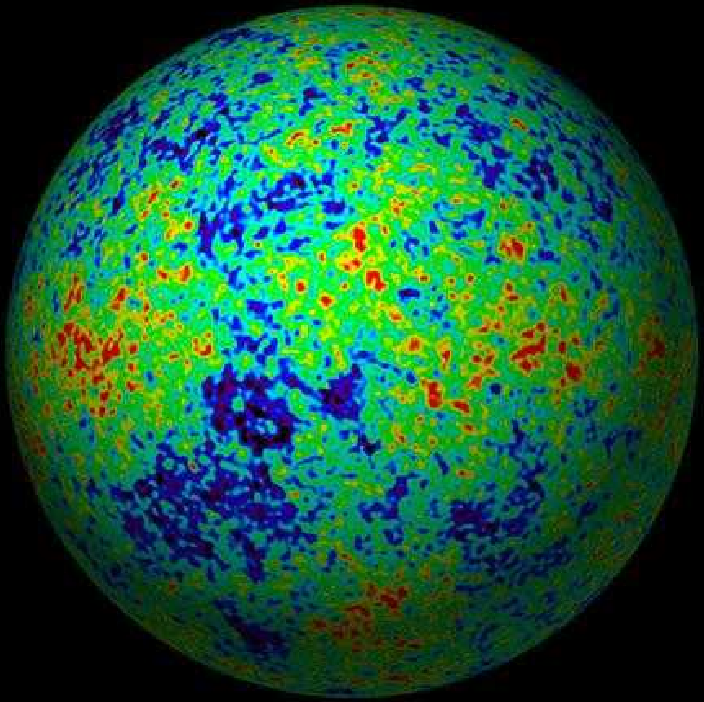

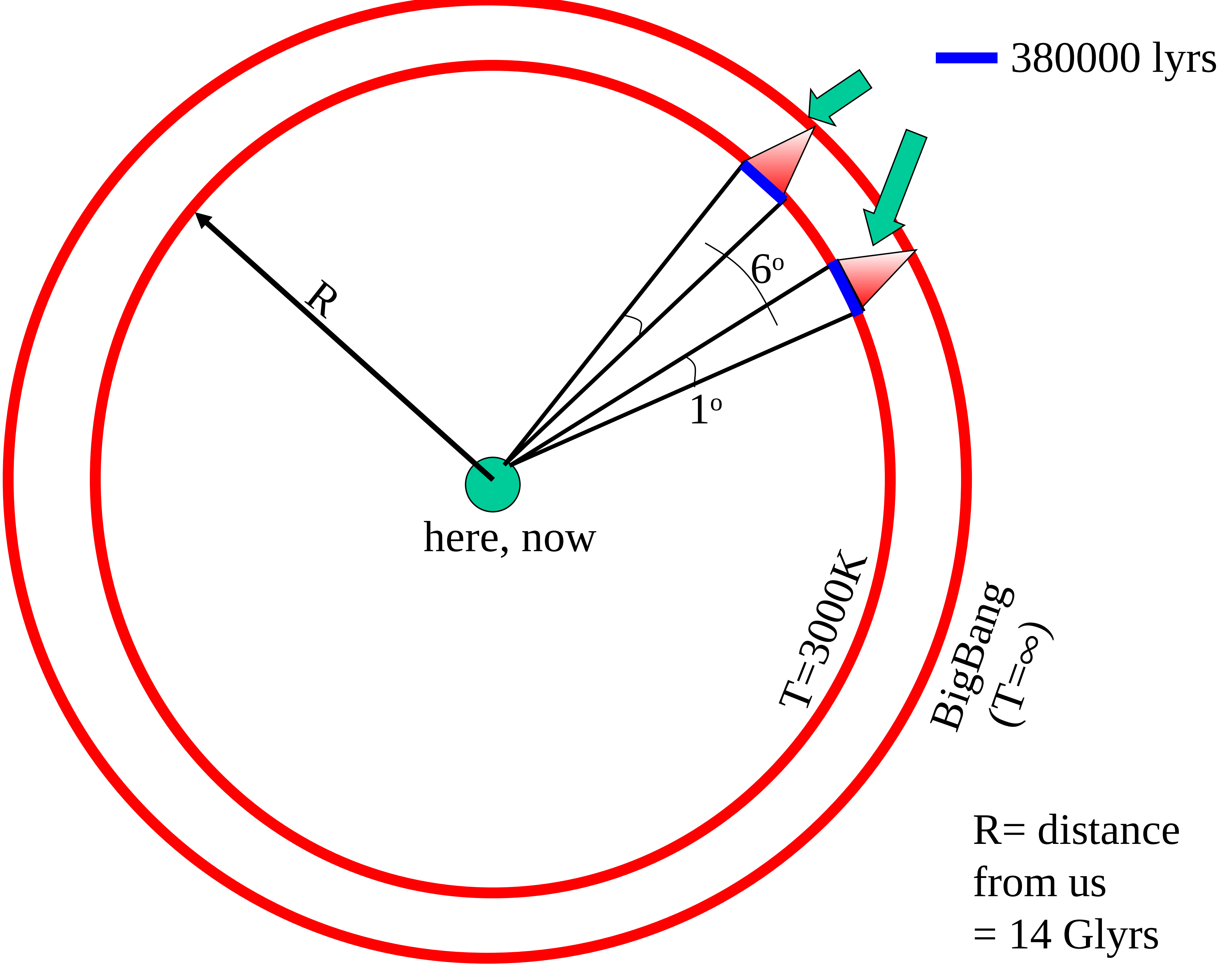

380000 lyrs
R
6°
1°
here, now
T=3000K
BigBang
(T=∞)
R= distance
from us
= 14 Glyrs

Density perturbations ($\Delta\rho/\rho$) were **oscillating** in the primeval plasma (as a result of the opposite effects of gravity and photon pressure).

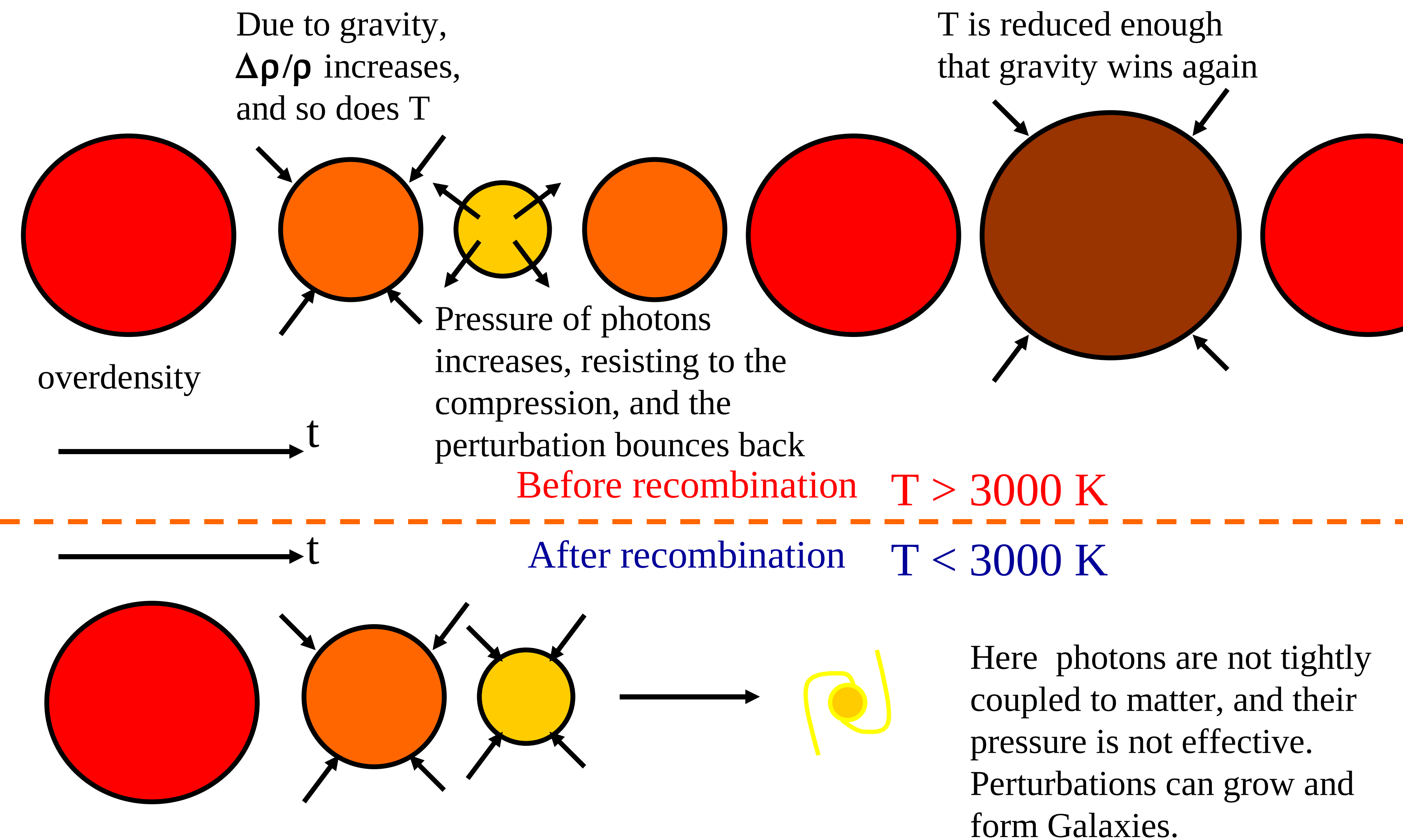

After recombination, density perturbation can **grow** and create the hierarchy of structures we see in the nearby Universe.

In the primeval plasma, photons/baryons density perturbations start to oscillate only when the sound horizon becomes larger than their linear size . Small wavelength perturbations oscillate faster than large ones.

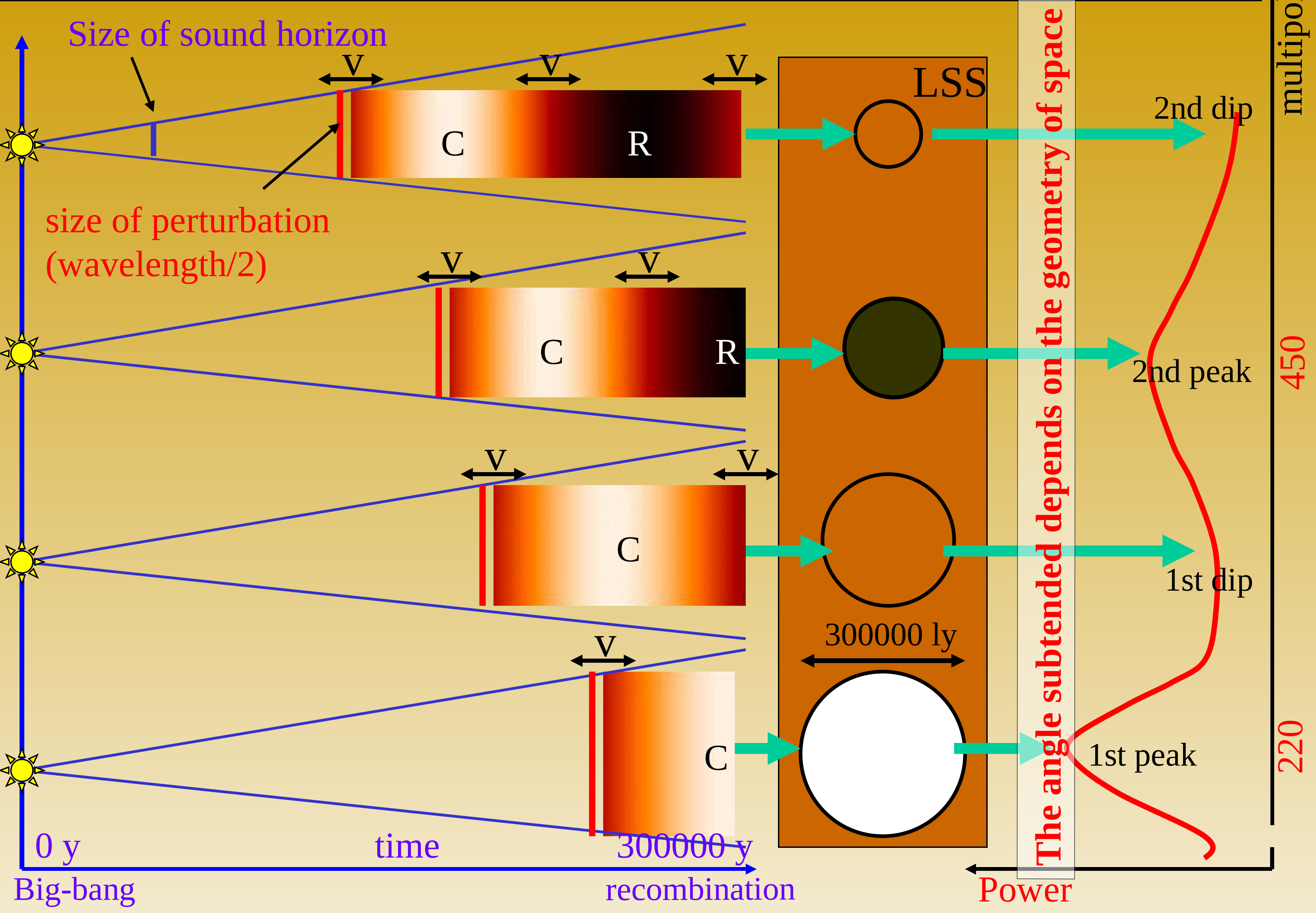

$$\frac{\Delta T}{T} = \sum a_{\ell,m} Y_\ell^m(\theta, \phi)$$

$$\boxed{c_\ell = \langle a^2_{\ell,m} \rangle}$$

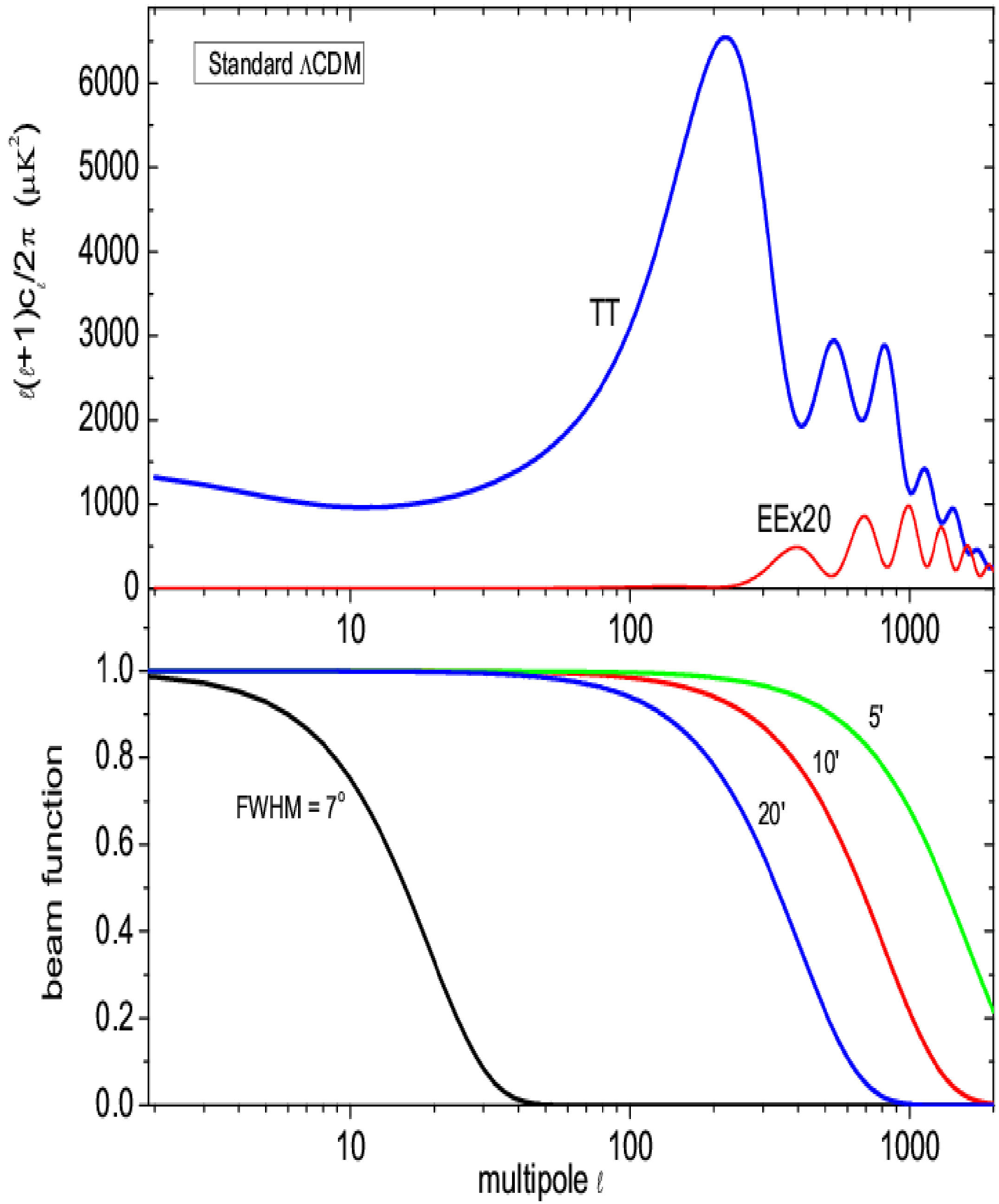

How can we measure this image of the early universe ?

- We need a mm-wave telescope.
- The earth atmosphere is emissive and not perfectly transparent at mm waves, due to the presence of water vapor.
- The telescope must operate from a very cold and dry site. Or from the stratosphere, above the water vapor layer.

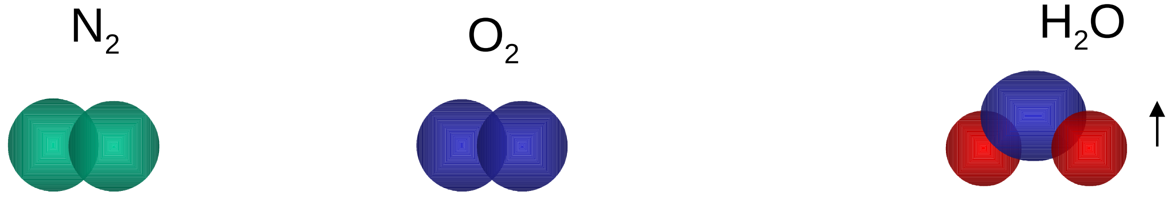

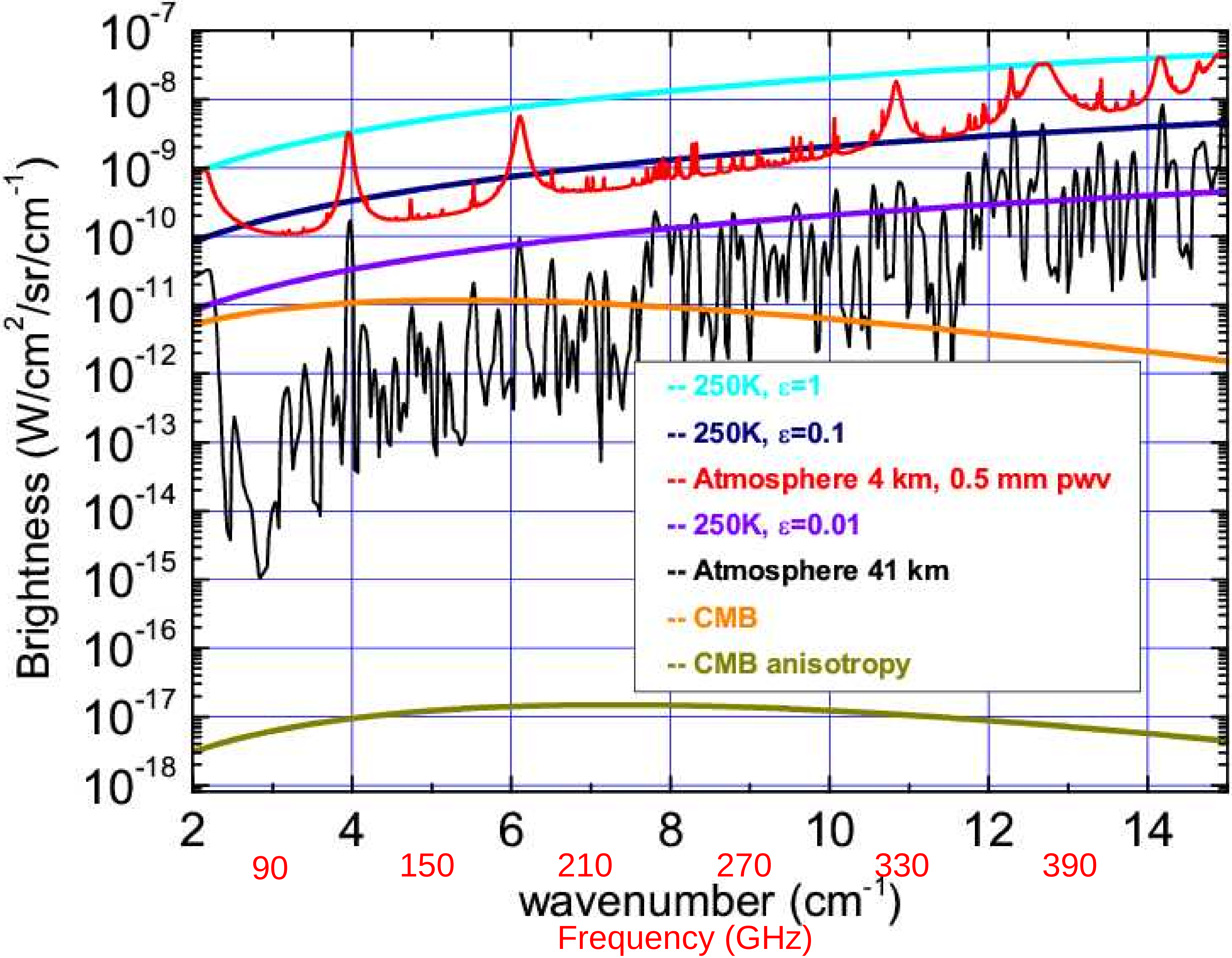

Brightness (W/cm²/sr/cm⁻¹)
10⁻⁷
10⁻⁸
10⁻⁹
10⁻¹⁰
10⁻¹¹
10⁻¹²
10⁻¹³
10⁻¹⁴
10⁻¹⁵
10⁻¹⁶
10⁻¹⁷
10⁻¹⁸
-- 250K, ε=1
-- 250K, ε=0.1
-- Atmosphere 4 km, 0.5 mm pwv
-- 250K, ε=0.01
-- Atmosphere 41 km
-- CMB
-- CMB anisotropy
2
4
6
8
10
12
14
90
150
210
270
330
390
wavenumber (cm⁻¹)
Frequency (GHz)

http: // oberon.roma1.infn.it / boomerang
http: // www.physics.ucsb.edu / ~boom

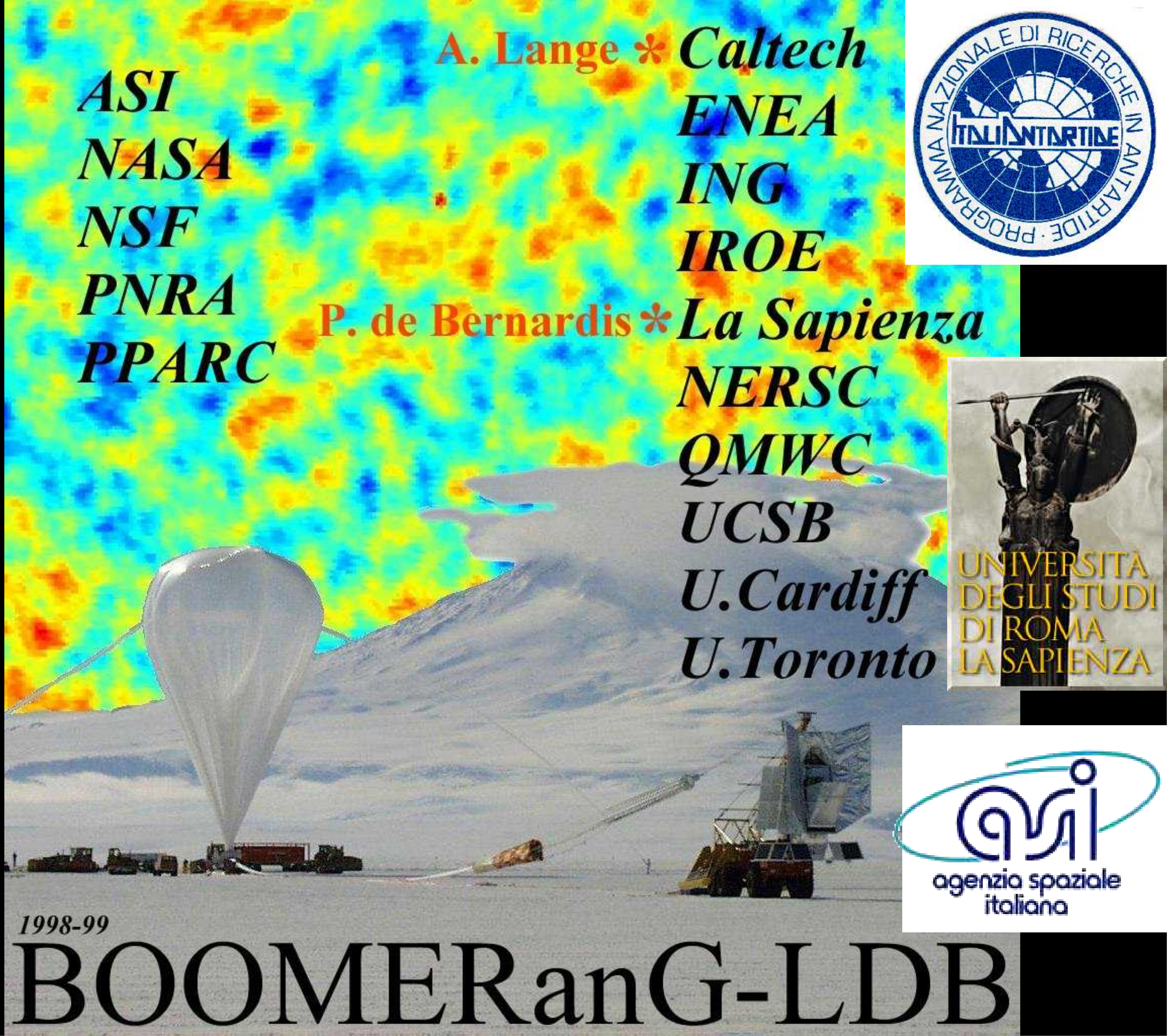

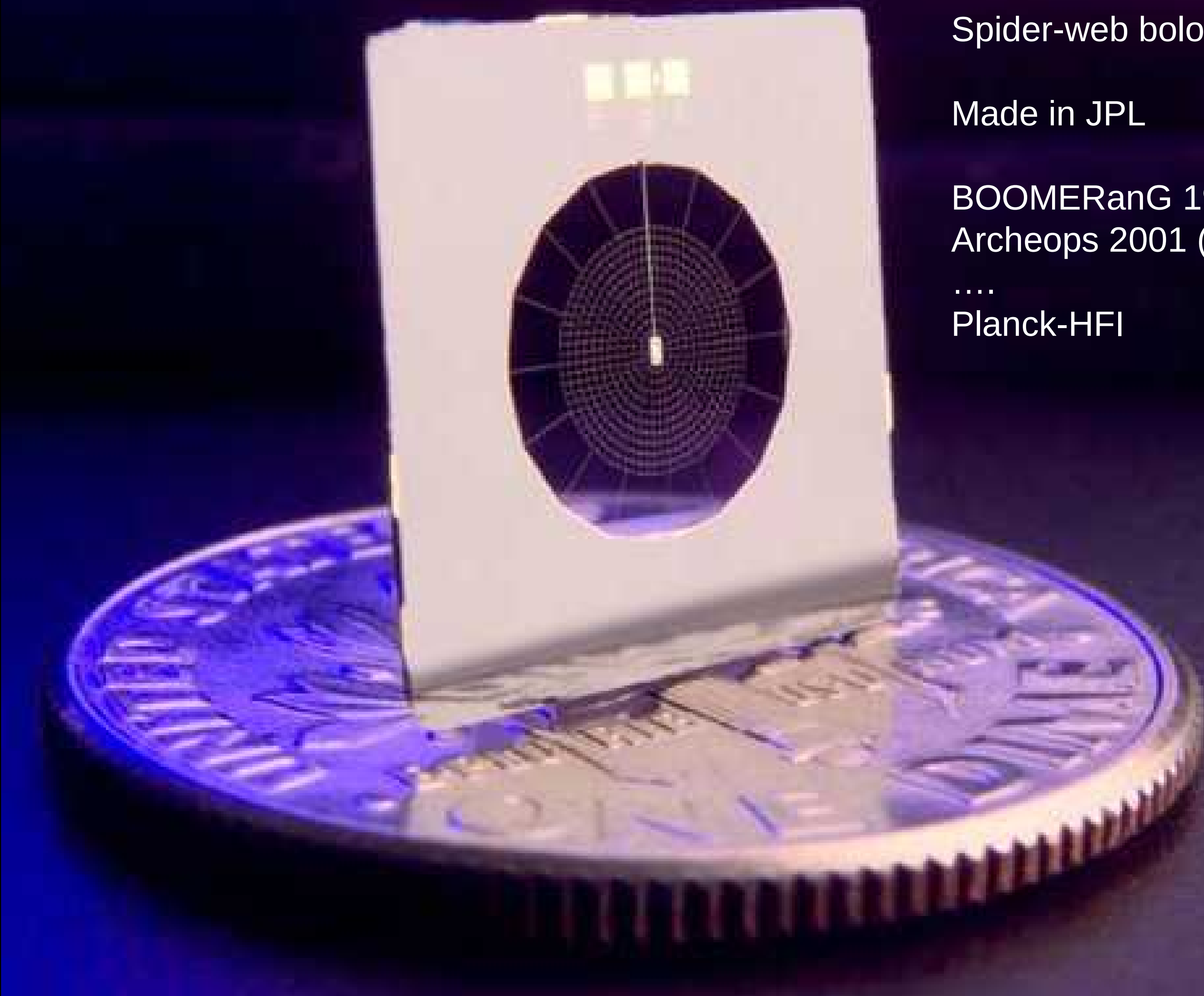

Spider-web bolometers

Made in JPL

BOOMERanG 1998 (0.3K),
Archeops 2001 (0.1K),
….
Planck-HFI

BOOMERanG (1998, 2003)

PROGRAMMA NAZIONALE DI RICERCHE IN ANTARTIDE

ITALIANTARTIDE

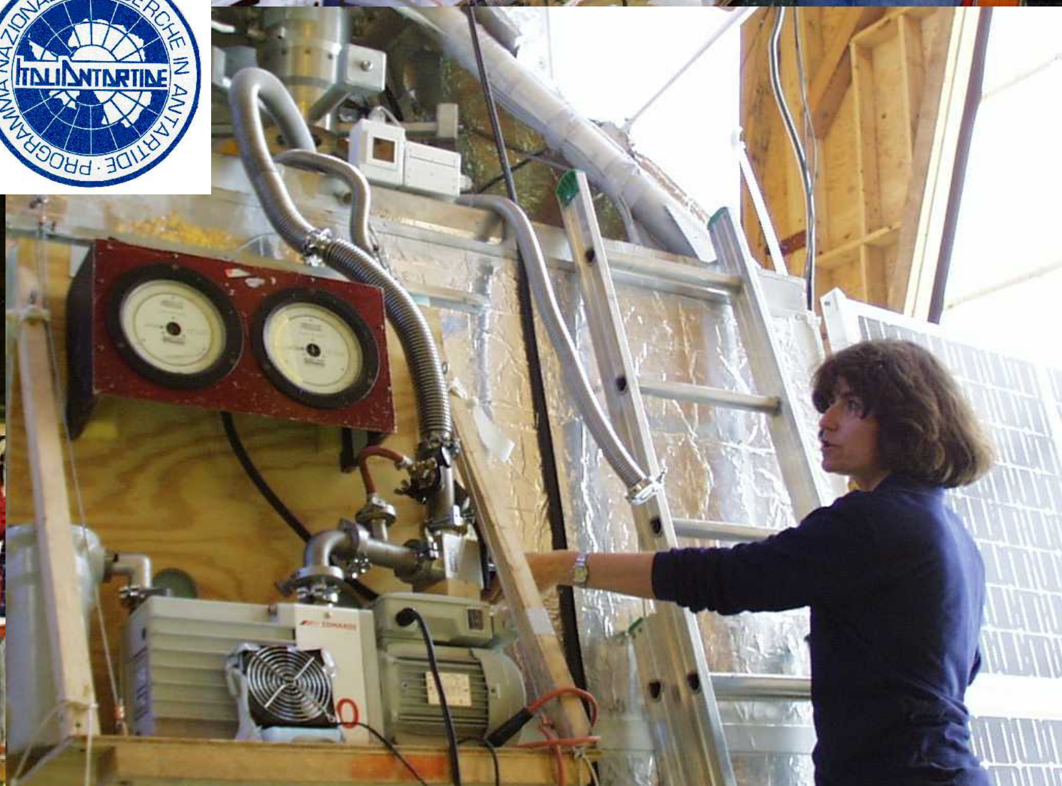

BOOMERanG

Il lancio

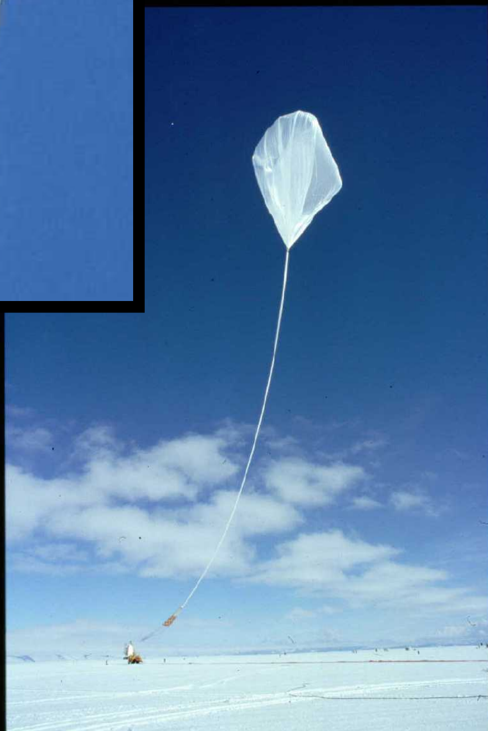

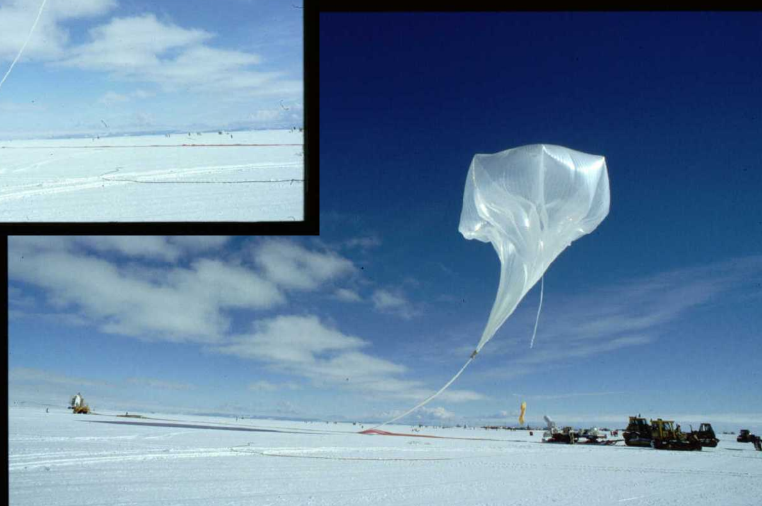

PROGRAMMA NAZIONALE DI RICERCHE IN ANTARTIDE · ITALIANTARTIDE

ACS

Firenze

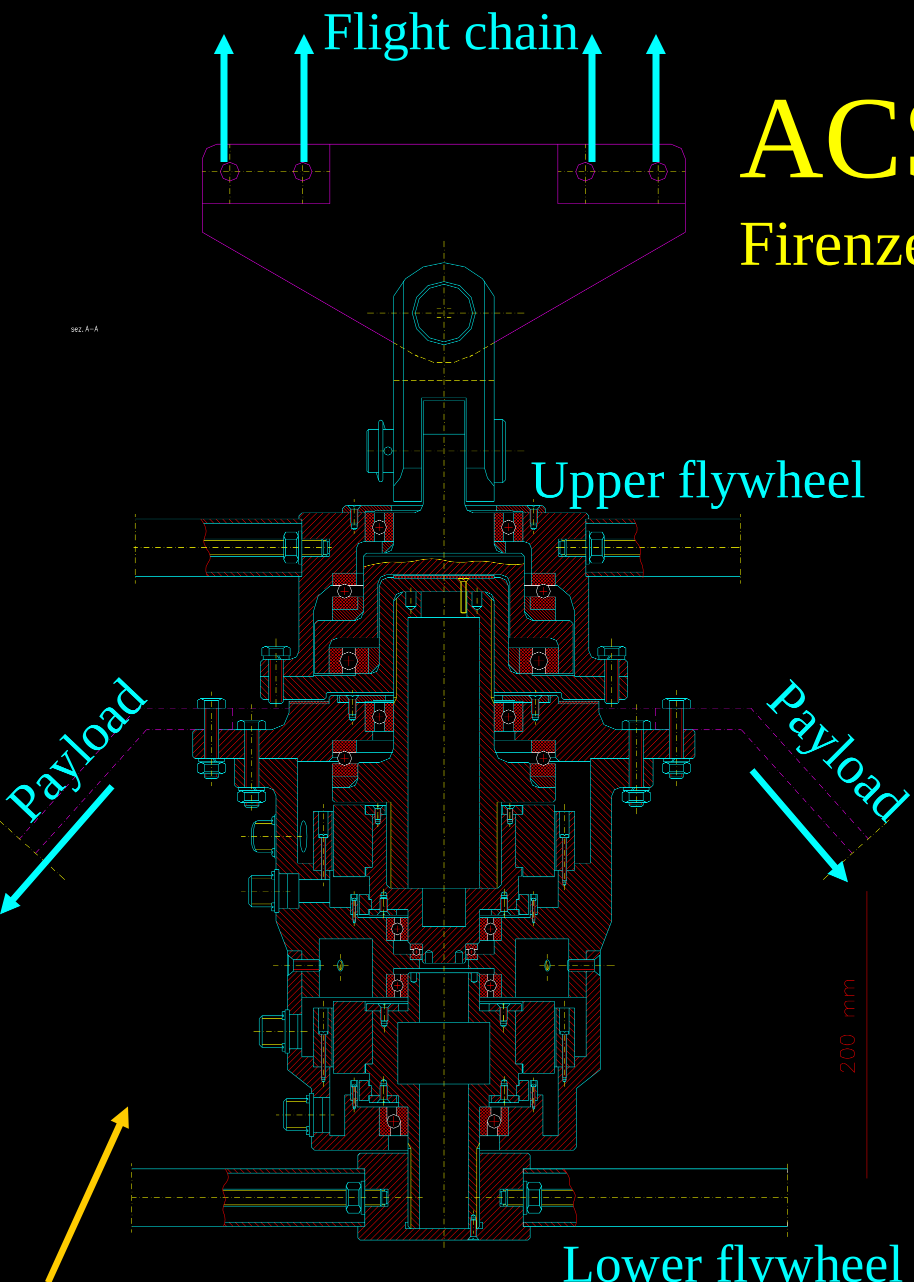

The pivot is qualified for payload weights as high as 2 tons

- The scan is obtained and controlled by means of a Attitude Control System, mainly built in IROE-CNR (Firenze).
- Actuators: inertia wheels for azimuth pointing (1 torquing against the flight chain, 1 free); ball screw for inner frame elevation
- Day-time sensors: sun sensors, laser gyros, differential GPS
- Night-time sensors: magnetometer, vibrating gyros, star camera
- Passive pendulation damper
- Feedback: optimal digital feedback with redundant CPU
- Performance: better than 0.5’ rms (measured with CCD camera in BOOM97 test flight and MAXIMA-0,1,2

The sky scan

- The image of the sky is obtained by slowly scanning in azimuth ($\pm 30^{o}$) at constant elevation
- The optimal scan speed is between 1 and 2 deg/s in azimuth

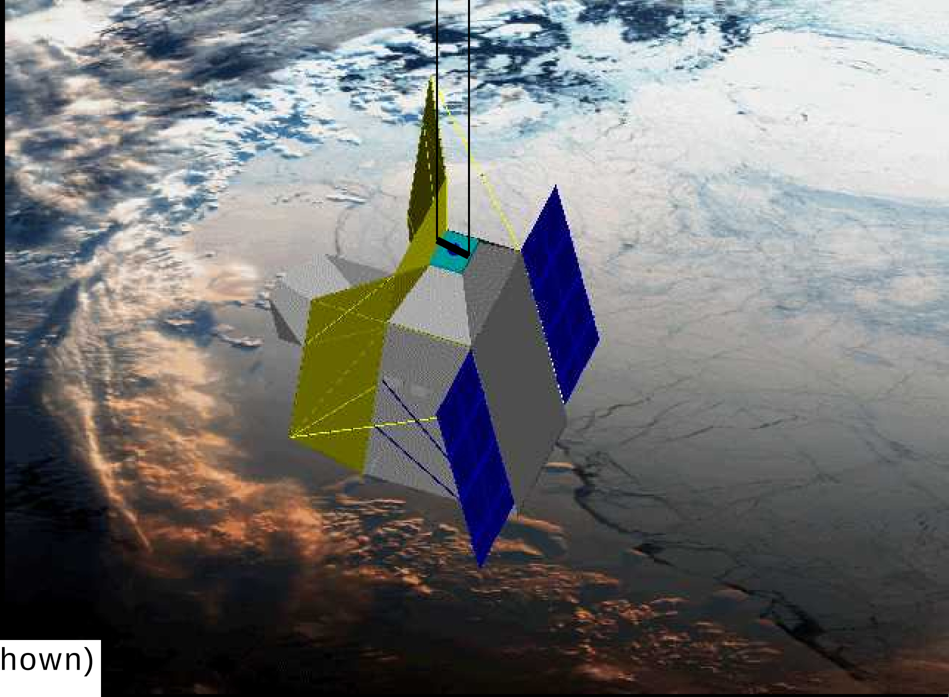

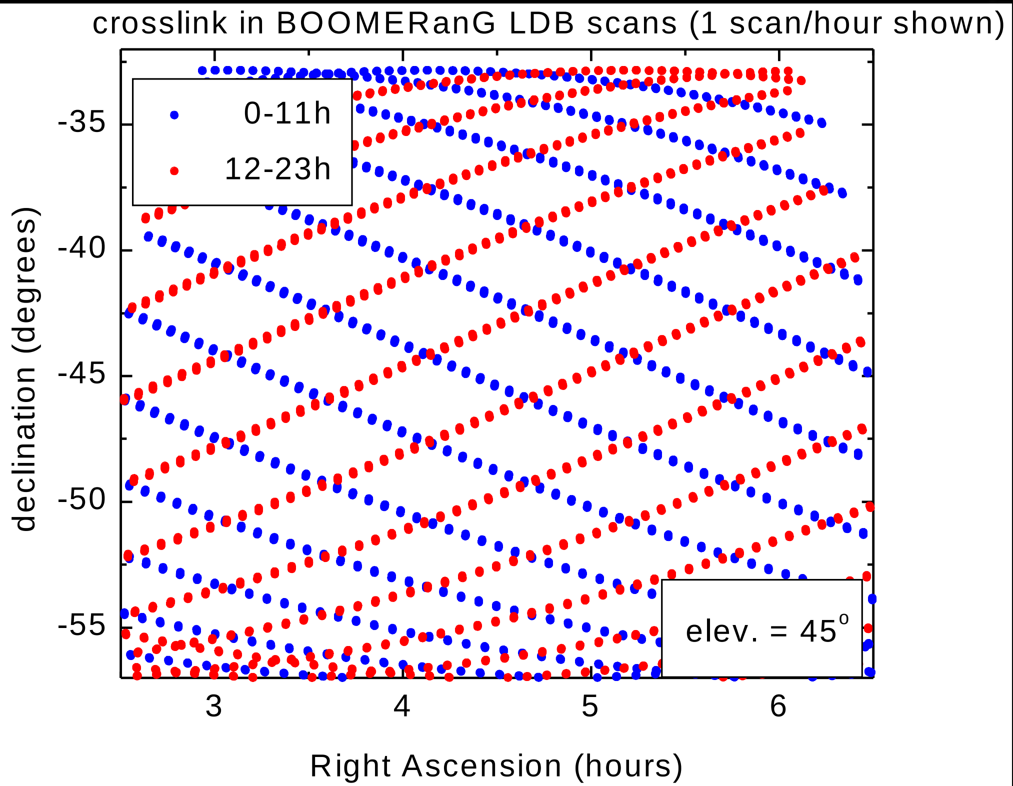

- The scan center constantly tracks the azimuth of the lowest foreground region
- Every day we obtain a fully crosslinked map.

From time-ordered data to the map

- Pointing reconstruction (gyros + differential GPS + fine Sun Sensor)
- Bolometer data editing (cosmic rays hits and other instrumental events, <4% of the data removed)
- All our maps use HEALPIX pixelization (http://www.eso.org/~kgorski/healpix/)
- 1) “Naive” coadded maps (E.Hivon, B.Crill, F.Piacentini) with high pass ($\theta>10^o$ removed)
- 2) “Rigorous” method: Maximum likelihood maps
- $$m = (A^T N^{-1} A)^{-1} A^T N^{-1} d$$

Time ordered data 57×10^6 samples

Map, 10^5 pixels

Time-time noise correlation matrix $57\times10^6 \times 57\times10^6$

Pointing matrix $57\times10^6 \times 10^5$

- Needs:
  - estimate of noise N^{-1}: iterative method (Prunet et al. Astro-ph/0006052).
  - MADCAP(Borrill, astro-ph/9903204) http://cfpa.berkeley.edu/~borrill/cmb/madcap.html
- Outputs:
  - M=maximum likelihood map
  - $v = (A^T N^{-1} A)^{-1} A^T N^{-1} n$ $\gamma = \langle v v^T \rangle = (A^T N^{-1} A)^{-1}$ pixel-pixel noise covariance

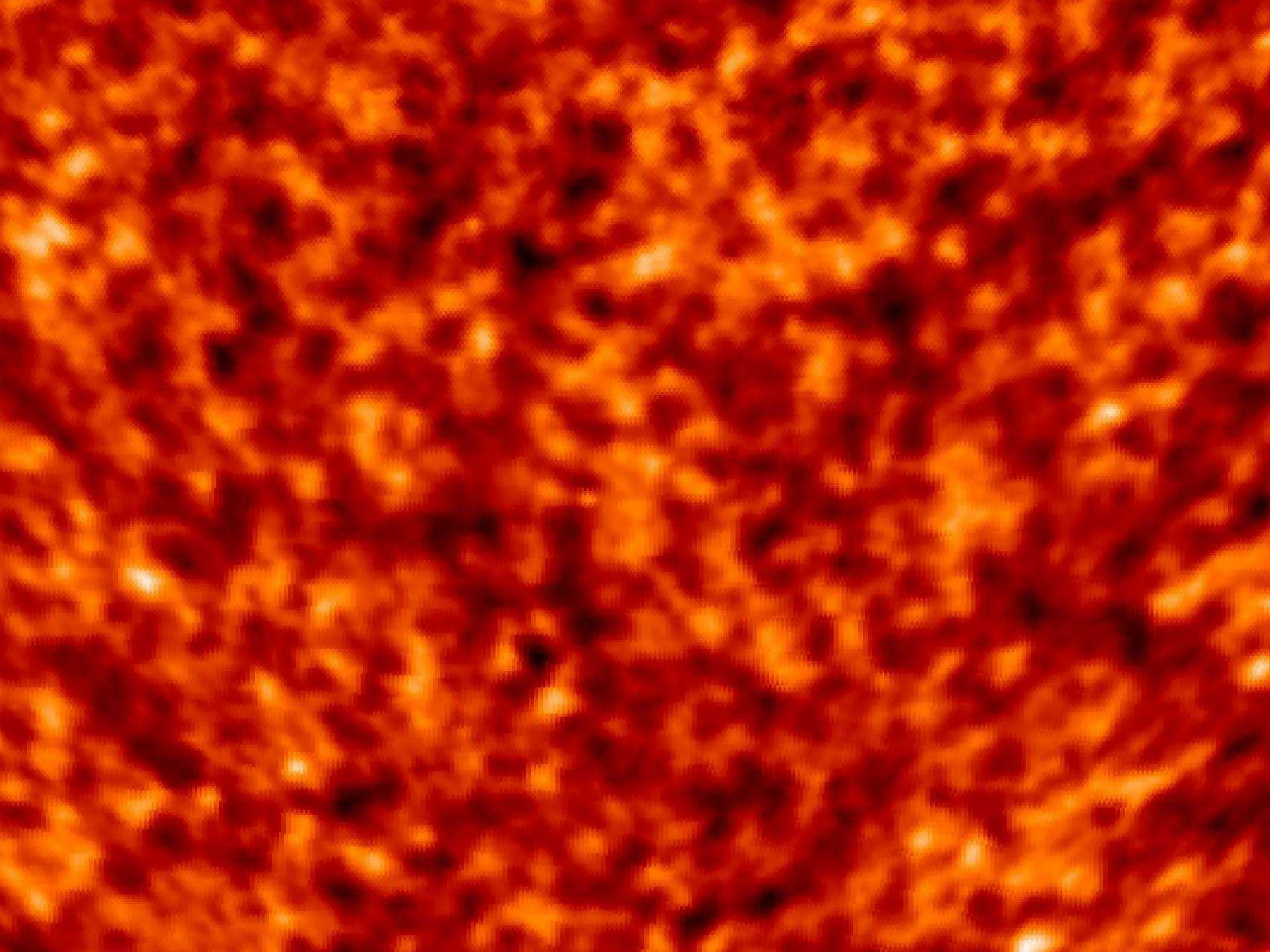

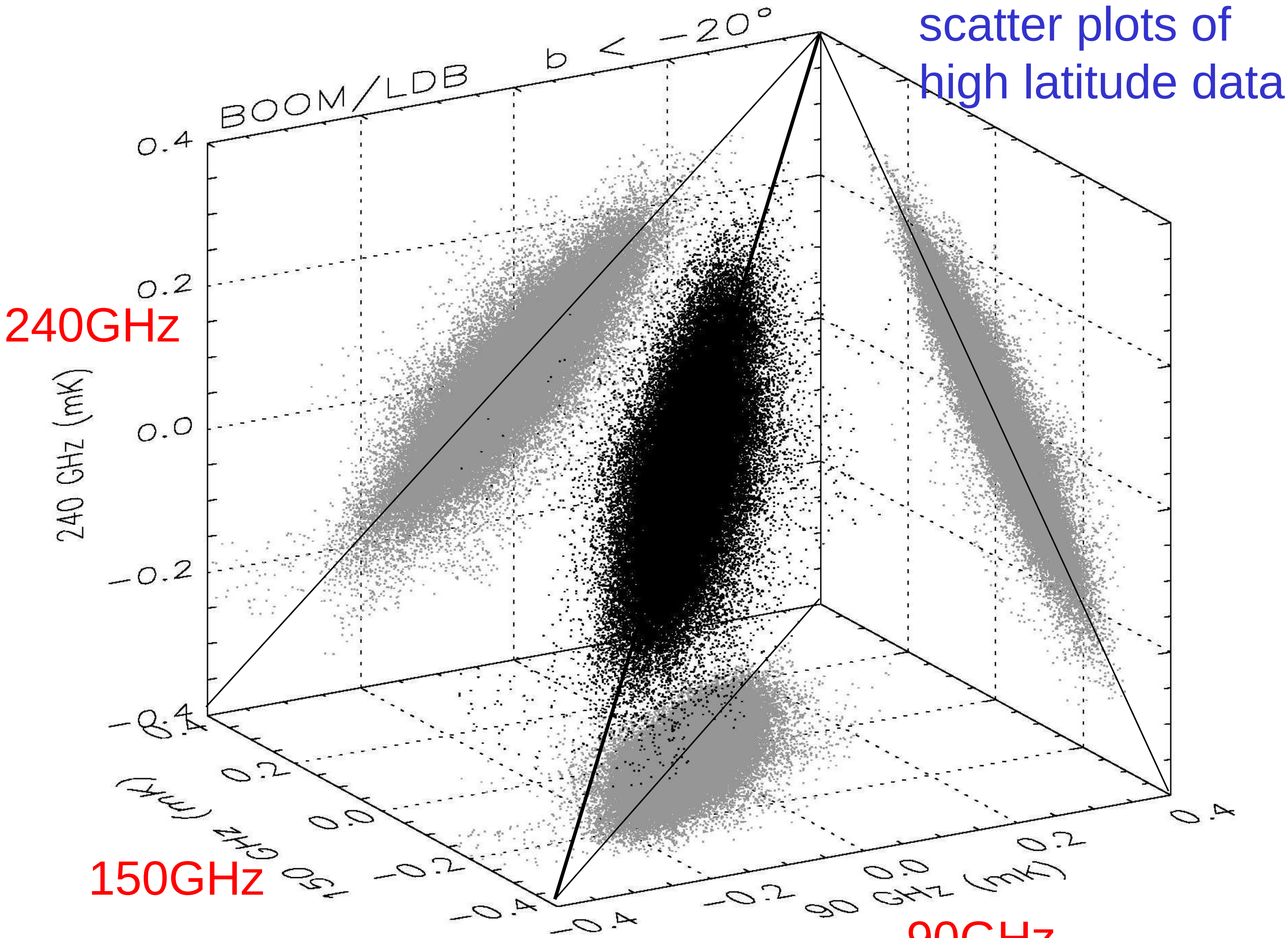

Astro-ph/0011469

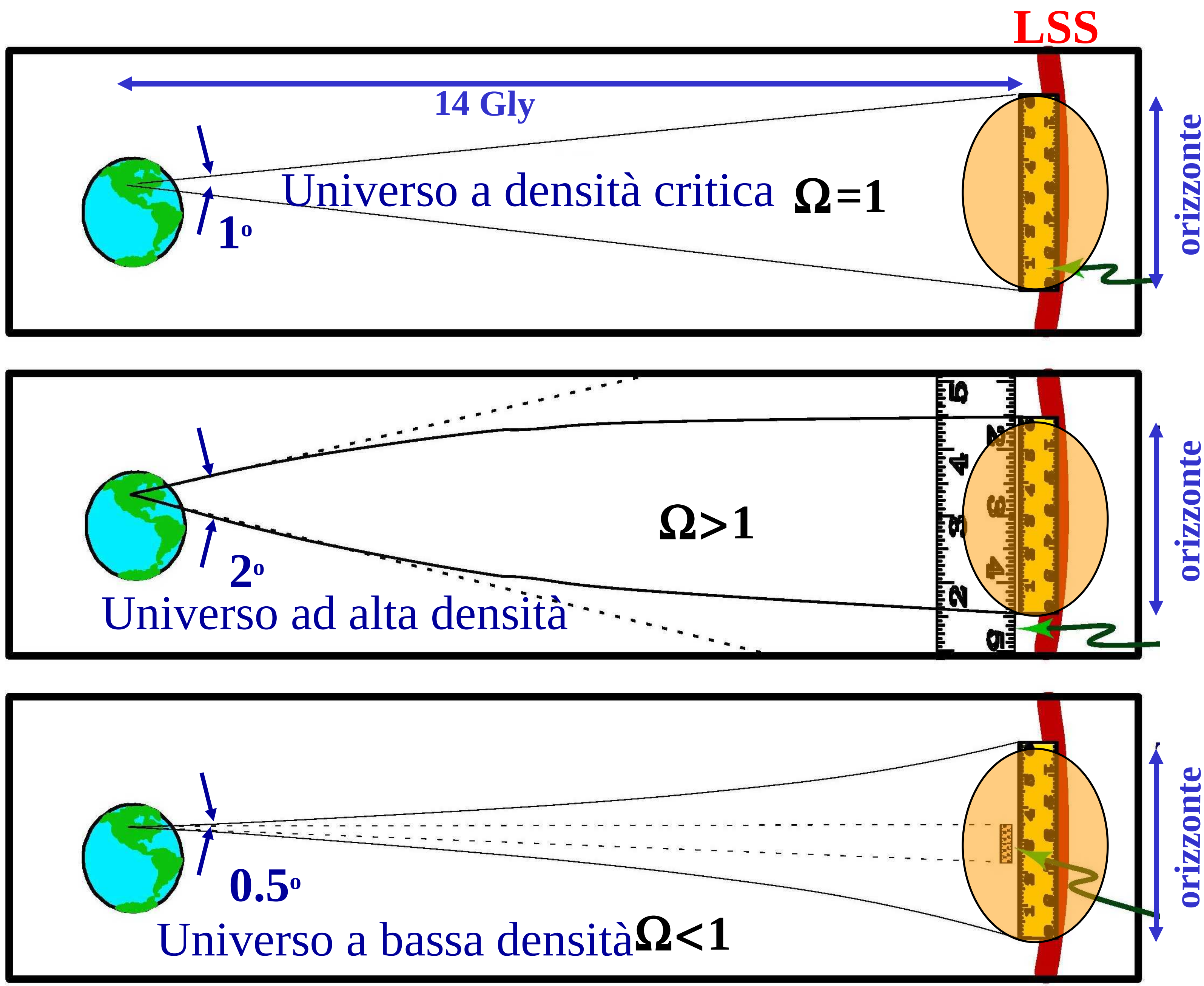

LSS
14 Gly
Universo a densità critica
Ω=1
1°
orizzonte
Ω>1
2°
Universo ad alta densità
orizzonte
0.5°
Universo a bassa densità
Ω<1
orizzonte

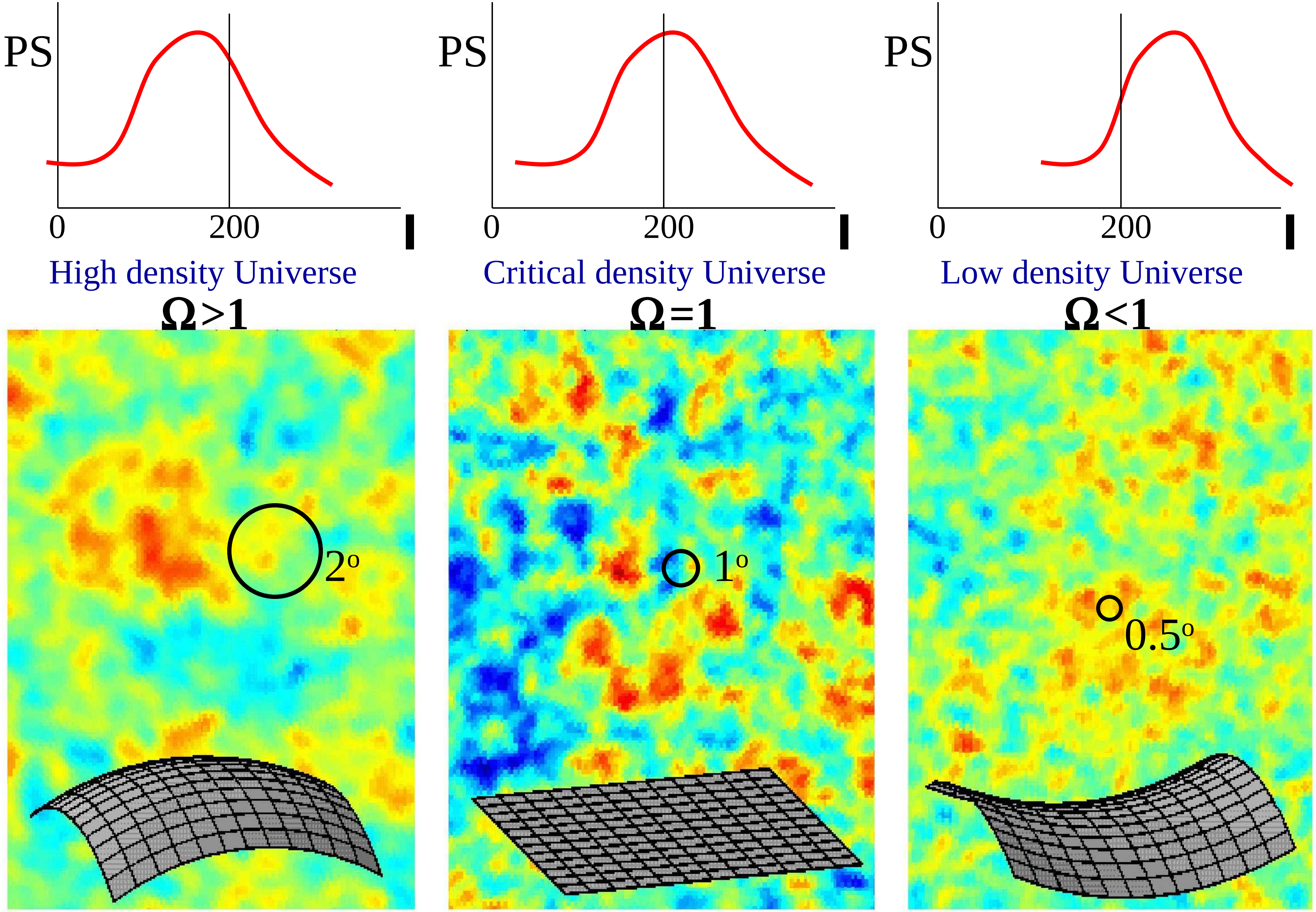
PS
0
200
l
High density Universe
Ω>1
2°
PS
0
200
l
Critical density Universe
Ω=1
1°
PS
0
200
l
Low density Universe
Ω<1
0.5°

THE ASTROPHYSICAL JOURNAL, 564:559–566, 2002 January 10

MULTIPLE PEAKS IN THE ANGULAR POWER SPECTRUM OF THE COSMIC MICROWAVE BACKGROUND: SIGNIFICANCE AND CONSEQUENCES FOR COSMOLOGY

P. DE BERNARDIS,[1] P. A. R. ADE,[2] J. J. BOCK,[3] J. R. BOND,[4] J. BORRILL,[5] A. BOSCALERI,[6] K. COBLE,[7] C. R. CONTALDI,[4] B. P. CRILL,[8] G. DE TROIA,[1] P. FARESE,[7] K. GANGA,[9] M. GIACOMETTI,[1] E. HIVON,[9] V. V. HRISTOV,[8] A. IACOANGELI,[1] A. H. JAFFE,[10] W. C. JONES,[8] A. E. LANGE,[8] L. MARTINIS,[11] S. MASI,[1] P. MASON,[8] P. D. MAUSKOPF,[12] A. MELCHIORRI,[13] T. MONTROY,[7] C. B. NETTERFIELD,[14] E. PASCALE,[6] F. PIACENTINI,[1] D. POGOSYAN,[4] G. POLENTA,[1] F. PONGETTI,[15] S. PRUNET,[4] G. ROMEO,[15] J. E. RUHL,[7] AND F. SCARAMUZZI[11]

Received 2001 May 18; accepted 2001 September 11

ABSTRACT

Three peaks and two dips have been detected in the power spectrum of the cosmic microwave background by the BOOMERANG experiment, at $l = (213^{+10}_{-13})$, (541^{+20}_{-32}), (845^{+12}_{-25}) and $l = (416^{+22}_{-12})$, (750^{+20}_{-750}), respectively. Using model-independent analyses, we find that all five features are statistically significant, and we measure their location and amplitude. These are consistent with the adiabatic inflationary model. We also calculate the mean and variance of the peak and dip locations and amplitudes in a large seven-dimensional parameter space of such models, which gives good agreement with the model-independent estimates. We forecast where the next few peaks and dips should be found if the basic paradigm is correct. We test the robustness of our results by comparing Bayesian marginalization techniques on this space with likelihood maximization techniques applied to a second seven-dimensional cosmological parameter space, using an independent computational pipeline, and find excellent agreement: $\Omega_{tot} = 1.02^{+0.05}_{-0.06}$ versus 1.04 ± 0.05, $\Omega_b h^2 = 0.022^{+0.004}_{-0.003}$ versus $0.019^{+0.005}_{-0.004}$, and $n_s = 0.96^{+0.09}_{-0.08}$ versus 0.90 ± 0.08. The determination of the best fit by the maximization procedure effectively ignores nonzero optical depth of reionization $\tau_C > 0$, and the difference in primordial spectral index n_s between the two methods is thus a consequence of the strong correlation of n_s with the τ_C.

Subject headings: cosmic microwave background — cosmological parameters — cosmology: observations

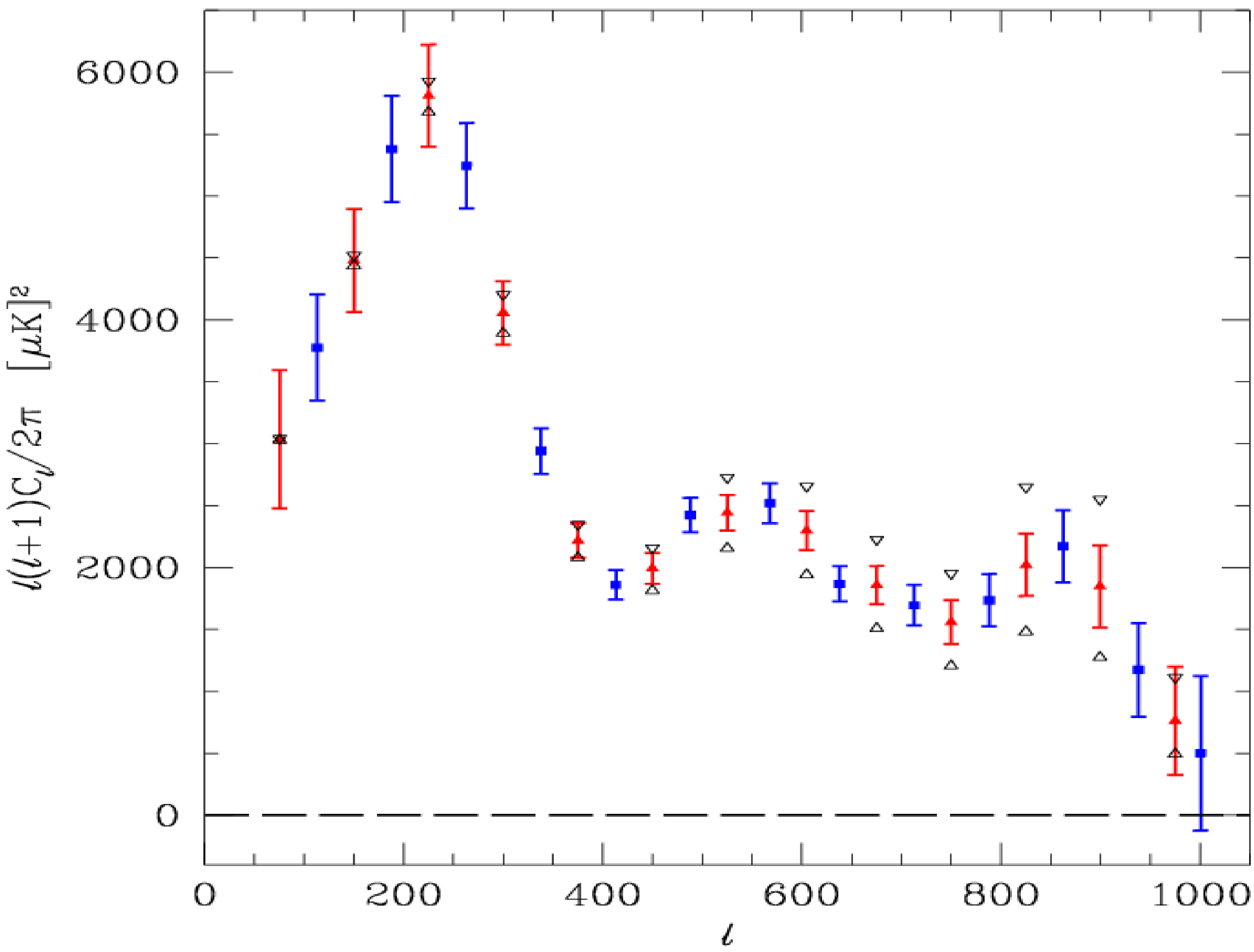

Netterfield et al. 2001, de Bernardis et al. 2002

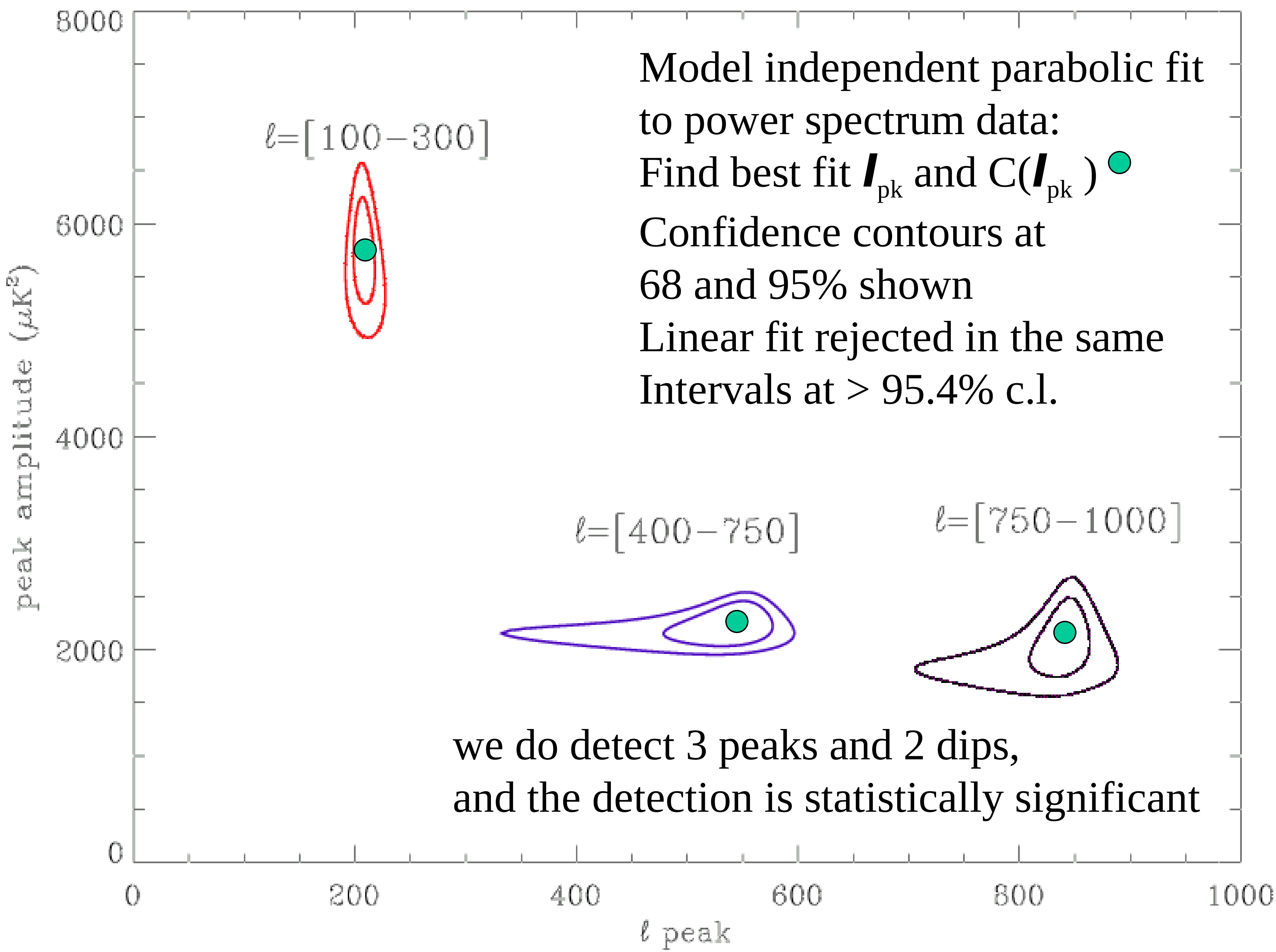

Model independent parabolic fit
to power spectrum data:
Find best fit l_{pk} and C(l_{pk})
Confidence contours at
68 and 95% shown
Linear fit rejected in the same
Intervals at > 95.4% c.l.
we do detect 3 peaks and 2 dips,
and the detection is statistically significant
ℓ=[100−300]
ℓ=[400−750]
ℓ=[750−1000]
peak amplitude (μK^2)
ℓ peak
8000
6000
4000
2000
0
0
200
400
600
800
1000

WMAP (2002)

Wilkinson Microwave Anisotropy Probe

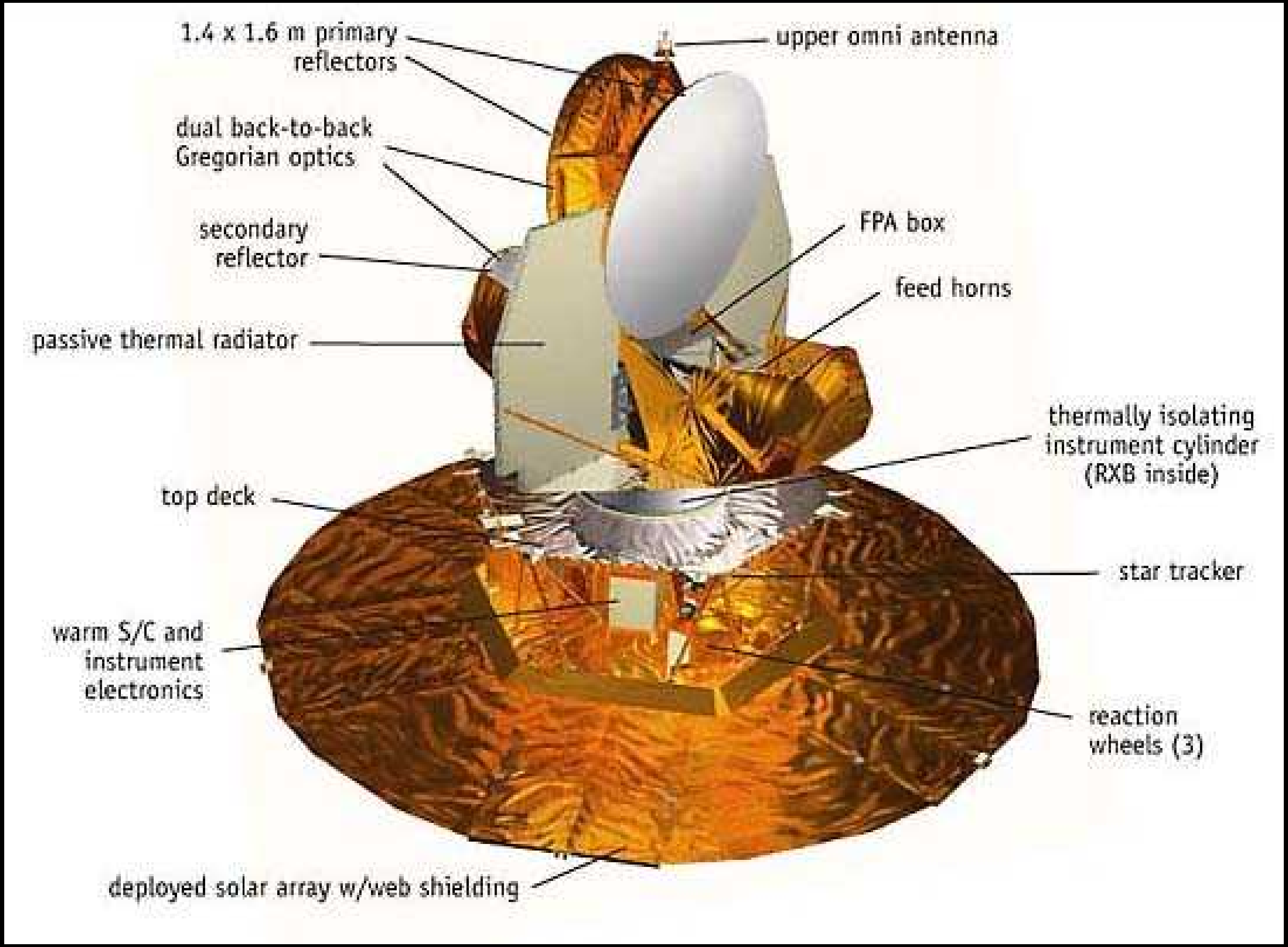

WMAP in L_2 : sun, earth, moon are all well behind the solar shield.

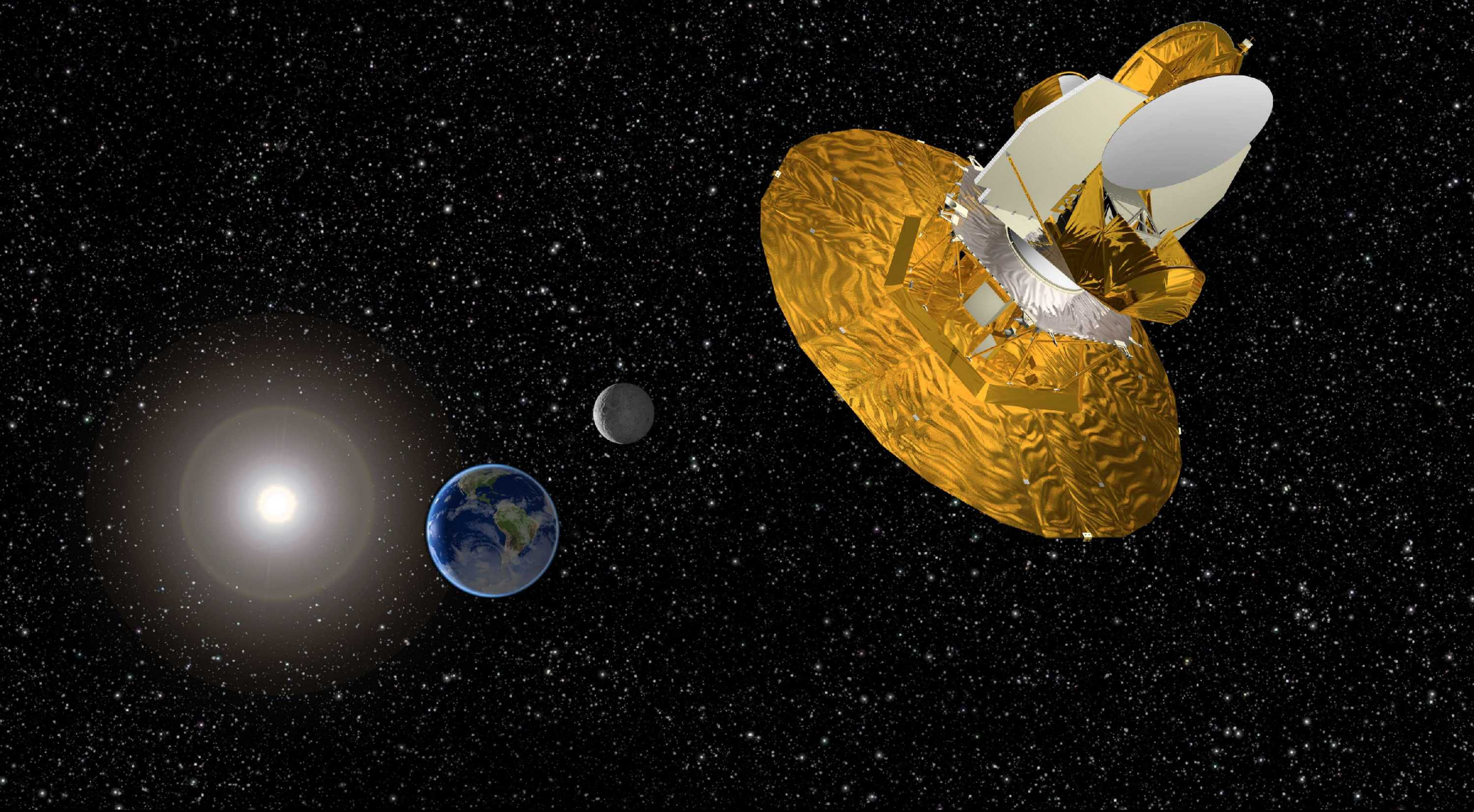

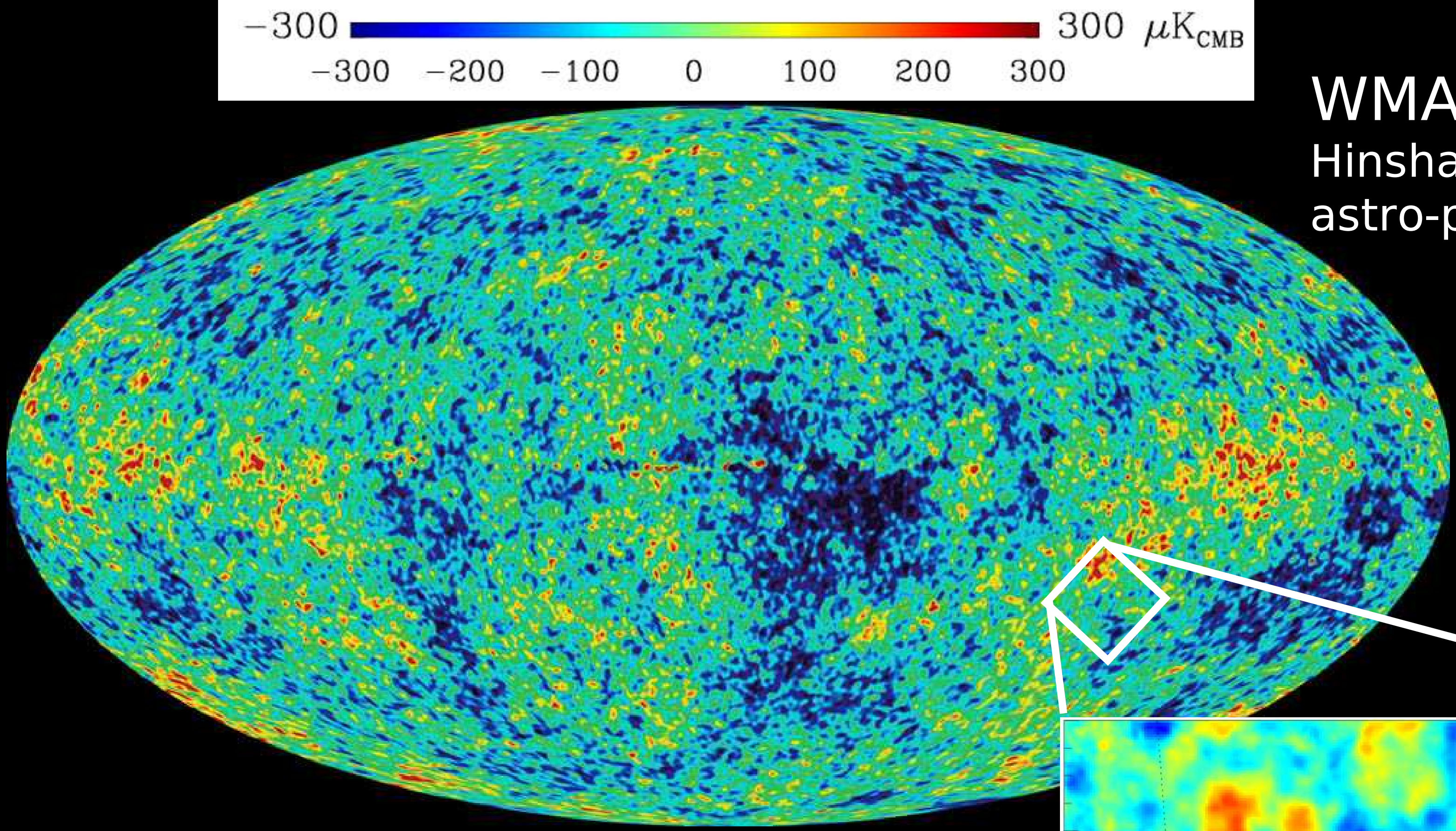

WMAP
Hinshaw et al. 2006
astro-ph/0603451

Detailed Views of the Recombination Epoch (z=1088, 13.7 Gyrs ago)

BOOMERanG
Masi et al. 2005
astro-ph/0507509

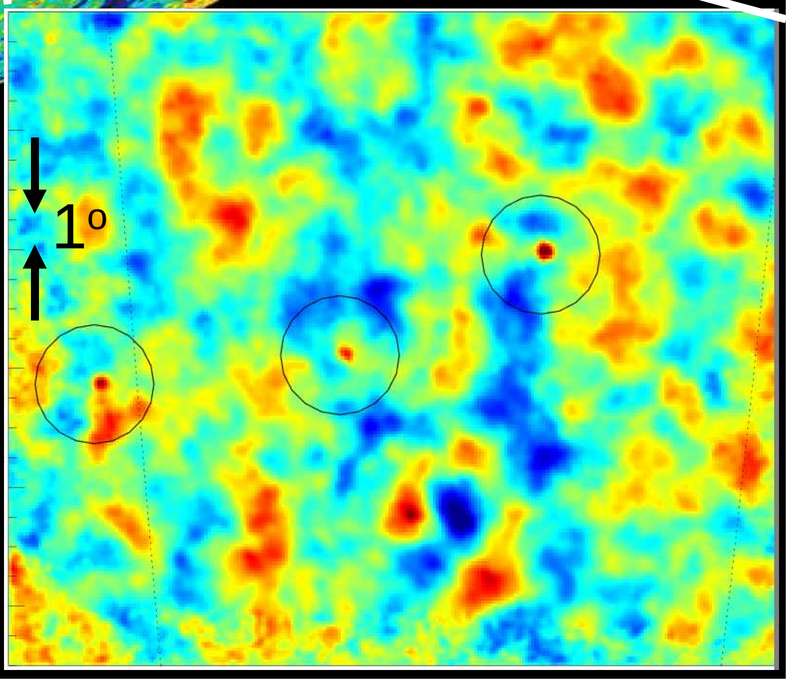

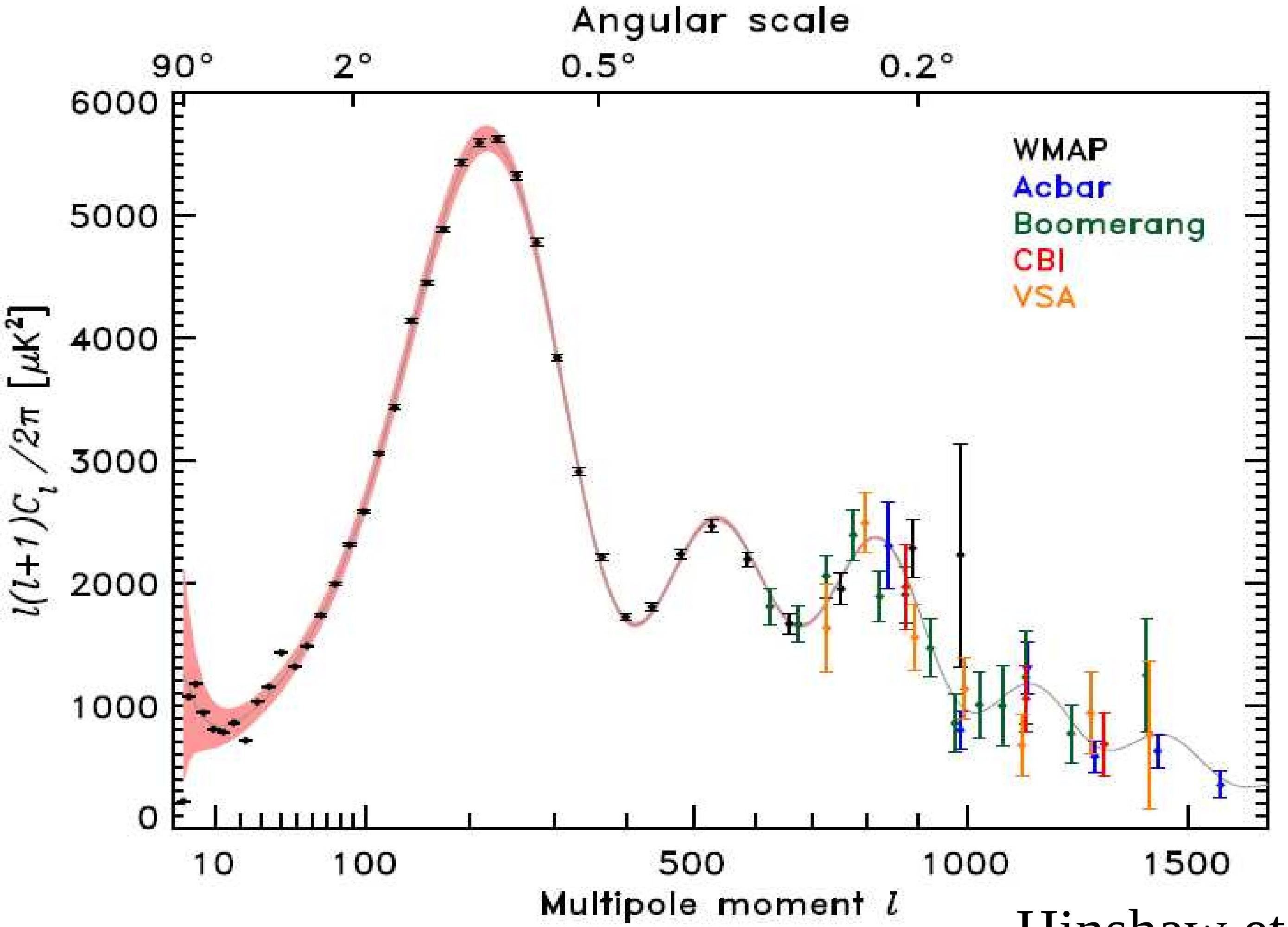

Hinshaw et al. 2006

Fig. 18.— The *WMAP* three-year power spectrum (in black) compared to other recent measurements of the CMB angular power spectrum, including Boomerang (Jones et al. 2005), Acbar (Kuo et al. 2004), CBI (Readhead et al. 2004), and VSA (Dickinson et al. 2004). For clarity, the $l < 600$ data from Boomerang and VSA are omitted; as the measurements are consistent with *WMAP*, but with lower weight. These data impressively confirm the turnover in the 3rd acoustic peak and probe the onset of Silk damping. With improved sensitivity on sub-degree scales, the *WMAP* data are becoming an increasingly important calibration source for high-resolution experiments.

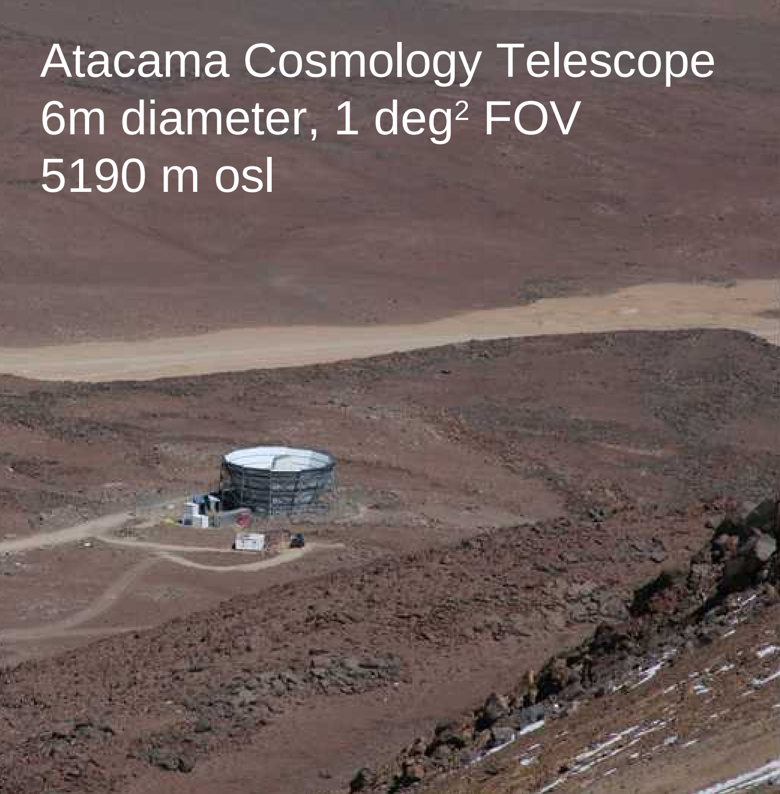
Atacama Cosmology Telescope
6m diameter, 1 deg^2 FOV
5190 m osl

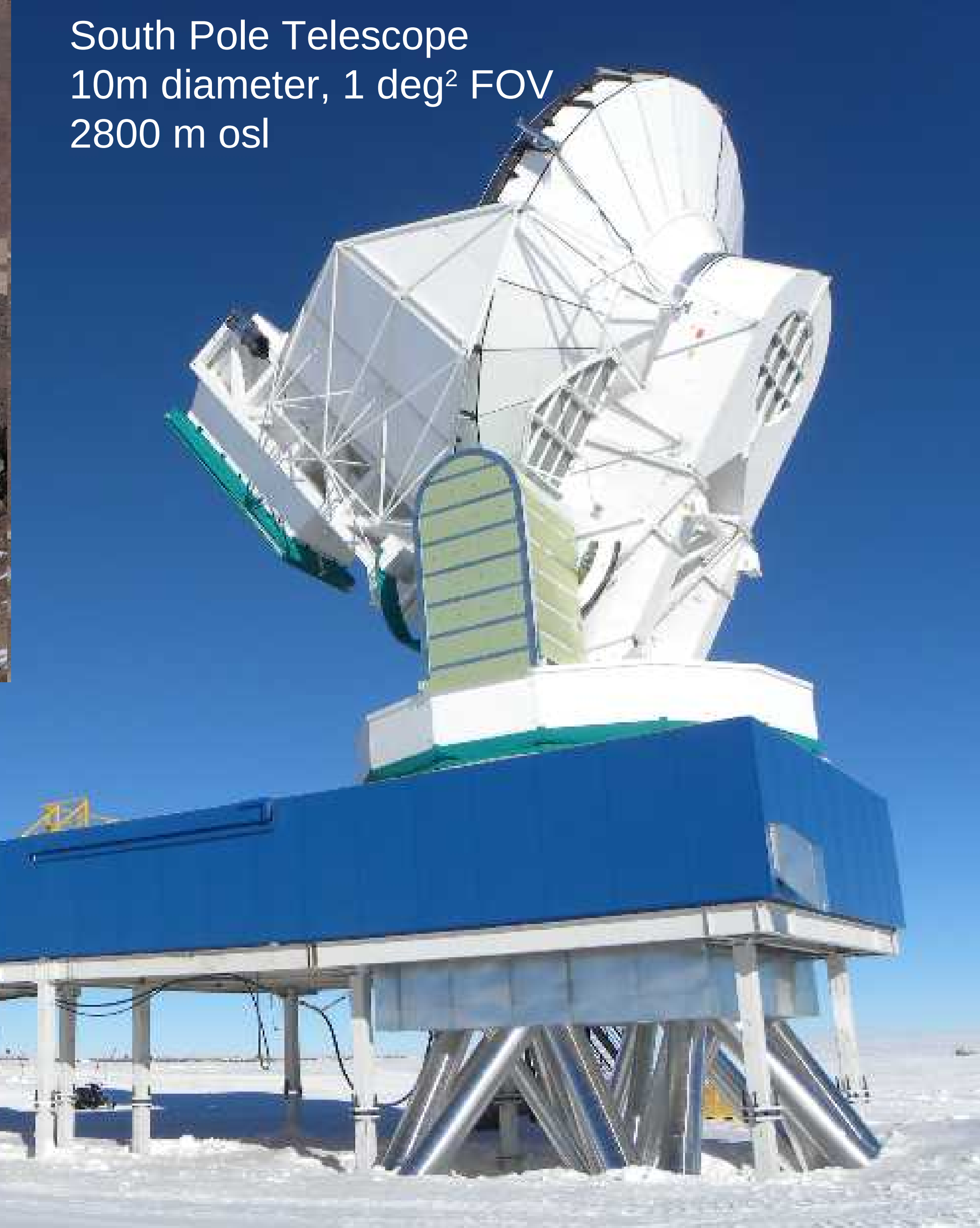
South Pole Telescope
10m diameter, 1 deg^2 FOV
2800 m osl

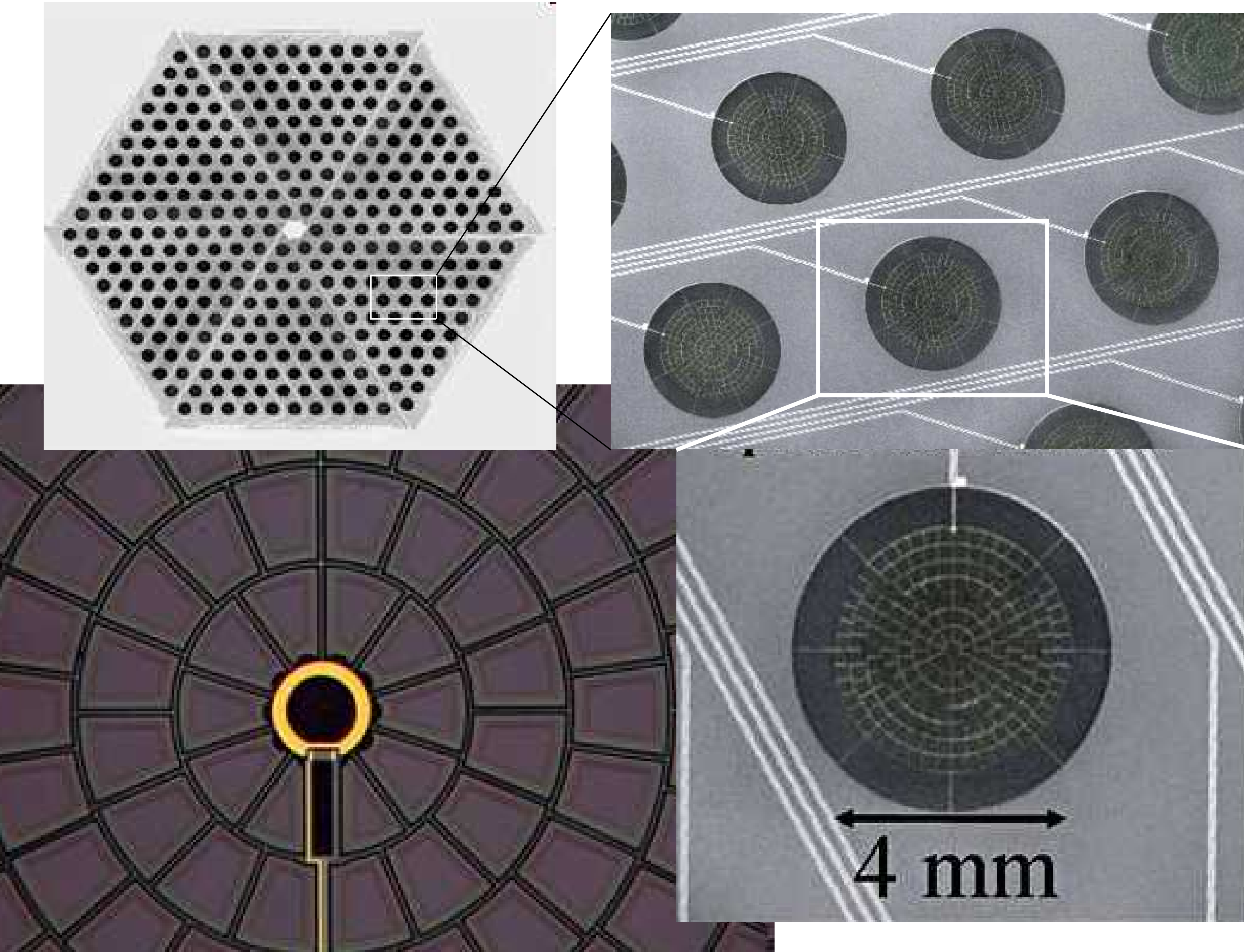
4 mm

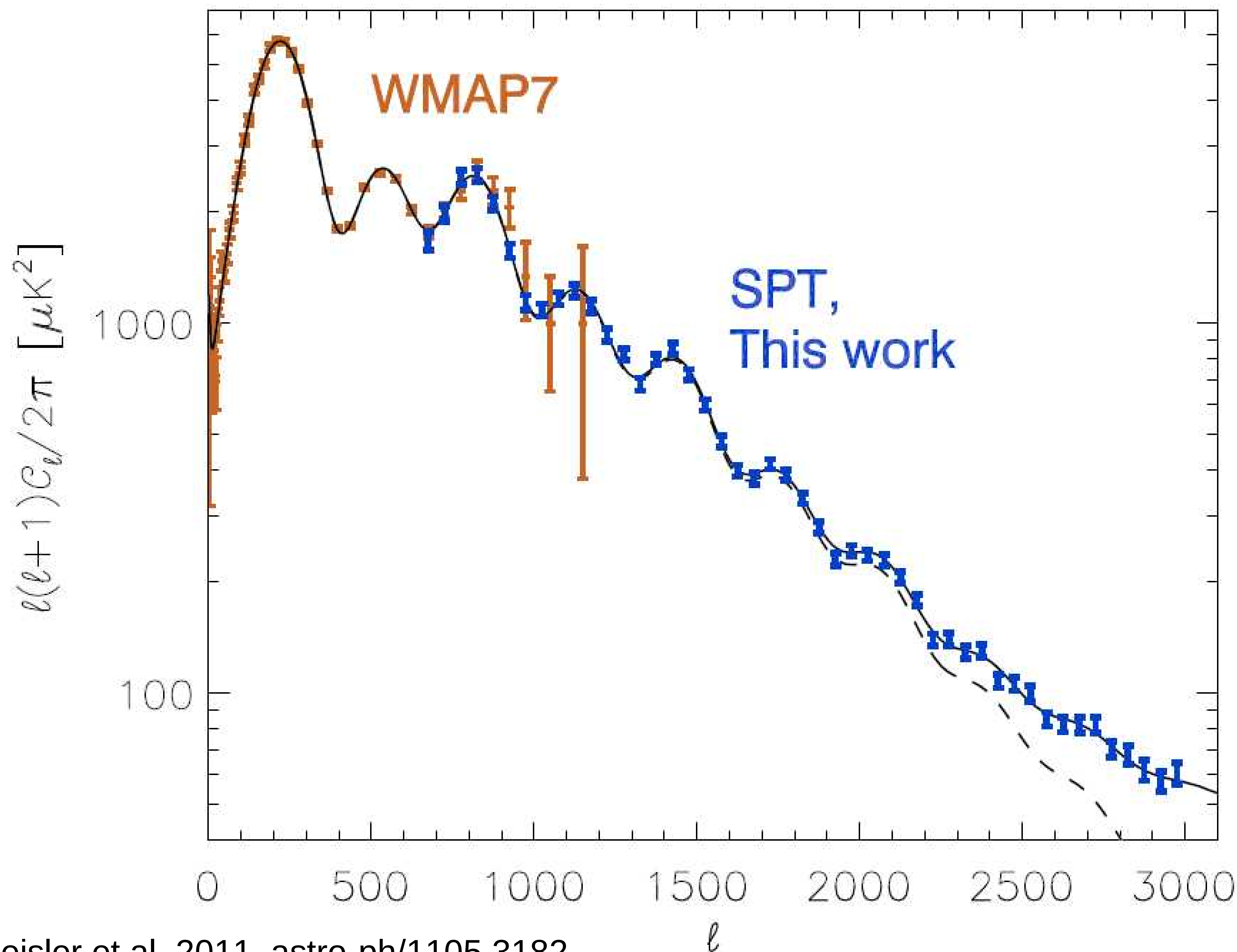

Keisler et al. 2011, astro-ph/1105.3182

Radiazione
< 0.3%

Materia Normale
4%

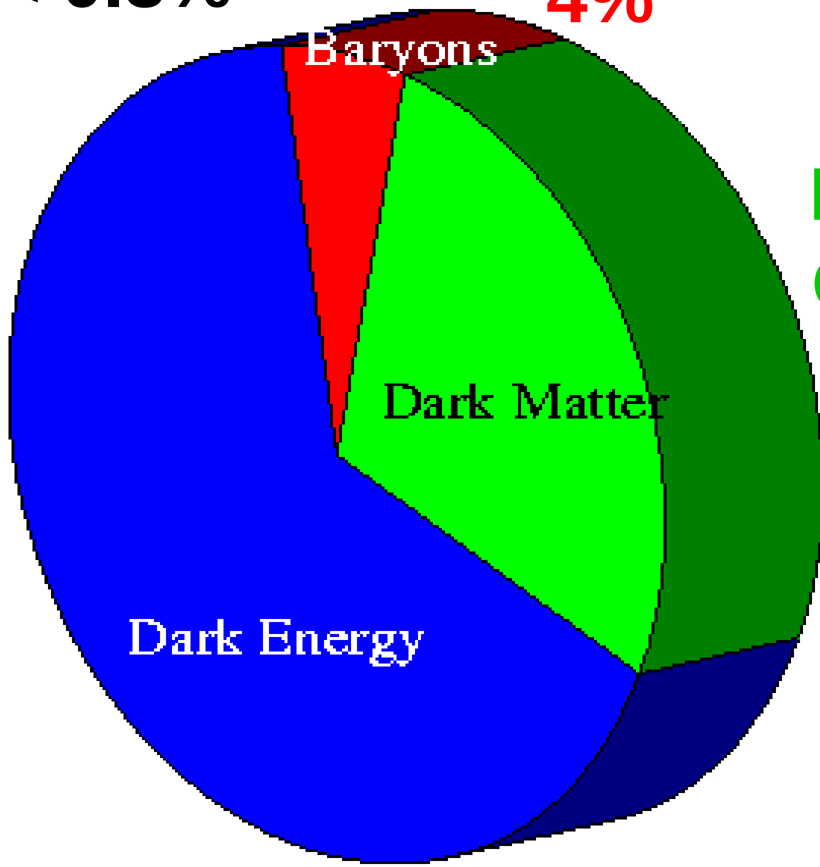

Materia Oscura
22%

Energia Oscura
74%

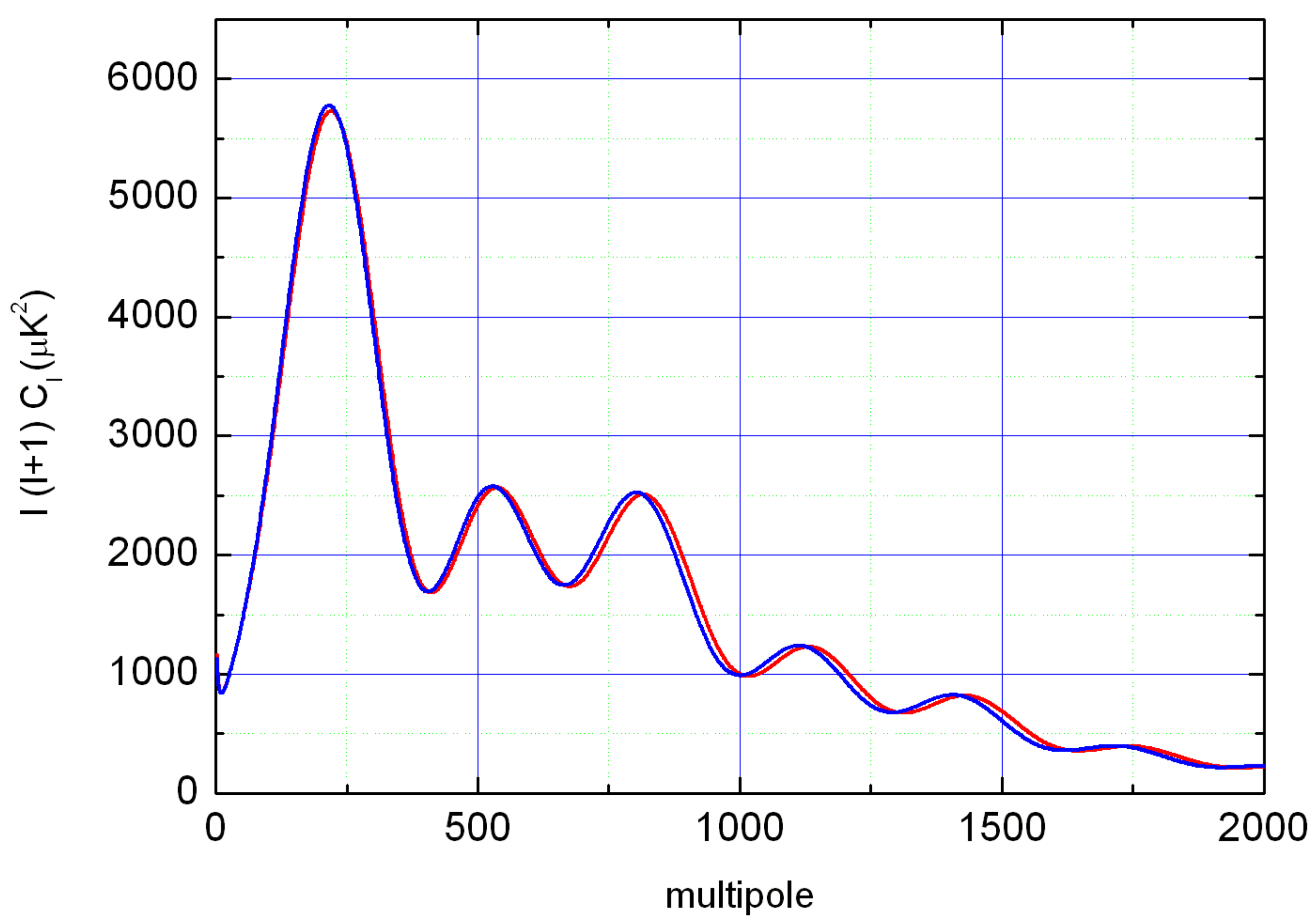

- **Effect on massive neutrinos on CMB anisotropy power spectrum (red: Nν=3, Σmν=0.65 eV)**

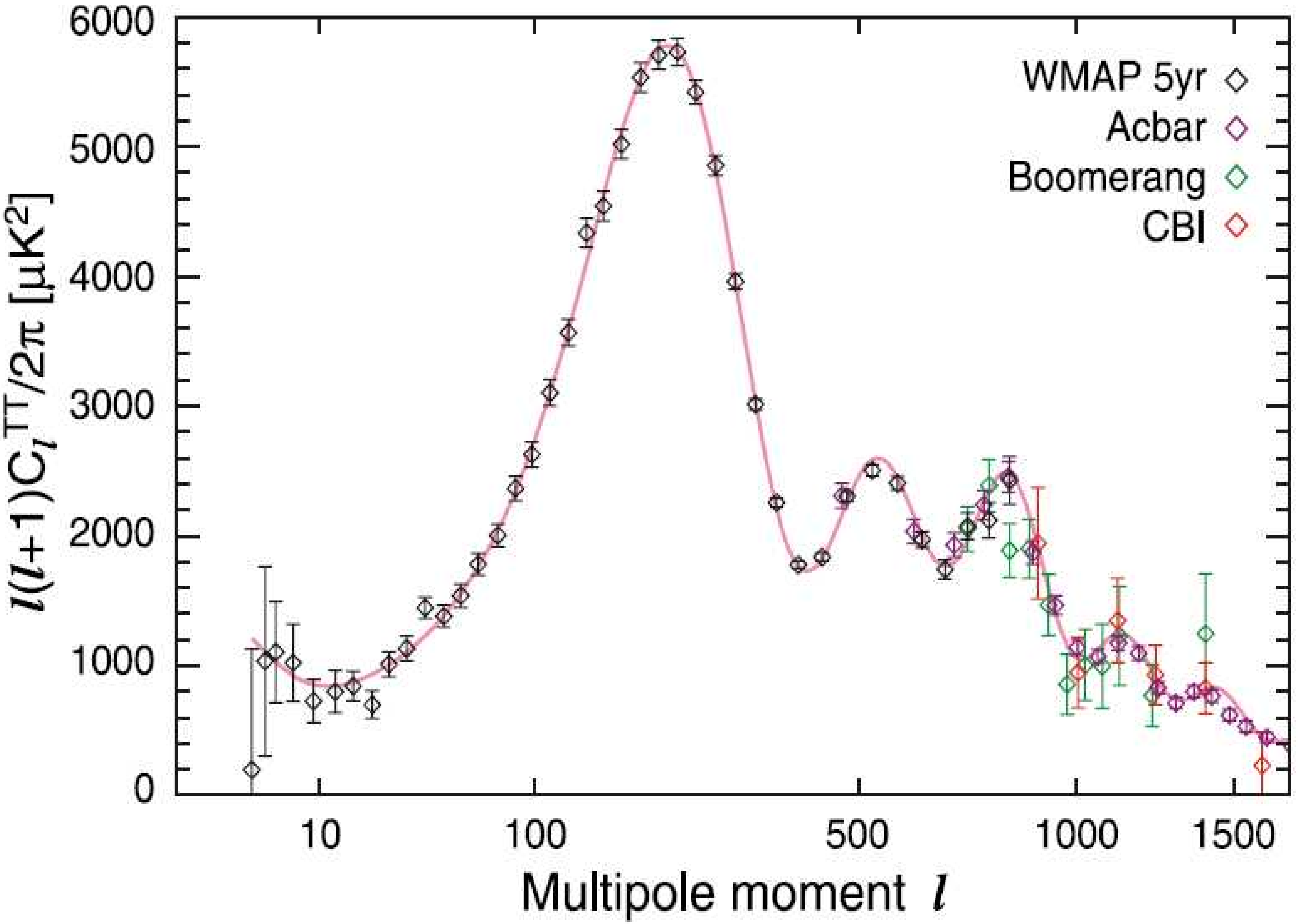

6000
5000
4000
3000
2000
1000
0
10
100
500
1000
1500
Multipole moment l
l(l+1)C_l^TT/2π [μK²]
WMAP 5yr
Acbar
Boomerang
CBI

TABLE II: Representative cosmological data sets and corresponding 2σ (95% C.L.) constraints on the sum of ν masses Σ.

Case	Cosmological data set	Σ (at 2σ)
1	CMB	< 1.19 eV
2	CMB + LSS	< 0.71 eV
3	CMB + HST + SN-Ia	< 0.75 eV
4	CMB + HST + SN-Ia + BAO	< 0.60 eV
5	CMB + HST + SN-Ia + BAO + Lyα	< 0.19 eV

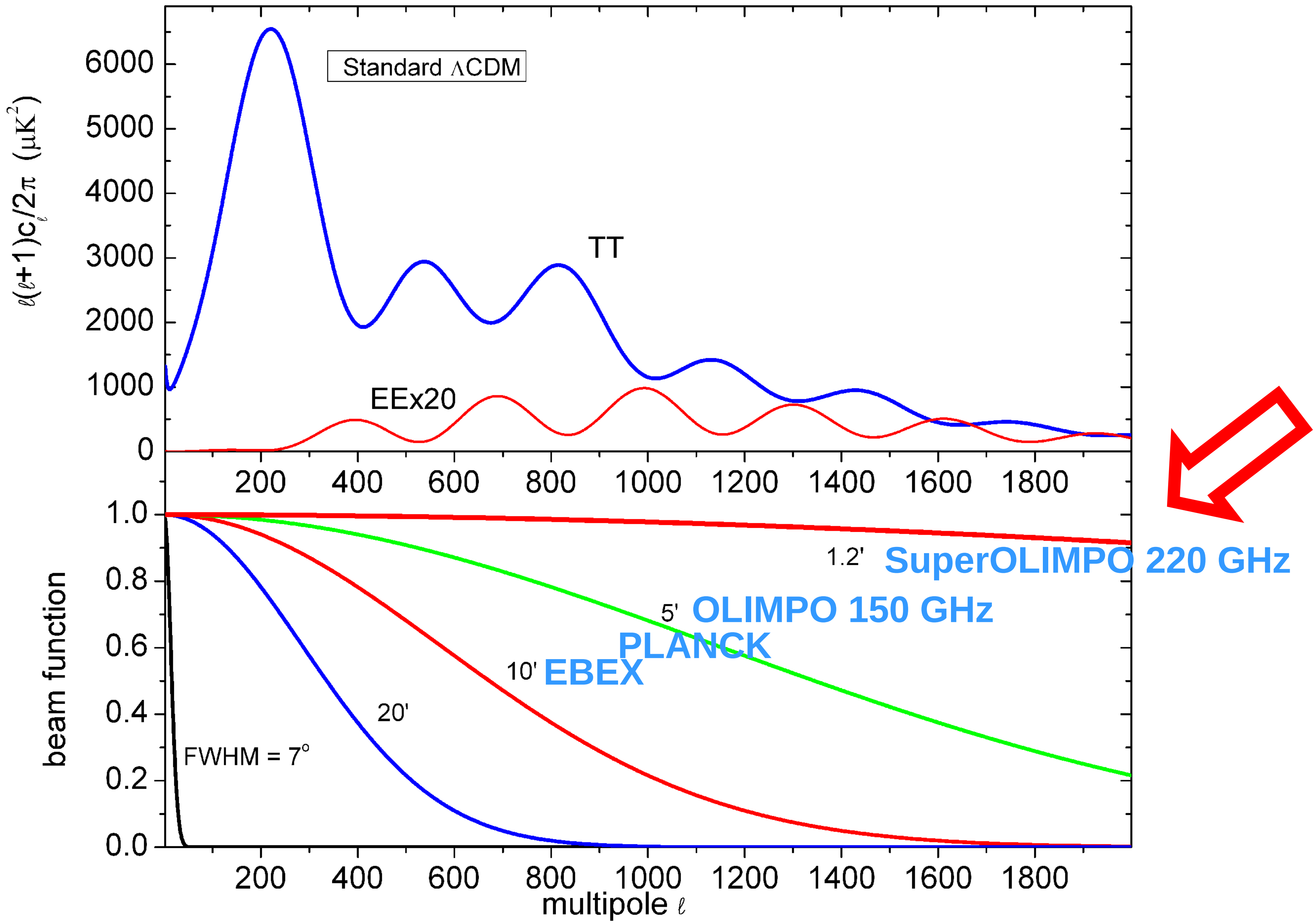

- Angular resolution is the key !

Super-OLIMPO: performance

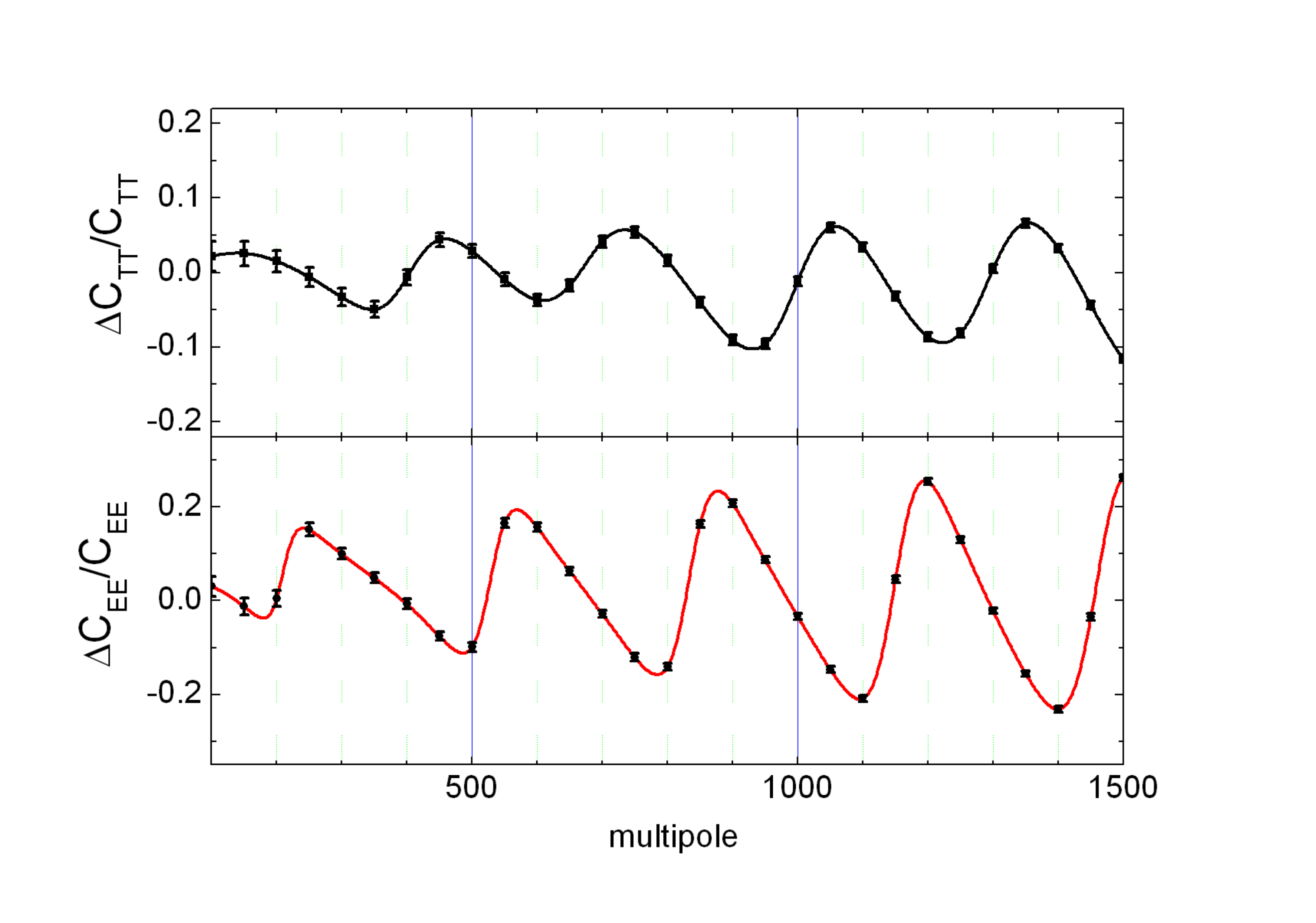

- **Effect on massive neutrinos on CMB anisotropy and polarization spectra (Nν=3, Σmν=0.65 eV)**

Super-OLIMPO: performance

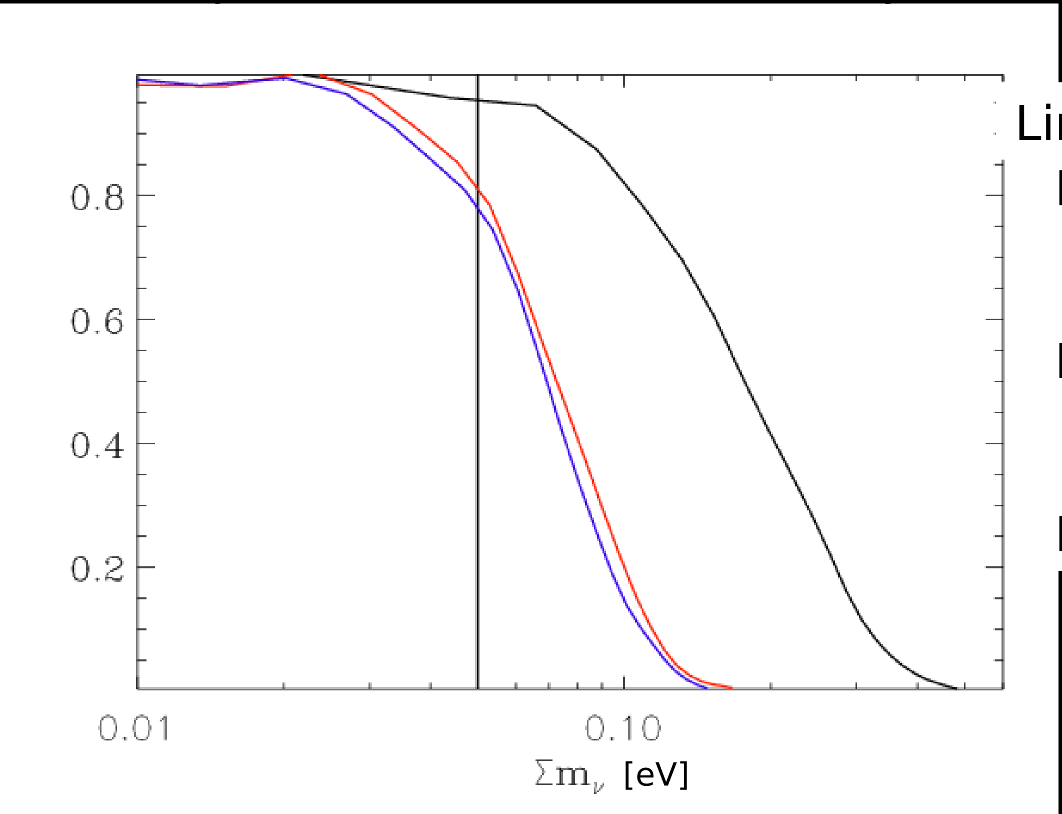

Limits at 95% c.l.:

Black: Planck $\sum m_n < 0.28\ eV$

Red: Planck+1000 bol $\sum m_n < 0.098\ eV$

Blue: Planck+5000 bol $\sum m_n < 0.093\ eV$

- **constraints on neutrino masses (from Pagano & Melchiorri)**

Constraints on Neutrino Masses from CMB + Priors

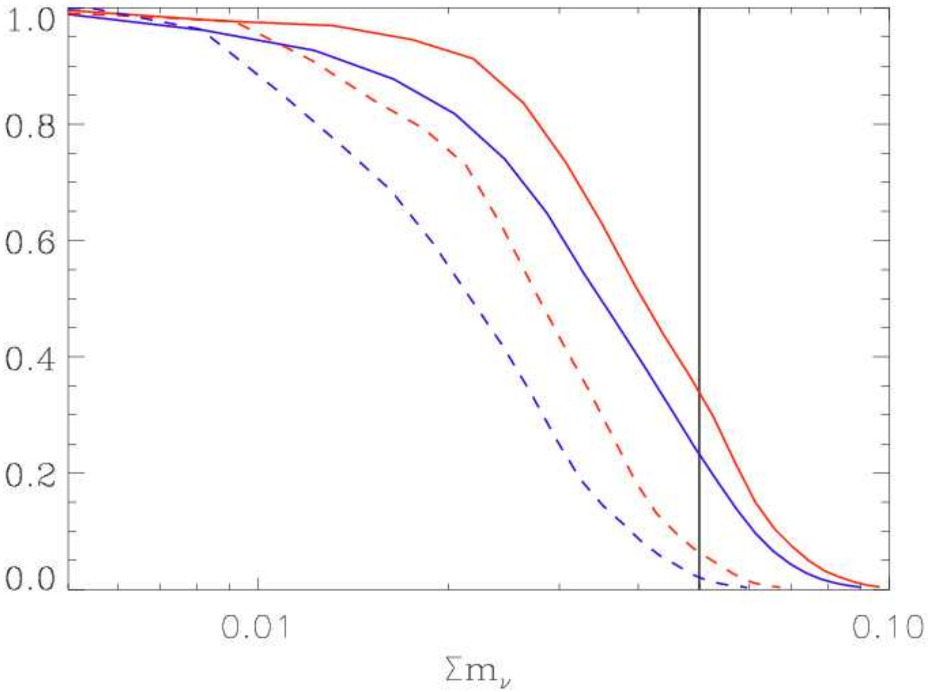

Limits at 95% c.l.:

Red: 1000 riv+
Prior 1% H0+
Priori 2% Ωm

$$\sum m_n < 0.057\ eV$$

Blue: 5000 riv+
Prior 1% H0+
Priori 2% Ωm

$$\sum m_n < 0.054\ eV$$

Red Dashed: 1000 riv+
Prior 0.5% H0+
Priori 1% Ωm

$$\sum m_n < 0.040\ eV$$

Blue Dashed: 5000 riv+
Prior 0.5% H0+
Priori 1% Ωm

$$\sum m_n < 0.035\ eV$$

ith external priors on the Hubble parameter nd the matter density also the Normal ierarchy can be probed: safe detection of neutrino mass.

- **constraints on neutrino masses (from Pagano & Melchiorri)**

Chi crea le strutture ? Inflation !

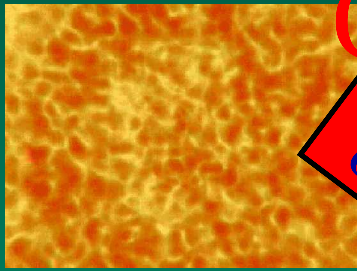

Inflazione Cosmica

Dimensioni subatomiche
$t=10^{-32}$s
Fluttuazioni quantistiche del campo di energia primordiale

Energie tipiche:
10^{16} GeV
(100 milioni di miliardi di milardi di eV)

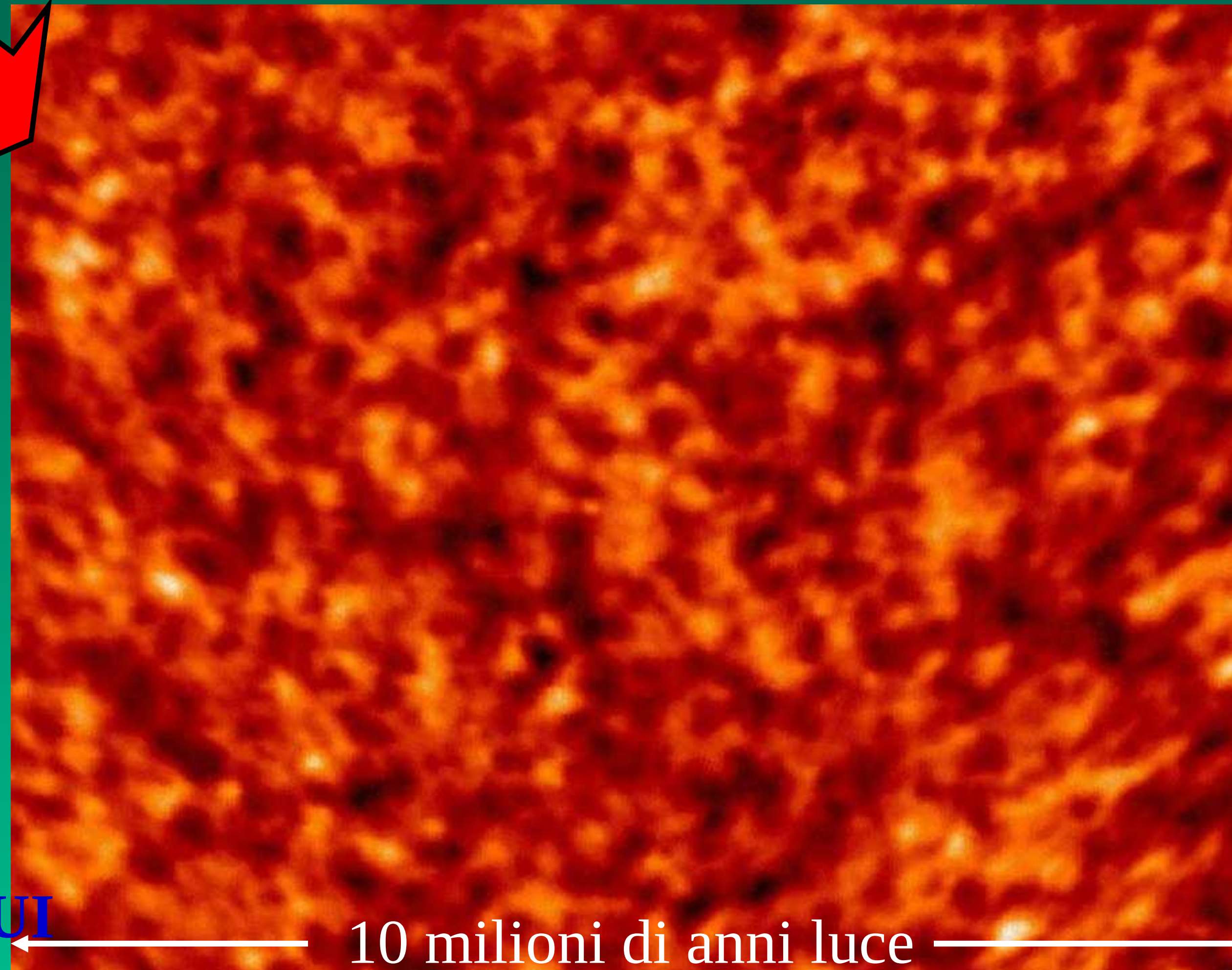

10 milioni di anni luce
t=380000 anni
Fluttuazioni di densita' illuminate dalla luce del fondo cosmico

UNA FINESTRA SUI PRIMI ISTANTI E SULLA FISICA DELLE ALTISSIME ENERGIE

CMB Polarization – Why ?

- An **inflation** phase at **E=10^{16}–10^{15} GeV** (t=10^{-36}-10^{-33} s) is currently the most popular scenario to explain
  - The origin of our universe
  - The geometry of our universe
  - The origin and morphology of structures in our universe
  - The lack of defects, and the smoothness of the CMB at super-horizon scales.
- Inflation is a **predictive** theory:
  - Any initial curvature is flattened by the huge expansion: we expect an Euclidean universe.
  - Adiabatic, gaussian density perturbations are produced from quantum fluctuations. This is the physical origin for structures in the Universe.
  - The power spectrum of scalar perturbations is approximately scale invariant, $P(k)=Ak^{n-1}$ with n slightly less than 1.
  - Tensor perturbations produce a background of primordial gravitational waves (PGW)
- 1.,2.,3. have been confirmed already by measurements of CMB anisotropy
- 4. can be tested measuring CMB polarization

CMB Polarization – Why ?

- Linear Polarization of CMB photons is induced via Thomson scattering by quadrupole anisotropy at recombination (z=1100, *t* =1.2x10^{13}s).

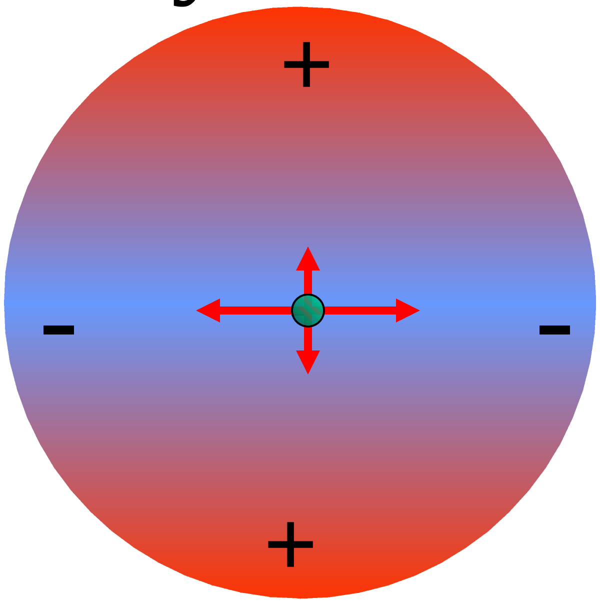

- In turn, quadrupole anisotropy is induced by
  - Density perturbations (*scalar* relics of inflation) producing a curl-free polarization vectors field (**E-modes**)
  - Gravitational waves (*tensor* relics of inflation) producing both curl-free and curl polarization fields (**B-modes**)

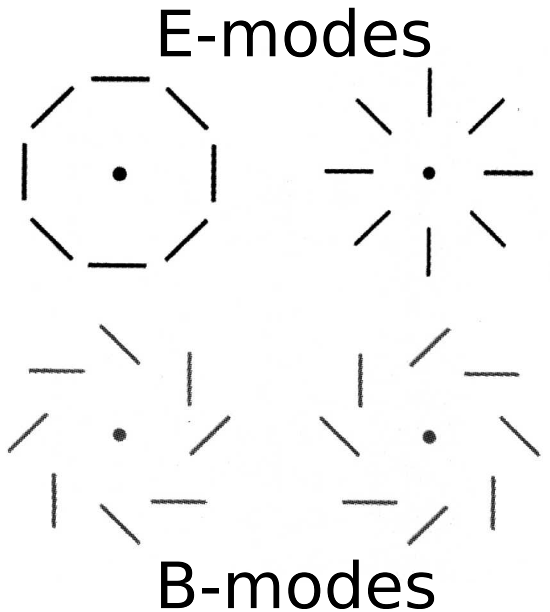

- No other sources for a curl polarization field of the CMB at large angular scales:
- **B-modes are a clear signature of inflation**.

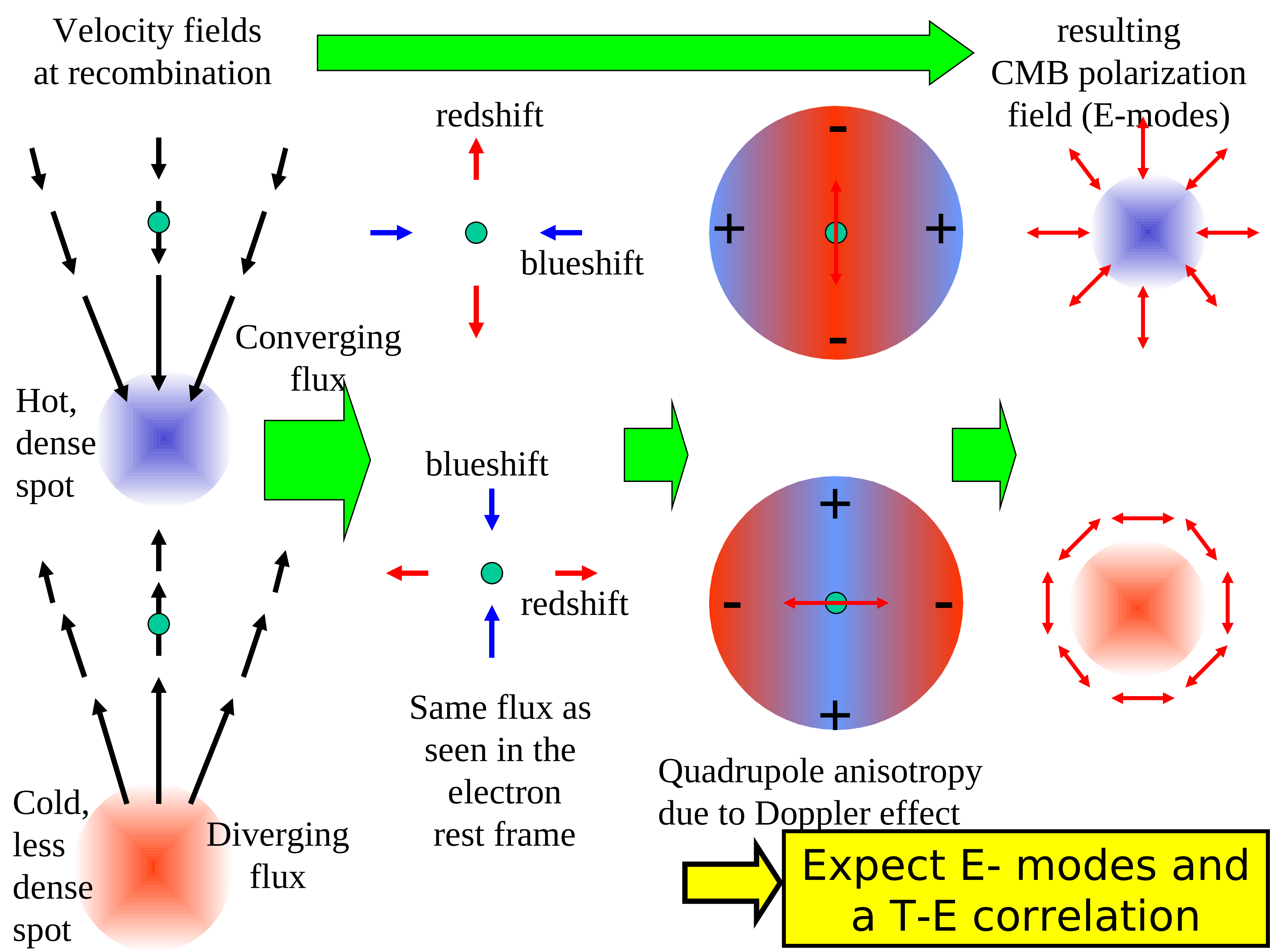

Velocity fields
at recombination
resulting
CMB polarization
field (E-modes)
redshift
blueshift
Converging
flux
Hot,
dense
spot
blueshift
redshift
Cold,
less
dense
spot
Diverging
flux
Same flux as
seen in the
electron
rest frame
Quadrupole anisotropy
due to Doppler effect
Expect E- modes and
a T-E correlation

E-modes & B-modes

Spin-2 quantity Spin-2 basis

$$(Q \pm iU)(n) = \sum_{\ell,m} \left(a_{\ell m}^{E} \pm i a_{\ell m}^{B} \right) {}_{\pm 2}Y_{\ell m}(n)$$

- From the measurements of the Stokes Parameters $\boldsymbol{Q}$ and $\boldsymbol{U}$ of the linear polarization field we can recover both irrotational and rotational a_{lm} by means of modified Legendre transforms:

E-modes produced by scalar and tensor perturbations

$$a_{\ell m}^{E} = \frac{1}{2} \int d\Omega W(\vec{n}) \left[(Q + iU)(\vec{n})\, {}_{+2}Y_{\ell m}(\vec{n}) + (Q - iU)(\vec{n})\, {}_{-2}Y_{\ell m}(\vec{n}) \right]$$

B-modes produced **only** by tensor perturbations

$$a_{\ell m}^{B} = \frac{1}{2i} \int d\Omega W(\vec{n}) \left[(Q + iU)(\vec{n})\, {}_{+2}Y_{\ell m}(\vec{n}) - (Q - iU)(\vec{n})\, {}_{-2}Y_{\ell m}(\vec{n}) \right]$$

B-modes from P.G.W.

- The amplitude of this effect is very small, but depends on the Energy scale of inflation. In fact the amplitude of tensor modes normalized to the scalar ones is:

$$R = \left(\frac{T}{S}\right)^{1/4} \equiv \left(\frac{C_2^{GW}}{C_2^{Scalar}}\right)^{1/4} \cong \frac{V^{1/4}}{3.7\times 10^{16}\,\mathrm{GeV}}$$

Inflation potential

- and

$$\sqrt{\frac{\ell(\ell+1)}{2\pi}c^B_{\ell\max}} \cong 0.1\mu K\left[\frac{V^{1/4}}{2\times 10^{16}\,\mathrm{GeV}}\right]$$

- There are theoretical arguments to expect that the energy scale of inflation is close to the scale of GUT i.e. around 10^{16} GeV.
- The measurement of B-modes is a good way to investigate fundamental physics at extremely high energies.

The signal is extremely weak

- The current upper limit on anisotropy at large scales gives R<0.5 (at 2σ)
- A competing effect is lensing of E-modes, which is important at large multipoles.
- Nobody really knows how to detect this.
  - Pathfinder experiments are needed
- Whatever smart, ambitious experiment we design to detect the B-modes:
  - It needs to be extremely sensitive
  - It needs an extremely careful control of systematic effects
  - It needs careful control of foregrounds
  - It will need independent experiments with orthogonal systematic effects.
- A lot has been done, but there is still a long way to go: ...

E-modes : 3 μK (2002…)

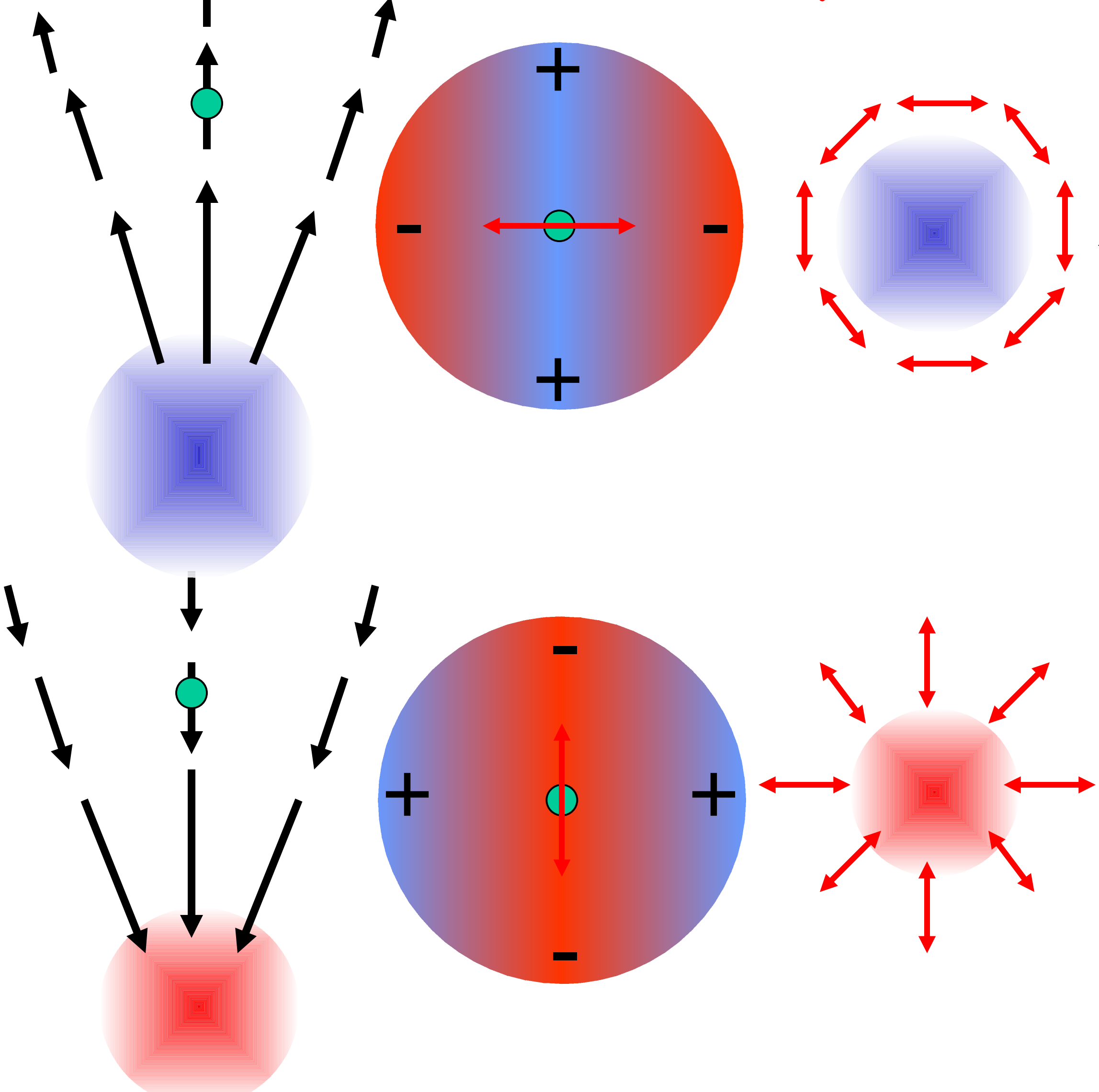

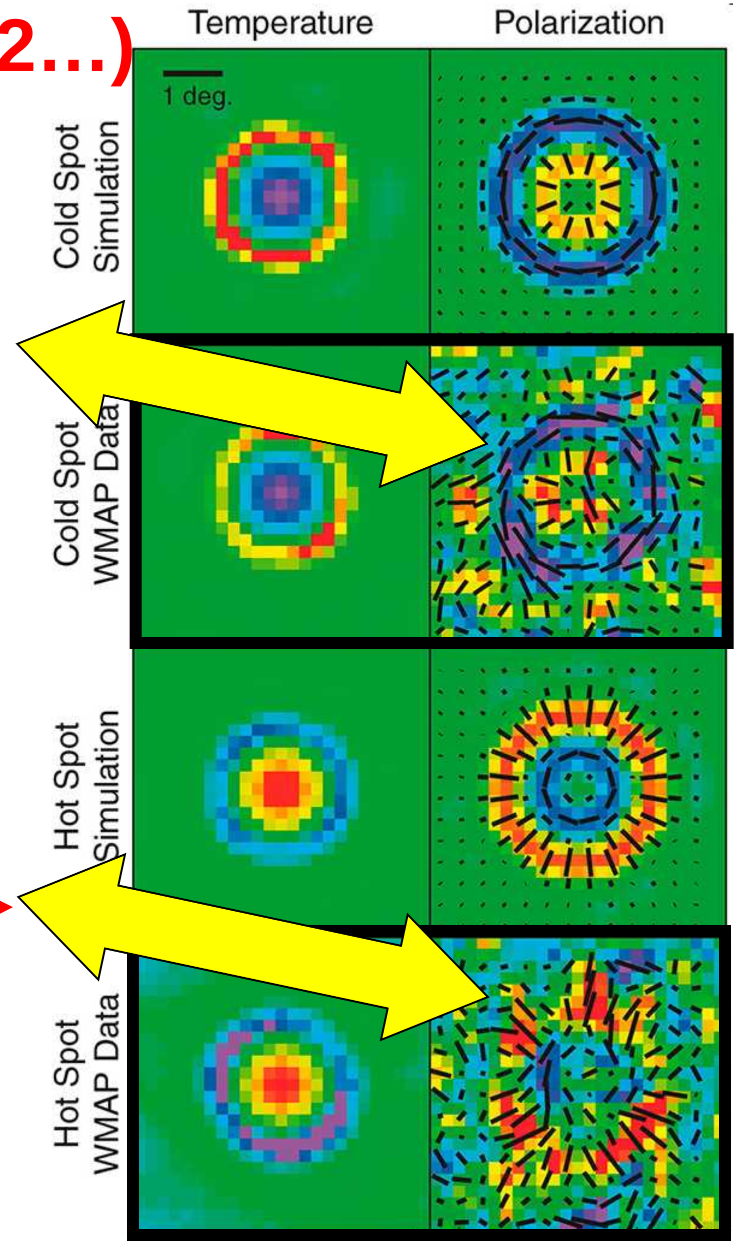

Velocity field near density fluctuation

Resulting anisotropy seen by e-

Resulting polarization pattern

Komatsu et al. 2010 – astro-ph/1001.4538

WMAP7 measured data (stacked)

Chiang et al. 2010

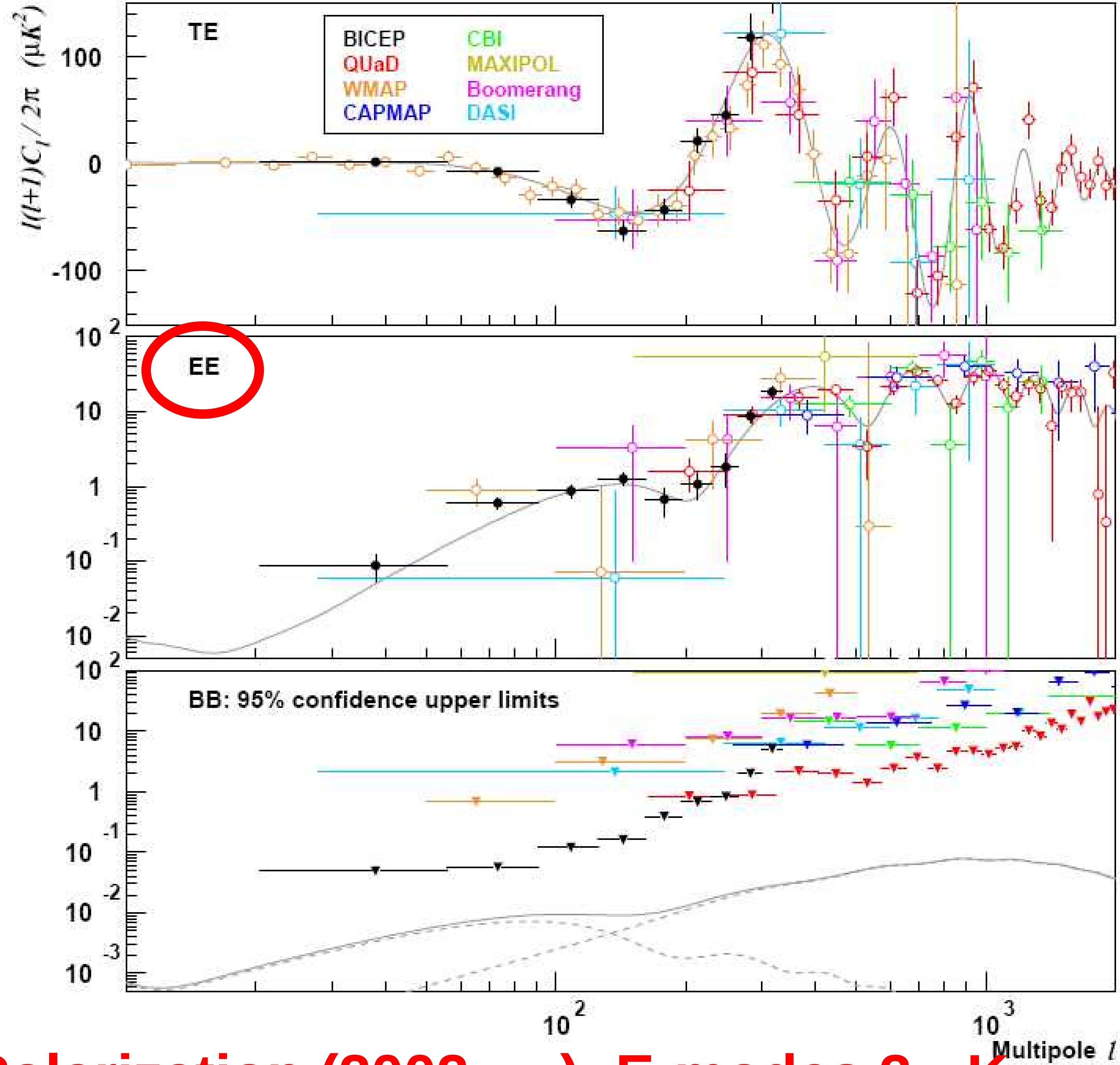

CMB Polarization (2002 …): E-modes 3 μK

Chiang et al. 2010

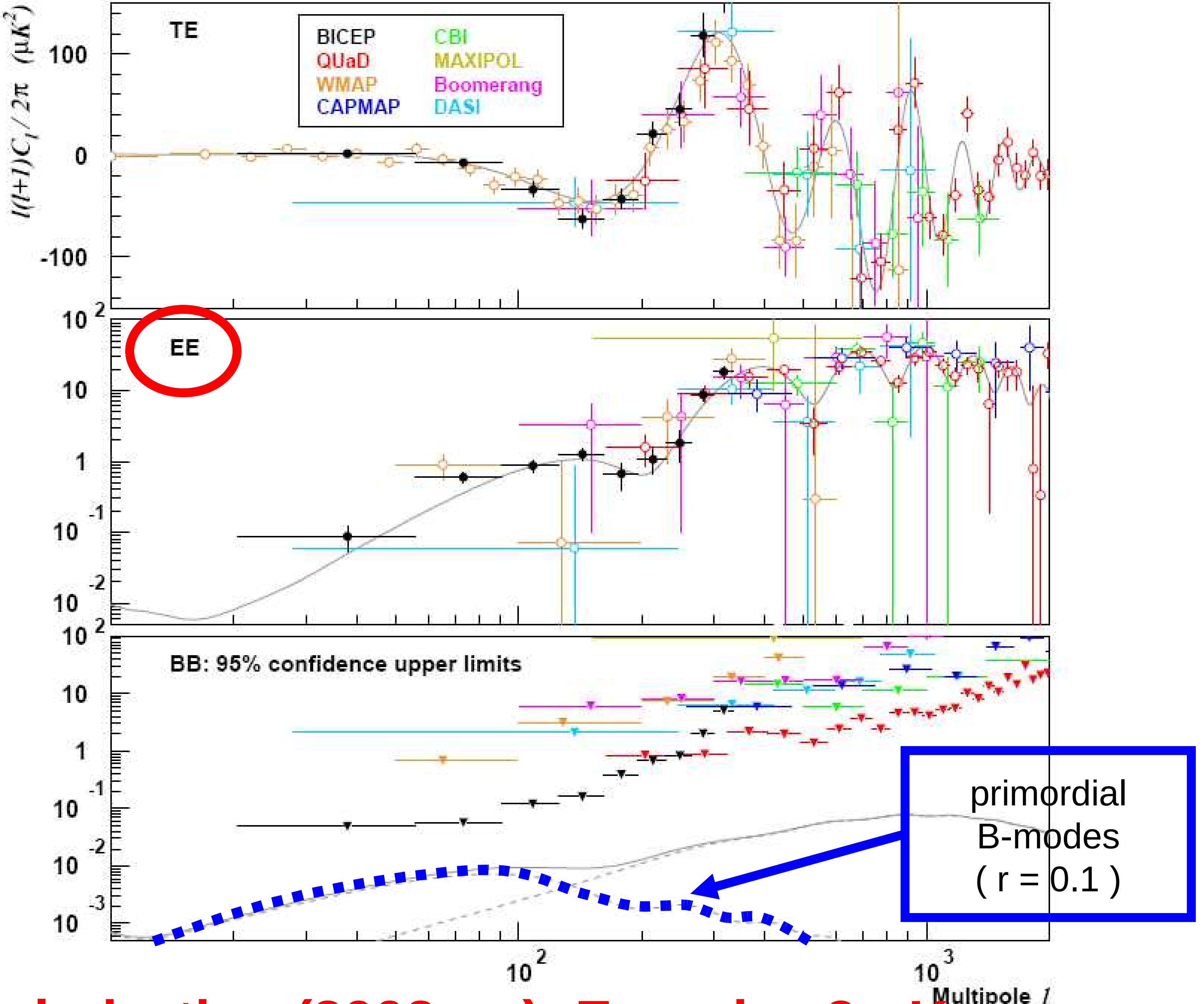

CMB Polarization (2002 …): E-modes 3 μK

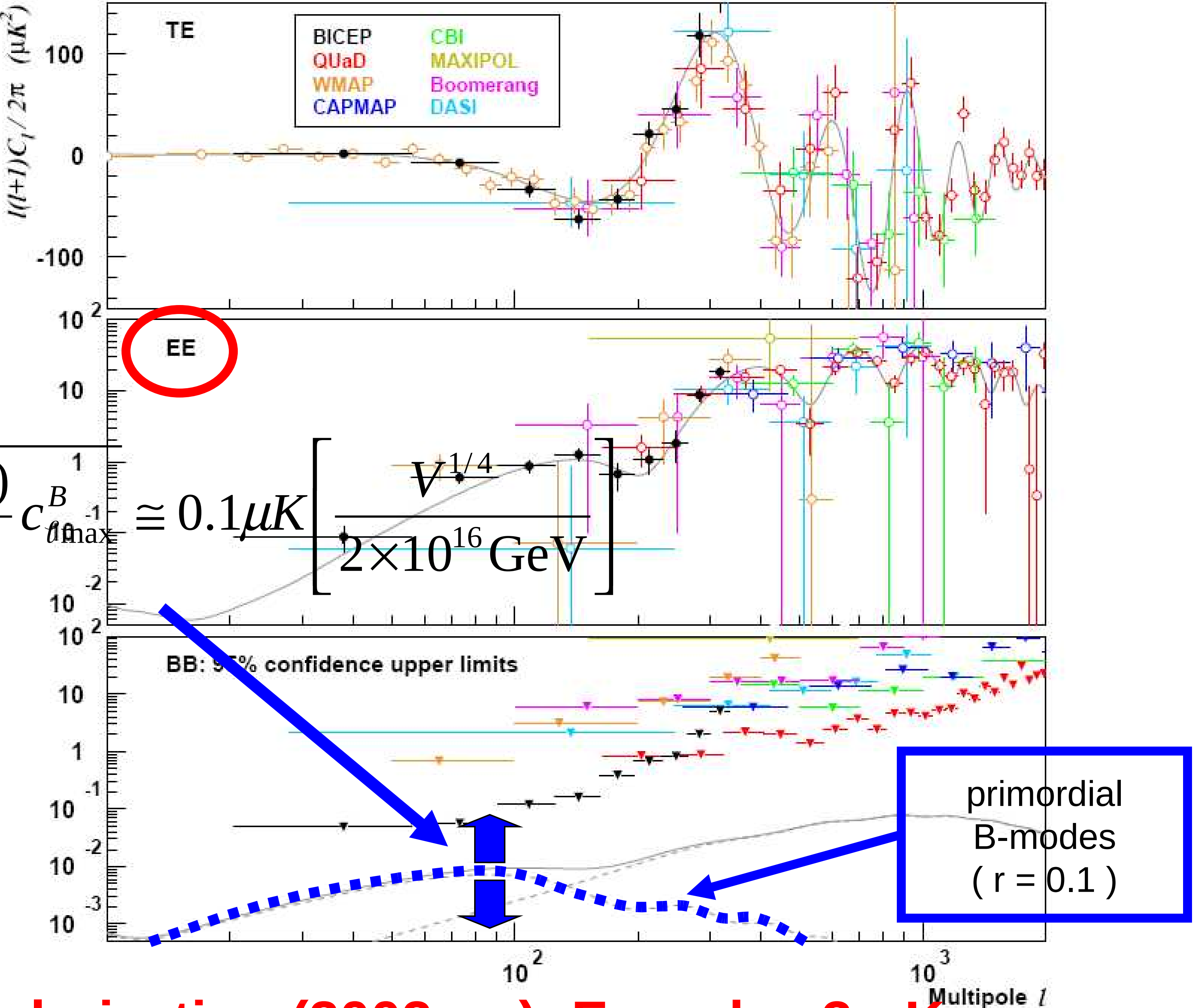

Chiang et al. 2010

$$\sqrt{\frac{\ell(\ell+1)}{2\pi}\,c^{B}_{\ell\,\max}} \cong 0.1\mu K\left[\frac{V^{1/4}}{2\times10^{16}\,\mathrm{GeV}}\right]$$

CMB Polarization (2002 …): E-modes 3 μK

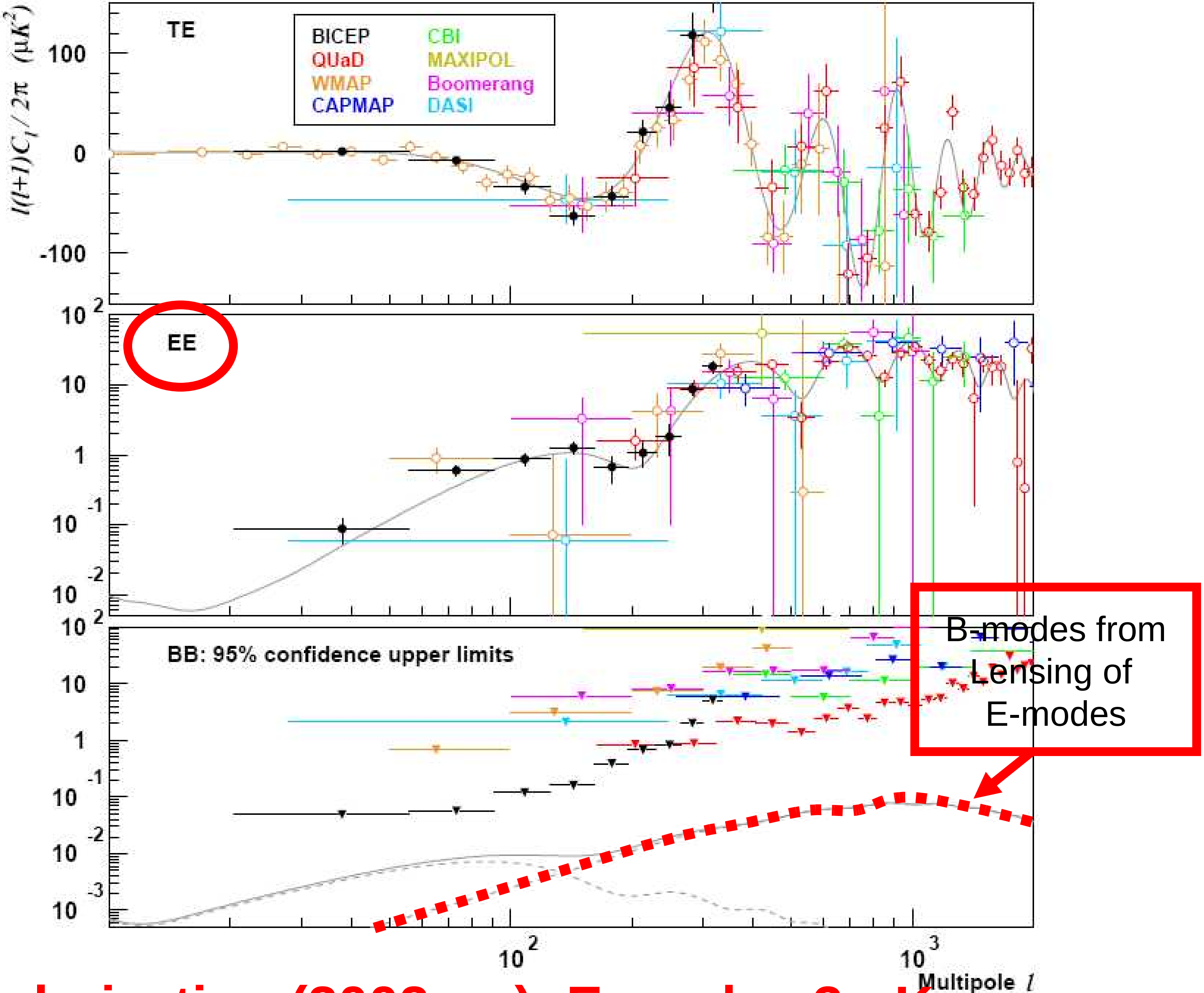

Chiang et al. 2010

CMB Polarization (2002 …): E-modes 3 μK

Lensing of E-modes

- E-modes have been measured already with good accuracy, and will be measured with exquisite accuracy by Planck and other experiments.
- They depend on the distribution of mass (mainly dark matter) so their study can shed light on the nature of dark matter (including massive neutrinos).
- While the primordial B-mode is maximum at multipoles around 100 (θ=2°), the lensed B-mode is maximum at multipoles around 1000 (θ=0.2°), requiring high angular resolution polarization experiments

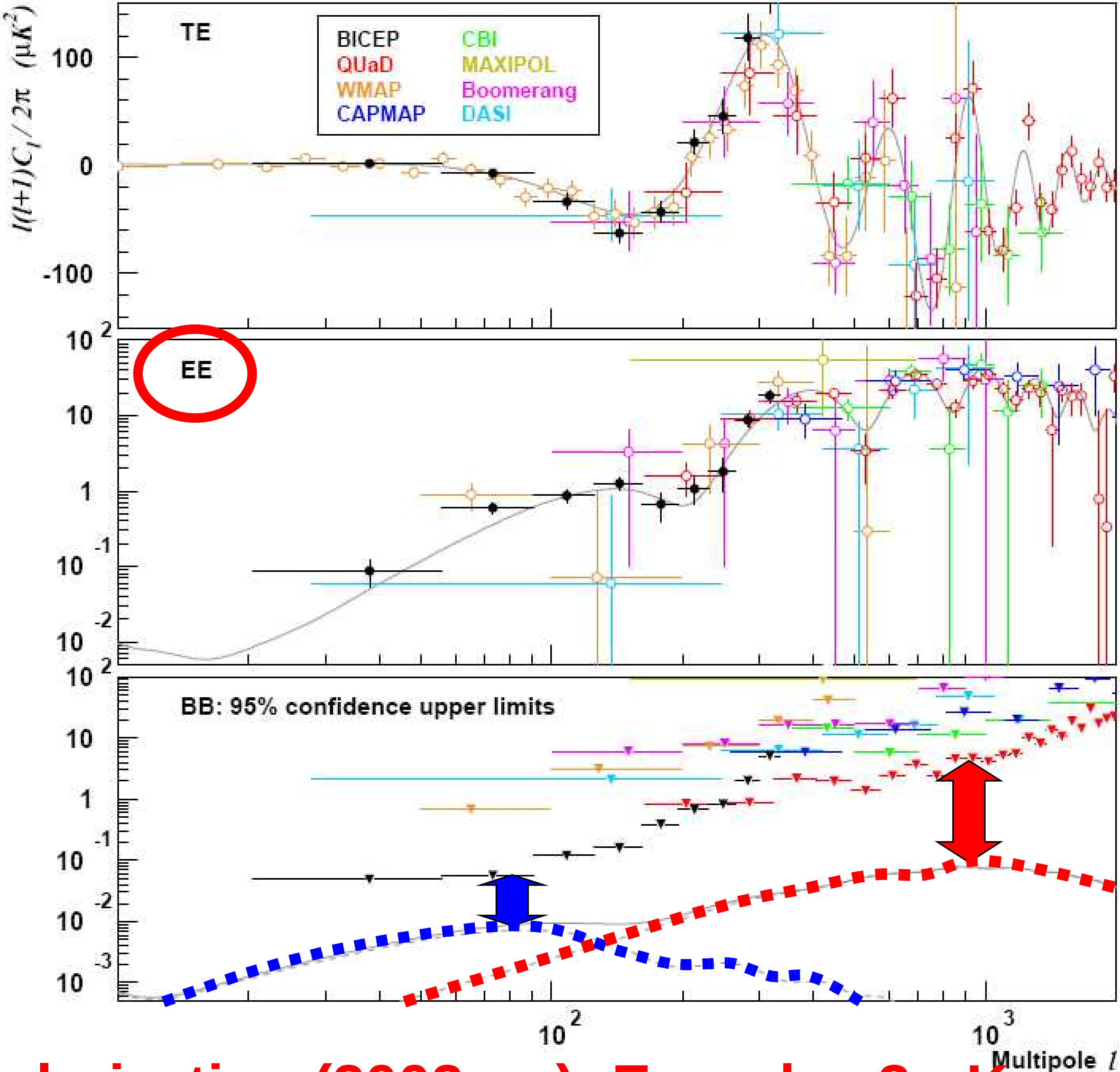

Chiang et al. 2010

CMB Polarization (2002 …): E-modes 3 μK

How to improve ?

1. Knowledge of Foregrounds
   (Planck)

- Sensitivity
- Control of Systematic Effects

1. Knowledge of the foregrounds

- WMAP results: Page et al. 2006.
- Main message: primordial B-modes are extremely difficult to detect, because Galactic contamination is higher than E-modes **at these wavelengths and in the average high-latitude sky.**

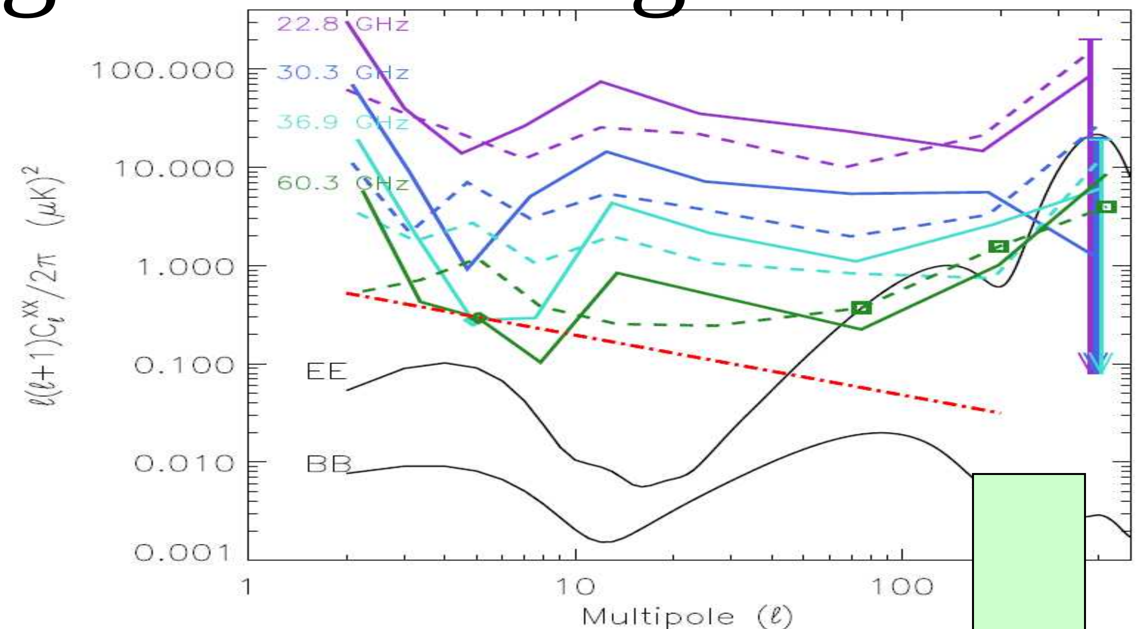

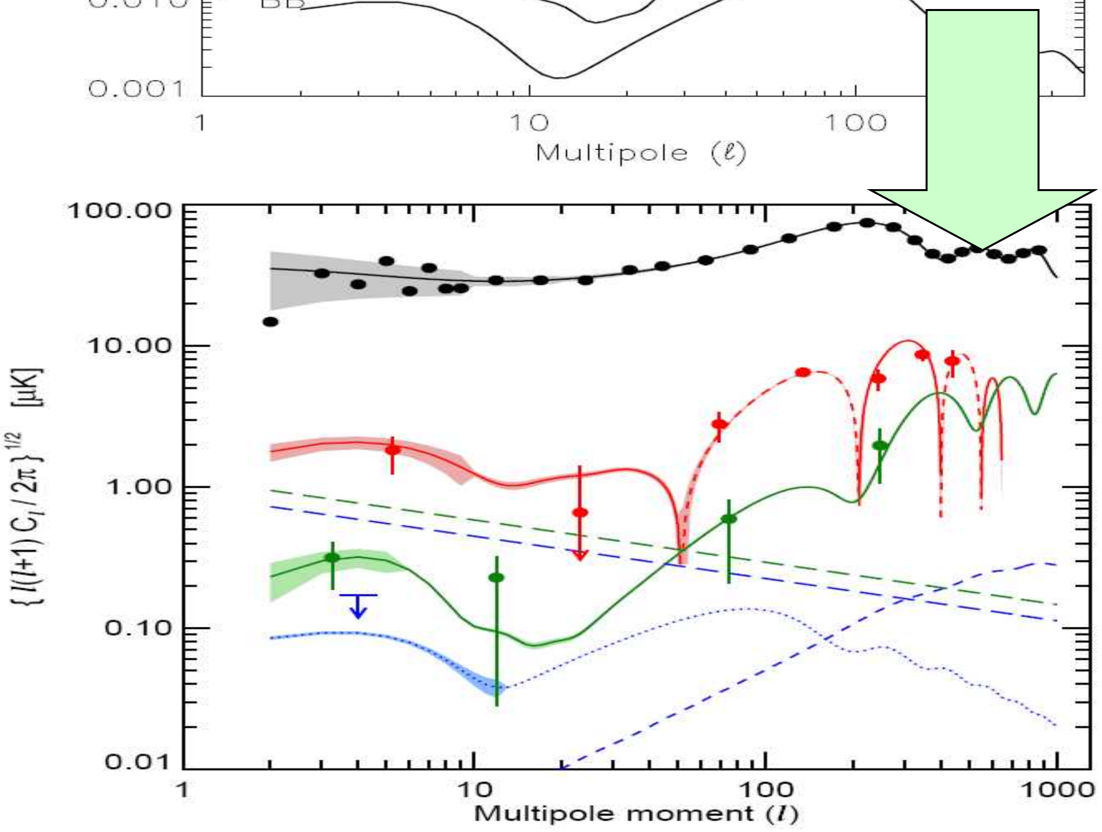

Sweet spots (anisotropy)

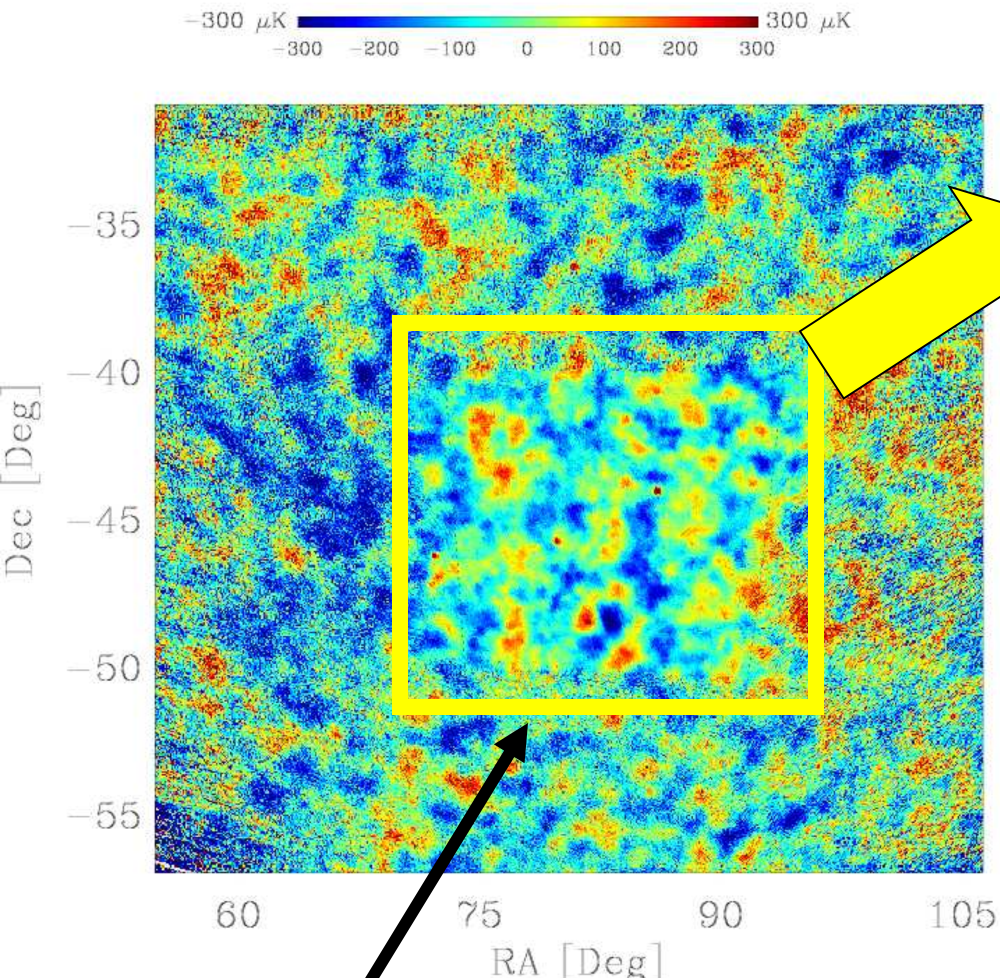

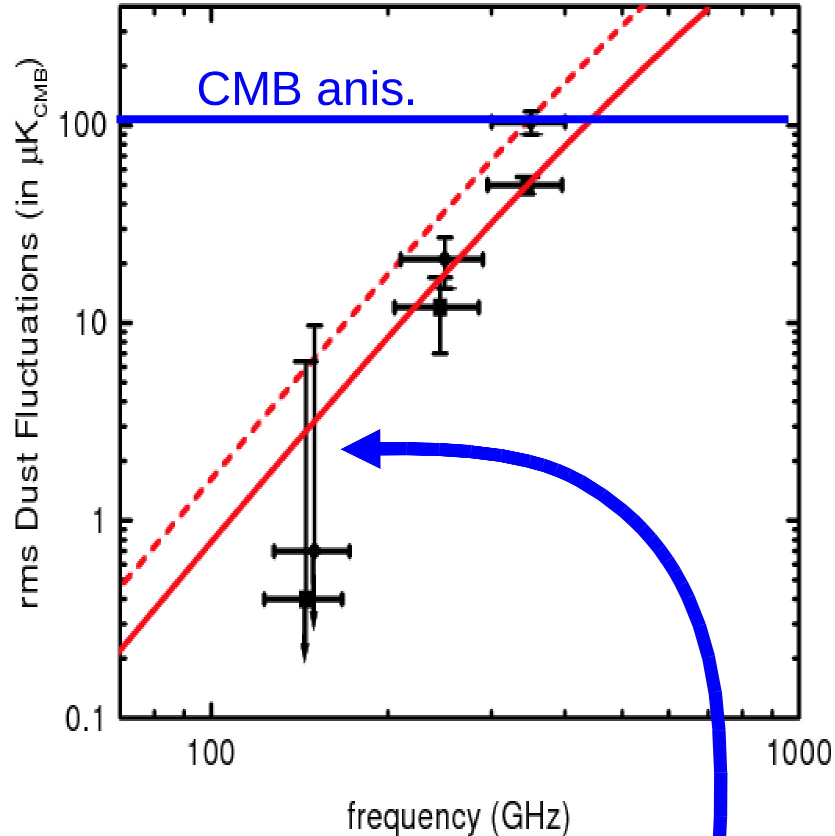

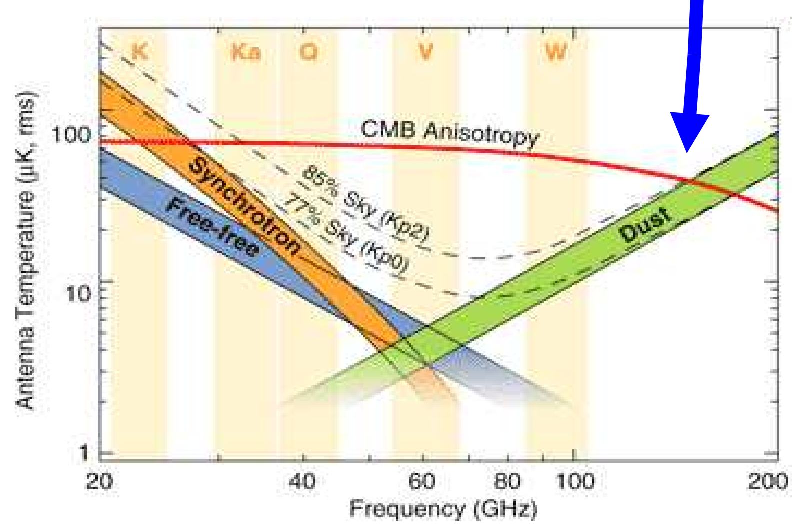

BOOMERanG deep region (Masi et al. 2006):
dust anisotropy << CMB anisotropy @ 150 GHz

Chiang et al. 2010

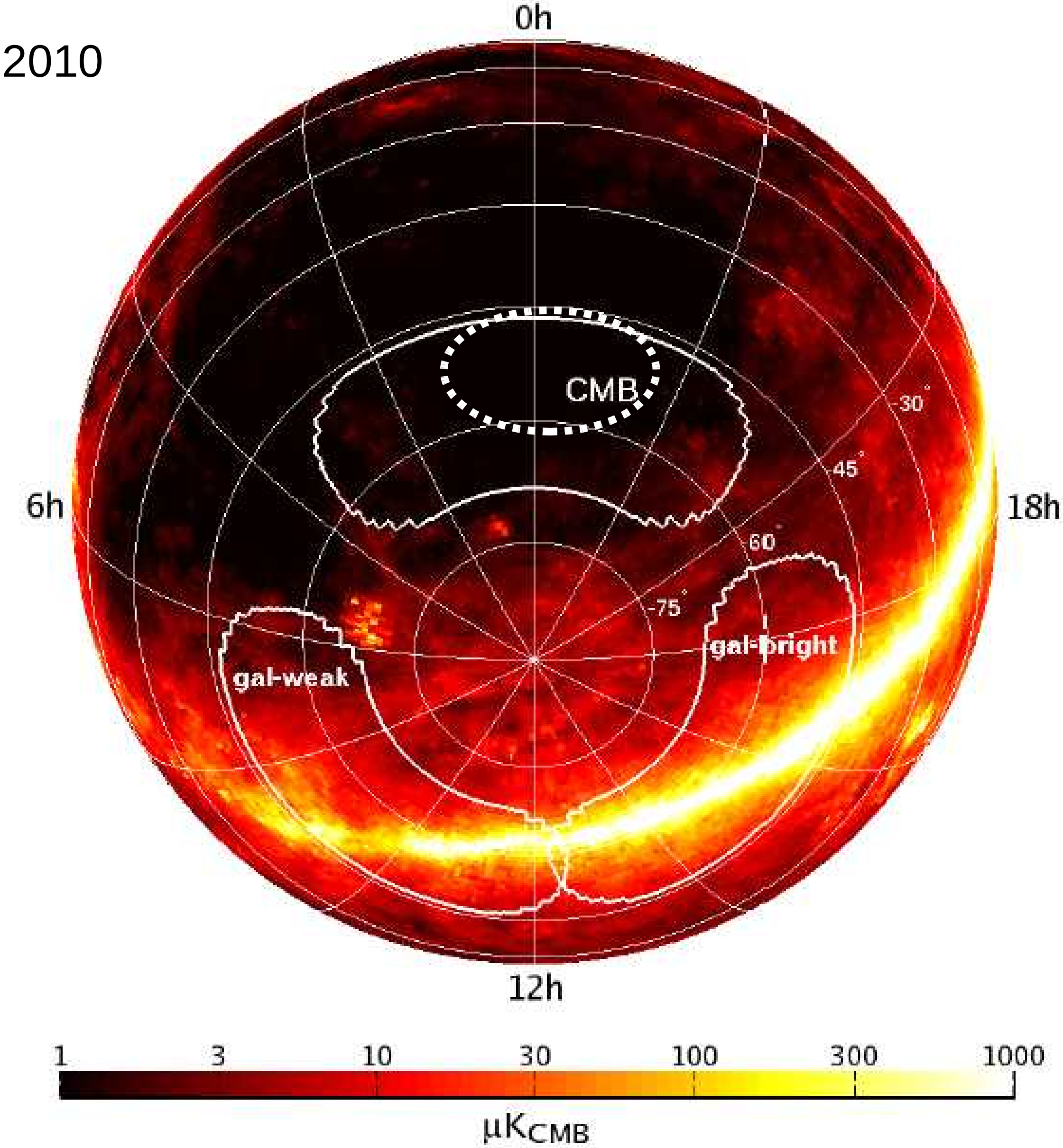

FIG. 1.— BICEP's CMB and Galactic fields are outlined on the 150-GHz FDS Model 8 prediction of dust emission (Finkbeiner et al. 1999), plotted here in equatorial coordinates.

Chiang et al. 2010
BICEP

Sweet Spots

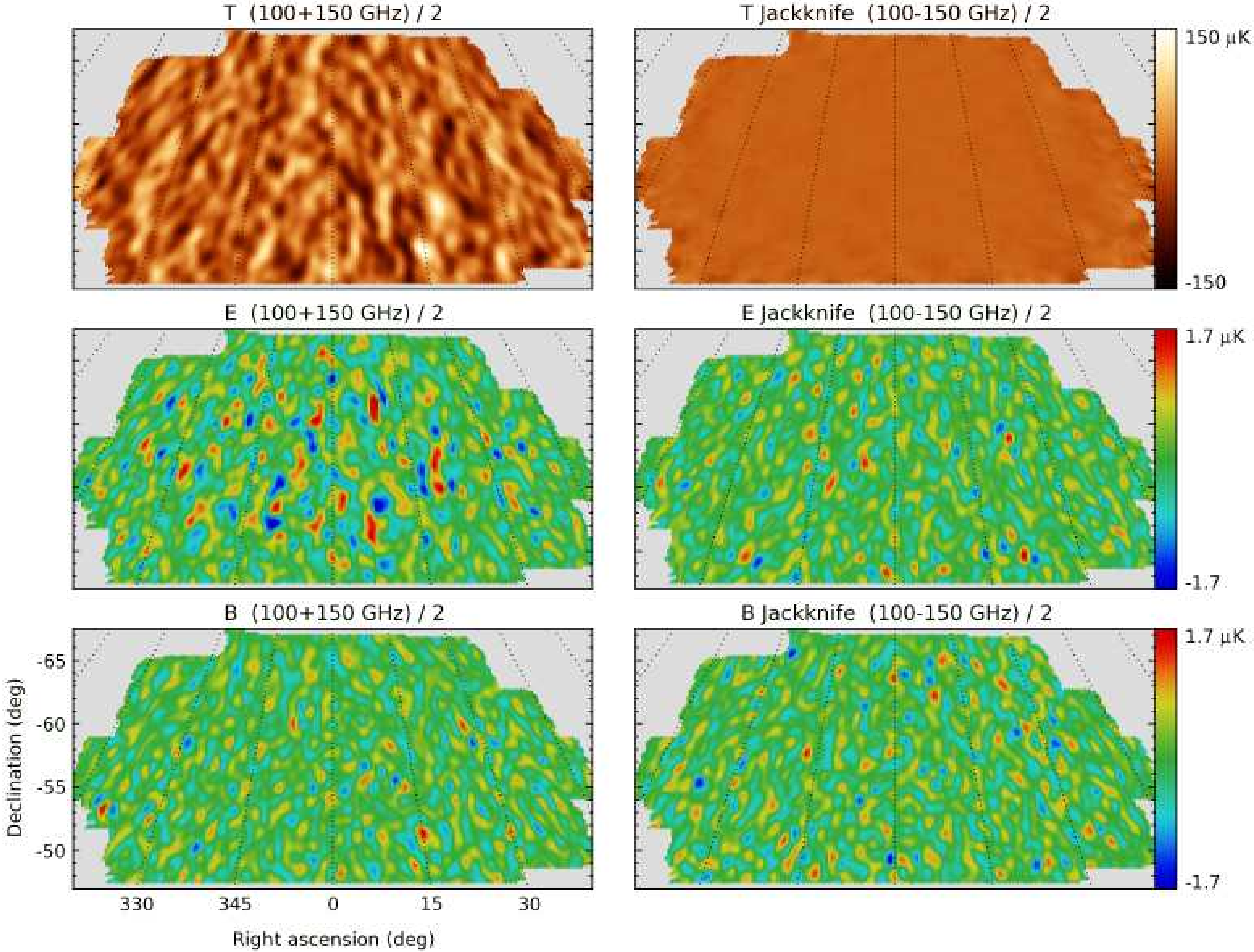

1. Knowledge of the foregrounds

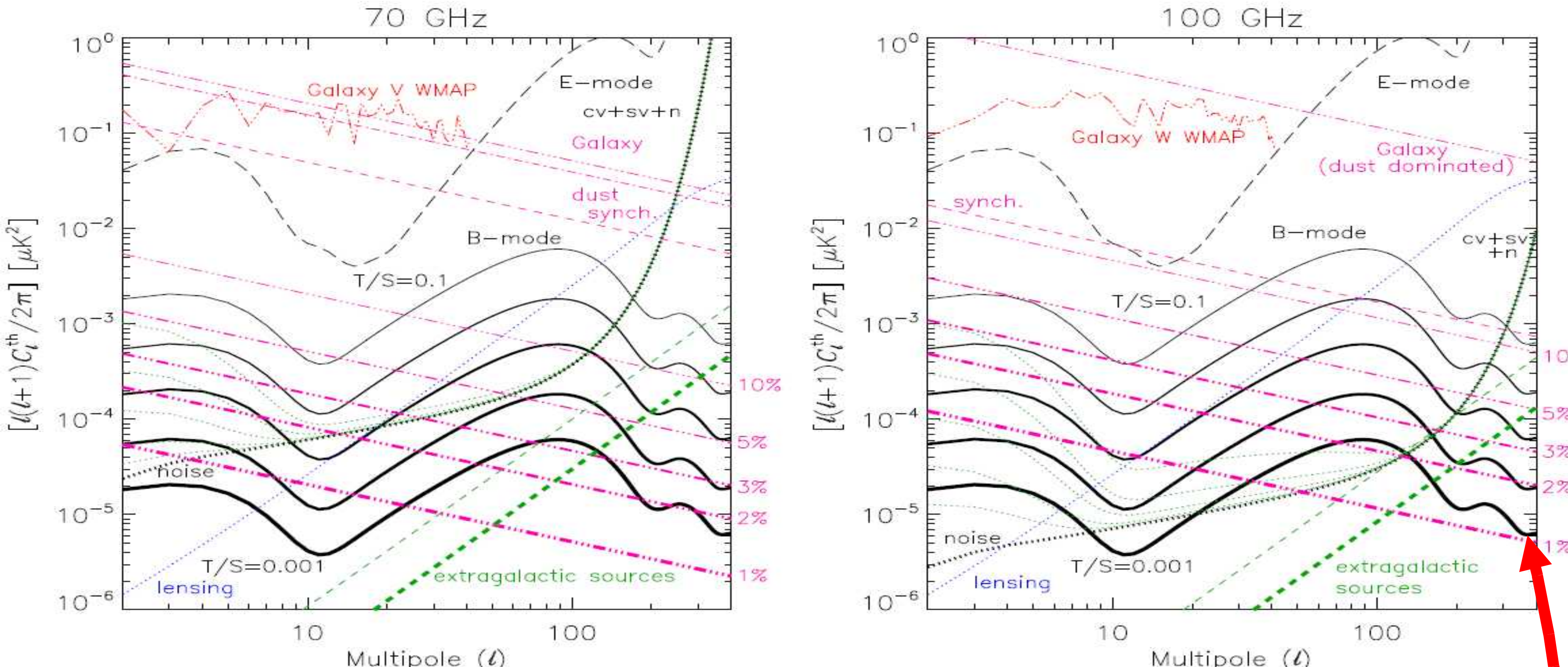

- This is the most difficult part of the path towards B-modes.
  - We need wide multiband observations
  - We need a detailed (3-D) model of galactic emission, able to predict the local polarized signal with <1% accuracy

PdB et al., Exp.Astron. 23, 5-16 (2009), astro-ph/0808.1881. www.b-pol.org

Planck is a very ambitious experiment.

It carries a complex CMB experiment (the state of the art, a few years ago) all the way to L2,

improving the sensitivity wrt WMAP by at least a factor 10,

extending the frequency coverage towards high frequencies by a factor about 10

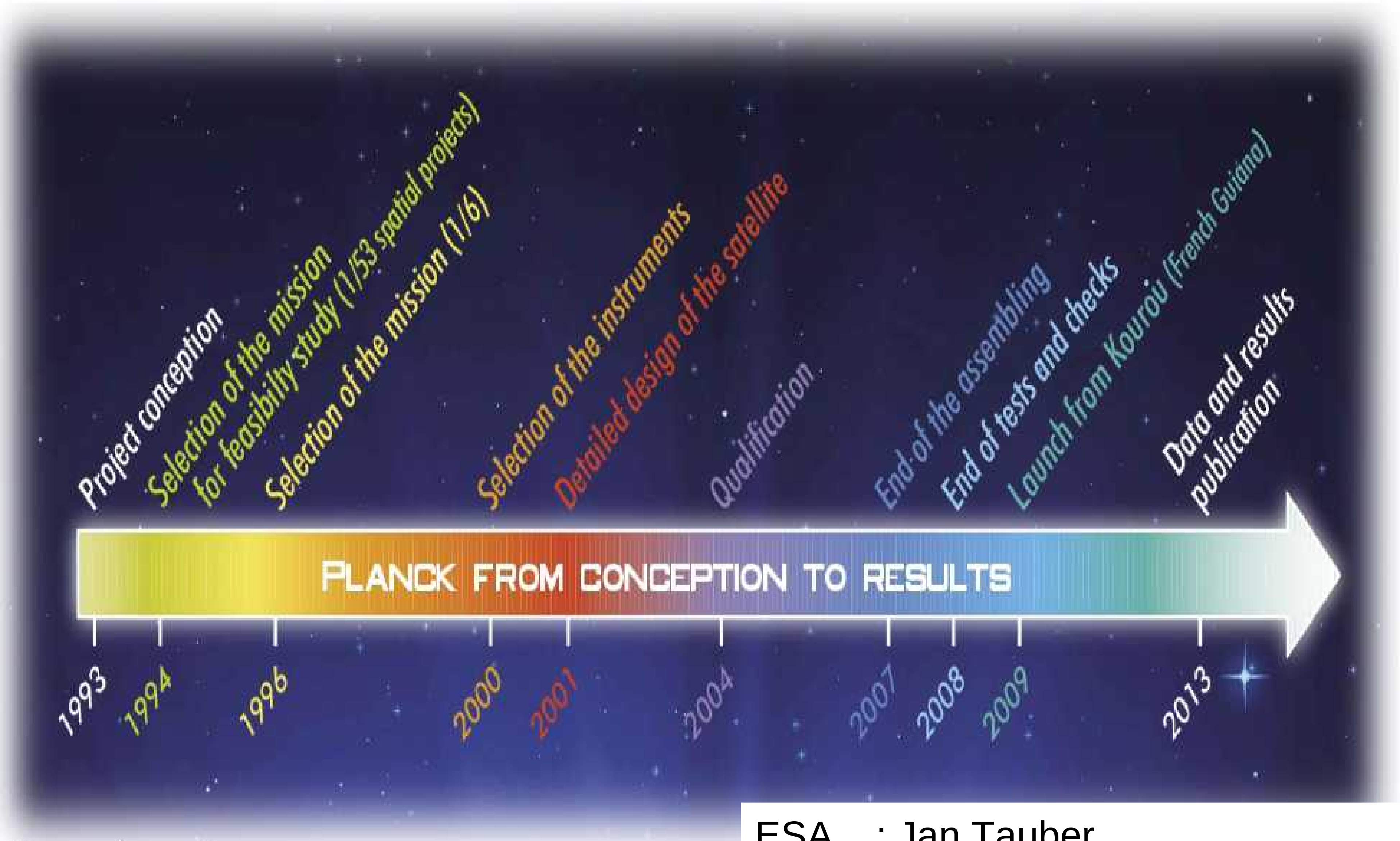

Almost 20 years of hard work of a very large team, coordinated by:

ESA : Jan Tauber
HFI PI : Jean Loup Puget (Paris)
HFI IS : Jean Michel Lamarre (Paris)
LFI PI : Reno Mandolesi (Bologna)
LFI IS : Marco Bersanelli (Milano)

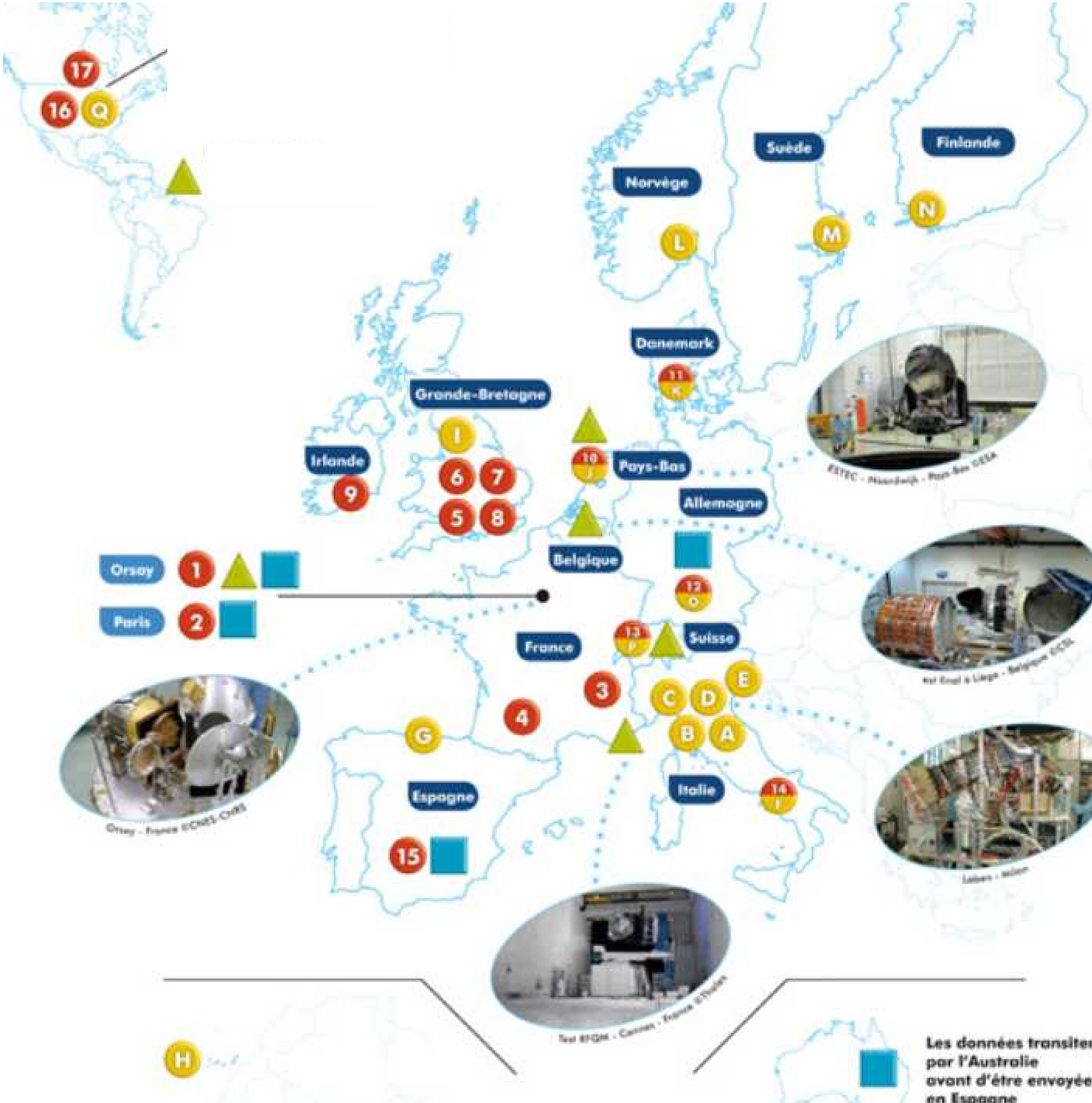

National Agencies

Scientific Laboratories

HFI PI Puget

LFI PI Mandolesi

Satellite

+ subcontractors

Observing strategy

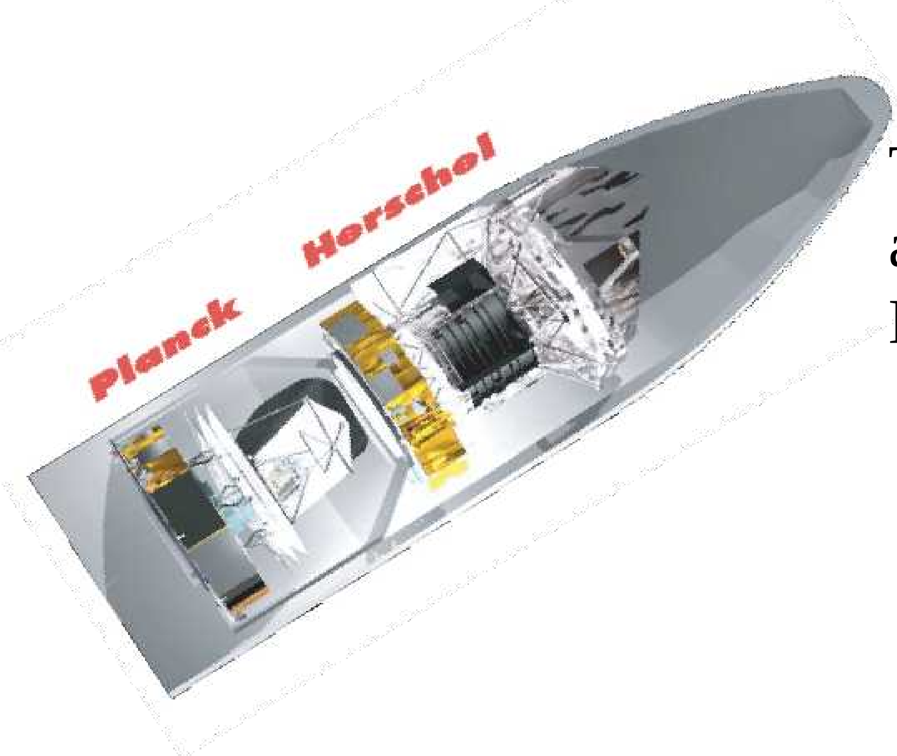

The payload will work from L2, to avoid the emission of the Earth, of the Moon, of the Sun

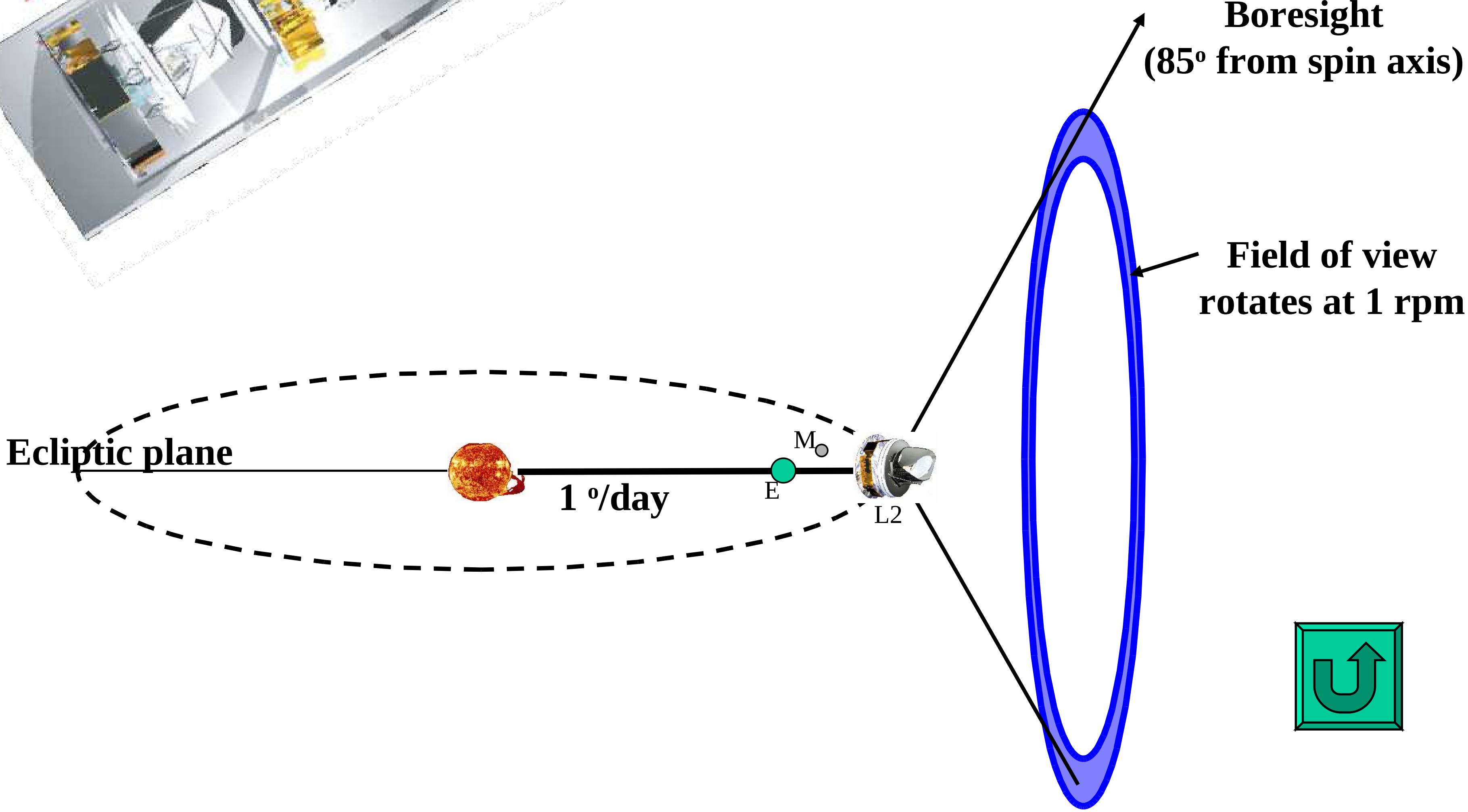

Why so far ?

- Good reasons to go in deep space:
  - Atmosphere
  - Sidelobes
  - Stability

- In the case of CMB observations, the detected brightness is the sum of the brightness from the sky (dominant for the solid angles directed towards the sky, in the main lobe) and the Brightness from ground (dominant for the solid angles directed towards ground, in the sidelobes).

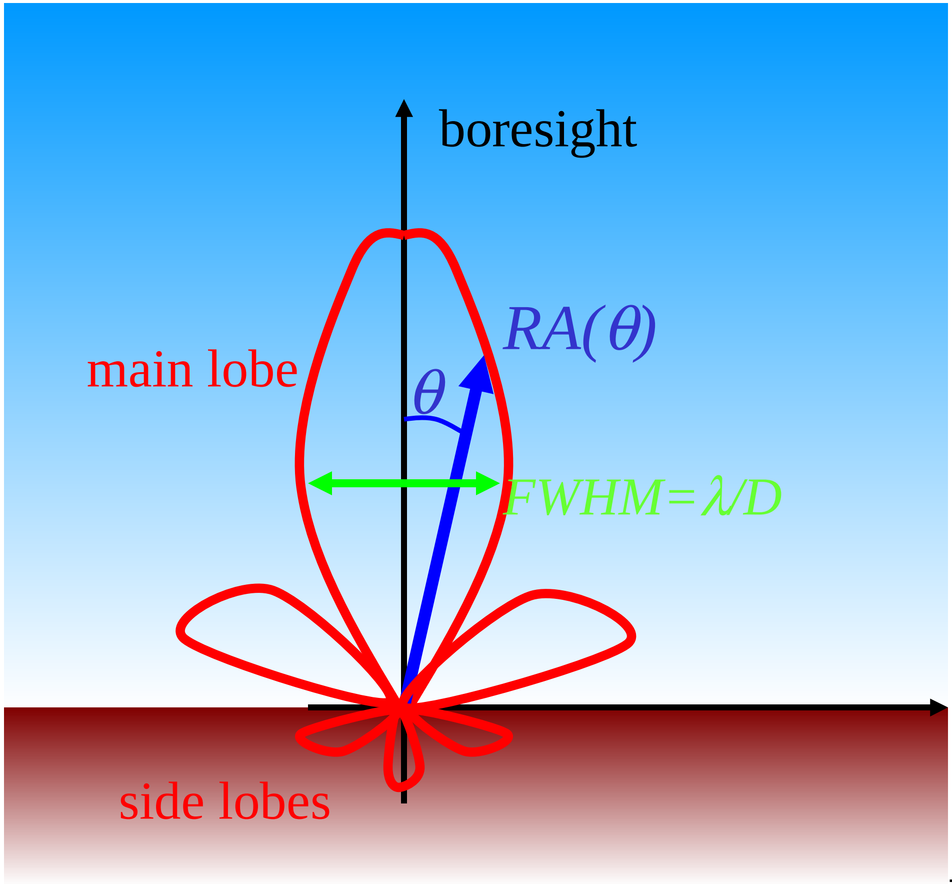

$$W = A\left[\int_{\substack{main\\lobe}} B_{sky}(\theta,\varphi)RA(\theta,\varphi)d\Omega + \int_{\substack{side\\lobes}} B_{Ground}(\theta,\varphi)RA(\theta,\varphi)d\Omega\right]$$

- The angular response (beam pattern) $RA(\theta,\phi)$ is usually polarization-dependent

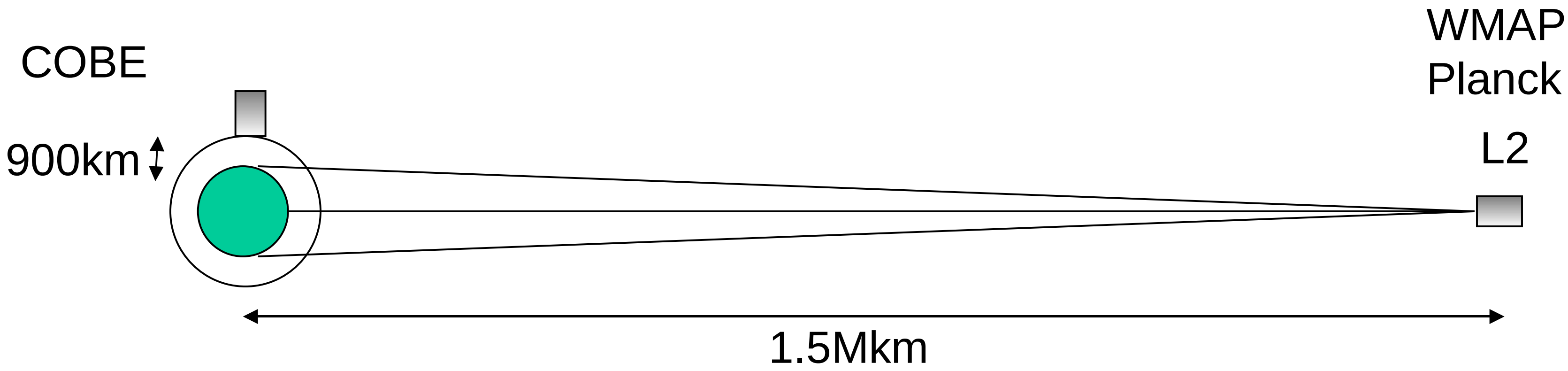

Going to L2 reduces the solid angle occupied by the Earth by a factor $2\pi/2\times10^{-4}$=31000, thus relaxing by the same factor the required off-axis rejection.

FWHM	$\Omega_{mainlobe}$	$<RA_{sidelobes}>$
10^o	2×10^{-2} srad	$<<1$
1^o	2×10^{-4} srad	$<<0.01$
10’	7×10^{-6} srad	$<<3\times10^{-4}$
1’	7×10^{-8} srad	$<<3\times10^{-6}$

No day-night changes up there … extreme stability

PLANCK

ESA's mission to map the Cosmic Microwave Background

Image of the whole sky at wavelengths near the intensity peak of the CMB radiation, with

- high instrument sensitivity ($\Delta T/T \sim 10^{-6}$)
- high resolution (≈5 arcmin)
- wide frequency coverage (25 GHz-950 GHz)
- high control of systematics
- Sensitivity to polarization

Launch: 14/May/2009; payload module: 2 instruments + telescope

- Low Frequency Instrument (LFI, uses HEMTs)
- High Frequency Instrument (HFI, uses bolometers)
- Telescope: primary (1.50x1.89 m ellipsoid)

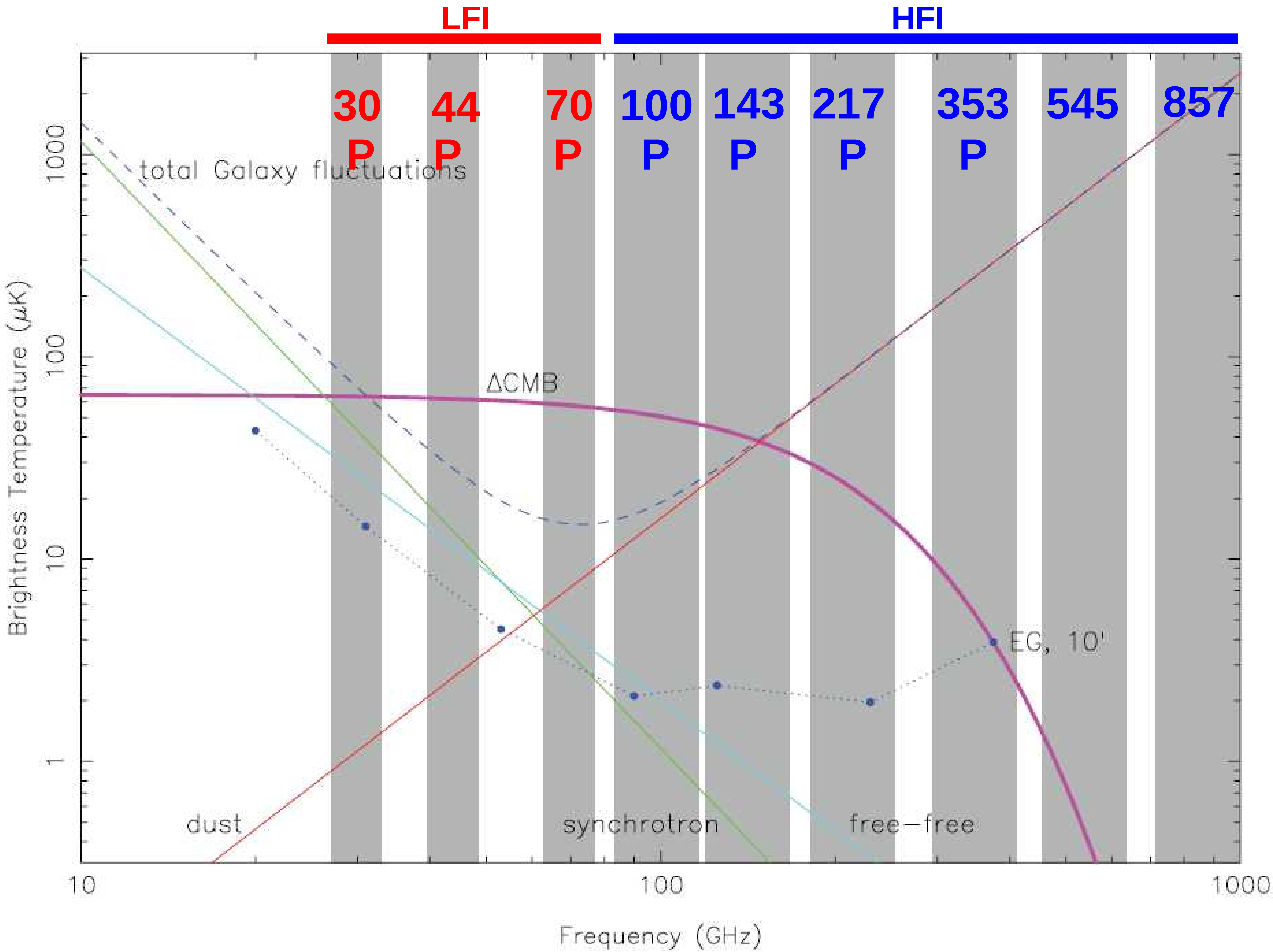

LFI
HFI
30 P
44 P
70 P
100 P
143 P
217 P
353 P
545
857
total Galaxy fluctuations
ΔCMB
EG, 10'
dust
synchrotron
free−free
Brightness Temperature (μK)
Frequency (GHz)
1000
100
10
1
10
100
1000

Planck – HFI polarization sensitive focal plane

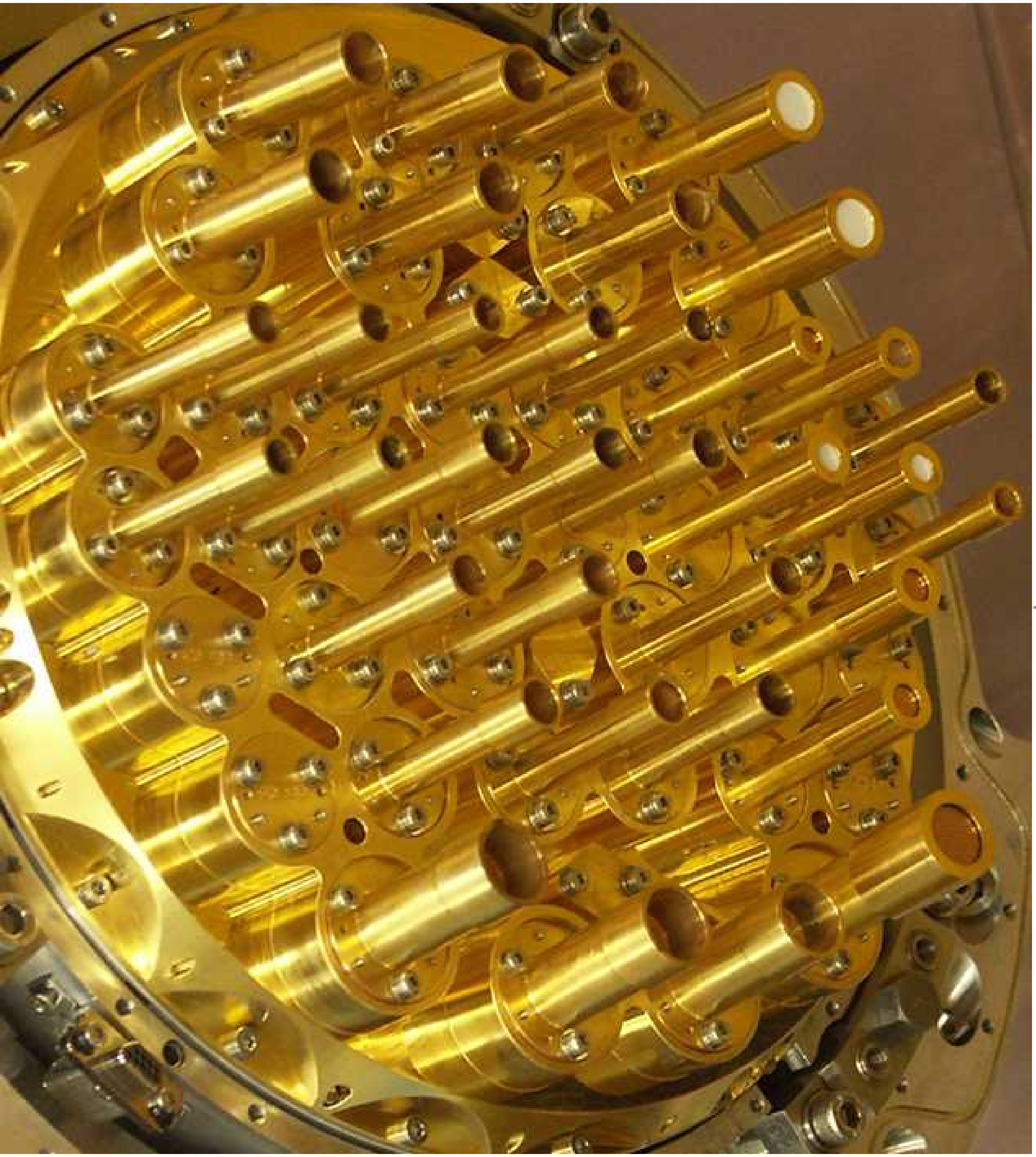

Ponthieu et al. 2010

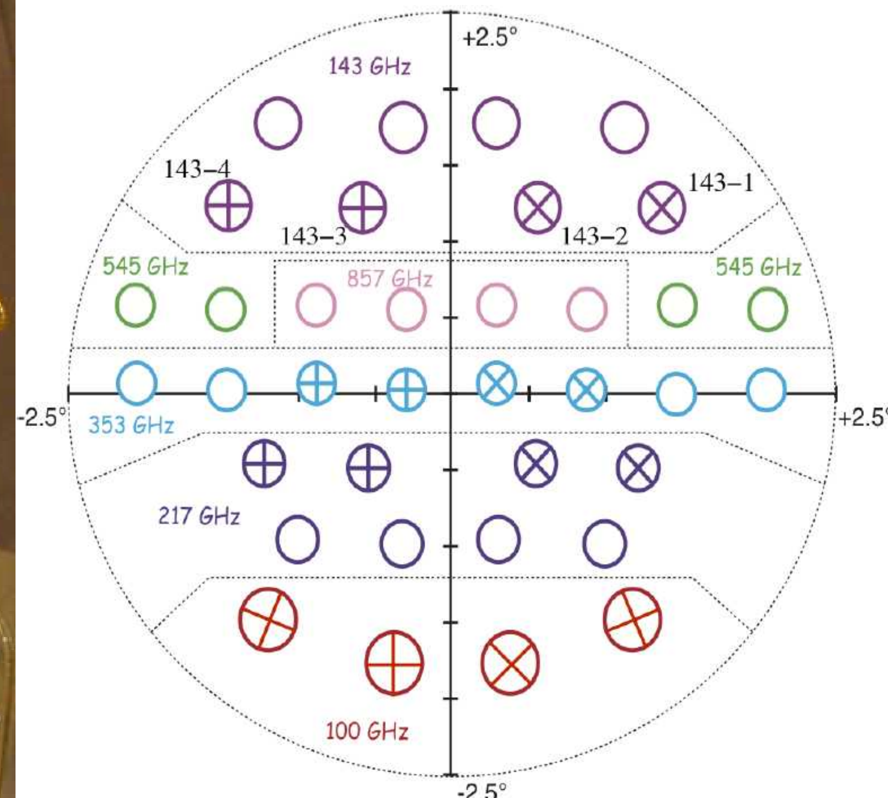

Scan direction

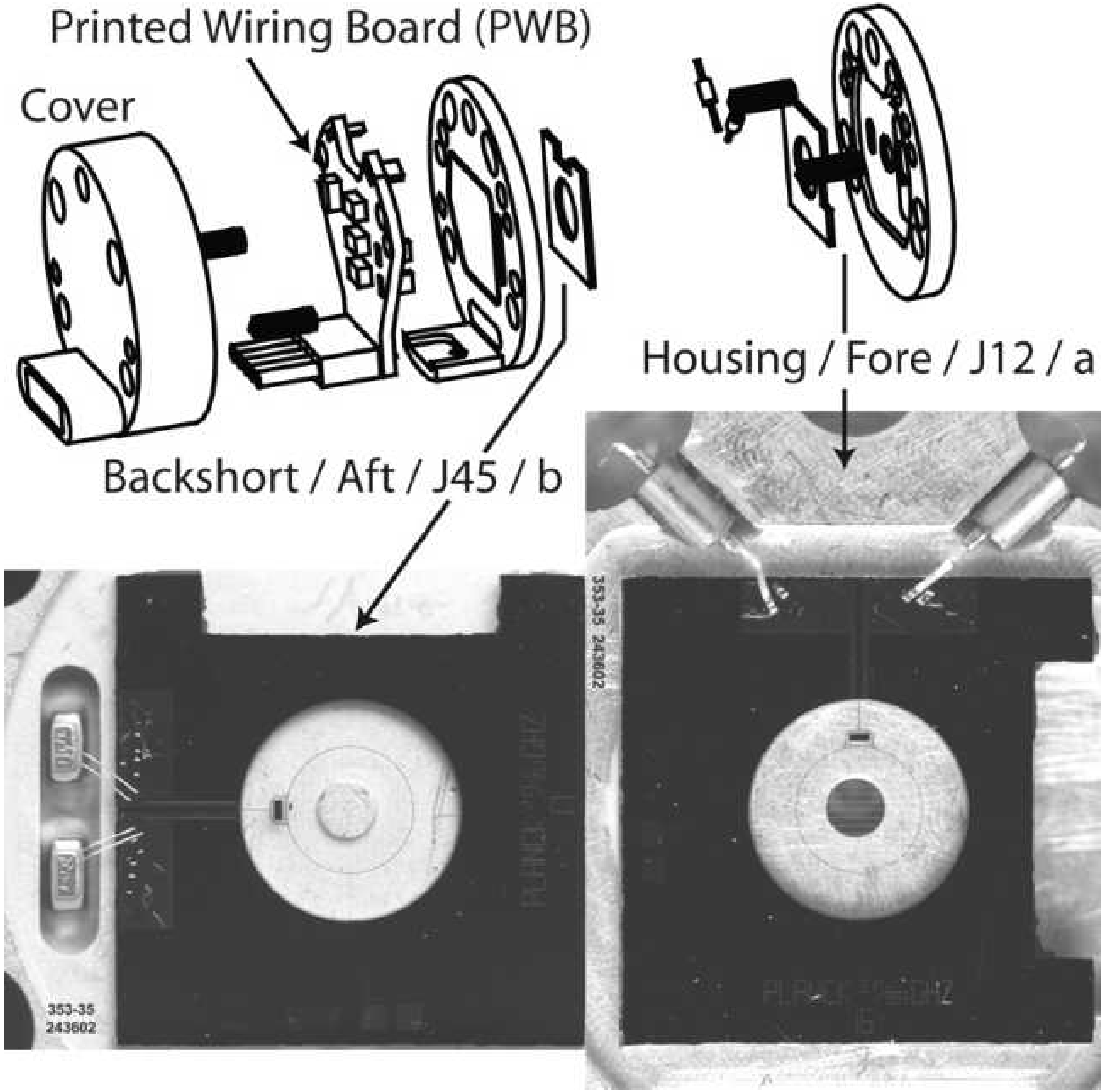
Printed Wiring Board (PWB)
Cover
Housing / Fore / J12 / a
Backshort / Aft / J45 / b
353-35 243602
353-35 243602

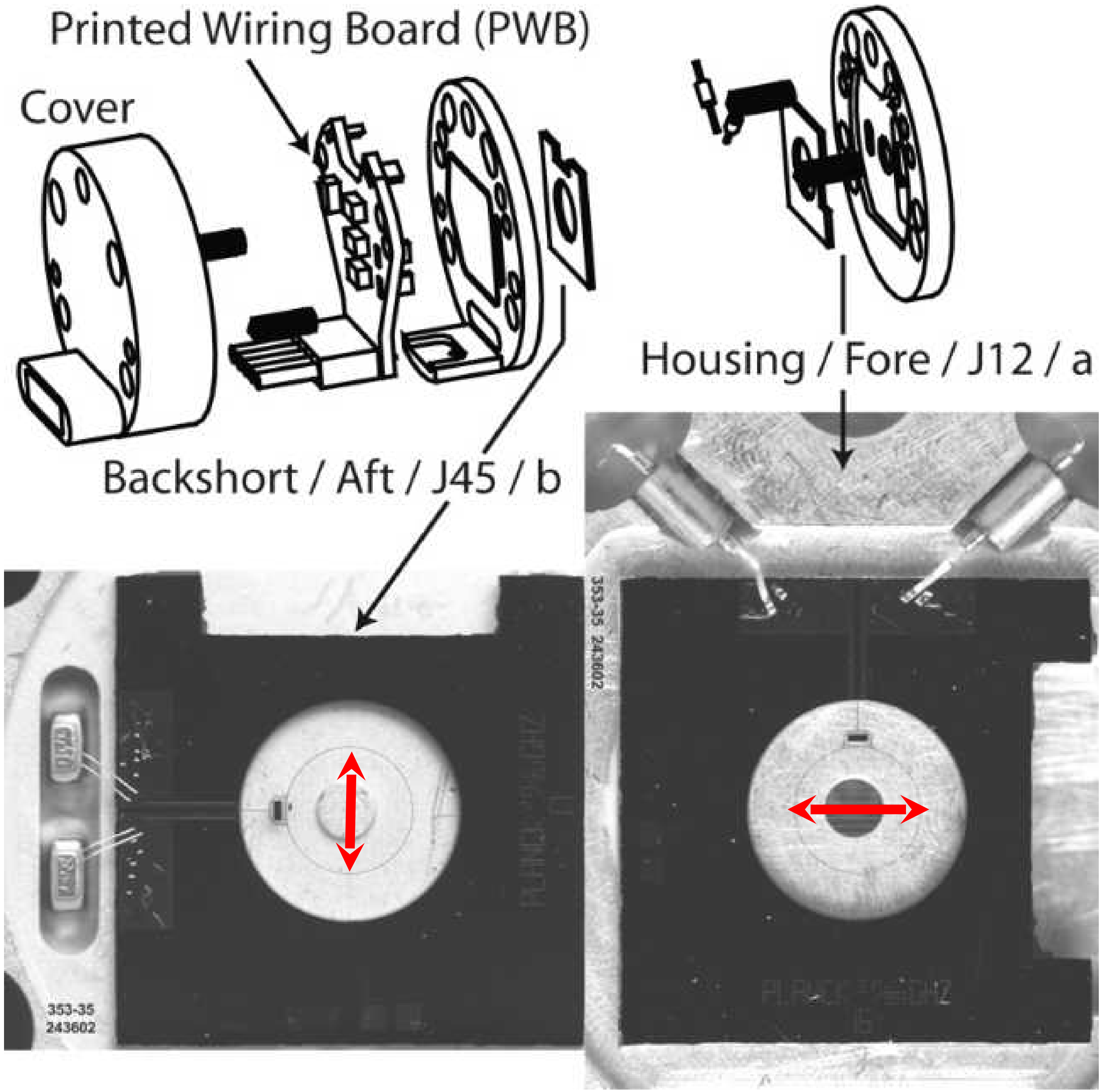

Printed Wiring Board (PWB)
Cover
Housing / Fore / J12 / a
Backshort / Aft / J45 / b
353-35 243602
353-35
243602

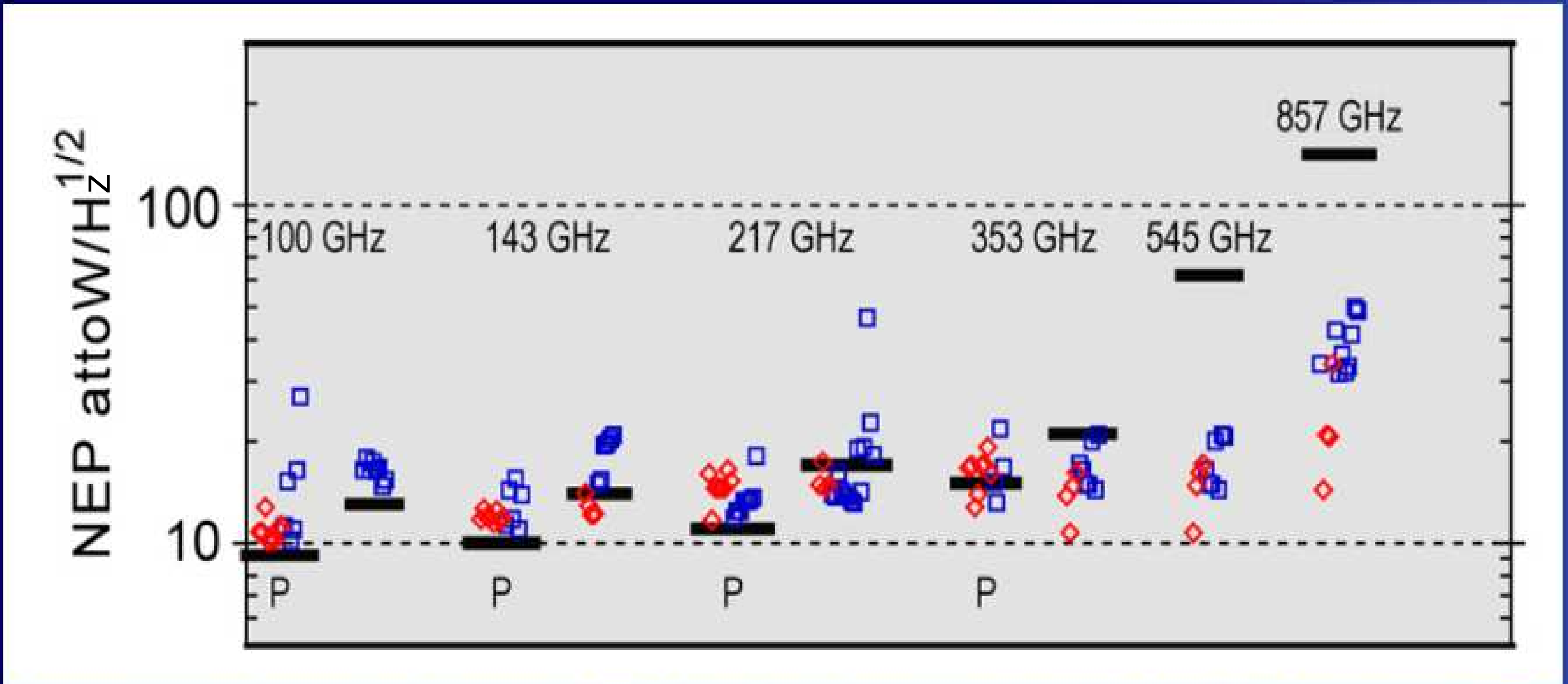

Measured dark noise equivalent power (NEP) of the focal plane detectors, including 6.5 nV / sqrt(Hz) amplifier noise at nominal bias. The open diamond symbols are the NEP for detectors installed in the focal plane. The open square symbols are the NEP of spare bolometers. The thick solid line segments indicate the photon background limit from a 35 K telescope and astrophysical sources in each band for a 30% bandwidth and 30% in band optical efficiency. Unpolarized detectors at 100 GHz were made and delivered but were replaced by polarized detectors. (from Holmes et al. (2008))

NEP_b = 15 aW/Hz$^{1/2}$ -> 70 μK/Hz$^{1/2}$

Total NET (bolo+photon) = 85 μK/Hz$^{1/2}$

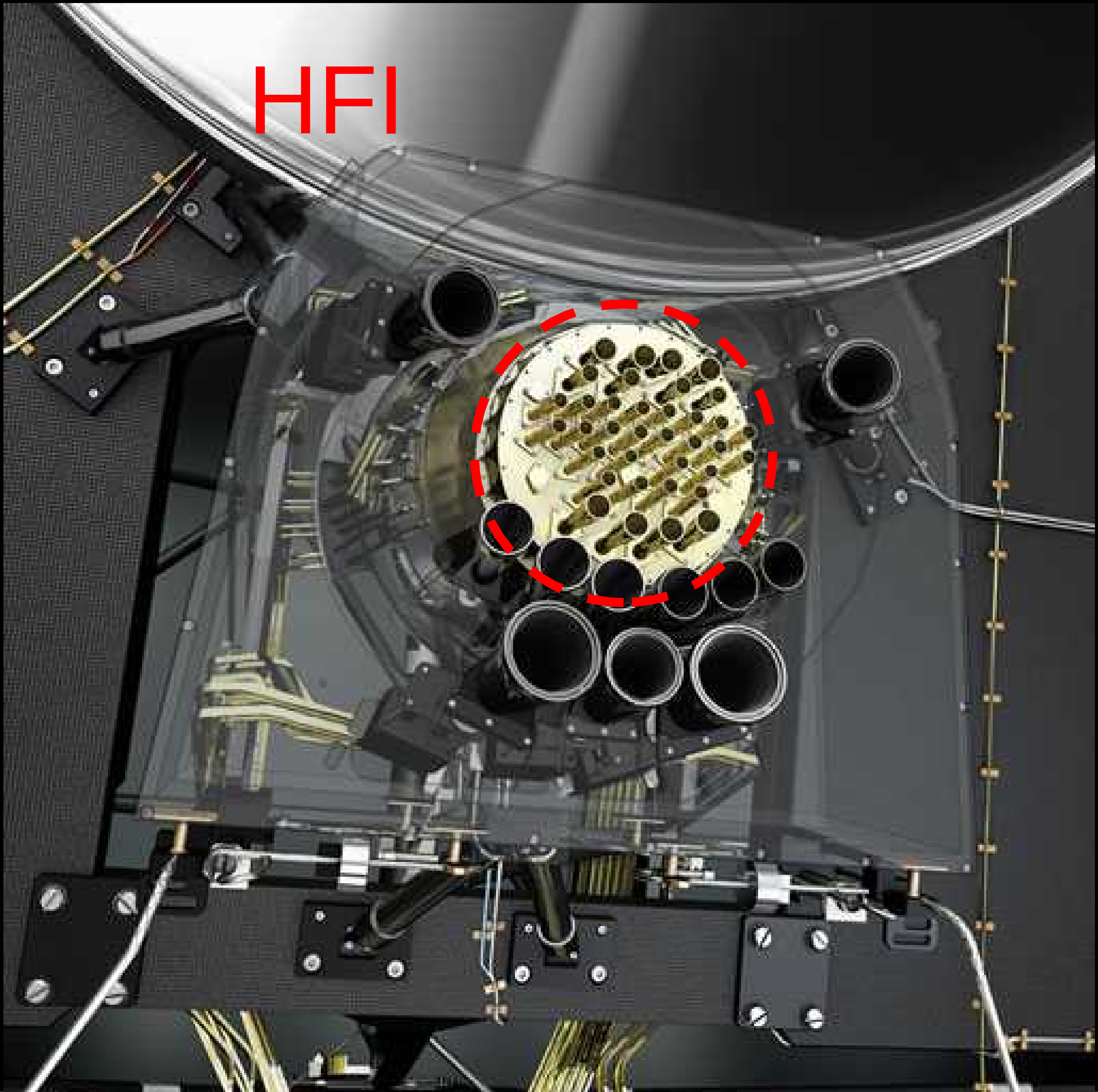
HFI

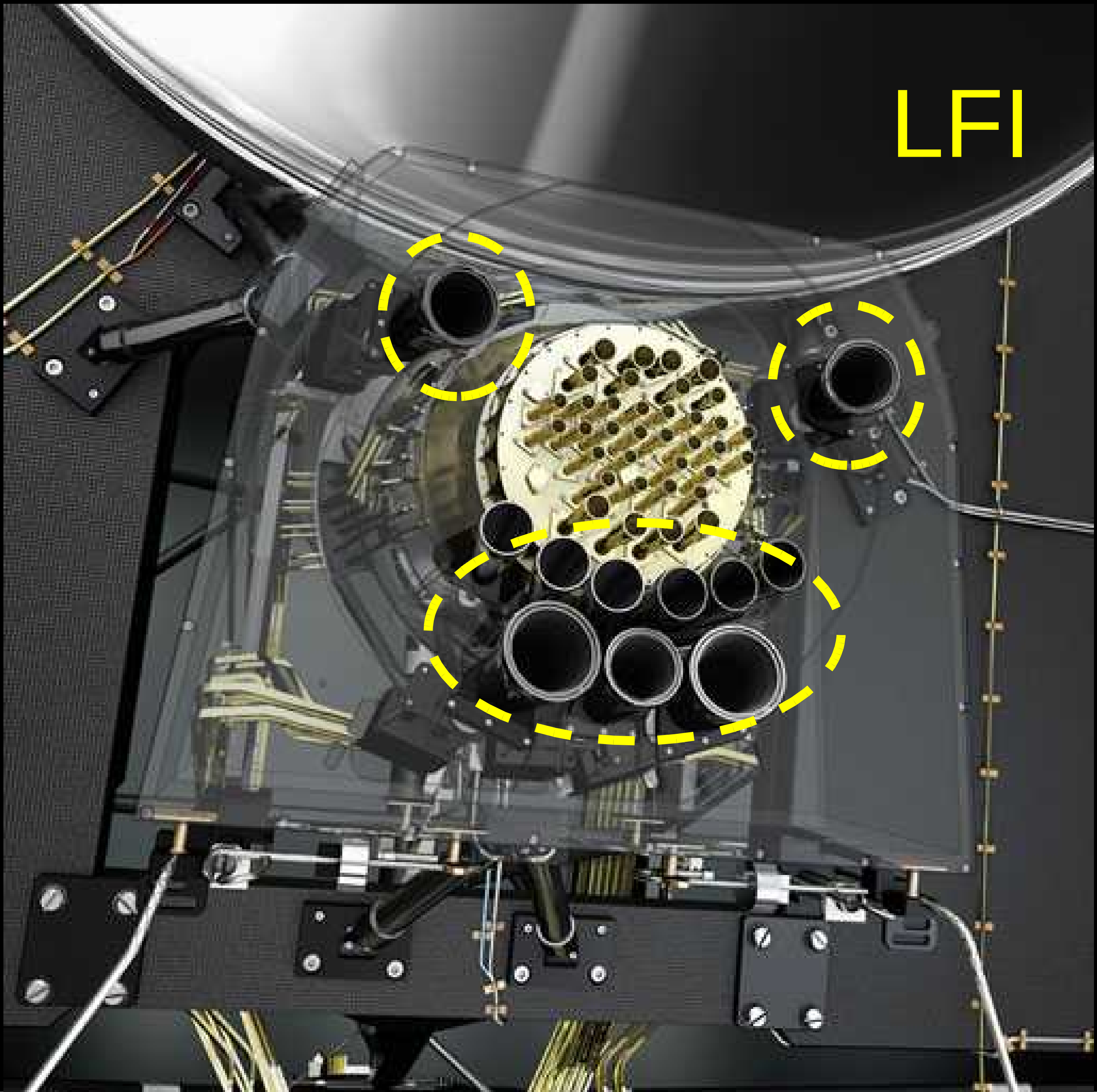
LFI

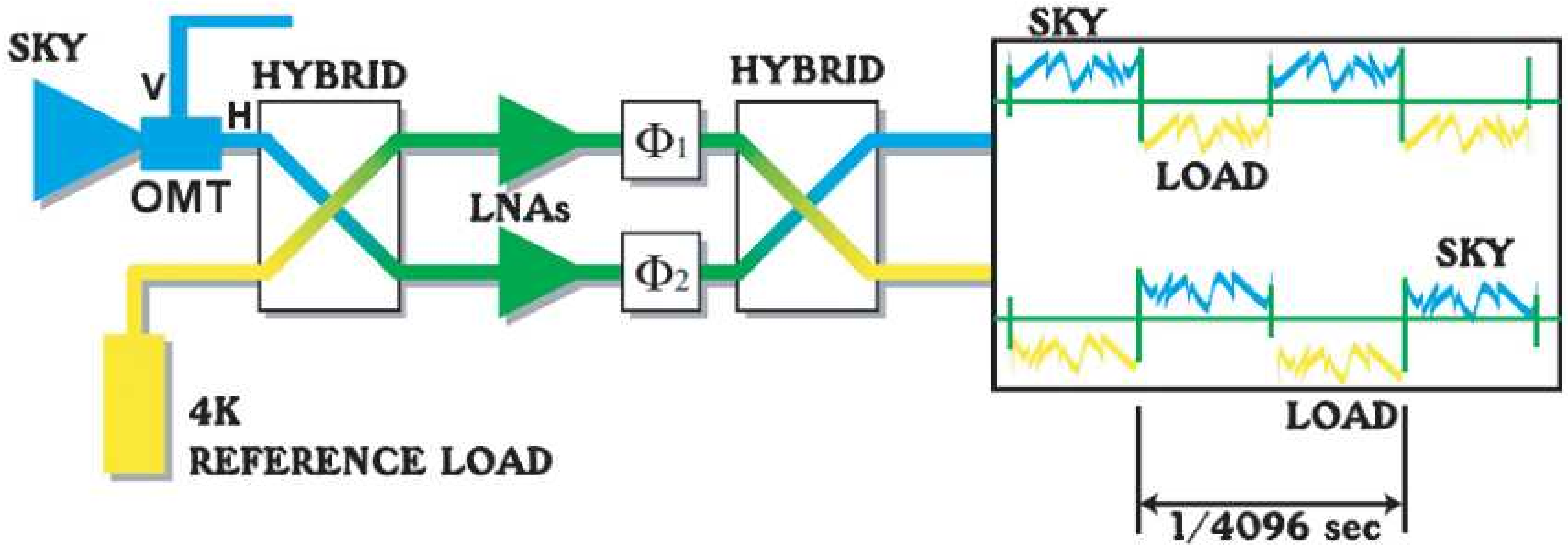

LFI
Pseudo-correlation
Differential radiometer
Measures I,Q,U
30, 44, 70 GHz

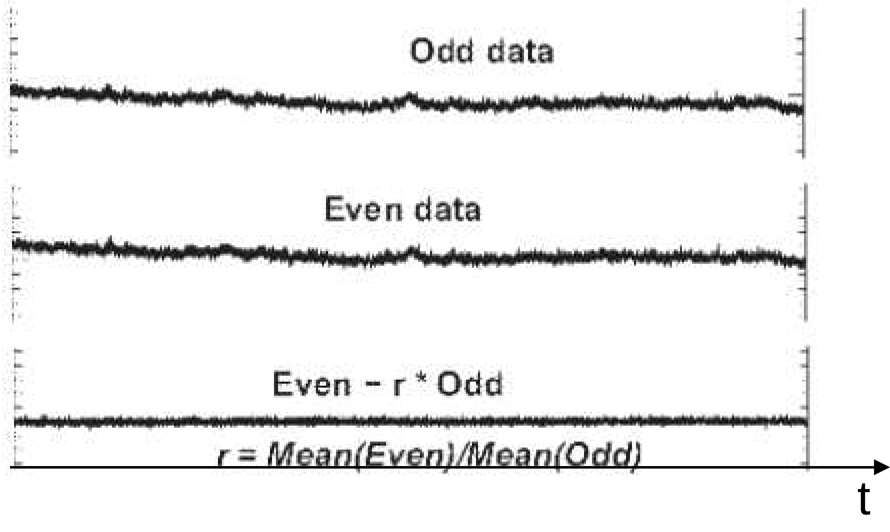

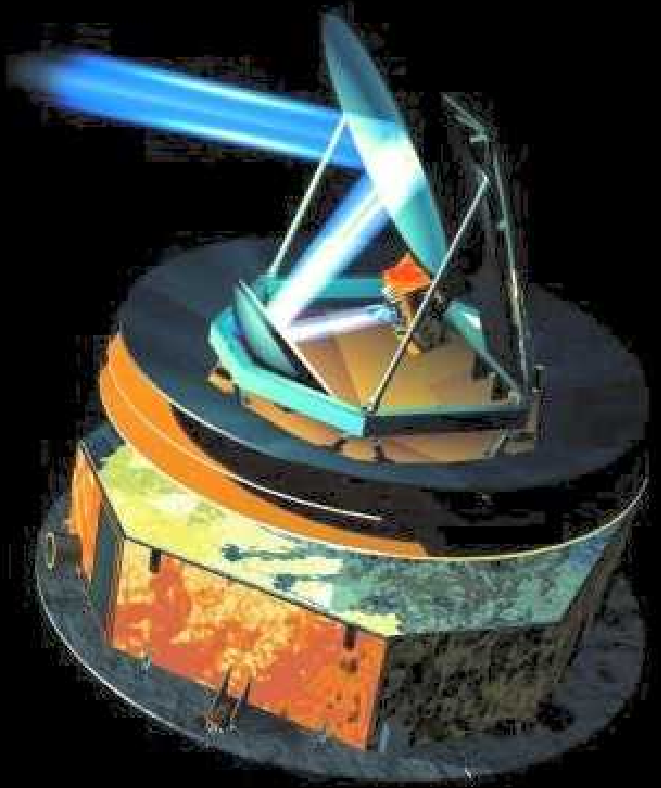

Off-axis Dragone Telescope, wide field, good polarization properties, 1.89mx1.50m aperture

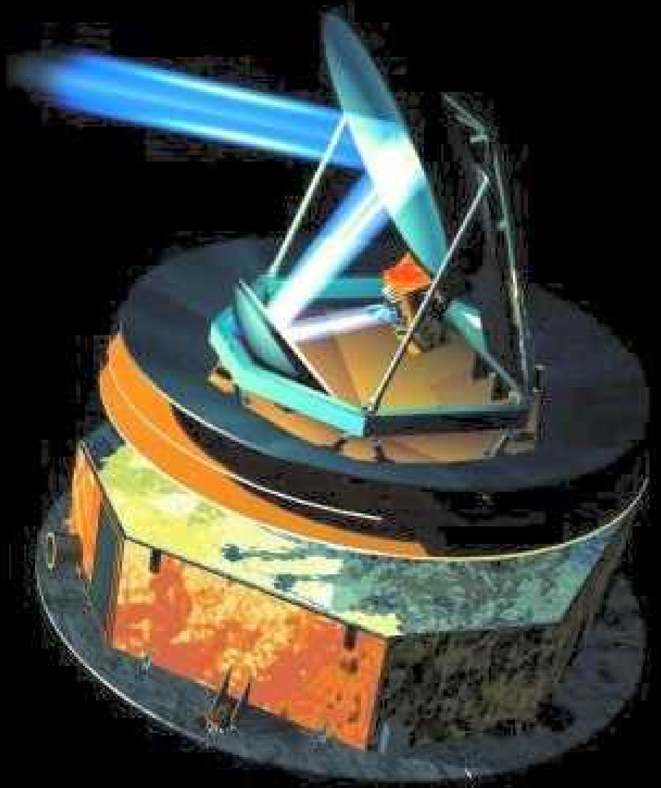

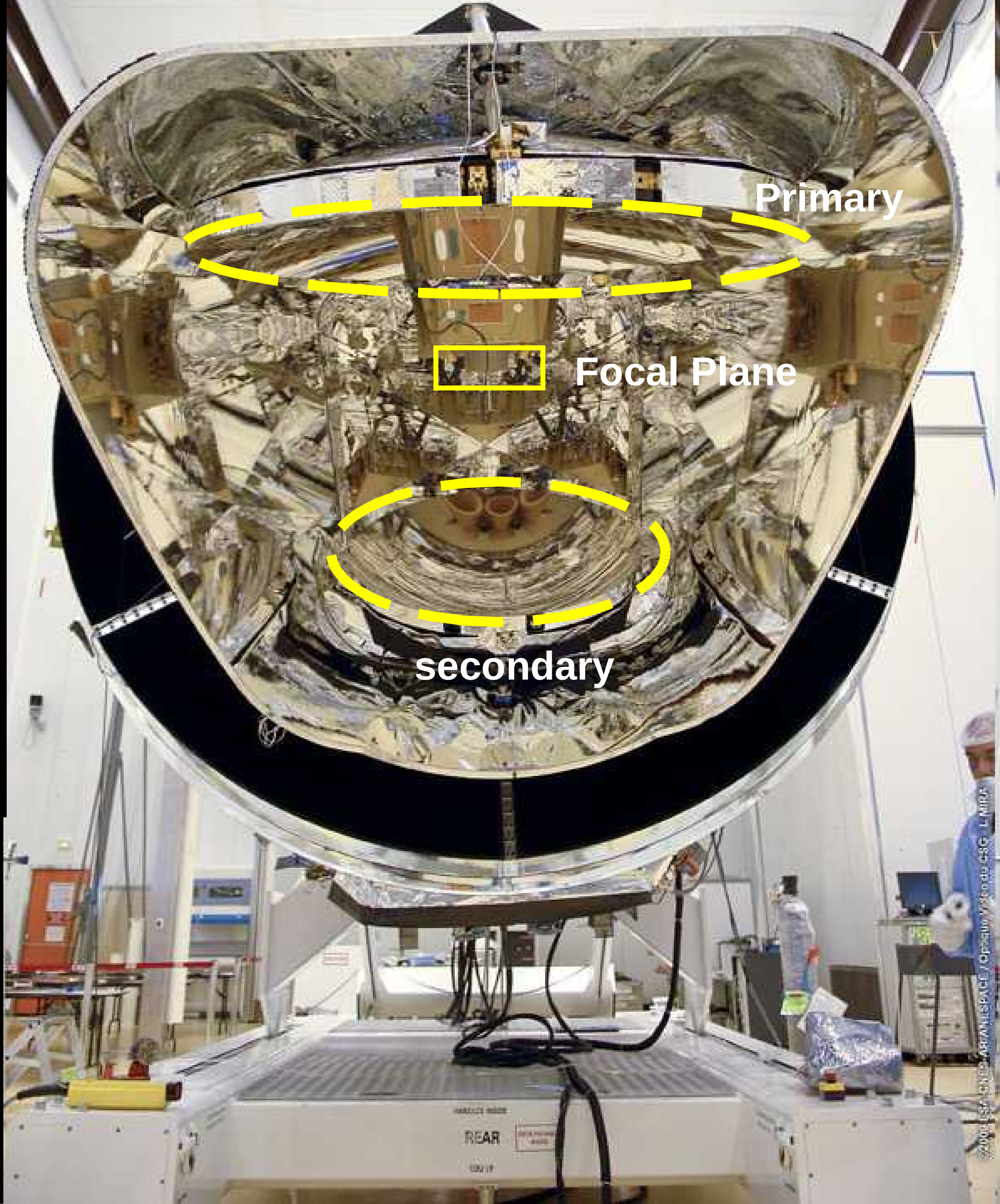

Off-axis Dragone Telescope, wide field, good polarization properties, 1.89mx1.50m aperture

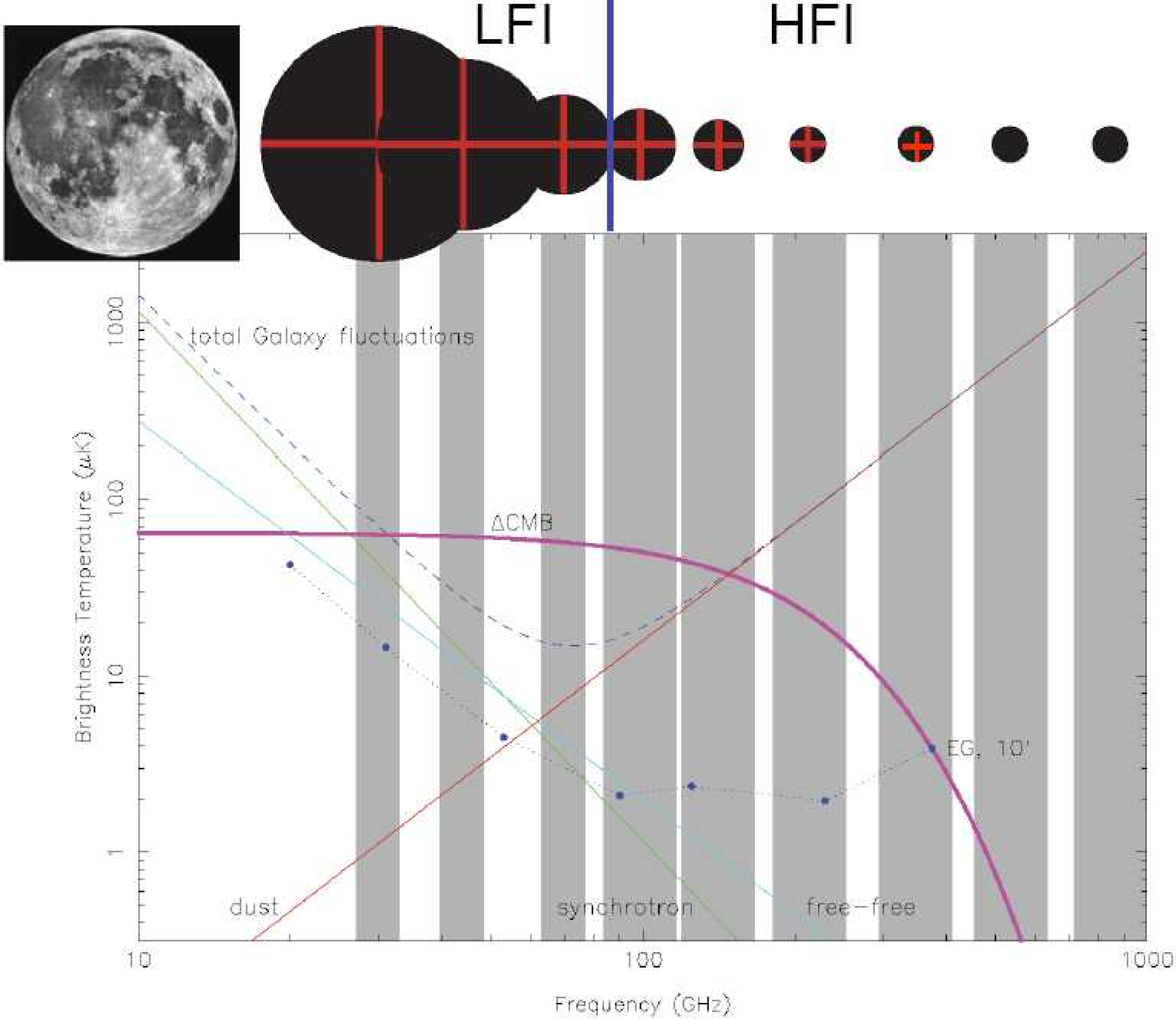
LFI
HFI
total Galaxy fluctuations
ΔCMB
EG, 10'
dust
synchrotron
free-free
Brightness Temperature (μK)
1000
100
10
1
10
100
1000
Frequency (GHz)

Cooling system

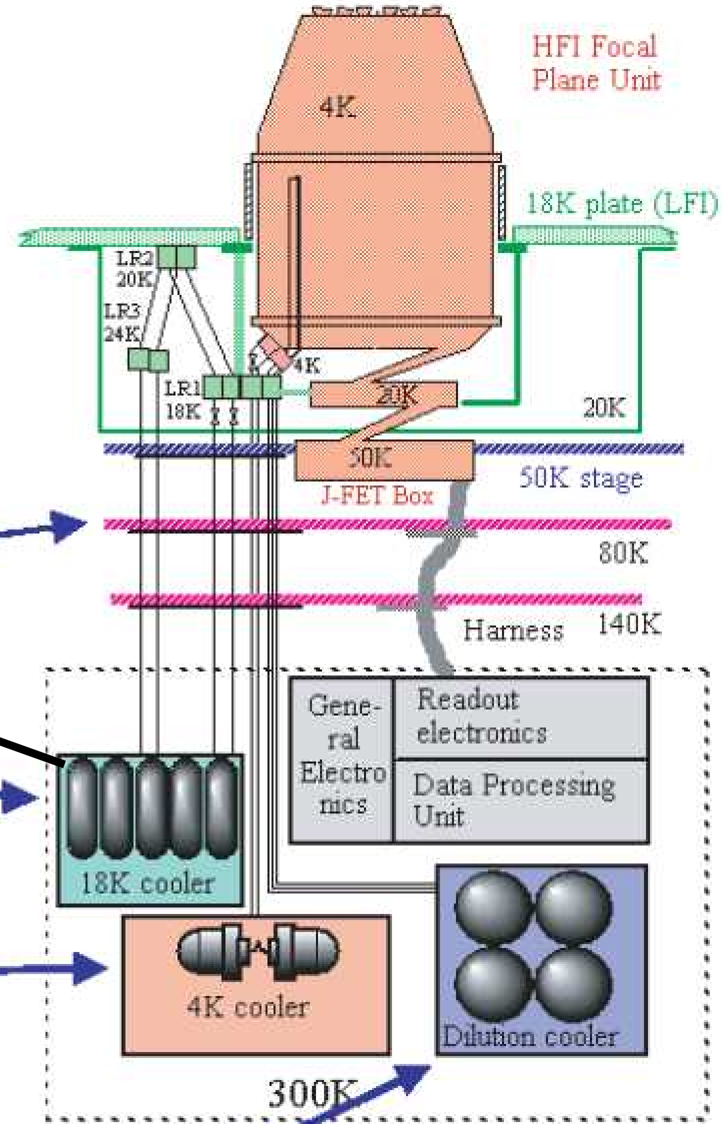

V-groove radiators (to 60 K)

LFI Focal
Plane Unit

20 K H_2 sorption coolers (JPL)

4 K Stirling cooler (RAL/MMS)

0.1 K ^{3}He/^{4}He dilution cooler (CRTBT)

TABLE 1.1

SUMMARY OF PLANCK INSTRUMENT CHARACTERISTICS

Instrument Characteristic	LFI			HFI					
Detector Technology	HEMT arrays			Bolometer arrays					
Center Frequency [GHz]	30	44	70	100	143	217	353	545	857
Bandwidth ($\Delta\nu/\nu$)	0.2	0.2	0.2	0.33	0.33	0.33	0.33	0.33	0.33
Angular Resolution (arcmin)	33	24	14	10	7.1	5.0	5.0	5.0	5.0
$\Delta T/T$ per pixel (Stokes I)[a]	2.0	2.7	4.7	2.5	2.2	4.8	14.7	147	6700
$\Delta T/T$ per pixel (Stokes Q & U)[a]	2.8	3.9	6.7	4.0	4.2	9.8	29.8	...	...

[a] Goal (in μK/K) for 14 months integration, 1σ, for square pixels whose sides are given in the row "Angular Resolution".

From the Blue Book (2005)

Launch
May 14th, 2009

Cruise
May-June 2009

First All-sky survey
Completed May 2010

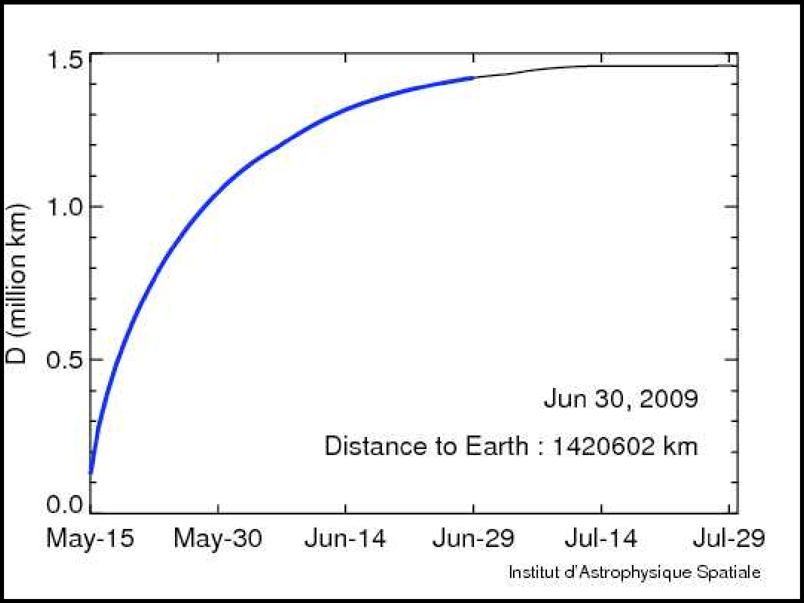

Thermal performance :
Planck collaboration: astro-ph/1101:2023

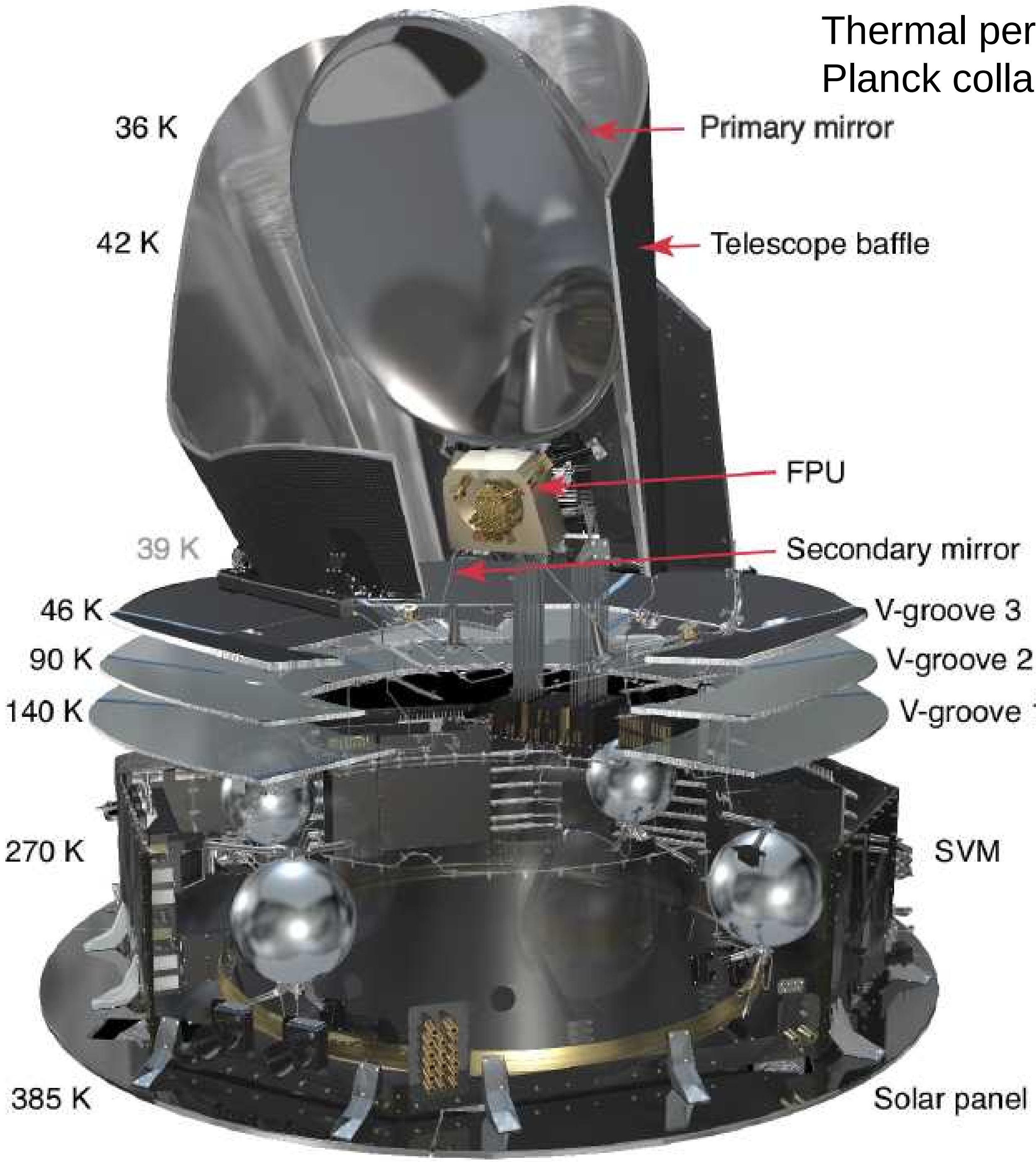

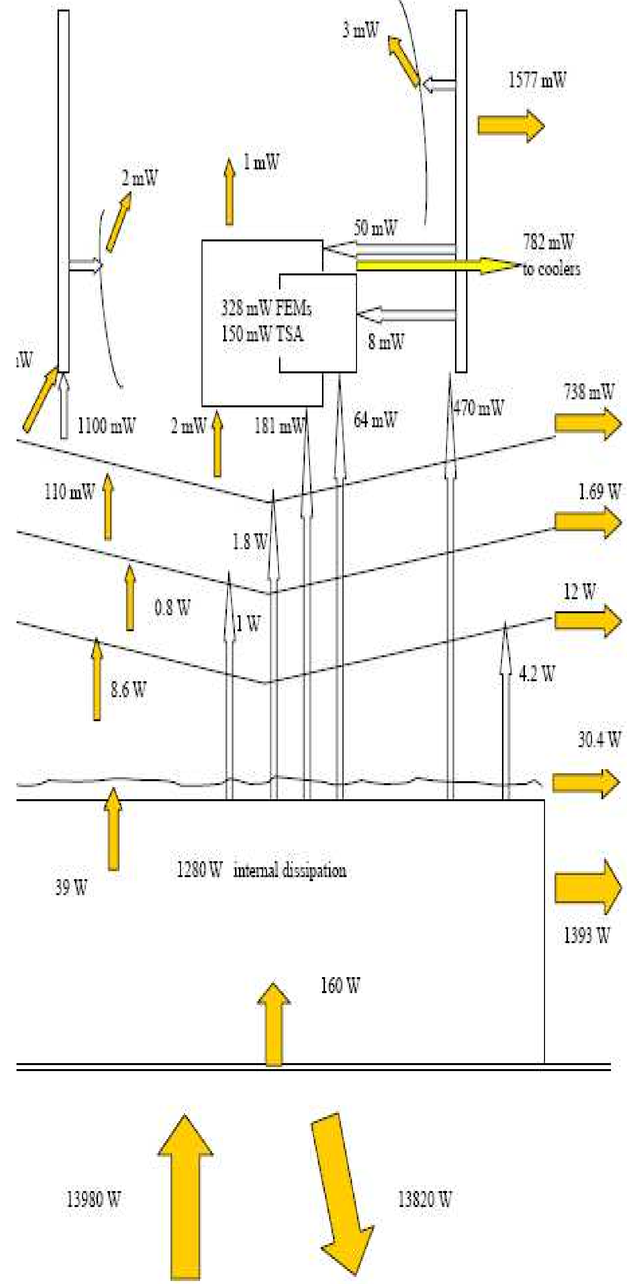

Thermal performance :
Planck collaboration: astro-ph/1101:2023

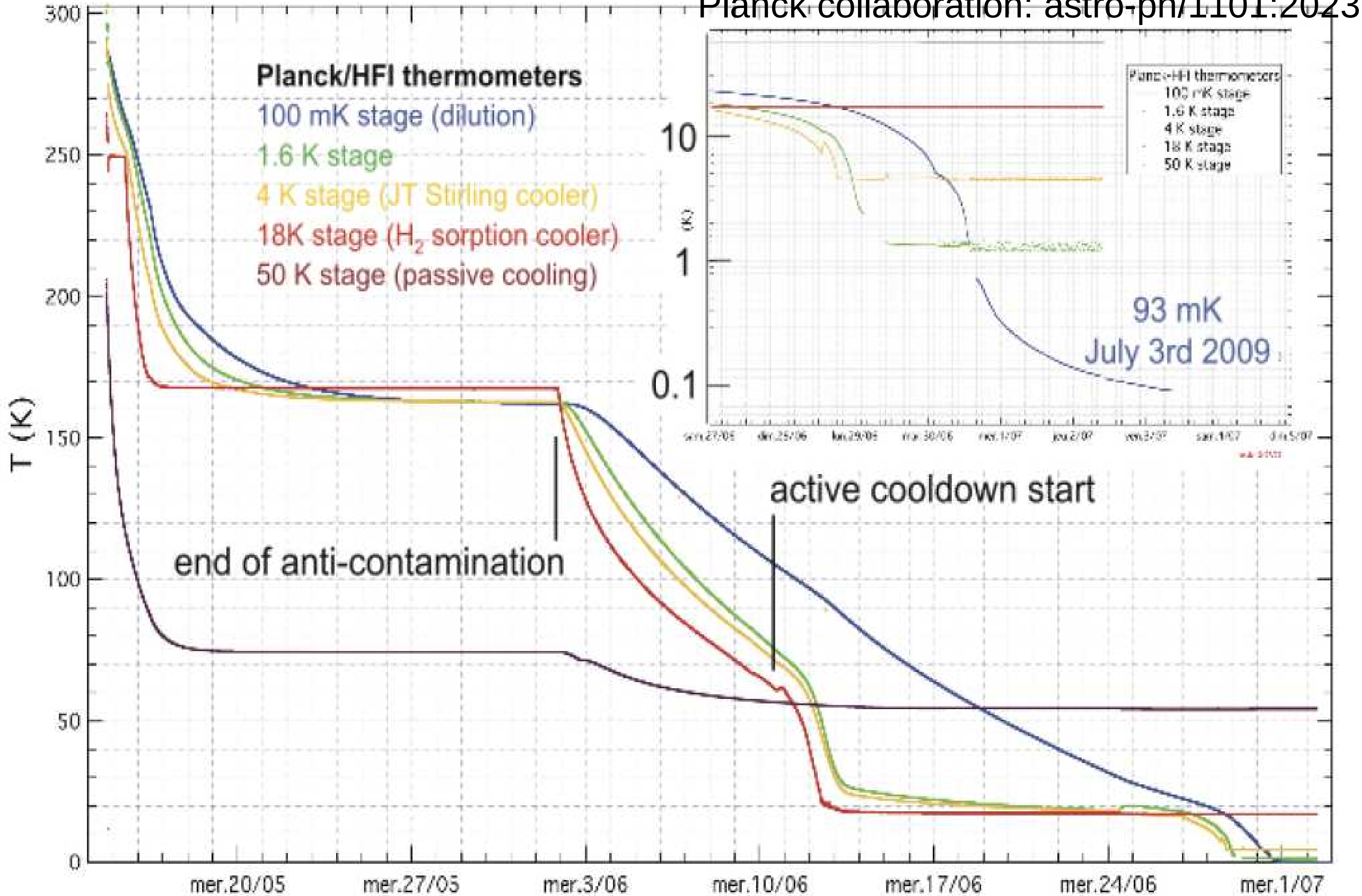

Mission :
Planck collaboration: astro-ph/1101:2022

Table 1. *Planck* coverage statistics.

	30 GHz	100 GHz	545 GHz	
Mean[a]	2293	4575	2278	sec deg^2
Minimum	440	801	375	sec deg^2
$<$ half Mean[b]	14.4	14.6	15.2	%
$> 4\times$ Mean[c]	1.6	1.5	1.2	%
$> 9\times$ Mean[d]	0.41	0.42	0.41	%

[a] Mean over the whole sky of the integration time cumulated for all detectors (definition as in Table 3) in a given frequency channel.
[b] Fraction of the sky whose coverage is less than half the Mean.
[c] Fraction of the sky whose coverage is larger than four times the Mean.
[d] Fraction of the sky whose coverage is larger than nine times the Mean.

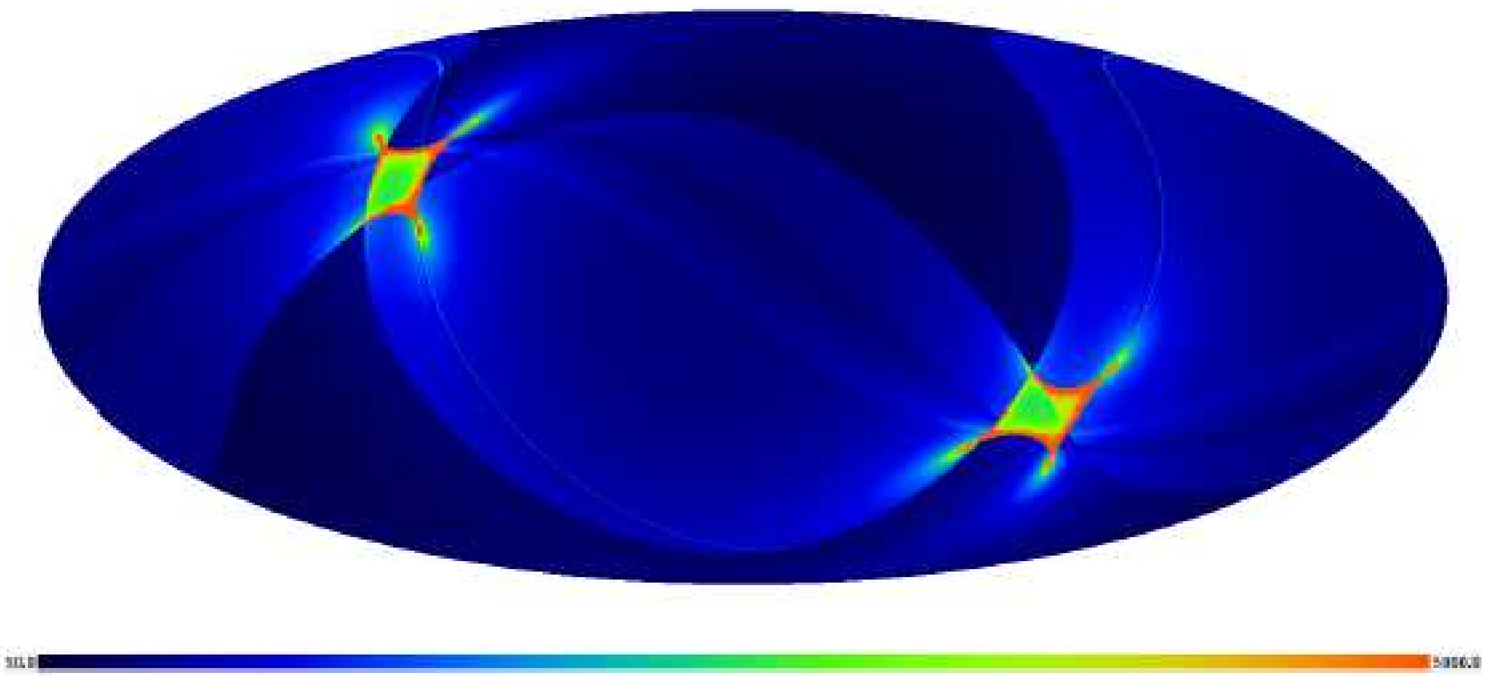

Mission : Planck collaboration: astro-ph/1101:2022

CHANNEL	$N_{\rm detectors}$[a]	$\nu_{\rm center}$[b] [GHz]	MEAN BEAM[c] FWHM	Ellipticity	WHITE-NOISE[d] SENSITIVITY [$\mu K_{RJ}\, s^{1/2}$]	[$\mu K_{CMB}\, s^{1/2}$]	CALIBRATION[e] UNCERTAINTY [%]	FAINTEST SOURCE[f] IN ERCSC $\lvert b \rvert > 30°$ [mJy]
30 GHz	4	28.5	32.65	1.38	143.4	146.8	1	480
44 GHz	6	44.1	27.92	1.26	164.7	173.1	1	585
70 GHz	12	70.3	13.01	1.27	134.7	152.6	1	481
100 GHz	8	100	9.37	1.18	17.3	22.6	2	344
143 GHz	11	143	7.04	1.03	8.6	14.5	2	206
217 GHz	12	217	4.68	1.14	6.8	20.6	2	183
353 GHz	12	353	4.43	1.09	5.5	77.3	2	198
545 GHz	3	545	3.80	1.25	4.9	...	7	381
857 GHz	3	857	3.67	1.03	2.1	...	7	655

[a] For 30, 44, and 70 GHz, each "detector" is a linearly polarised radiometer. There are two (orthogonally polarized) radiometers behind each horn. Each radiometer has two diodes, both switched at high frequency between the sky and a blackbody load at ~ 4 K (Mennella et al. 2011). For 100 GHz and above, each "detector" is a bolometer (Planck HFI Core Team 2011a). Most of the bolometers are sensitive to polarisation, in which case there are two orthogonally polarised detectors behind each horn; some of the detectors are spider-web bolometers (one per horn) sensitive to the total incident power.

[b] Mean center frequency of the N detectors at each frequency.

[c] Mean optical properties of the N beams at each frequency. FWHM ≡ FWHM of circular Gaussian with the same volume. Ellipticity gives the ratio of major axis to minor axis for a best-fit elliptical Gaussian. The actual point spread function of an unresolved object on the sky depends not only on the optical properties of the beam, but also on sampling and time domain filtering in signal processing, and the way the sky is scanned. For details on these aspects see § 4 of Mennella et al. (2011), § 4 of Zacchei et al. (2011), § 4.2 of Planck HFI Core Team (2011a), and § 6.2 of Planck HFI Core Team (2011b)

[d] Uncorrelated noise in 1 s for the array of N detectors, in Rayleigh-Jeans units and in thermodynamic CMB units. For a preliminary discussion of correlated noise and systematic effects, see Mennella et al. (2011), Planck HFI Core Team (2011a) , Zacchei et al. (2011) , and Planck HFI Core Team (2011b) .

[e] Absolute uncertainty, based on the known amplitude of the CMB dipole up to 353 GHz, and on FIRAS at 545 and 857 GHz (Zacchei et al. 2011; Planck HFI Core Team 2011b).

[f] Flux density of the faintest source included in the ERCSC (Planck Collaboration 2011c).

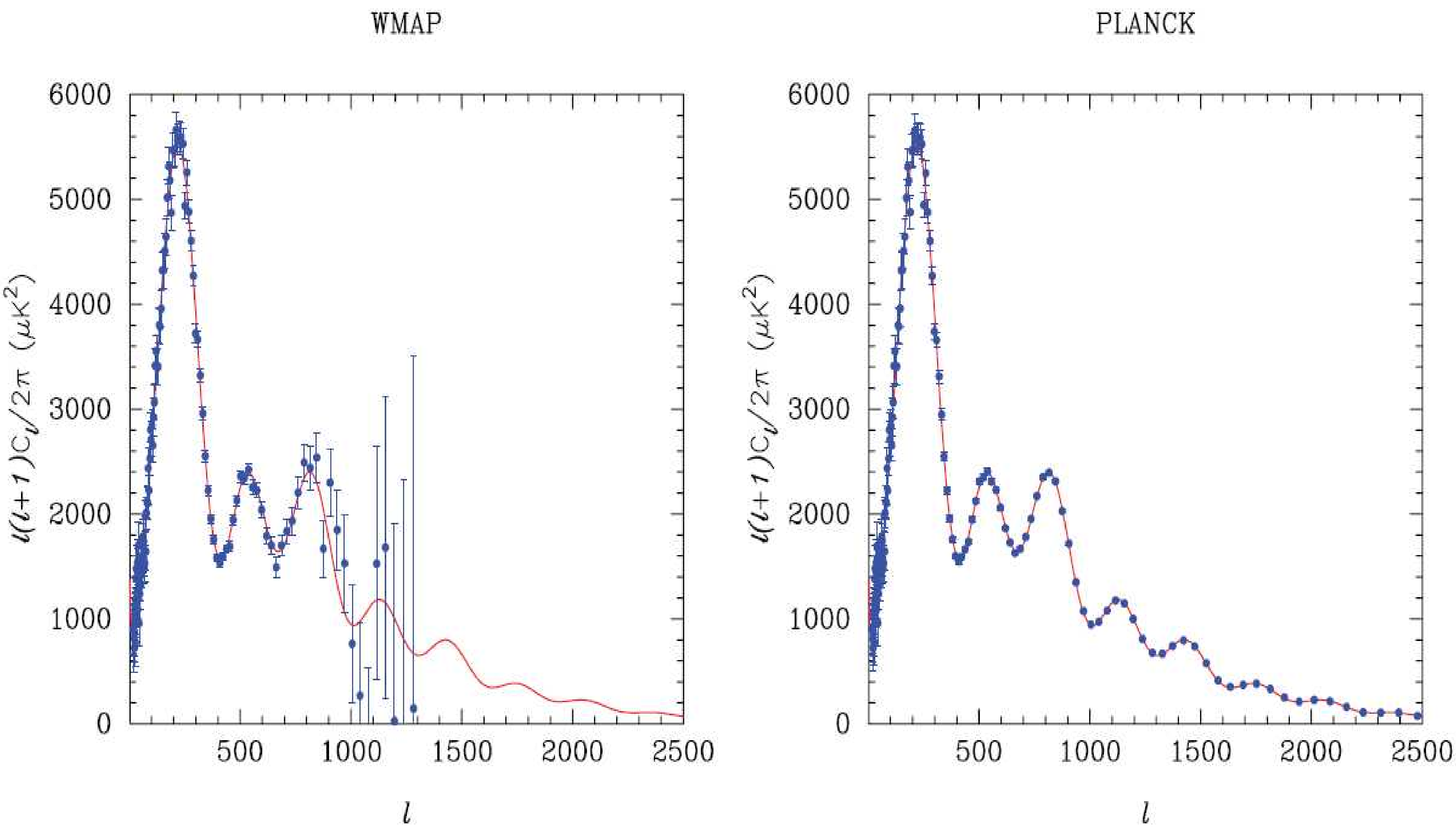

FIG 2.8.—The left panel shows a realisation of the CMB power spectrum of the concordance ΛCDM model (red line) after 4 years of *WMAP* observations. The right panel shows the same realisation observed with the sensitivity and angular resolution of *Planck*.

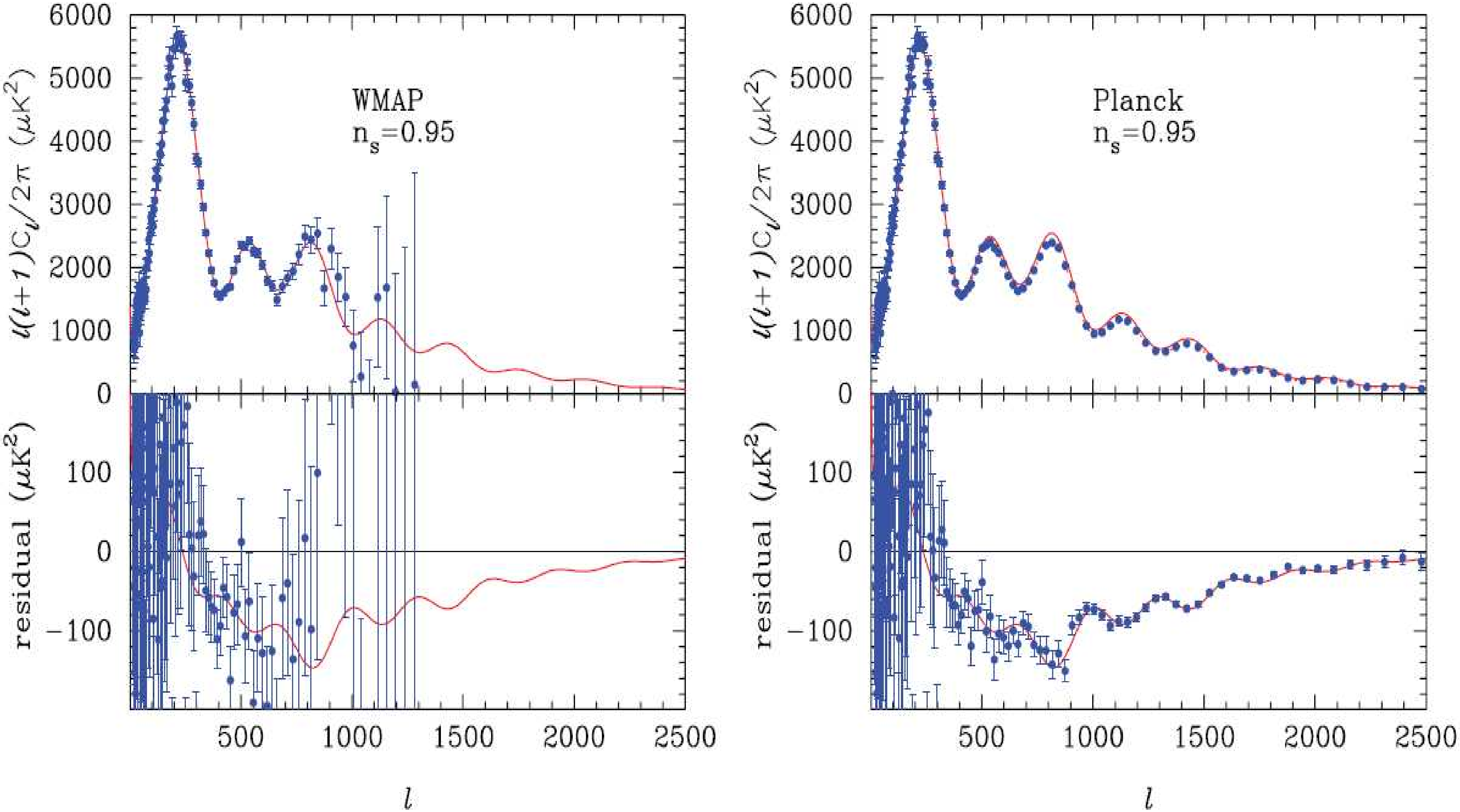

FIG 2.11.—The solid lines in the upper panels of these figures show the power spectrum of the concordance ΛCDM model with an exactly scale invariant power spectrum, $n_S = 1$. The points, on the other hand, have been generated from a model with $n_S = 0.95$ but otherwise identical parameters. The lower panels show the residuals between the points and the $n_S = 1$ model, and the solid lines show the theoretical expectation for these residuals. The left and right plots show simulations for *WMAP* and *Planck*, respectively.

ESA-SCI(2005)1

EE

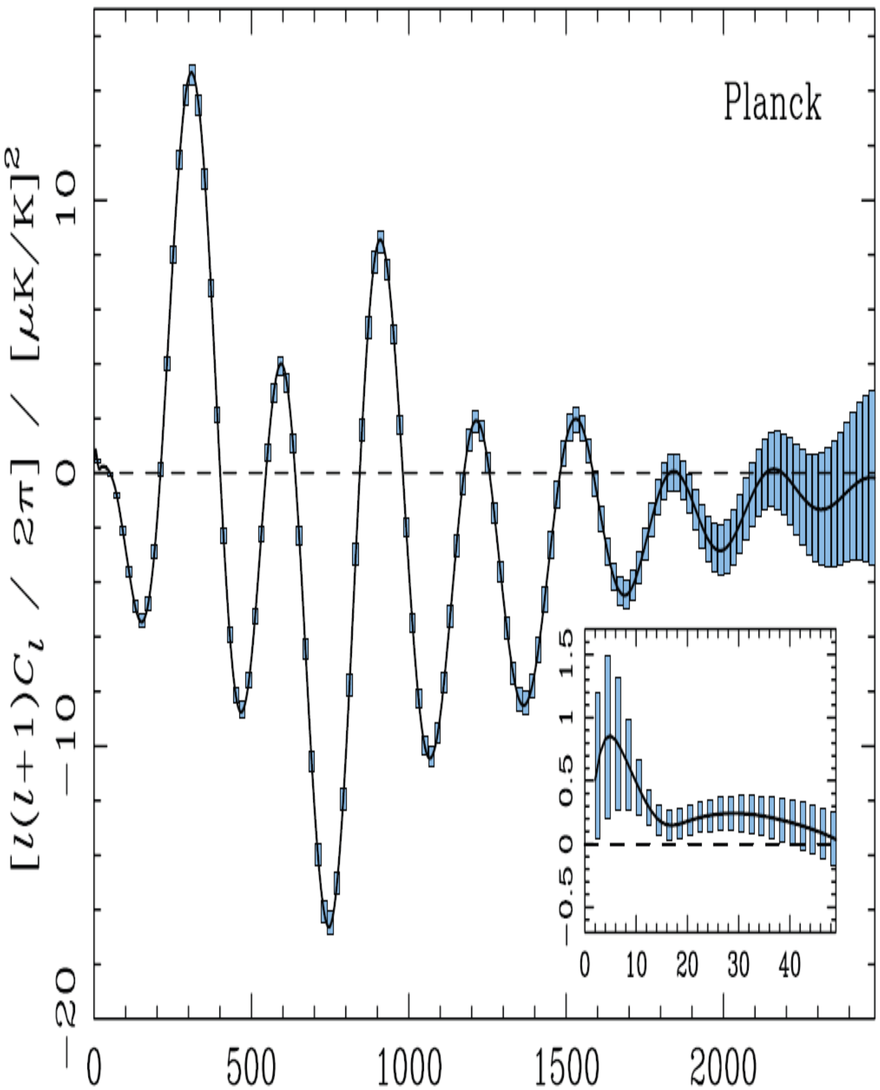

TE

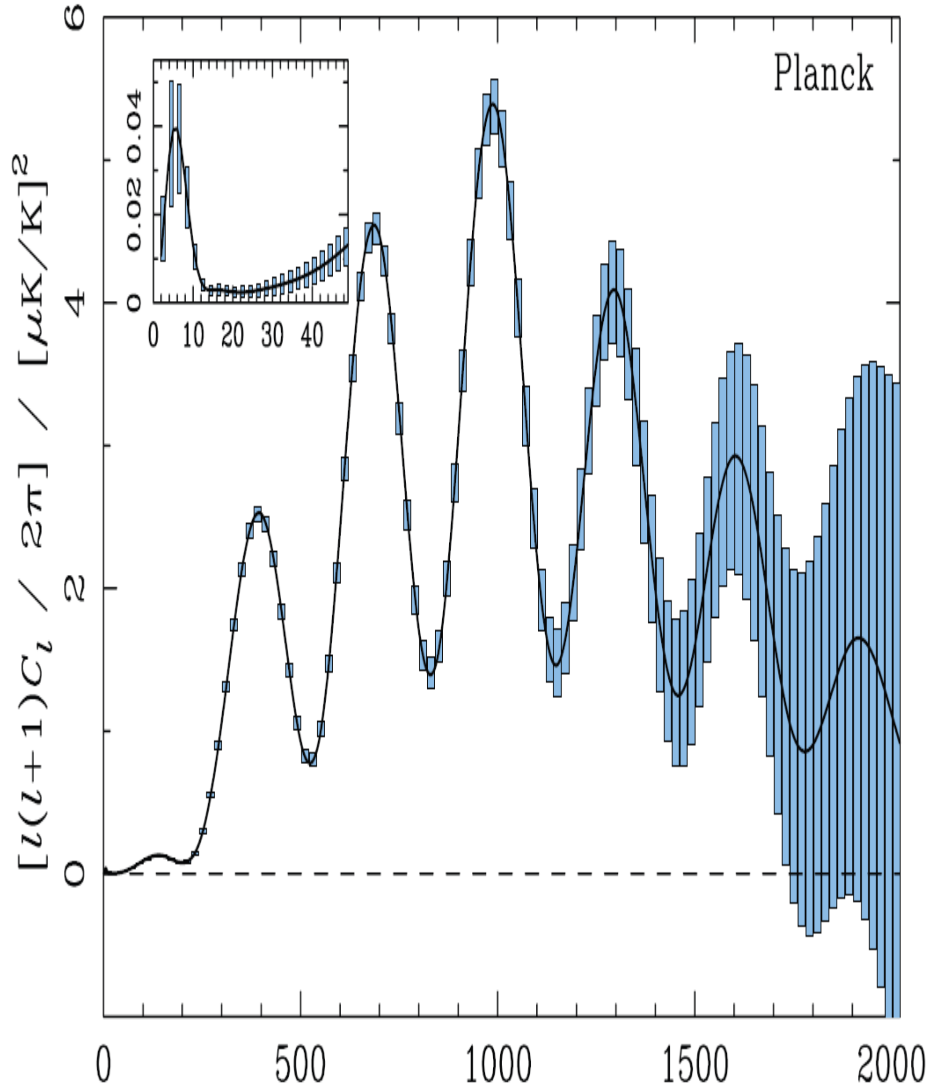

ESA-SCI(2005)1

TABLE II: Representative cosmological data sets and corresponding 2σ (95% C.L.) constraints on the sum of ν masses Σ.

Case	Cosmological data set	Σ (at 2σ)
1	CMB	< 1.19 eV
2	CMB + LSS	< 0.71 eV
3	CMB + HST + SN-Ia	< 0.75 eV
4	CMB + HST + SN-Ia + BAO	< 0.60 eV
5	CMB + HST + SN-Ia + BAO + Lyα	< 0.19 eV

From Fogli et al. 2008, Astro-ph/0805.2517

With Planck : < 0.2 eV

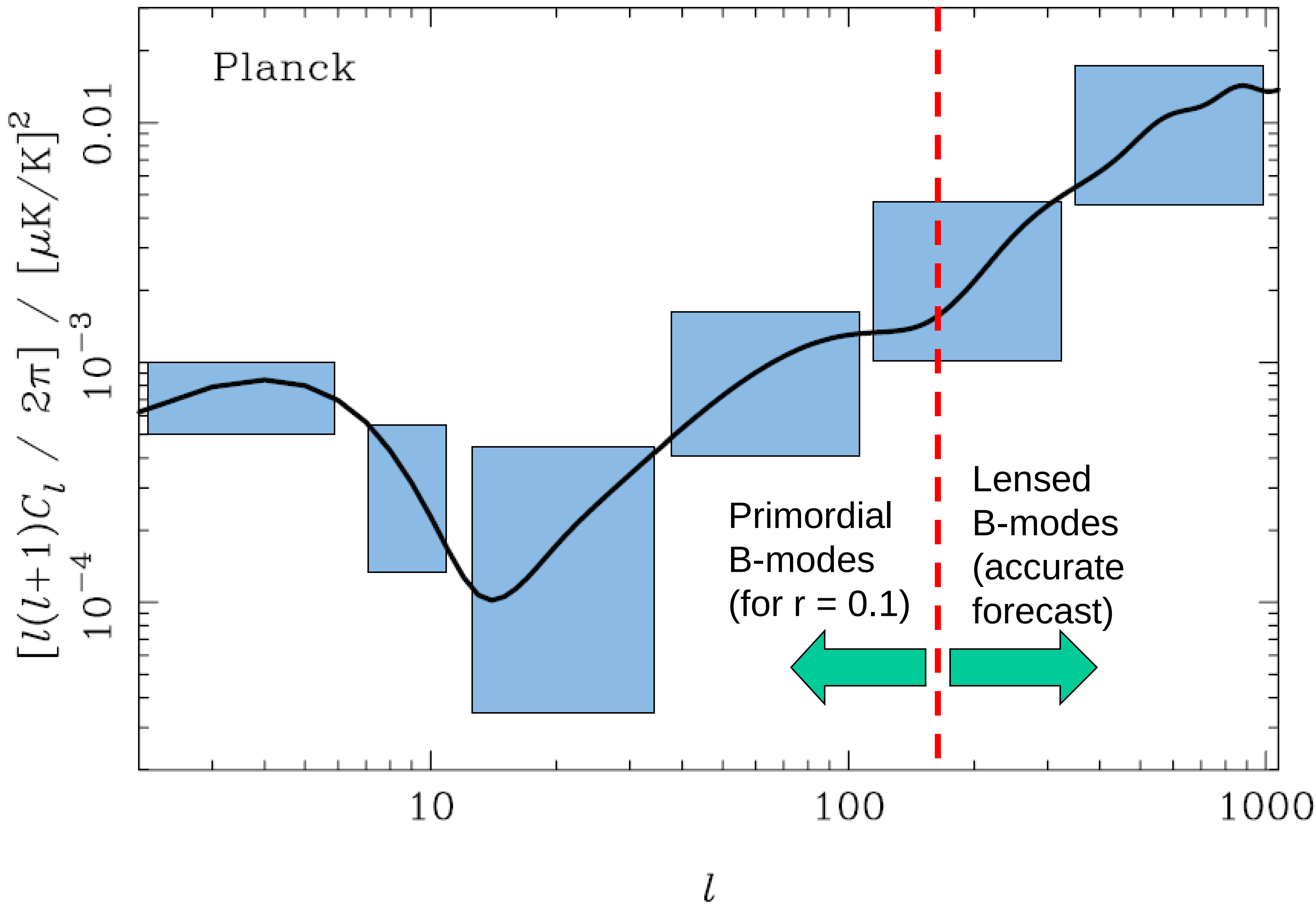

Planck
$[l(l+1)C_l \ / \ 2\pi] \ / \ [\mu K/K]^2$
0.01
10^{-3}
10^{-4}
10
100
1000
l
Primordial
B-modes
(for r = 0.1)
Lensed
B-modes
(accurate
forecast)

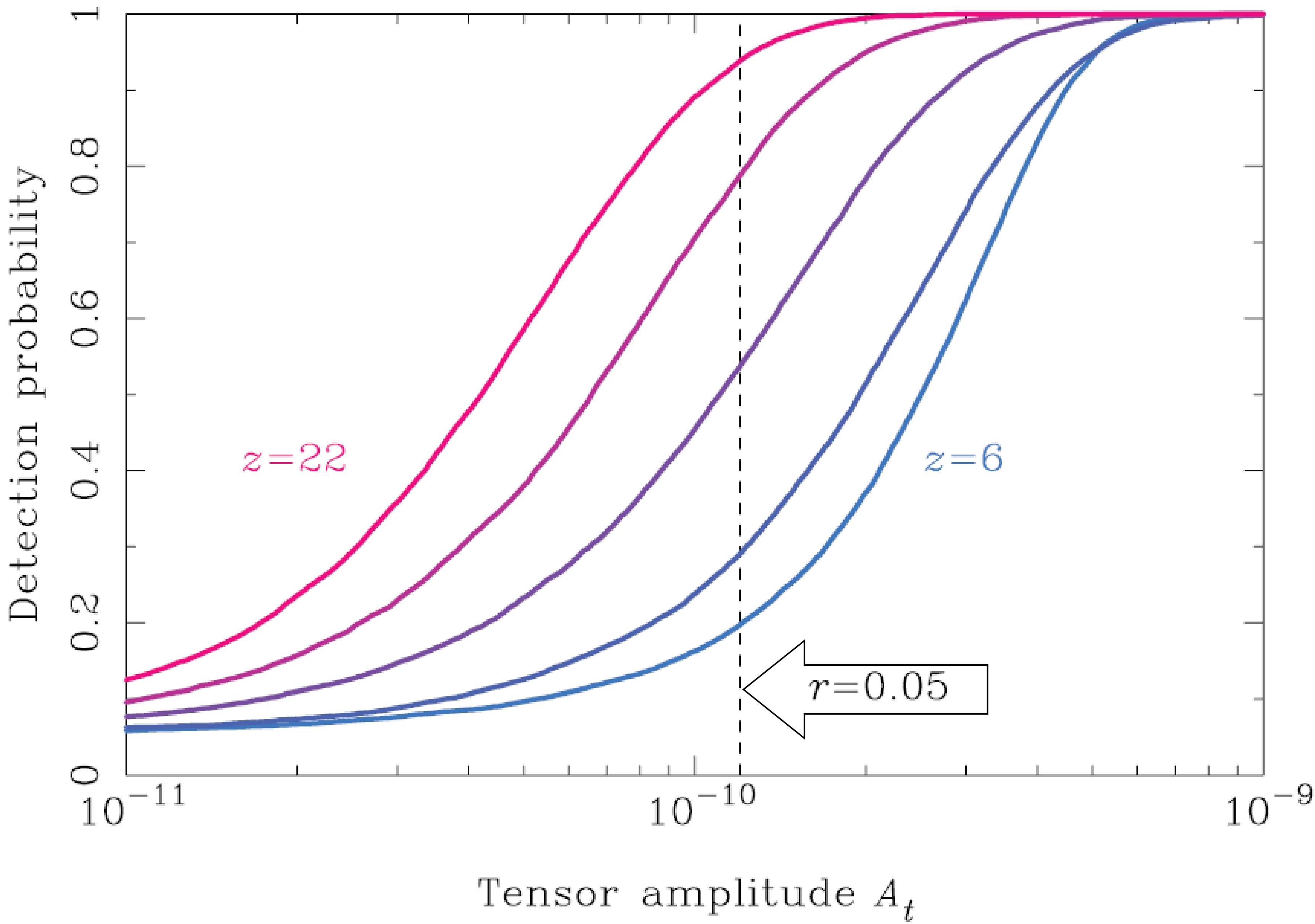

Detection probability
Tensor amplitude A_t
0
0.2
0.4
0.6
0.8
1
10^{-11}
10^{-10}
10^{-9}
z=22
z=6
r=0.05

From Efsthathiou & Gratton '09

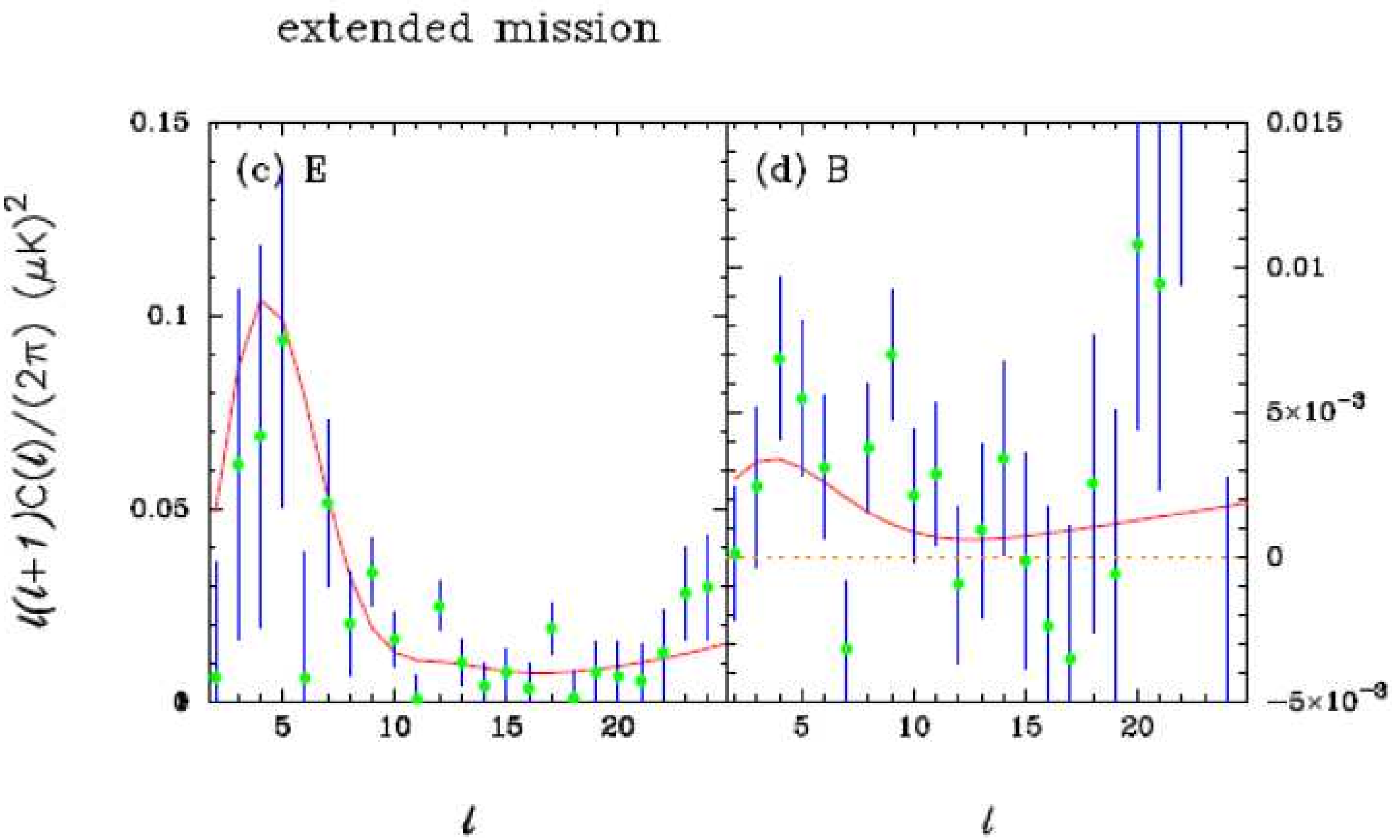

Figure 3. QML estimates of the E and B-mode polarization spectra for the simulations with $r = 0.05$. Figures 3a and 3b show power spectra for the nominal *Planck* mission. Figures 3c and 3d show power spectra for an extended *Planck* mission. The error bars are computed from the diagonal components of the inverse of the QML Fisher matrix using the theoretical input spectra for $r = 0.05$ (shown by the red lines).

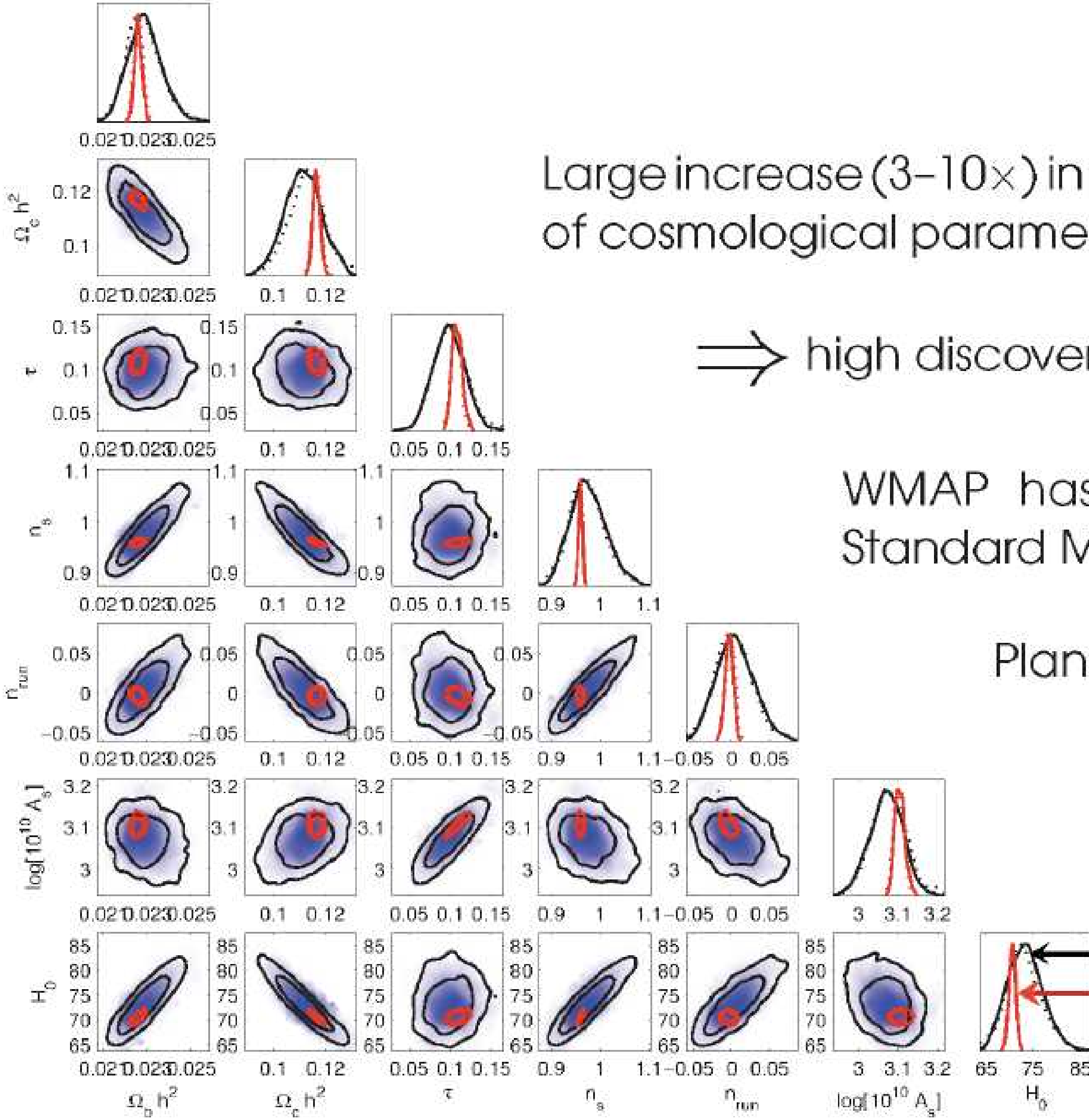

Large increase (3–10×) in precision of cosmological parameters

⇒ high discovery potential

WMAP has confirmed the Standard Model

Planck will challenge it

Projected WMAP likelihood

Projected Planck likelihood

on Hubble constant

Planck Bluebook

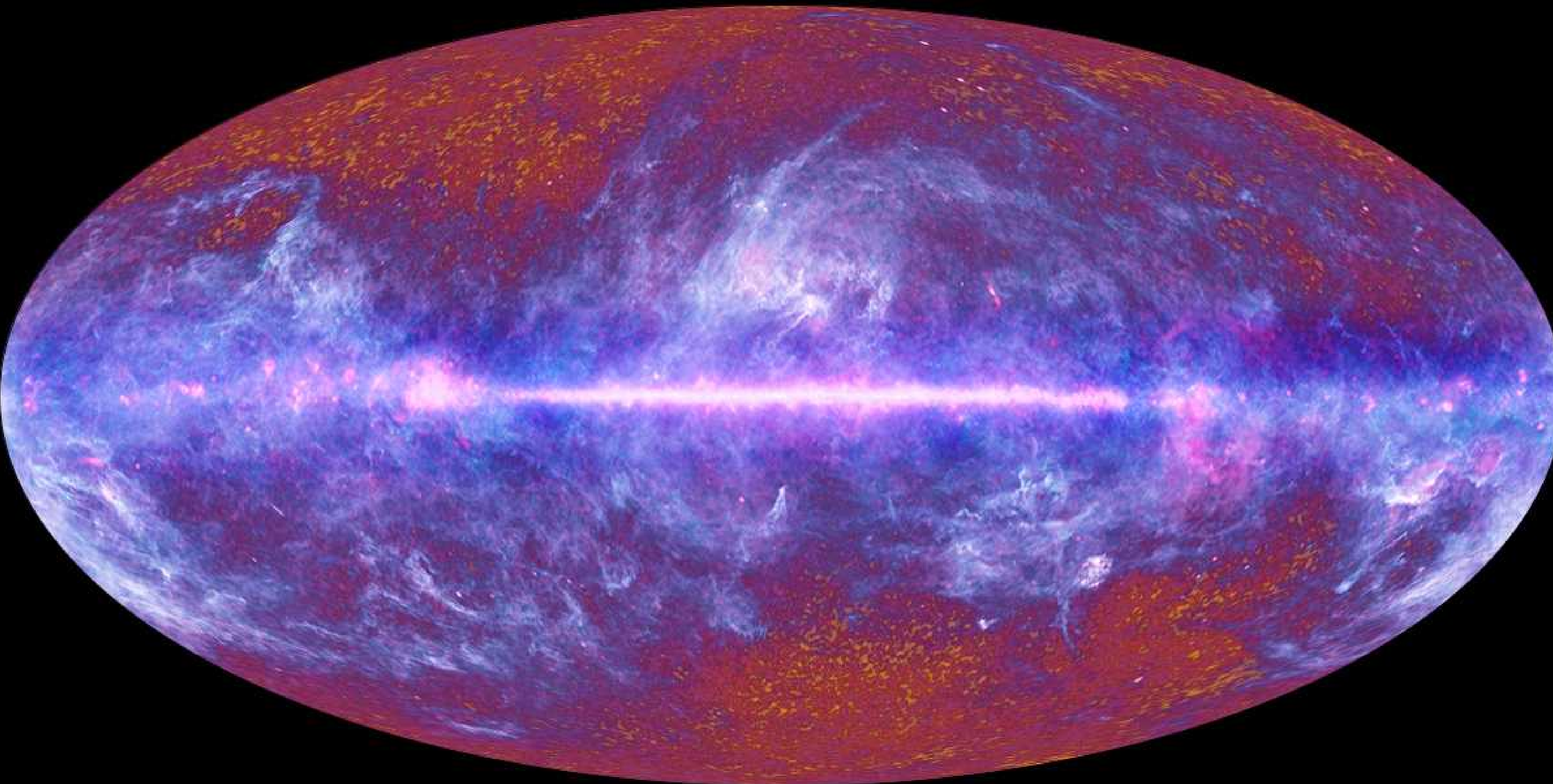

Planck one-year all-sky survey

(c) ESA, HFI and LFI consortia, J

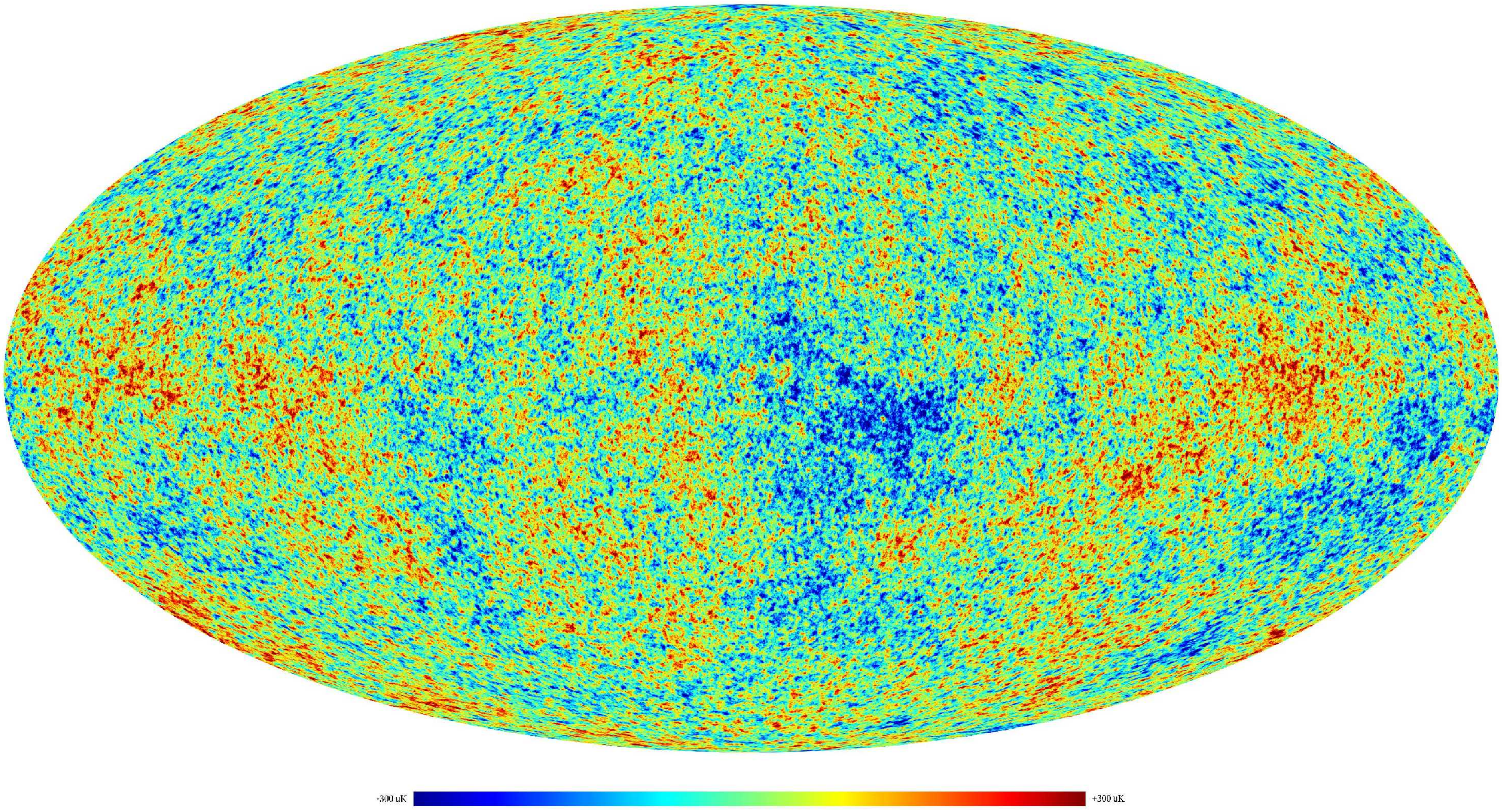

This is a simulation

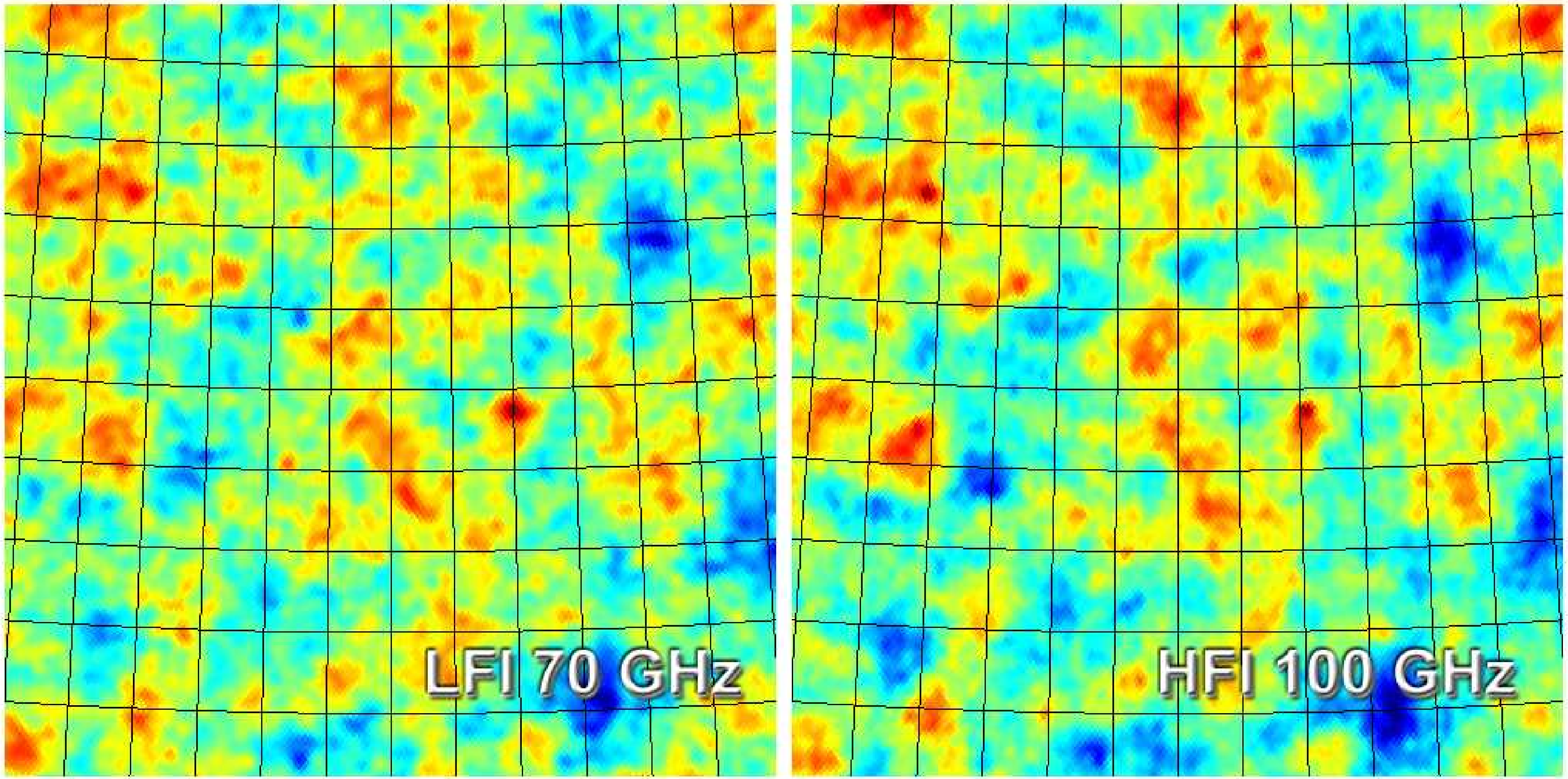

Real data (from just 15 days of operation)

Early Release Compact Source Catalogue

Jan. 11, 2010

ERCSC : Planck collaboration: astro-ph/1101:2041

Table 1. Comparison between all sky surveys with similar frequencies aligned in rows. The left column for each mission gives the frequency (ν in GHz) while the right column gives the spatial resolution as a full width at half maximum (FWHM) in arcminutes.

DMR		*WMAP*		*Planck*		*Akari*		*IRAS*		*WISE*	
ν	FWHM	ν	FWHM	ν	FWHM	ν	FWHM	ν	FWHM	ν	FWHM
		23	53								
32	420	33	40	30	32.65						
		41	31	44	27.00						
53	420	61	21	70	13.01						
90	420	94	13	100	9.94						
				143	7.04						
				217	4.66						
				353	4.41						
				545	4.47						
				857	4.23						
						1.9×10^3	0.8				
						2.1×10^3	0.7				
						3.3×10^3	0.45	3×10^3	5.2		
						4.6×10^3	0.32	5×10^3	3.9		
						16.7×10^3	0.09	12×10^3	4.5	13.6×10^3	0.2
						33×10^3	0.05	25×10^3	4.7	25×10^3	0.11
										65×10^3	0.11
										88×10^3	0.1

ERCSC :
Planck collaboration: astro-ph/1101:2041

Faintest source vs. frequency band

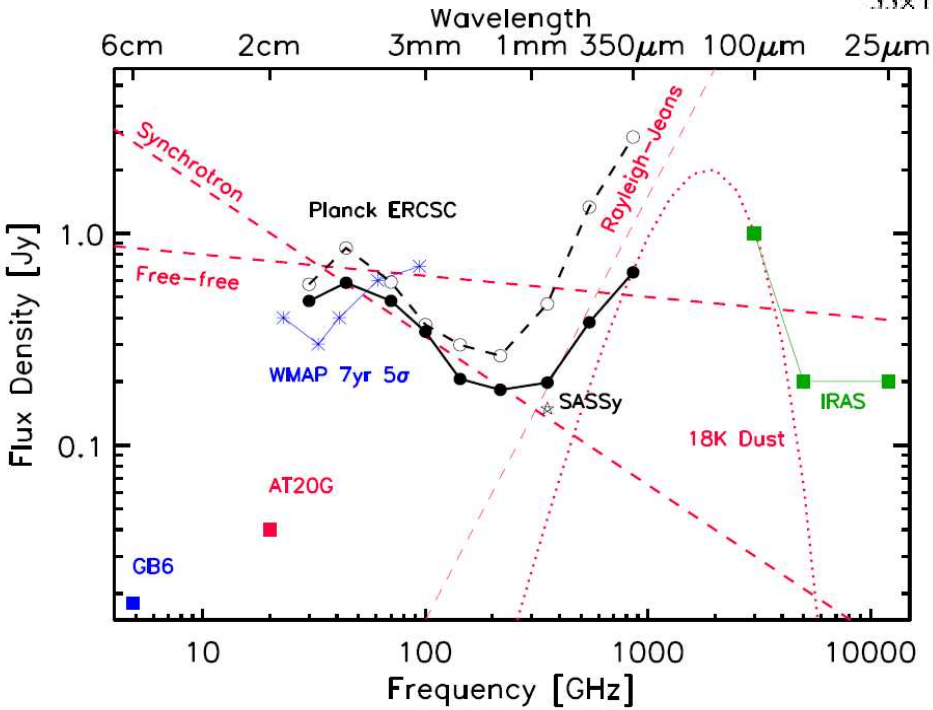

sources

Frequency	A	B	C	D
30	705	...	...	379
44	452	334	379	388
70	599	363	389	520
100	1381	496	520	1104
143	1764	929	1106	1357
217	5470	1067	1357	4190
353	6984	2848	4189	4244
545	7223	3404	4245	5363
857	8988	...	5365	...

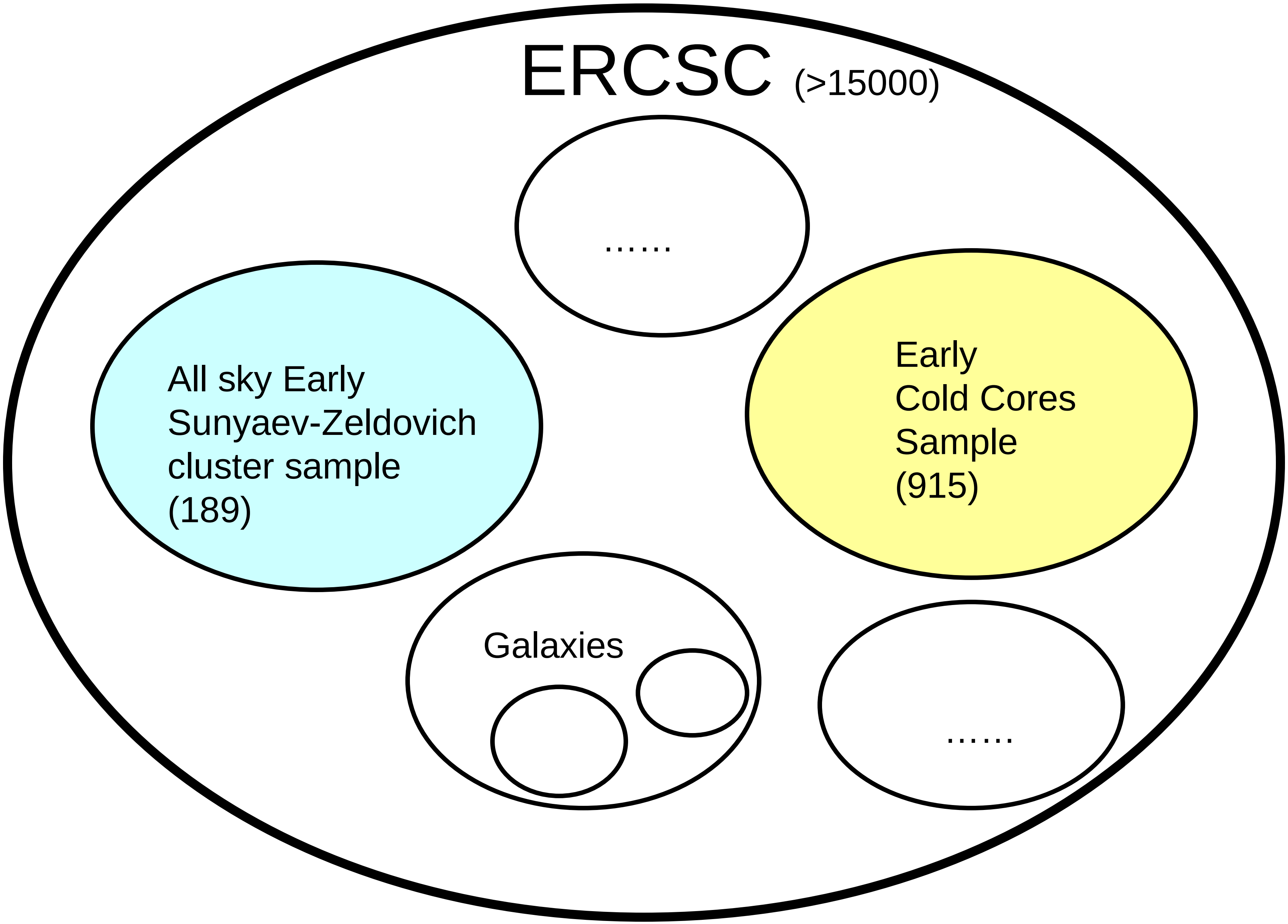

ERCSC (>15000)
......
All sky Early Sunyaev-Zeldovich cluster sample (189)
Early Cold Cores Sample (915)
Galaxies
......

Anomalous Microwave Emission

- Anomalous Microwave Emission (AME) has been detected by a number of experiments, at frequencies ~ 10–60 GHz.
- A number of physical emission mechanisms have been proposed, with electric dipole radiation from small spinning dust grains (“spinning dust”; Draine & Lazarian 1998) being the most widely accepted.

Spectrum of the Orion Nebula (a “regular” HII region used for comparison)
Note the agreement (better than 1%) between Planck and WMAP data

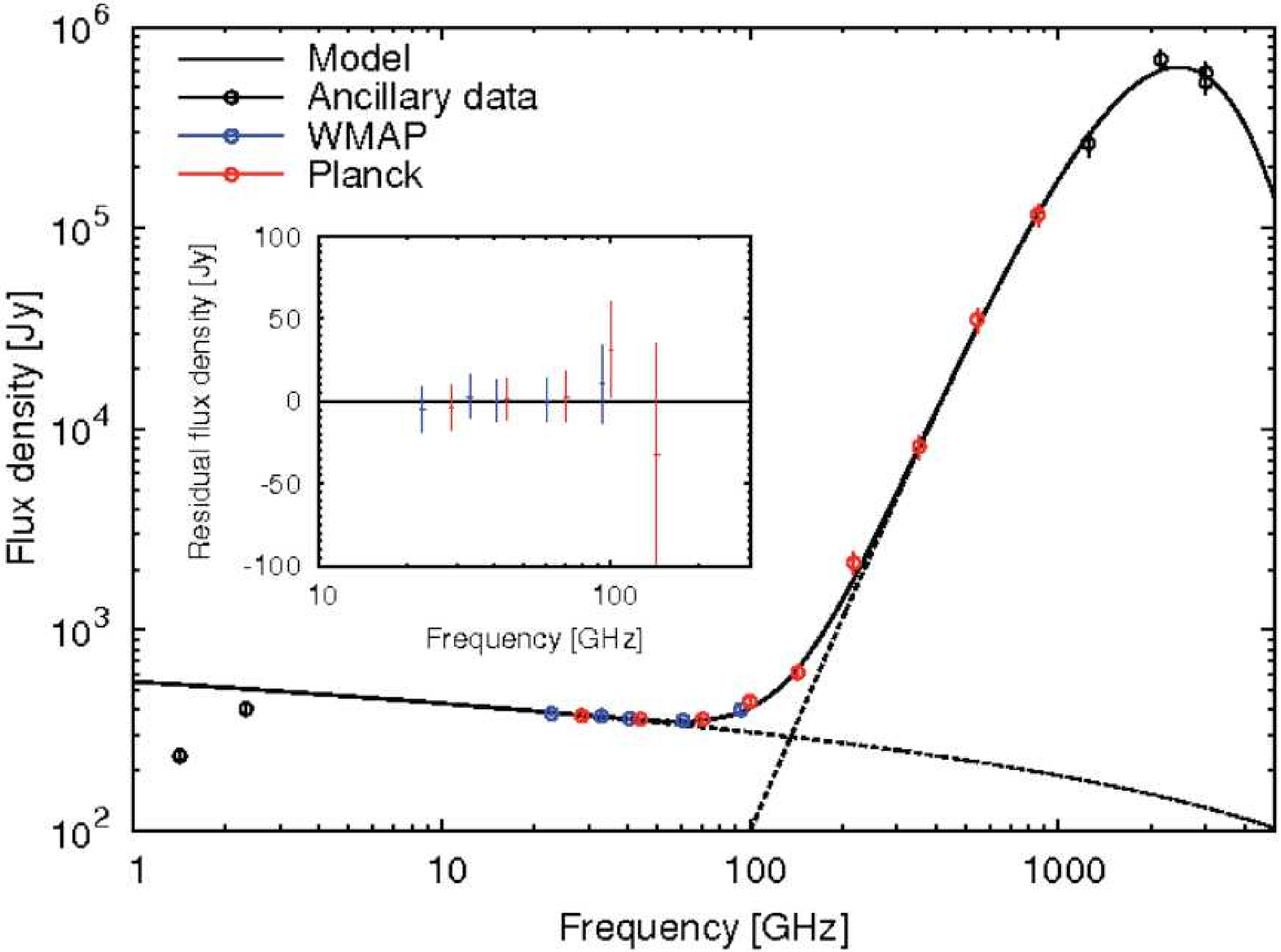

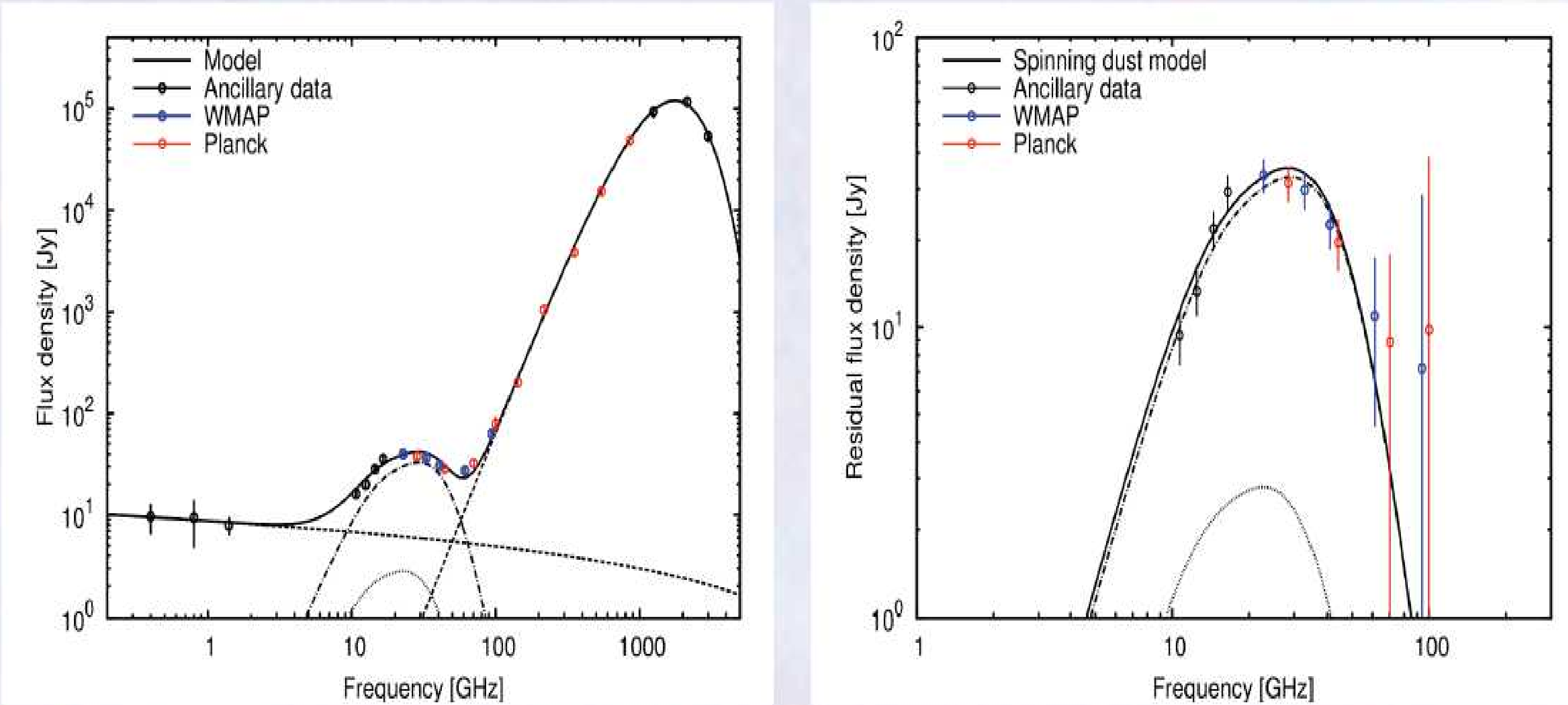

Fig. 3 Spectra for G162.26-18.62. Left: integrated spectrum. The best-fitting model for free-free, thermal dust and spinning dust is shown. Right: residual spectrum after removal of free-free, CMB and thermal dust components. The spinning dust model consists of 2 components for high density molecular gas (dashed line) and low density atomic gas (dotted line).

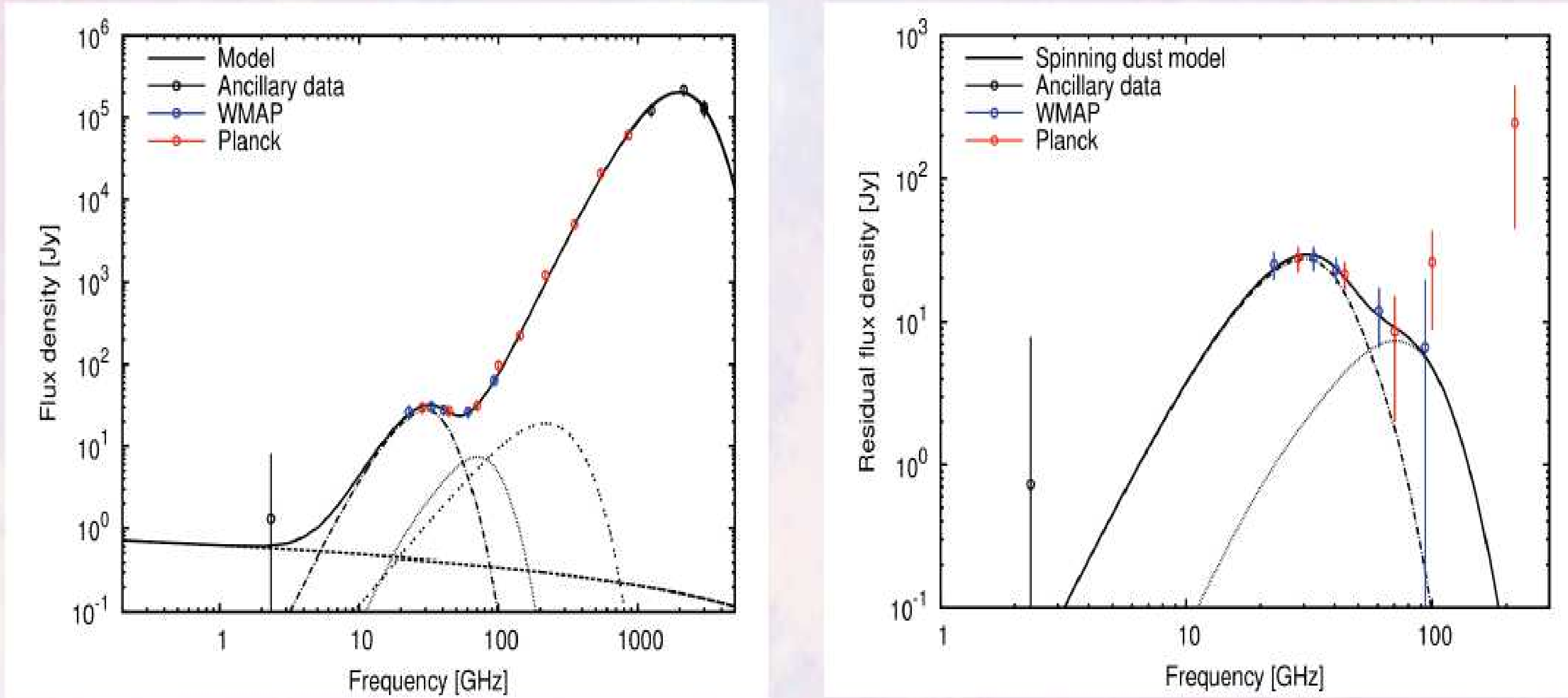

Fig. 5 *Spectra for G353.05+16.90. Left: integrated spectrum. The best-fitting model for free-free, thermal dust, CMB and spinning dust is shown. Right: residual spectrum after removal of free-free, CMB and thermal dust components. The spinning dust model consists of 2 components for high density molecular gas (dashed line) and irradiated low density atomic gas (dotted line).*

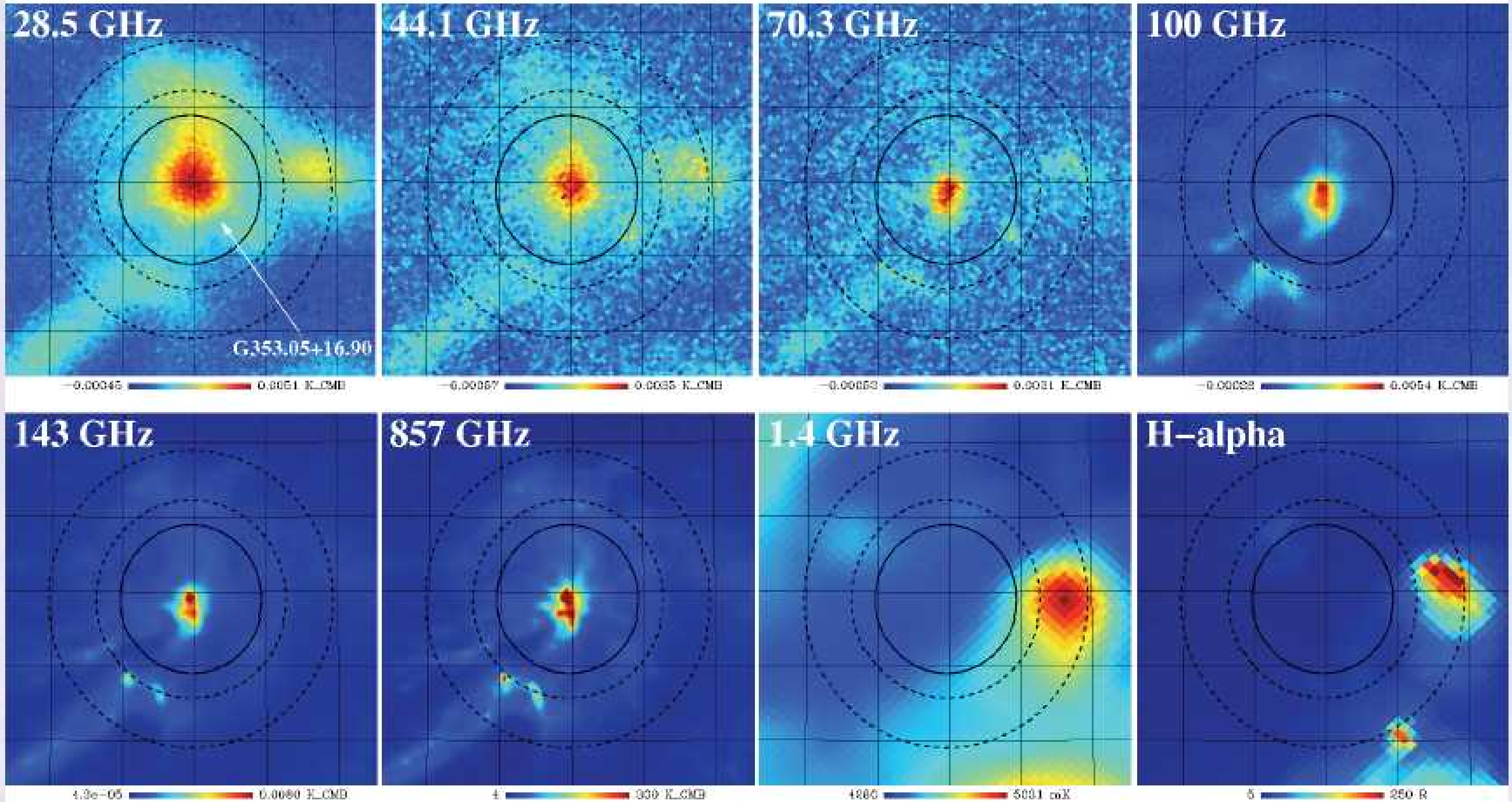

Fig. 4 *Maps of the ρ Ophiuchus molecular cloud region at their original angular resolution. From left to right, top row: Planck 28.5, 44.1, 70.3 and 100 GHz, bottom row: Planck 143 and 857 GHz, 1.4 GHz and Hα. The maps cover 5 deg on a side centered on (l,b) = (353.05,+16.90) and have linear color scales. The graticule has 1 deg spacing. The circular aperture and background annulus, used to calculate the flux density, is indicated. The strong AME is evident at 28.5 and 44.1 GHz.*

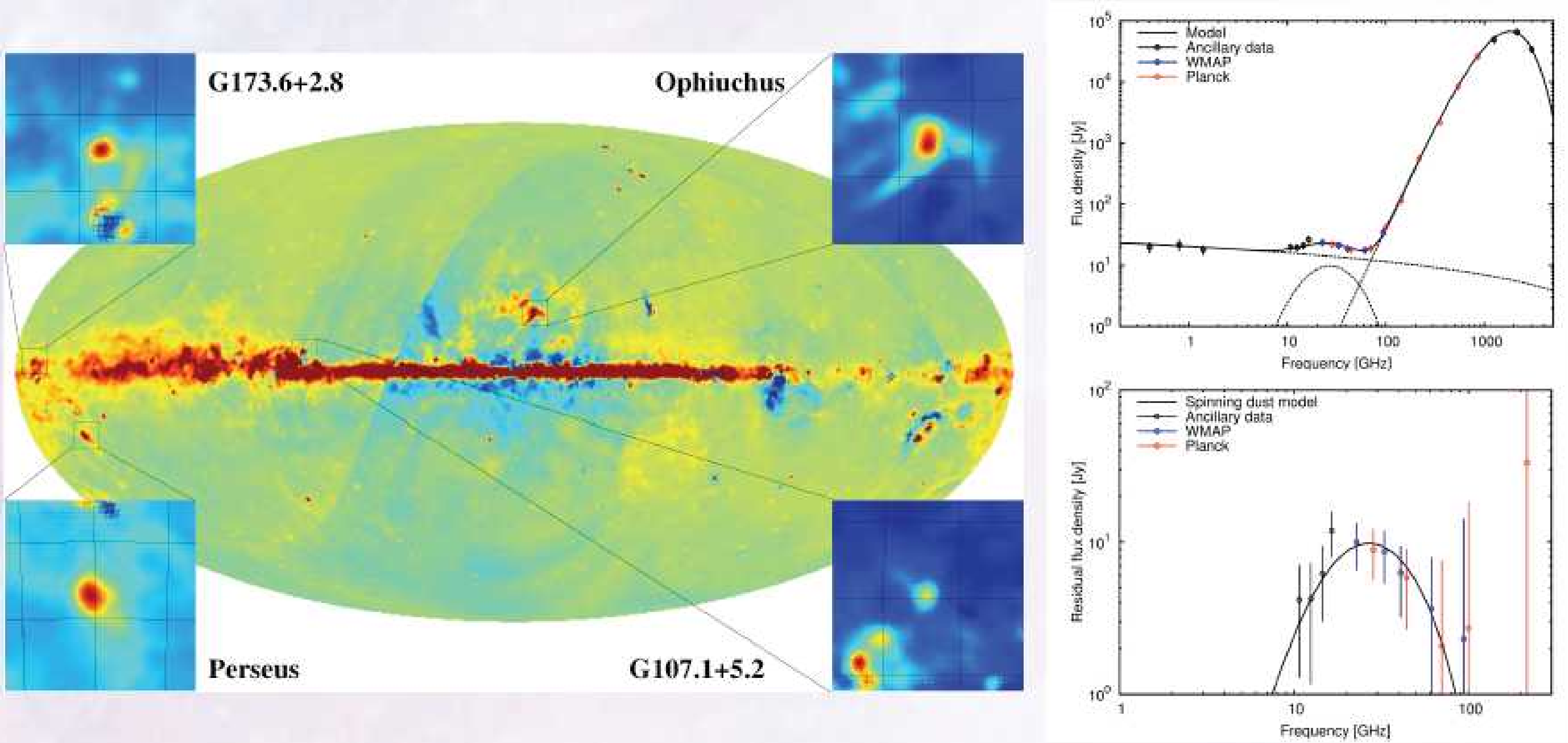

Fig. 6 *Left: Full-sky residual AME map at 28.5 GHz map after subtraction of synchrotron, free-free and thermal dust components. Cut-out maps of Perseus, Ophiuchus, and two new AME regions, are shown. Right: Integrated (top) and residual (bottom) spectrum for one of two new AME regions (G173.6+2.8). The spectrum is well-fitted by free-free, thermal dust and spinning dust components.*

First all-sky CO survey from Planck

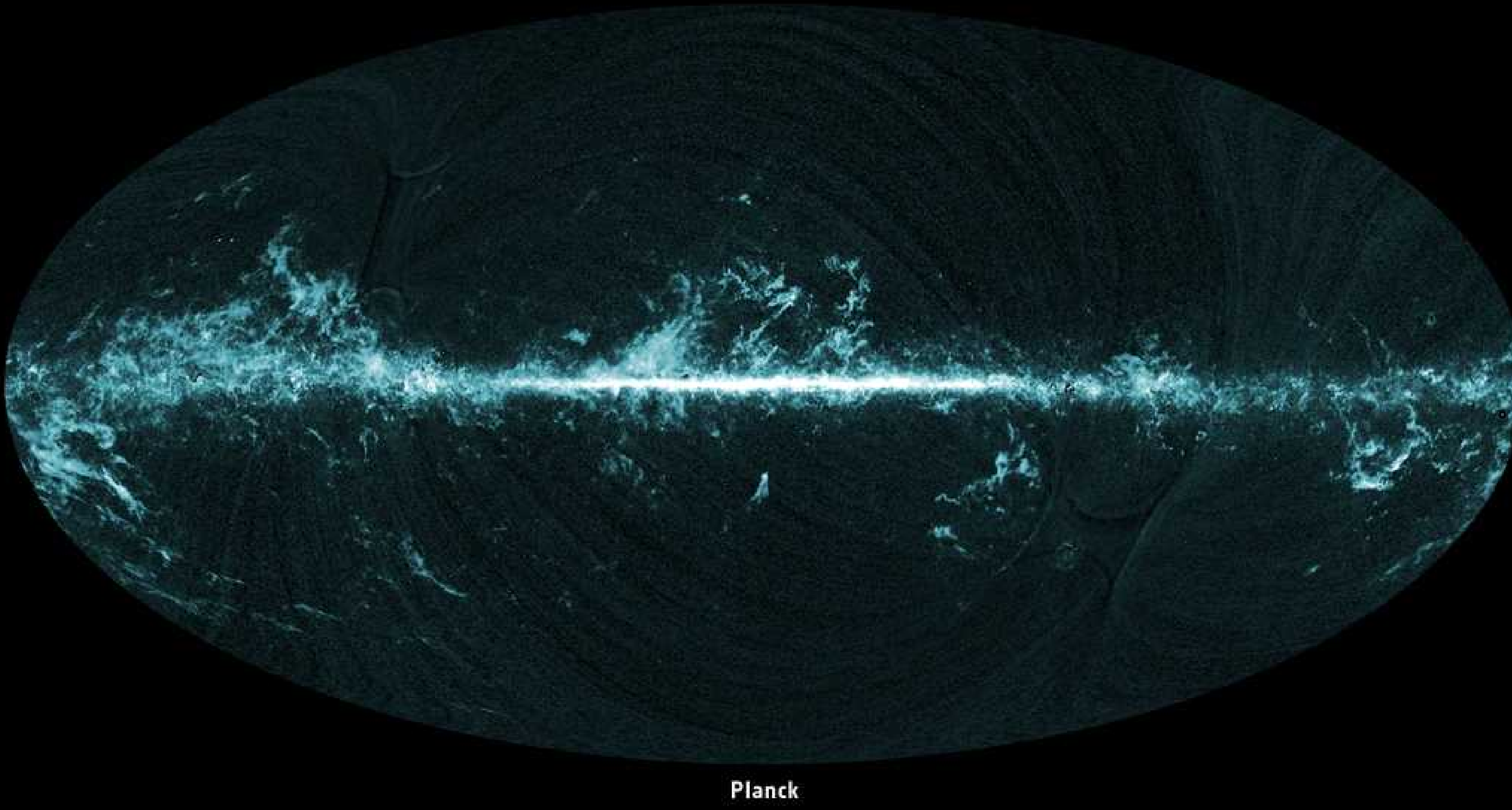

Feb. 2012

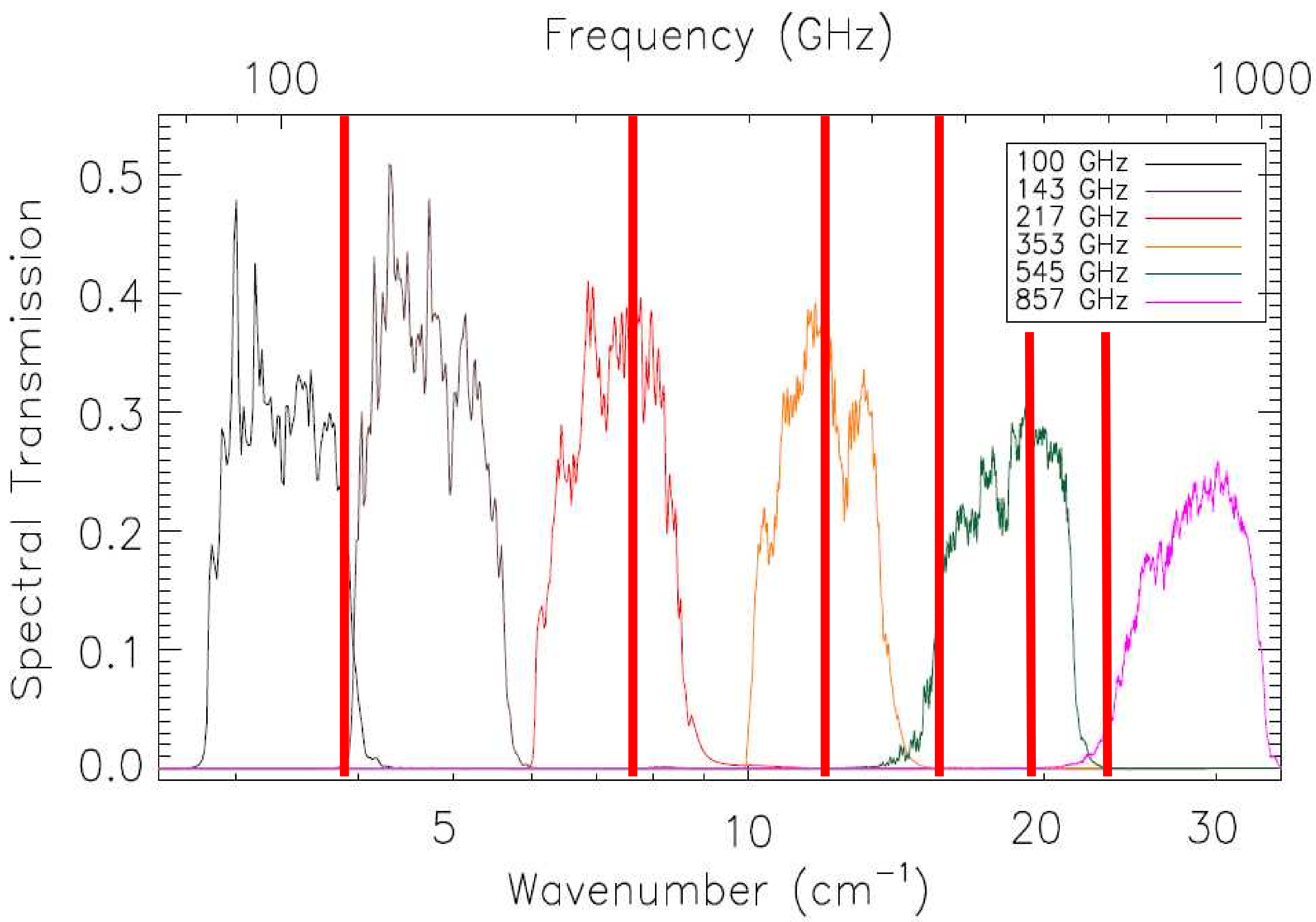

Frequency (GHz)
100
1000
Spectral Transmission
0.0
0.1
0.2
0.3
0.4
0.5
100 GHz
143 GHz
217 GHz
353 GHz
545 GHz
857 GHz
5
10
20
30
Wavenumber (cm^{-1})

After Planck

- New experiments have many more detectors than Planck (Sensitivity issue 1.)
- However,
  - it is difficult to obtain the same wide sky and frequency coverage if you are not working from space.
  - Sidelobes rejection is a big issue for large-scale surveys
- So I believe that the final word for primordial B-modes will come from a new space-based experiment
- Current and planned experiments are extremley useful to invent and test new configurations, to minimize and/or fully control systematic effects.

1. Sensitivity

- Reduce noise from the environment
  - Radiation noise from instrument, window, telescope, atmosphere
  - Get to astrophysical background limited conditions
  - Thermal noise in the detector

Space
+
Cryogenics

- Increase the number of detectors to boost the mapping speed.

Large Arrays of mm-wave detectors

Detector Arrays (ACDC & RIC projects)

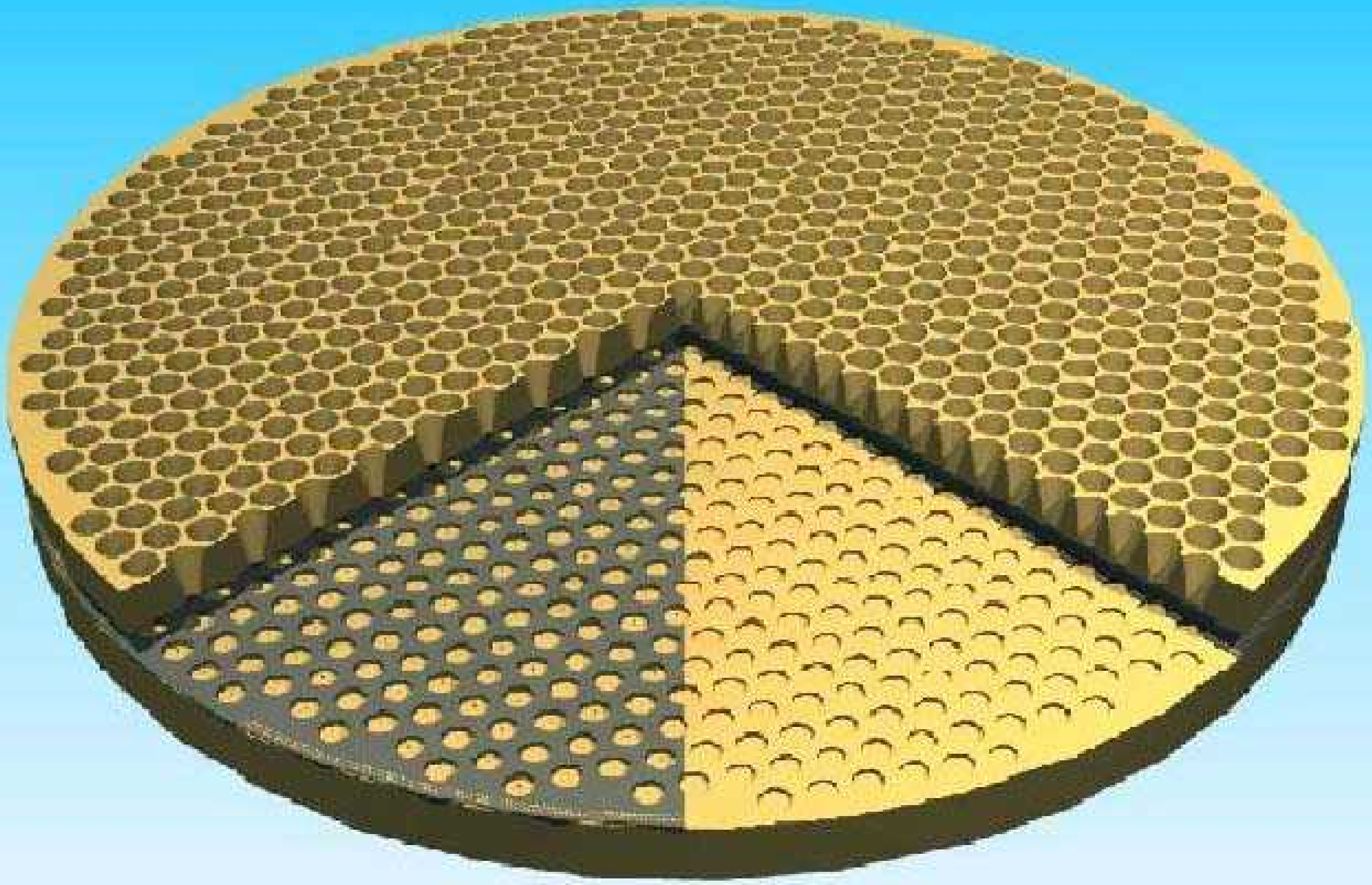

KIDs testbench: RIC INFN V

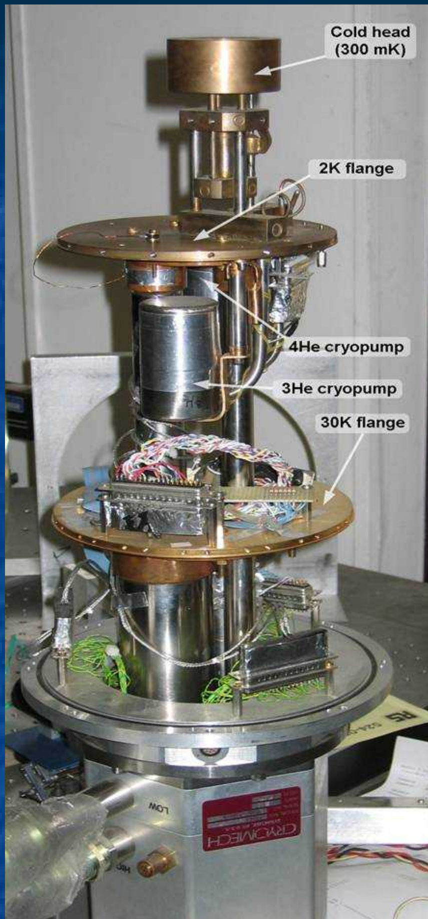

Cryostat modified to have RF ports

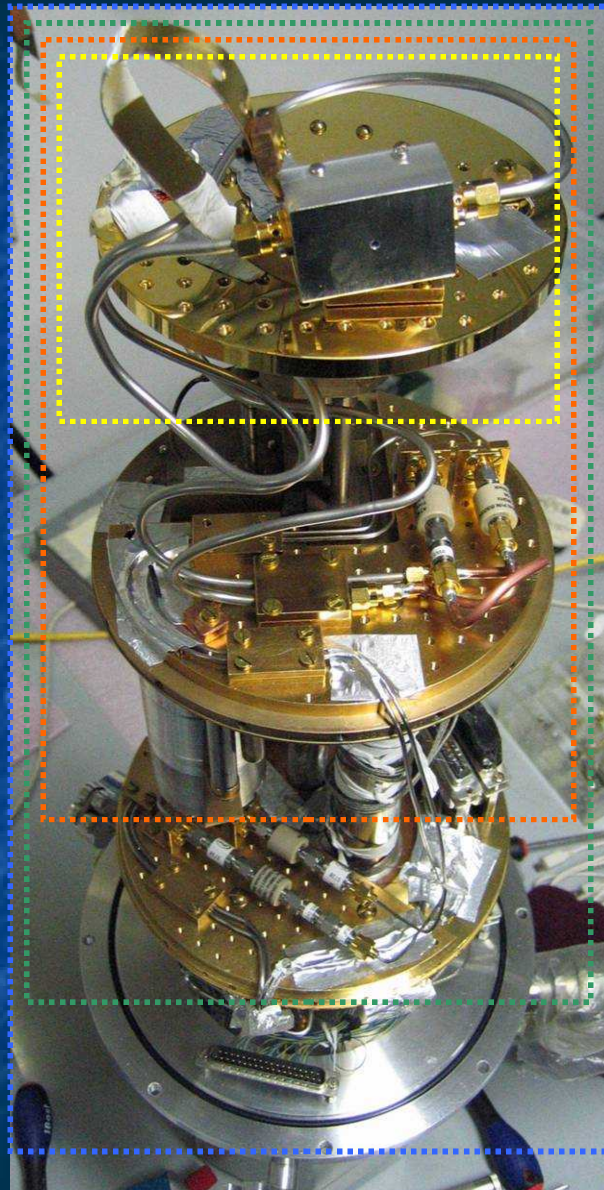

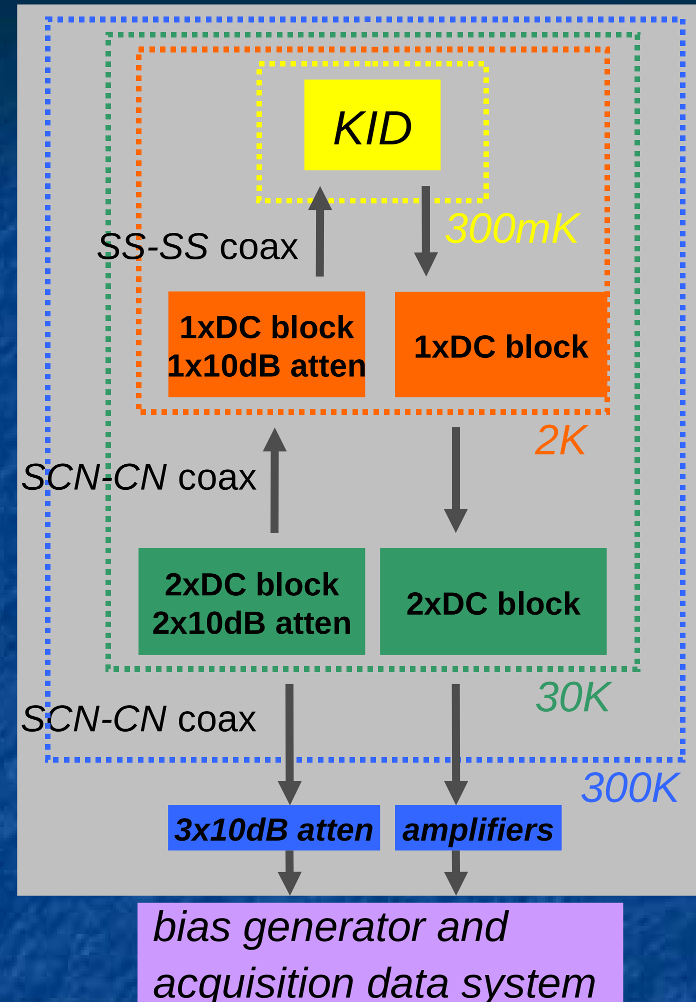

VNA : slower, easier, can give information on the sanity of the whole circuit. Ideal for the first runs.

IQ mixers: faster, essential to measure noise, QP lifetime... Need fast acquisition system

KIDs testbench: cryogenic system and RF circuit

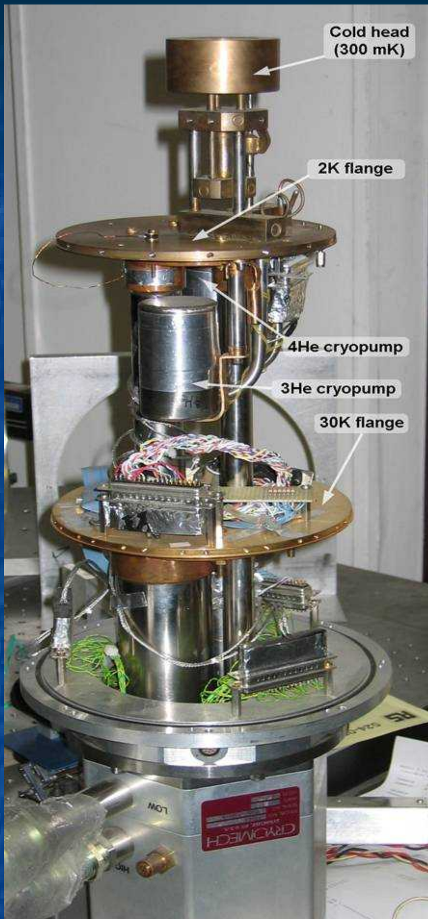

Cryostat modified to have RF ports

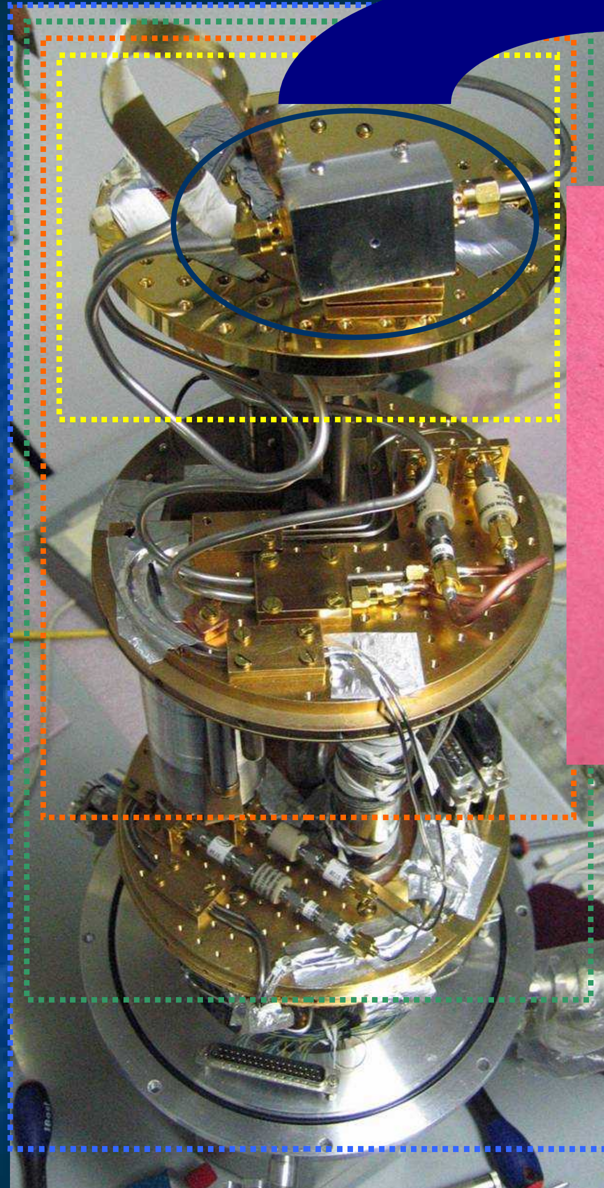

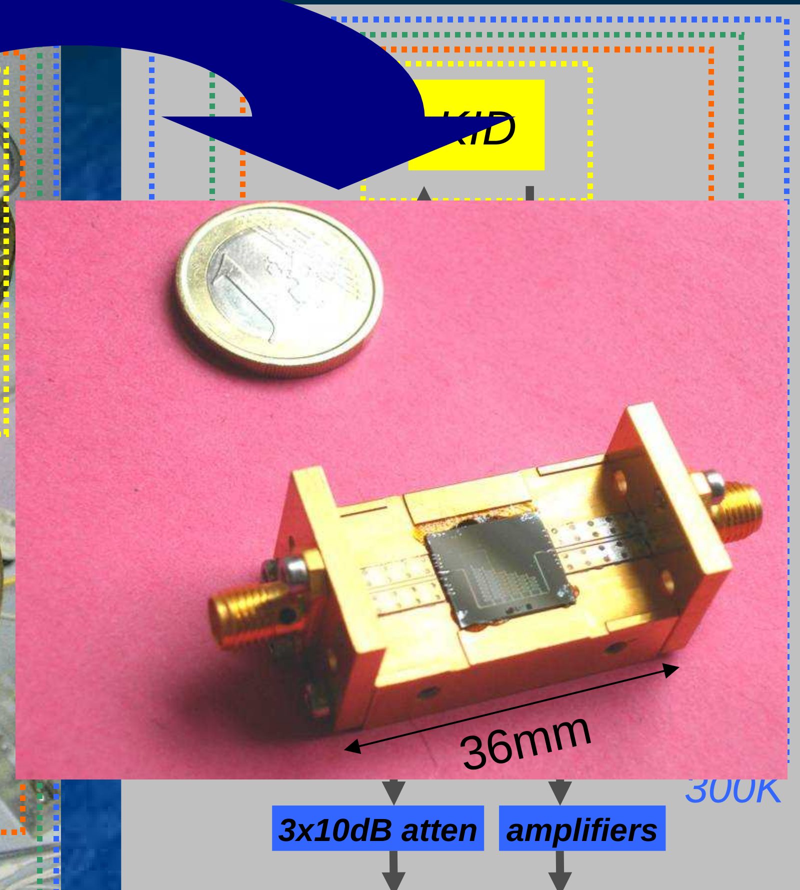

bias generator and acquisition data system

VNA : slower, easier, can give information on the sanity of the whole circuit. Ideal for the first runs.

IQ mixers: faster, essential to measure noise, QP lifetime... Need fast acquisition system

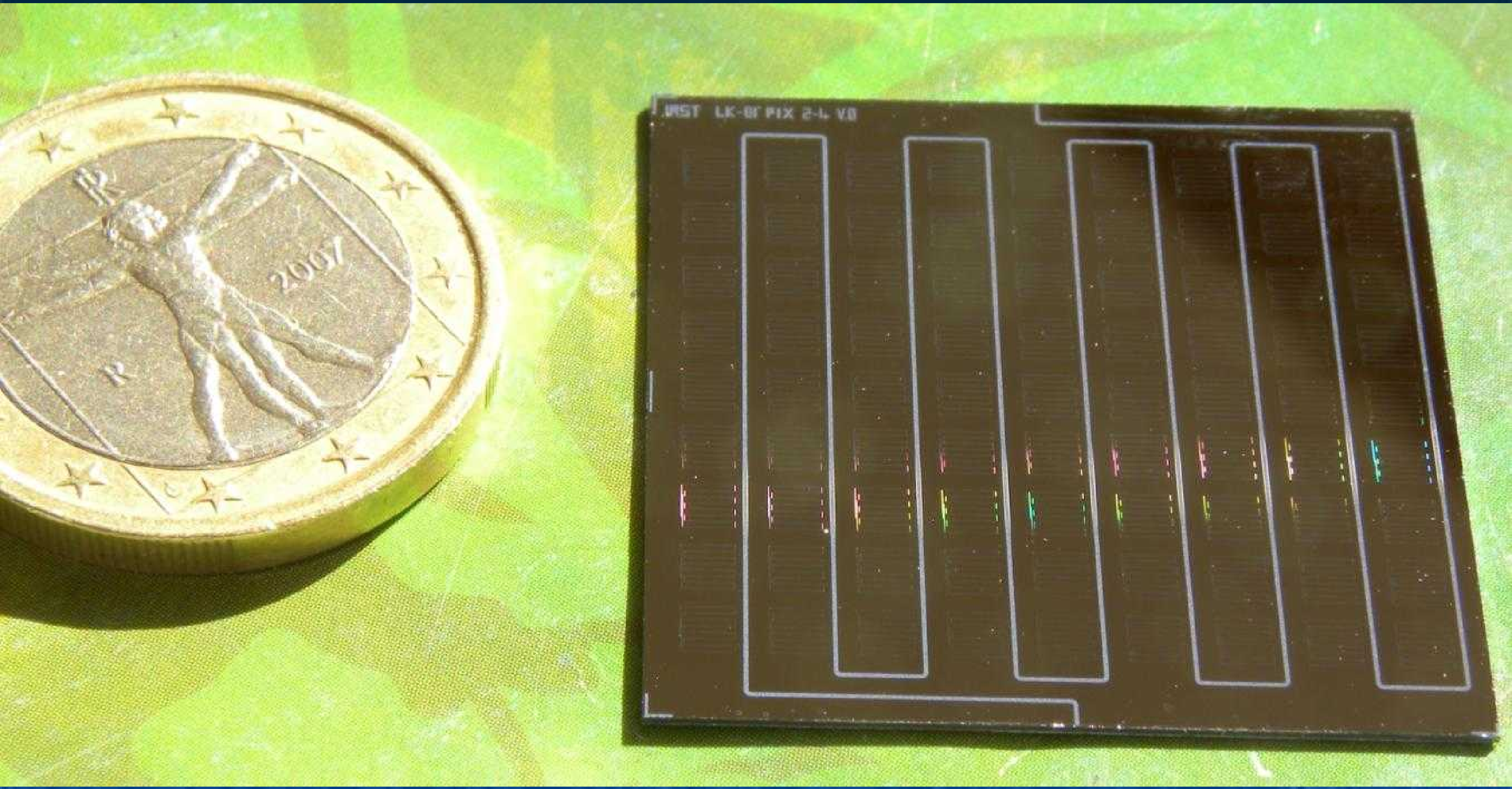

Array of 81 LKID
built by the RIC (INFN gruppo V) and ACDC (PNRA) collaborations

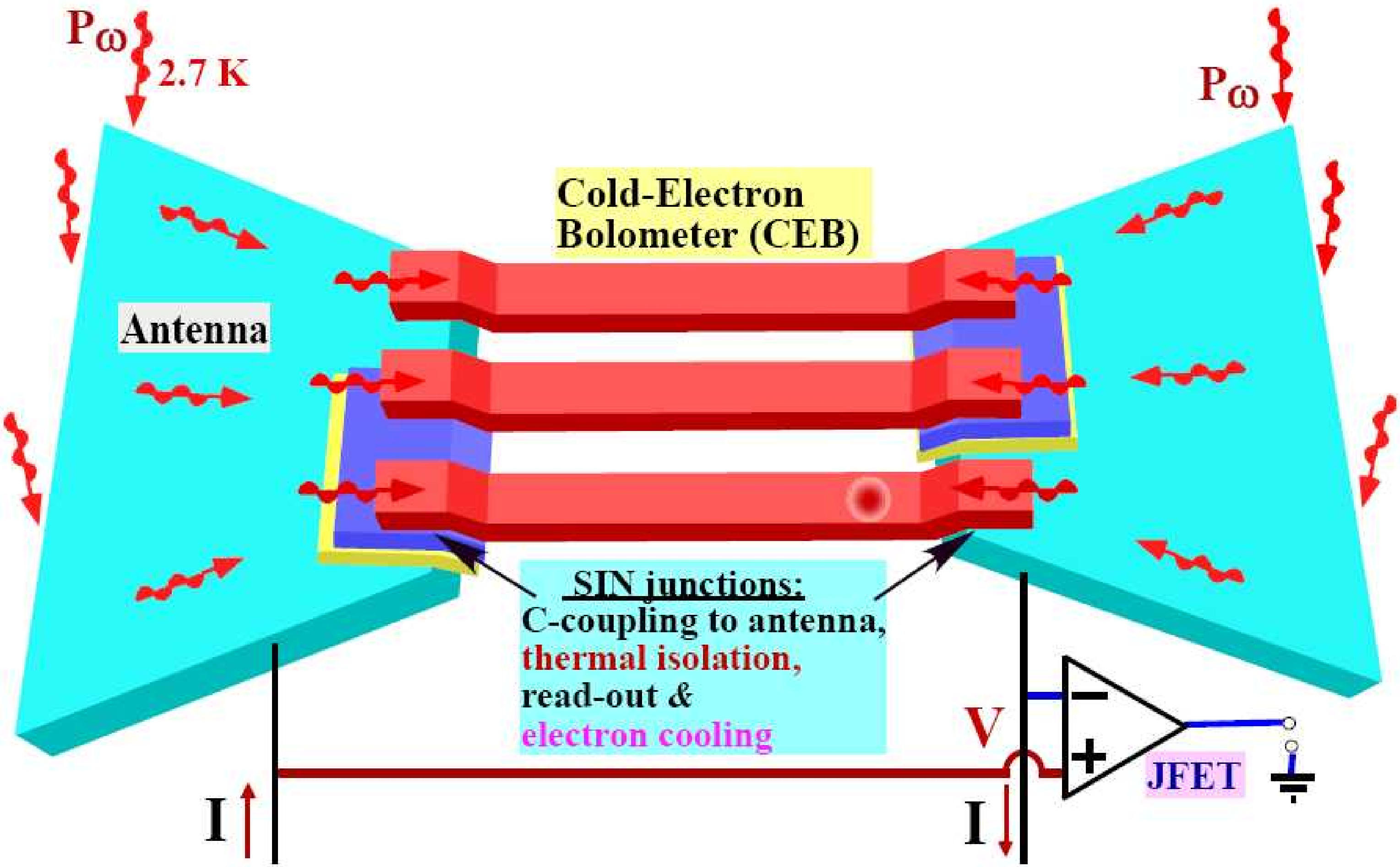

CEB Idea and development: Leonid Kuzmin and collaborators

CEBs: Cold Electrons Bolometers

- The concept is based on combination of several functions in a SIN tunnel junction:
  - RF capacitive coupling and effective thermal isolation
  - effect of electron cooling
  - temperature sensing
- The responsivity of CEB is extremely high due to the small volume of an absorber and a very low temperature.
- The CEB can reach remarkable sensitivities of NEP~10–19 W/Hz1/2 for space-borne telescopes with small optical power load.

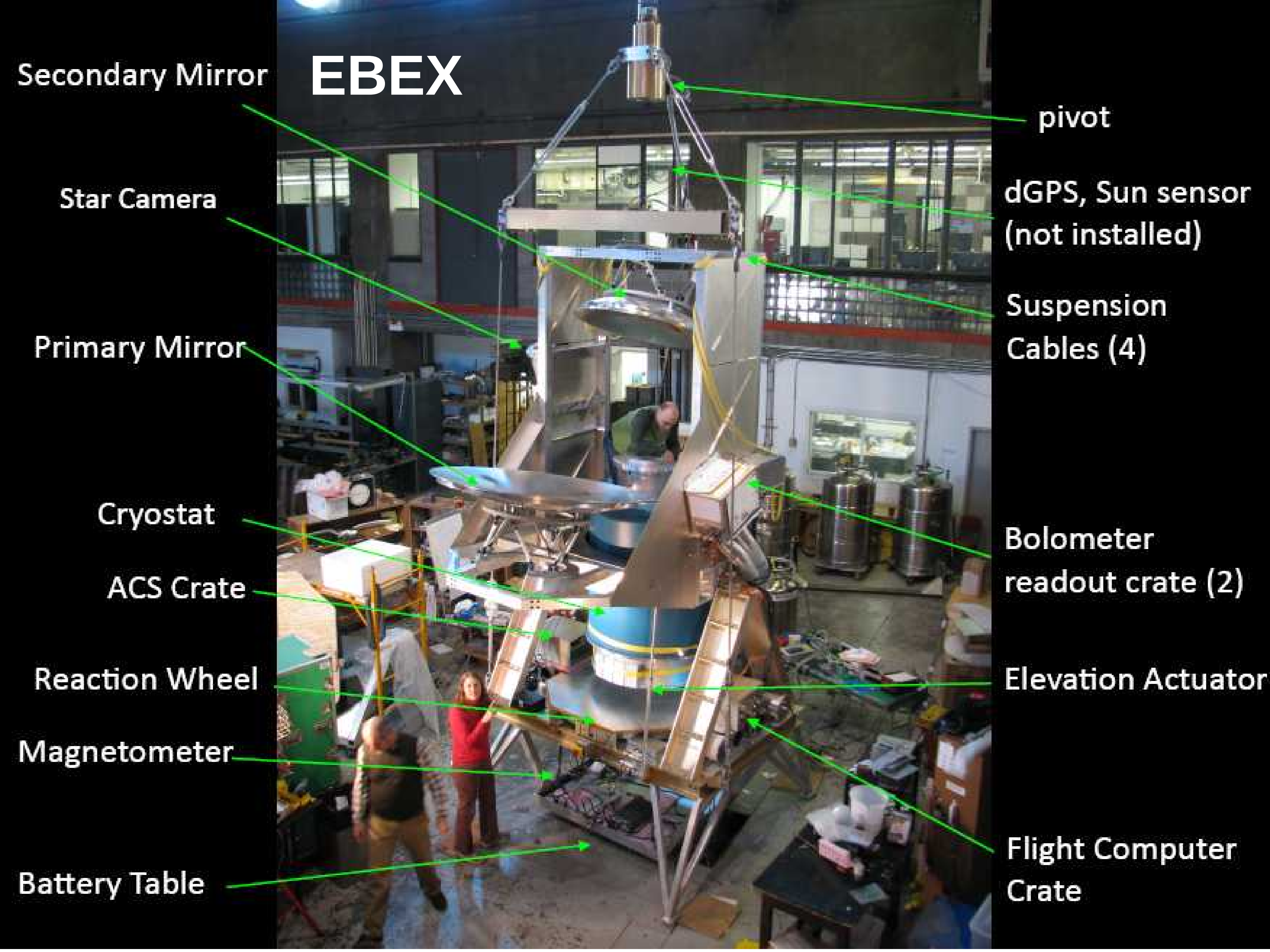
EBEX
Secondary Mirror
Star Camera
Primary Mirror
Cryostat
ACS Crate
Reaction Wheel
Magnetometer
Battery Table
pivot
dGPS, Sun sensor
(not installed)
Suspension
Cables (4)
Bolometer
readout crate (2)
Elevation Actuator
Flight Computer
Crate

EBEX Focal Plane

738 element array   141 element hexagon   Single TES

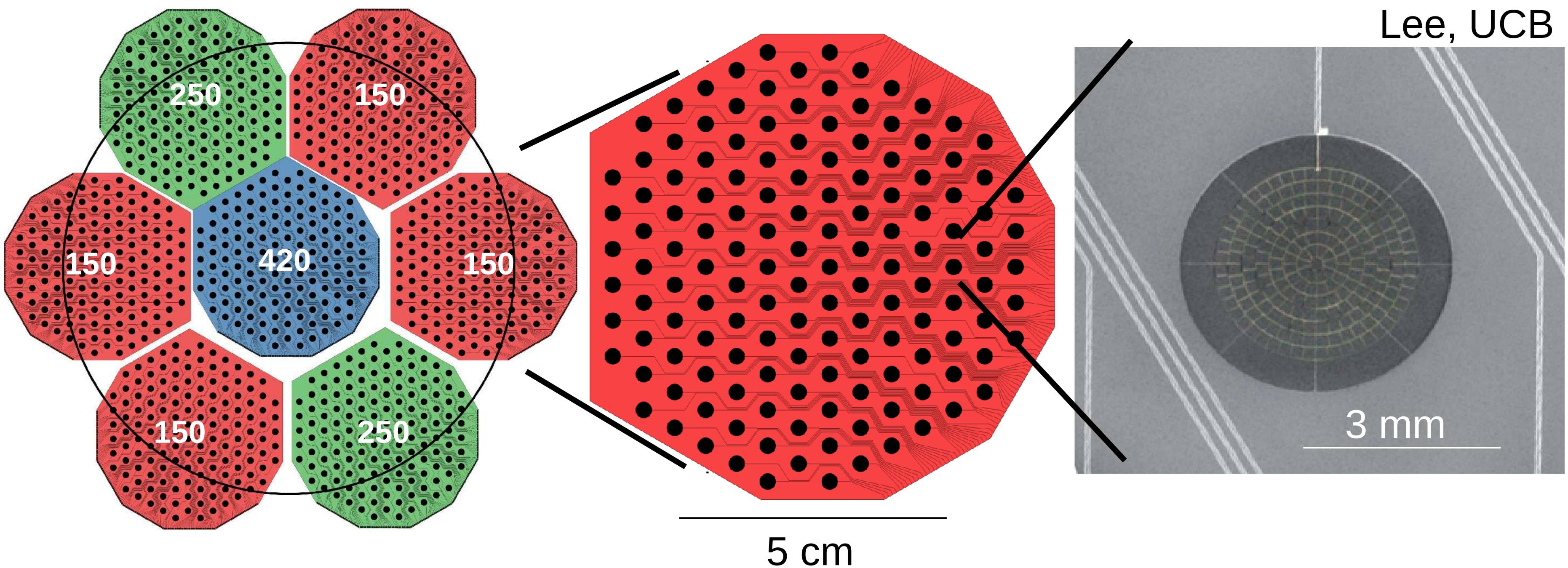

- Total of 1476 detectors
- Maintained at 0.27 K
- 3 frequency bands/focal plane

- G=15-30 pWatt/K
- NEP = 1.4e-17 (150 GHz)
- NEQ = 156 μK*rt(sec) (150 GHz)
- $\tau = 3$ msec,

Slide: Hanany

Science Goals

- Detect or set upper bound on inflation B-mode
- Measure lensing B-mode
- Understand Polarized Dust
- Improve estimation of cosmological parameters

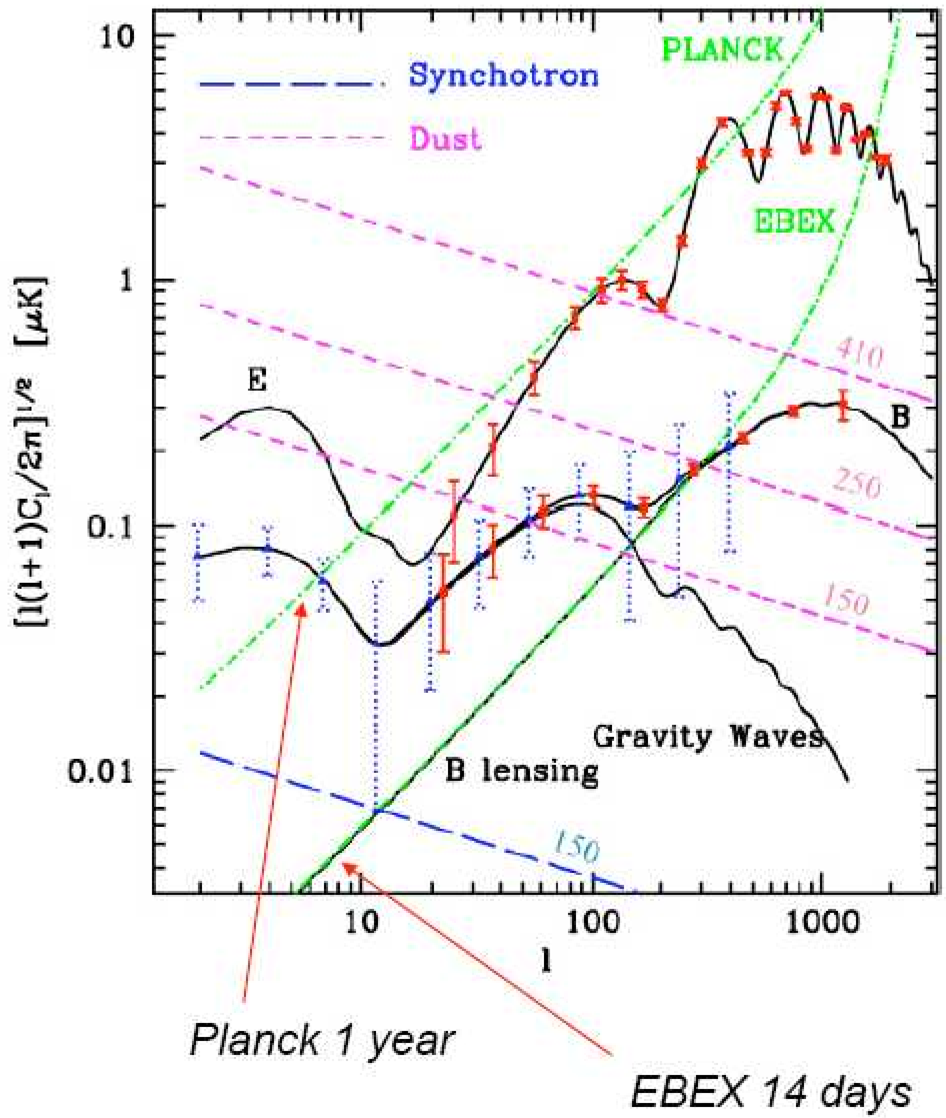

Focal Plane Hardware

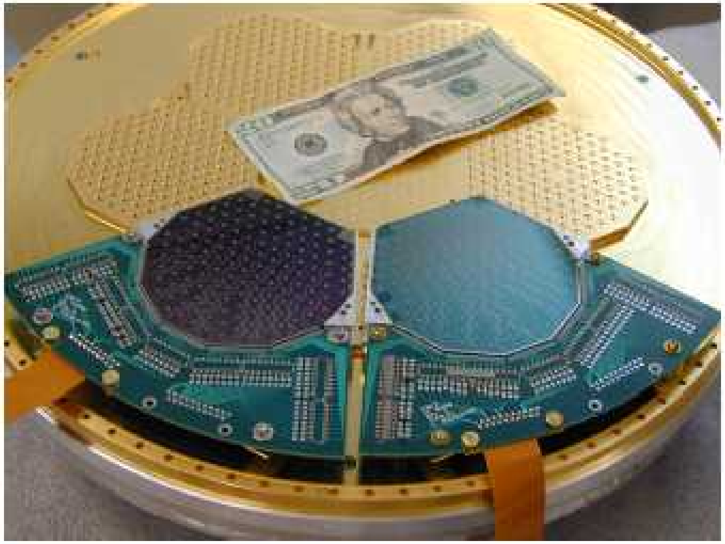

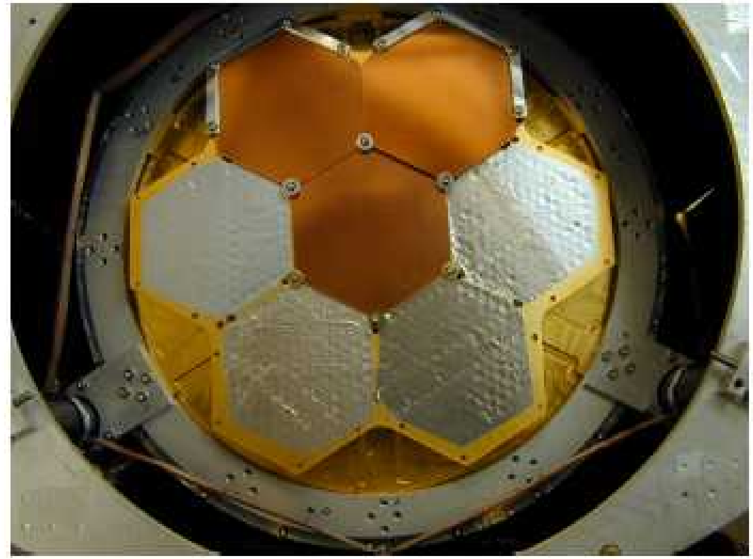

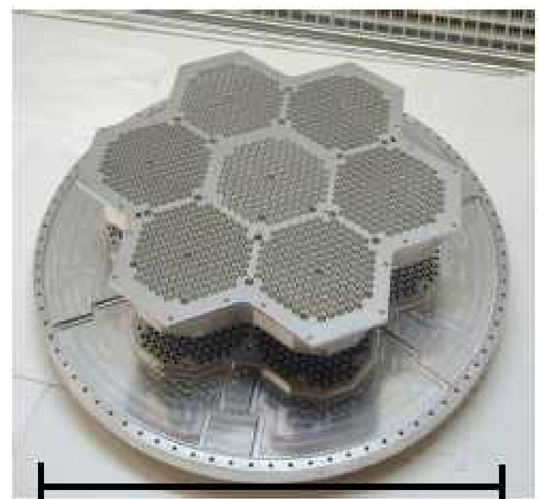

36 cm

SPIDER

Suborbital Polarimeter for Inflation Dust and the Epoch of Reionization

William Jones

Princeton University

for the

Spider Collaboration

The Path to CMBpol

June 31, 2009

Spider: A Balloon Borne CMB Polarimeter

Suborbital **P**olarimeter for **I**nflation **D**ust and the **E**poch of **R**eionization

- Long duration (~30 day cryogenic hold time) balloon borne polarimeter
- Surveys 60% of the sky each day of the flight, with ~0.5 degree resolution
- Broad frequency coverage to aid in foreground separation
- Will extract nearly all the information from the CMB E-modes
- Will probe B-modes on scales where lensing does not dominate
- Technical Pathfinder: solutions appropriate for a space mission

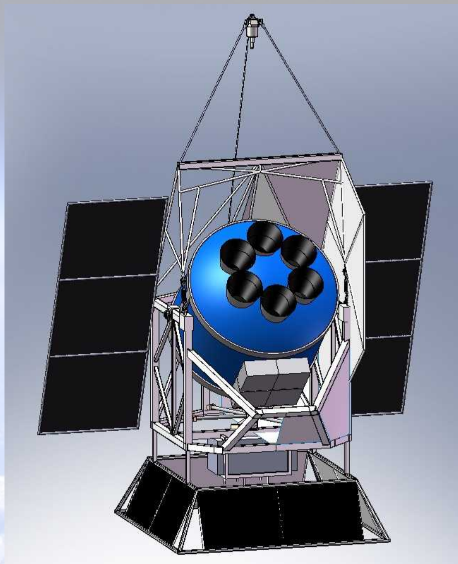

NASA CSA ASC C.S.B.F. PALESTINE, TEXAS NSERC CRSNG JPL CALIFORNIA INSTITUTE OF TECHNOLOGY UNIVERSITY OF TORONTO CASE WESTERN RESERVE UNIVERSITY EST. 1826 CARDIFF UNIVERSITY PRIFYSGOL CAERDYD UBC NIST PRINCETON UNIVERSITY CITA ICAT Canadian Institute for Theoretical Astrophysics L'institut canadien d'astrophysique théorique Imperial College London

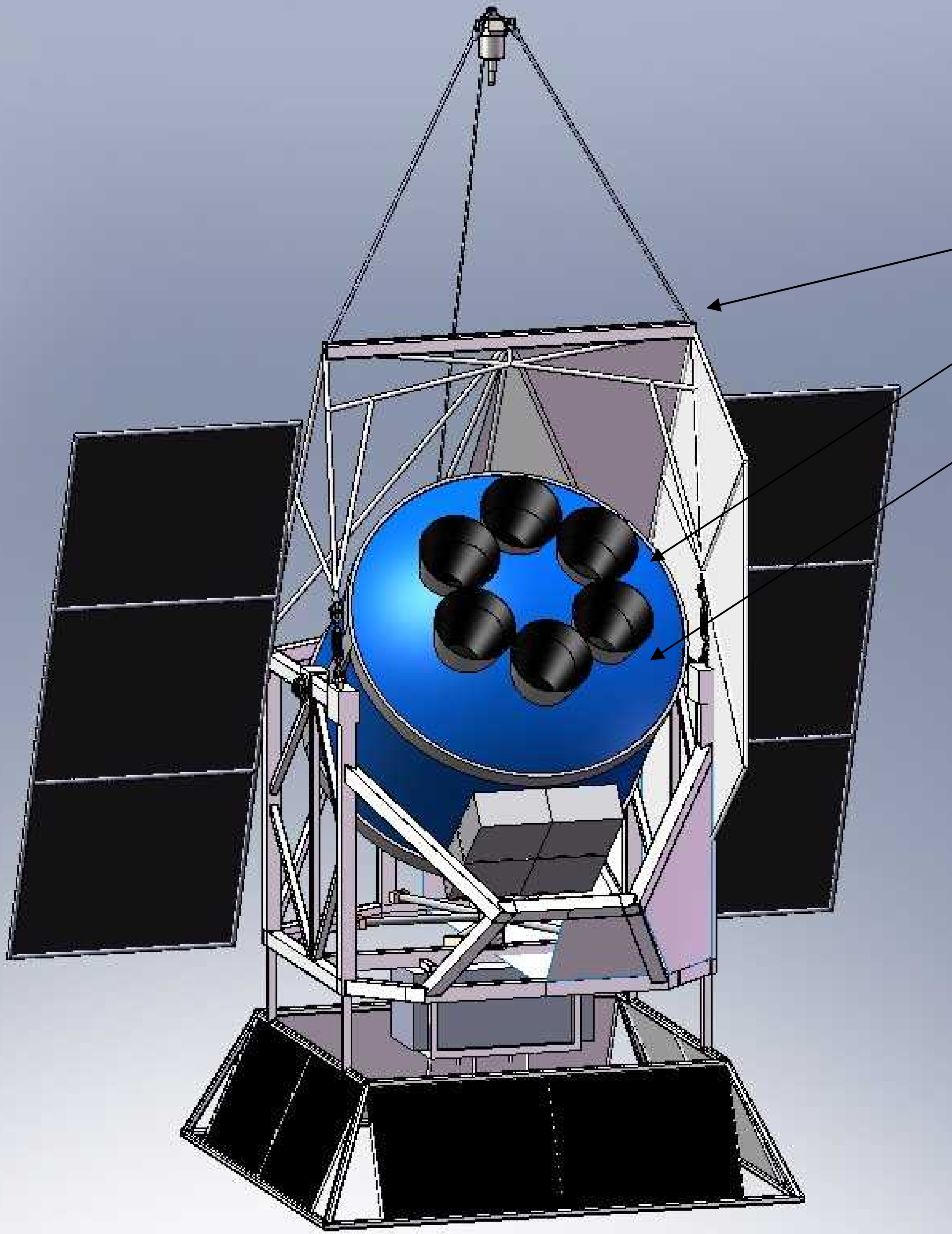

Carbon Fiber Gondola

Six single freq. telescopes

30 day, 1850 lb, 4K / 1.4 K cryostat

Attitude Control
- flywheel
- magnetometer
- rate gyros
- sun sensor

Pointing Reconstruction
- 2 pointed cameras
- boresight camera
- rate gyros

Flight Computers/ACS
- 1 TB for turnaround
- 5 TB for LDB

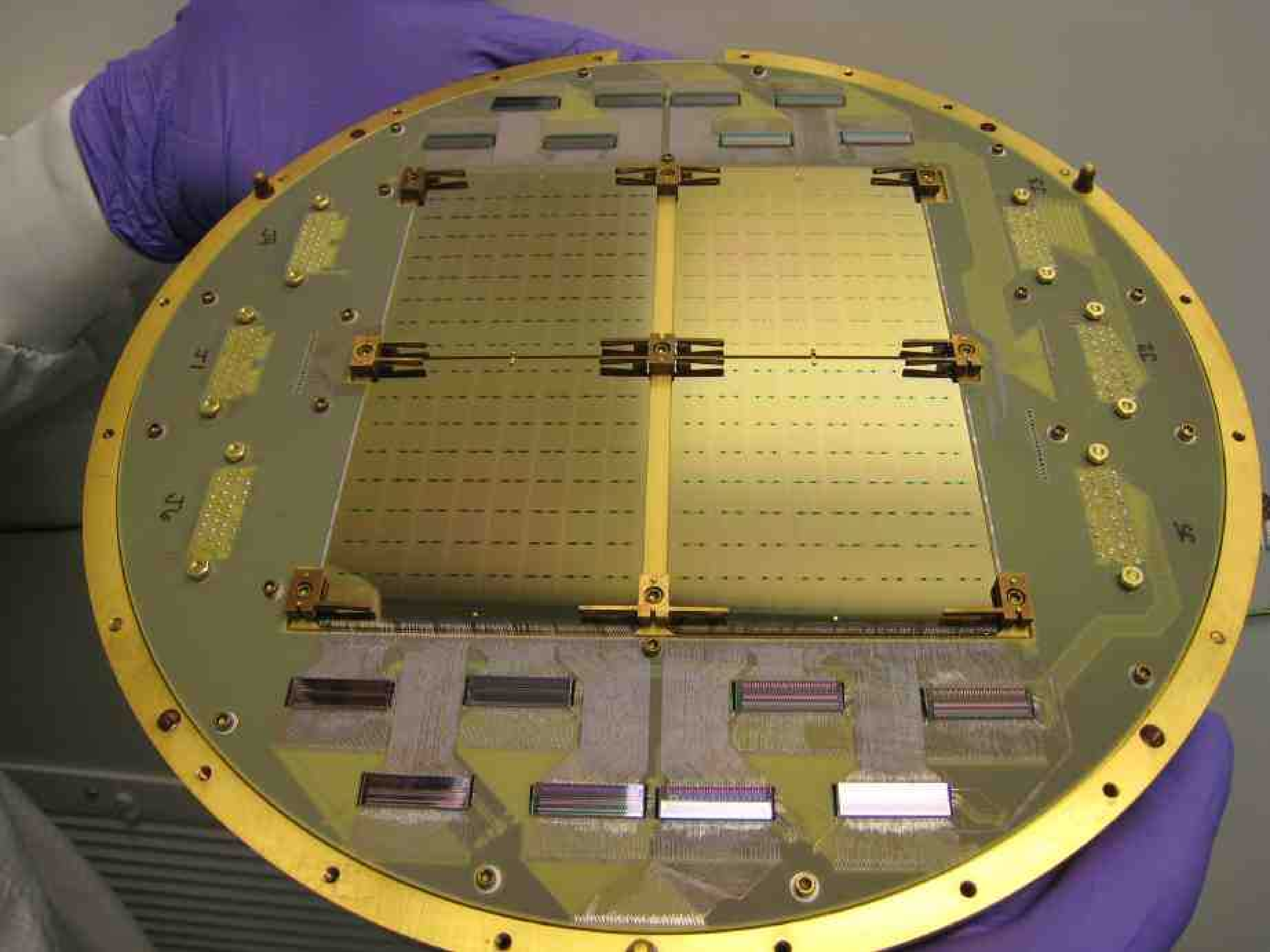

2. Control of systematic effects

- Polarized sidelobes (large baffles, space)
- Polarization modulators (many different methods)
- Orthogonal measurement methods:
  - Coherent imagers (QUIET, ..)
  - Bolometric imagers (BOOMERanG, MAXIPOL, Planck, BICEP, EBEX, SPIDER, PIPER, LSPE, …
  - Coherent interferometers (DASI, CBI, …)
  - Bolometric interferometers (MBI, QUBIC)

Astro-ph/0906.4069 Takahashi et al.

BICEP instrument characterization

TABLE 3
SYSTEMATIC ERRORS POTENTIALLY PRODUCING FALSE B-MODE POLARIZATION

	Benchmark[a]	Measured	Measurement notes	Reference
Relative gain uncertainty: $\Delta(g_1/g_2)/(g_1/g_2)$	0.9%	$<1.1\%$	Upper limit, rms error over the array.[b]	§3.1
Differential pointing: $(\mathbf{r}_1-\mathbf{r}_2)/\sigma$ [c]	1.9%	1.3%	Average, each repeatedly characterized to 0.4% precision.[d]	§3.2
Differential beam size: $(\sigma_1-\sigma_2)/\sigma$	3.6%	$<0.3\%$	Upper limit, rms over the array.	§3.2
Differential ellipticity: $(e_1-e_2)/2$	1.5%	$<0.2\%$	Upper limit, rms over the array.	§3.2
Polarization orientation uncertainty: $\Delta\psi$	2.3°	$<0.7°$	Upper limit, rms absolute orientation error over the array.	§3.3
Telescope pointing uncertainty: $\Delta\mathbf{b}$	$5'$	$0.2'$	Fit residual rms in optical star pointing calibration.	§3.4
Polarized sidelobes (100, 150 GHz)	-9, -4 dBi	-26, -17 dBi	Response at 30° from the beam center.	§3.5
Focal plane temperature stability: $\Delta T_{\rm FP}$	3 nK	1 nK	Scan-synchronous rms fluctuation on $\ell\sim100$ time scale.	§3.6
Optics temperature stability: $\Delta T_{\rm RJ}$	4 μK	0.7 μK	Scan-synchronous rms fluctuation on $\ell\sim100$ time scale.	§3.6

[a] Benchmarks correspond to values that result in a false B-mode signal of at most $r=0.1$. For $r=0.01$, all benchmarks would be lower by $\sqrt{10}$.
[b] If relative gain errors are detected, we anticipate removing their effects in future analyses using a CMB temperature template map.
[c] $\sigma = FWHM/\sqrt{8\ln(2)} = \{0.39°, 0.26°\}$ at $\{100, 150\}$ GHz.
[d] This measurement of differential pointing could be used in future analyses to remove the small predicted leakage of CMB temperature into polarization maps.

	Measured	max false B, equiv. r
1. Relative gain uncertainty: $\Delta(g_1/g_2)/(g_1/g_2)$	$< 1.1\%$	< 0.15
2. Differential pointing: $(\mathbf{r_1} - \mathbf{r_2})/\sigma$	1.3%	0.05
3. Focal plane temperature stability: ΔT_{FP}	1 nK	0.011
4. Polarization orientation uncertainty: $\Delta\psi$	$< 0.7°$	< 0.009
5. Optics temperature stability: ΔT_{RJ}	0.7 μK	0.003
6. Differential ellipticity: $(e_1 - e_2)/2$	$< 0.2\%$	< 0.002
7. Differential beam size: $(\sigma_1 - \sigma_2)/\sigma$	$< 0.3\%$	< 0.0007
8. Polarized sidelobes (100, 150 GHz)	-26, -17 dBi	0.0002
9. Telescope pointing uncertainty: $\Delta\mathbf{b}$	$0.2'$	0.0002

The result from BICEP 2 years is a 95% upper limit r < 0.73

Enitrely dominated by receiver noise and relative gain uncertainty .

	Measured	max false B, equiv. r
1. Relative gain uncertainty: $\Delta(g_1/g_2)/(g_1/g_2)$	$< 1.1\%$	< 0.15
2. Differential pointing: $(\mathbf{r_1} - \mathbf{r_2})/\sigma$	1.3%	0.05
3. Focal plane temperature stability: $\Delta T_{\rm FP}$	1 nK	0.011
4. Polarization orientation uncertainty: $\Delta\psi$	$< 0.7^\circ$	< 0.009
5. Optics temperature stability: $\Delta T_{\rm RJ}$	$0.7\ \mu$K	0.003
6. Differential ellipticity: $(e_1 - e_2)/2$	$< 0.2\%$	< 0.002
7. Differential beam size: $(\sigma_1 - \sigma_2)/\sigma$	$< 0.3\%$	< 0.0007
8. Polarized sidelobes (100, 150 GHz)	-26, -17 dBi	0.0002
9. Telescope pointing uncertainty: $\Delta\mathbf{b}$	$0.2'$	0.0002

A 10x improvement is possible:

- The best way to remove relative gain uncertainty is to use the same bolometer for both polarizations i.e. insert a polarization modulator.
- Then, to improve the sensitivity, boost the number of bolometers and reduce the background. EBEX, SPIDER, PIPER, LSPE are balloon borne instruments doing exactly this.

2. Control of systematic effects

- Polarized sidelobes (large baffles, space)
- Polarization modulators (many different methods)
- Orthogonal measurement methods:
  - Coherent imagers (QUIET, ..)
  - Bolometric imagers (BOOMERanG, MAXIPOL, Planck, BICEP, EBEX, SPIDER, PIPER, LSPE, …
  - Coherent interferometers (DASI, CBI, …)
  - Bolometric interferometers (MBI, QUBIC)

low sidelobes & reduced solid angle: Planck

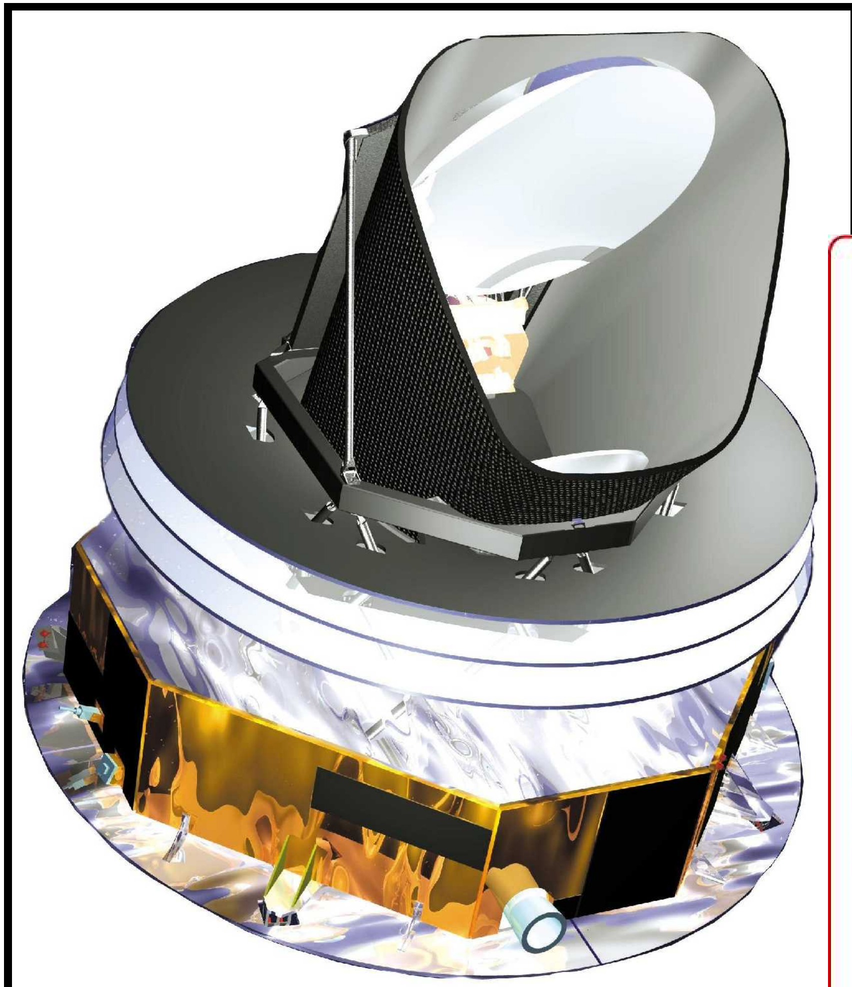

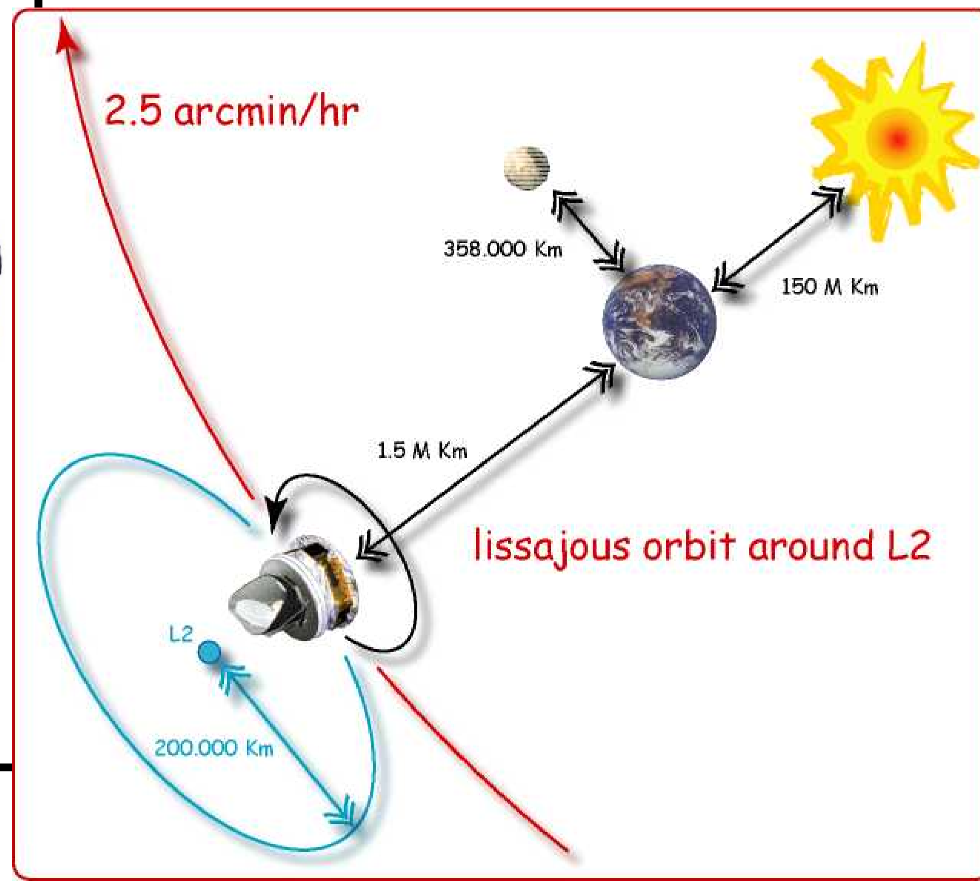

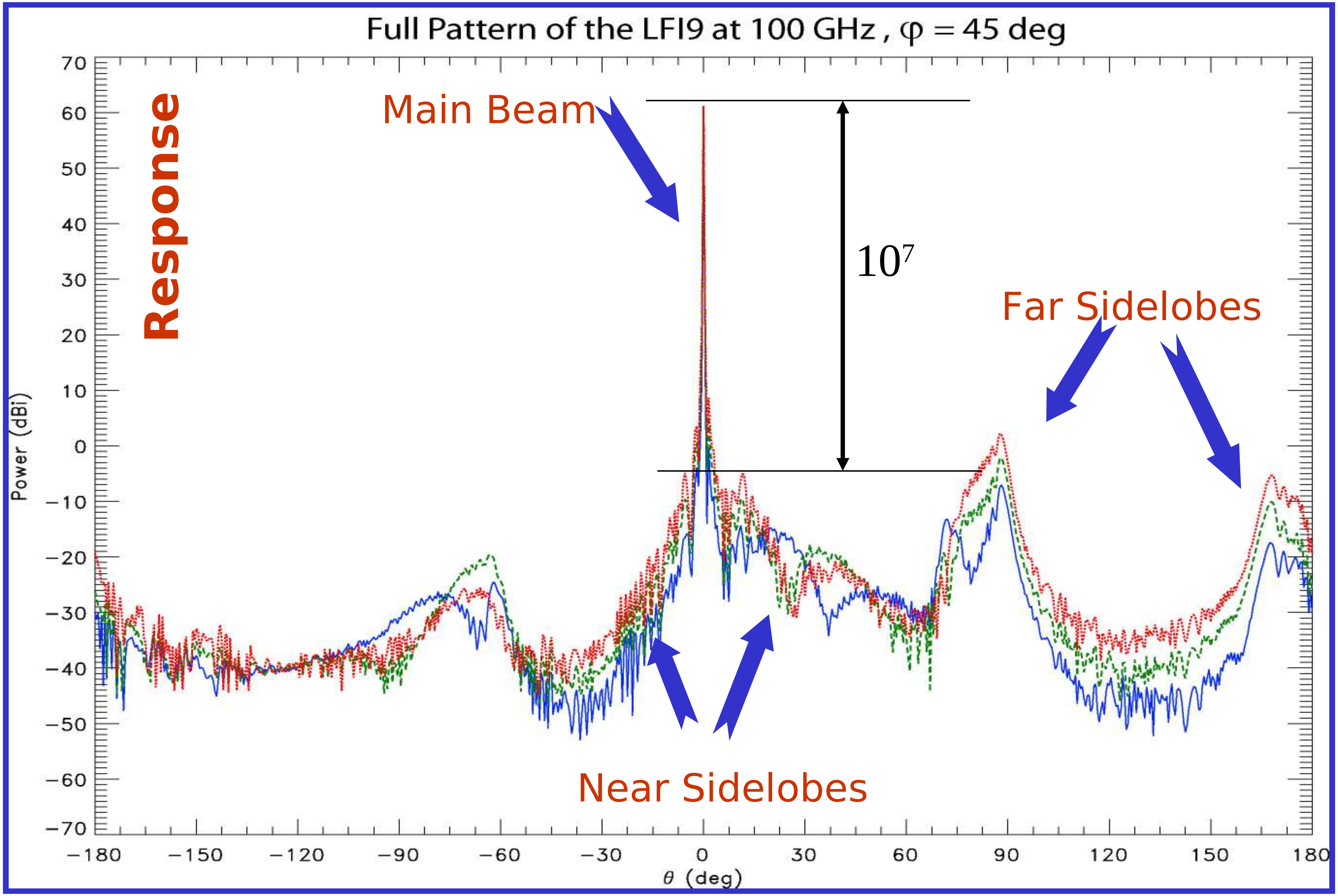

Angle from boresight

F. Villa, LFI

2. Control of systematic effects

- Polarized sidelobes
- Polarization modulators
- Orthogonal measurement methods:
  - Coherent imagers (QUIET, ..)
  - Bolometric imagers (BOOMERanG, MAXIPOL, Planck, BICEP, EBEX, SPIDER, PIPER, LSPE, …
  - Coherent interferometers (DASI, CBI, …)
  - Bolometric interferometers (MBI, QUBIC)

Polarization modulators (quasi-optical mode)

- Throughput advantage wrt coherent systems
- HWP + Polarizer (Stokes polarimetry)
  – Dielectric waveplates with ARC (EBEX, SPIDER, KECK…) Savini, Pisano, Hanany, Bryan
  – Metal mesh waveplates (LSPE …) Pisano
- Reflecting HWP (PolKA) Siringo
- VPM (Variable delay polarization modulator, PIPER) Kogut

Polarimetery with an achromatic Half Wave Plate

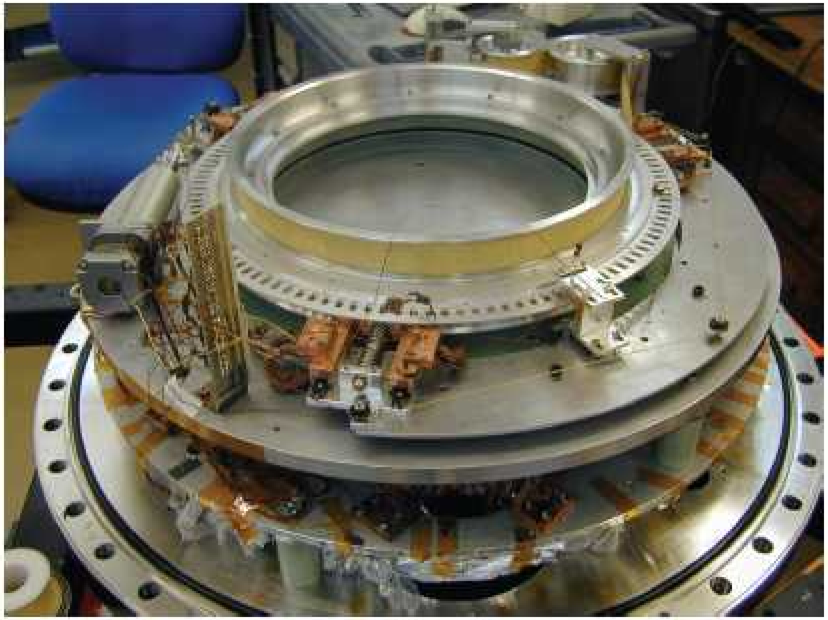

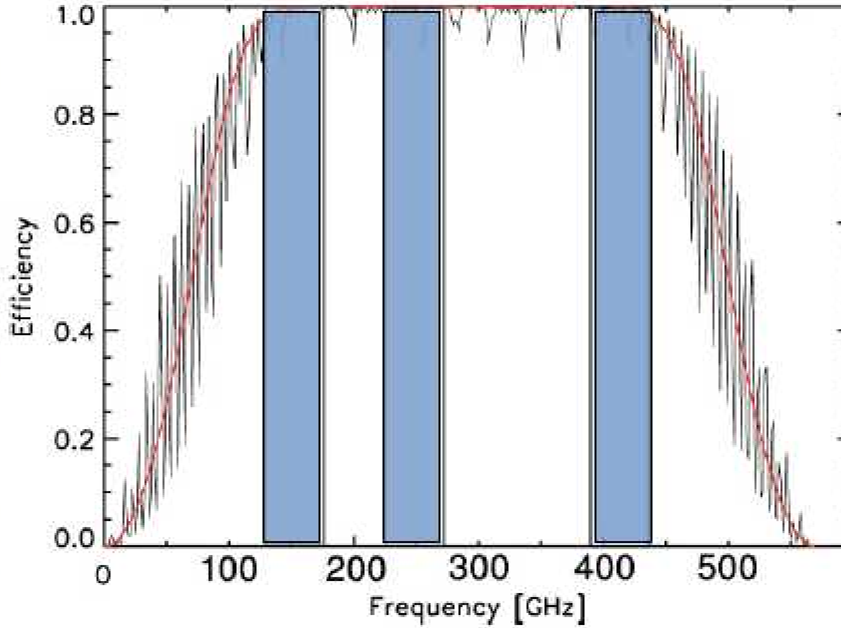

Rotates on a superconducting magnetic bearing

6 Hz rotation (2 Hz North American Flight)

0.25 degree angular encoding limited by sampling

< 10% attenuation from 3 msec time constant

5 stack achromatic HWP (sapphire)

0.98 efficiency for 120< ν < 420 Ghz

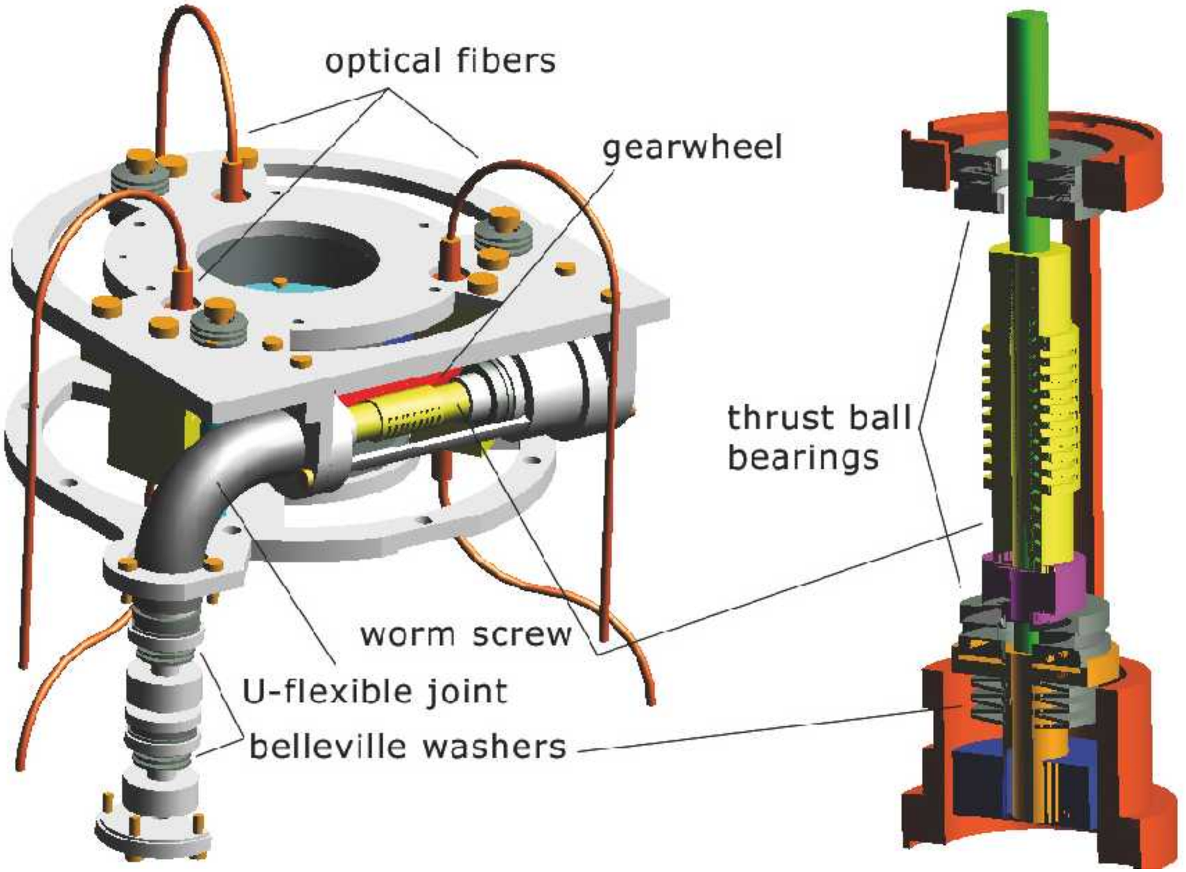

A cryogenic waveplate rotator for polarimetry at mm and sub-mm wavelengths

Maria Salatino, Paolo de Bernardis, Silvia Masi, astro-ph/1006.5392

Polarization Modulator

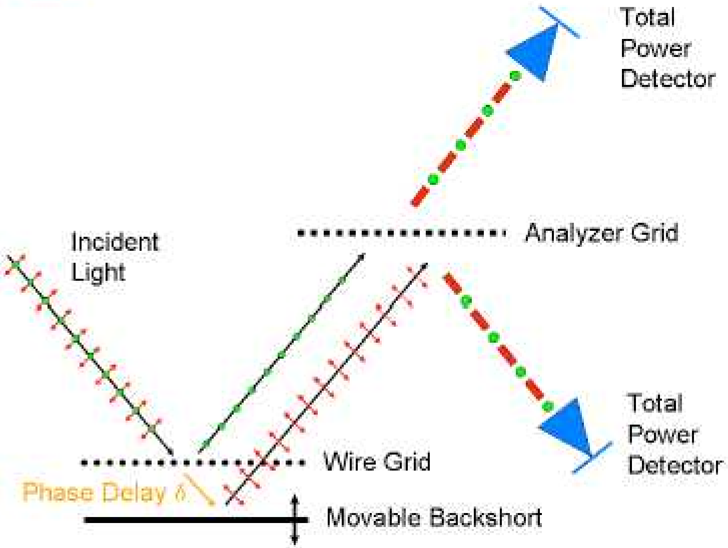

$$P_x = \frac{1}{2}(I + Q\cos\delta - V\sin\delta)$$

Measure linear and circular polarization!

$$P_y = \frac{1}{2}(I - Q\cos\delta + V\sin\delta)$$

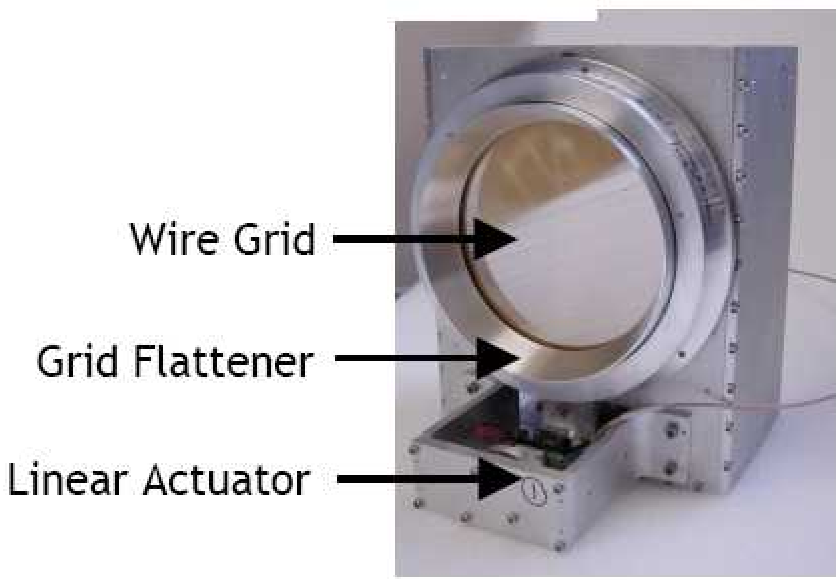

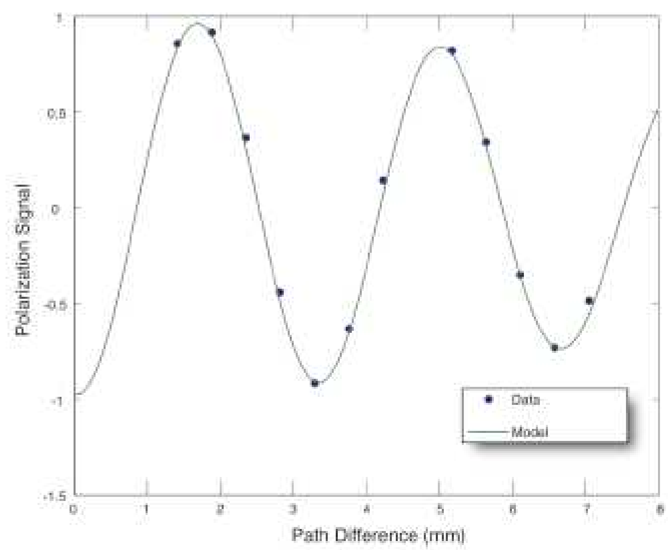

2. Control of systematic effects

- Polarized sidelobes
- Polarization modulators
- Orthogonal measurement methods:
  - Coherent imagers (QUIET, ..)
  - Bolometric imagers (BOOMERanG, MAXIPOL, Planck, BICEP, EBEX, SPIDER, PIPER, LSPE, …
  - Coherent interferometers (DASI, CBI, …)
  - Bolometric interferometers (MBI, QUBIC)

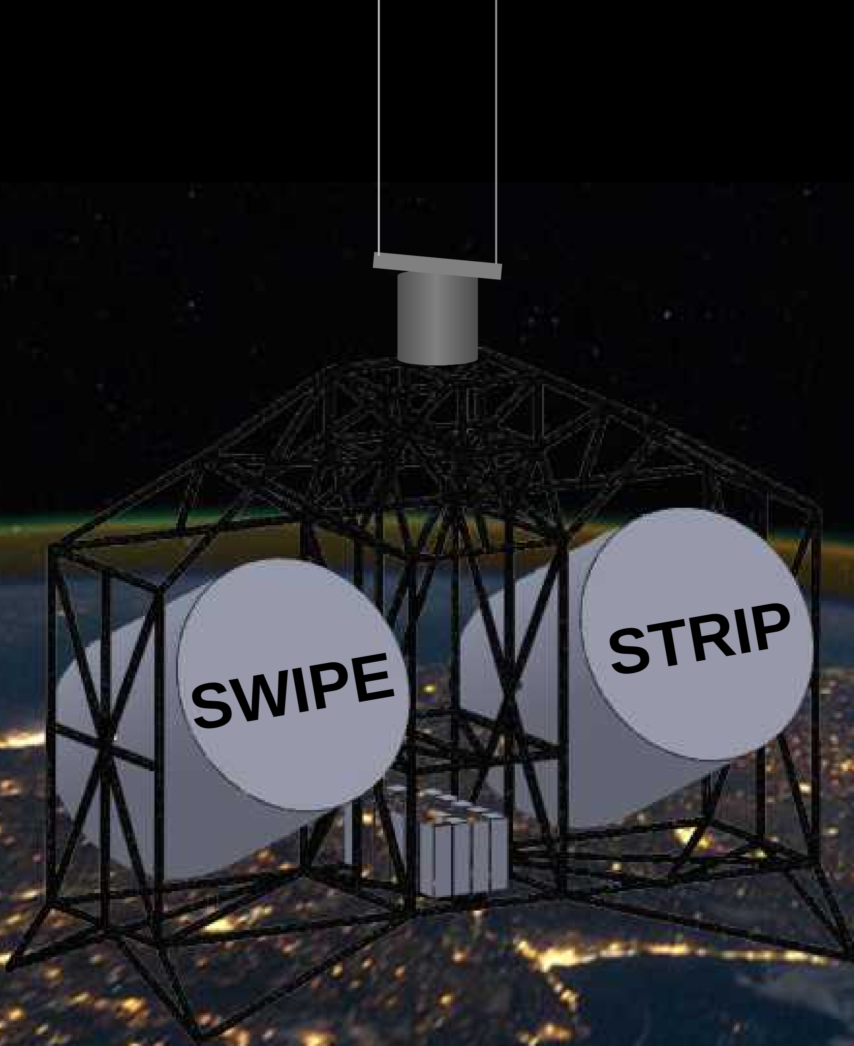

The Large Scale Polarization Explorer

P. de Bernardis, for the LSPE collaboration

The LSPE collaboration

Large Scale Polarization Explorer

Giorgio Amico, Elia Battistelli, Alessandro Baù, Paolo de Bernardis, Marco Bersanelli, Andrea Boscaleri, Francesco Cavaliere, Alessandro Coppolecchia, Angelo Cruciani, Francesco Cuttaia, Antonio D' Addabbo, Giuseppe D'Alessandro, Simone De Gregori, Francesco Del Torto, Marco De Petris, Lorenzo Fiorineschi, Cristian Franceschet, Enrico Franceschi, Massimo Gervasi, David Goldie, Anna Gregorio, Vic Haynes, Luca Lamagna, Bruno Maffei, Davide Maino, Silvia Masi, Aniello Mennella, Ng Ming Wah, Gianluca Morgante, Federico Nati, Luca Pagano, Andrea Passerini, Oscar Peverini, Francesco Piacentini, Lucio Piccirillo, Giampaolo Pisano, Sara Ricciardi, Paolo Rissone, Giovanni Romeo, Maria Salatino, Maura Sandri, Alessandro Schillaci, Luca Stringhetti, Andrea Tartari, Riccardo Tascone, Luca Terenzi, Maurizio Tomasi, Fabrizio Villa, Giuseppe Virone, Stafford Withington, Andrea Zacchei, Mario Zannoni

Short
Wavelength
Instrument for the
Polarization
Explorer
(bolometers, 80-250 GHz)
PI de Bernardis

STRatospheric
Italian
Polarimeter
(radiometers, 40-90 GHz)
PI Bersanelli

agenzia spaziale italiana

SAPIENZA Università di Roma | Università degli Studi di Milano | Università degli Studi di Milano Bicocca | IASF Bo | CNR IEIIT | IFAC | University of Cambridge | Manchester 1824

LSPE in a nutshell

- The Large-Scale Polarization Explorer is
  - a spinning stratospheric balloon payload
  - flying long-duration, in the polar night
  - aiming at CMB polarization at large angular scales
  - using polarization modulators to achieve high stability
- Frequency coverage: 40 – 250 GHz (5 channels)
- Angular resolution: 1.5 – 2.3 deg FWHM
- Sky coverage: 20-25% of the sky per flight
- Combined sensitivity: 10 μK *arcmin* per flight

The LSPE payload

A spinning gondola, rotated by torque motors around an azimuth pivot

Stokes polarimeter with cold stepping HWP and arrays of large-throughput bolometers at 90, 145, 220 GHz; FWHM 2.4° to 1.4°

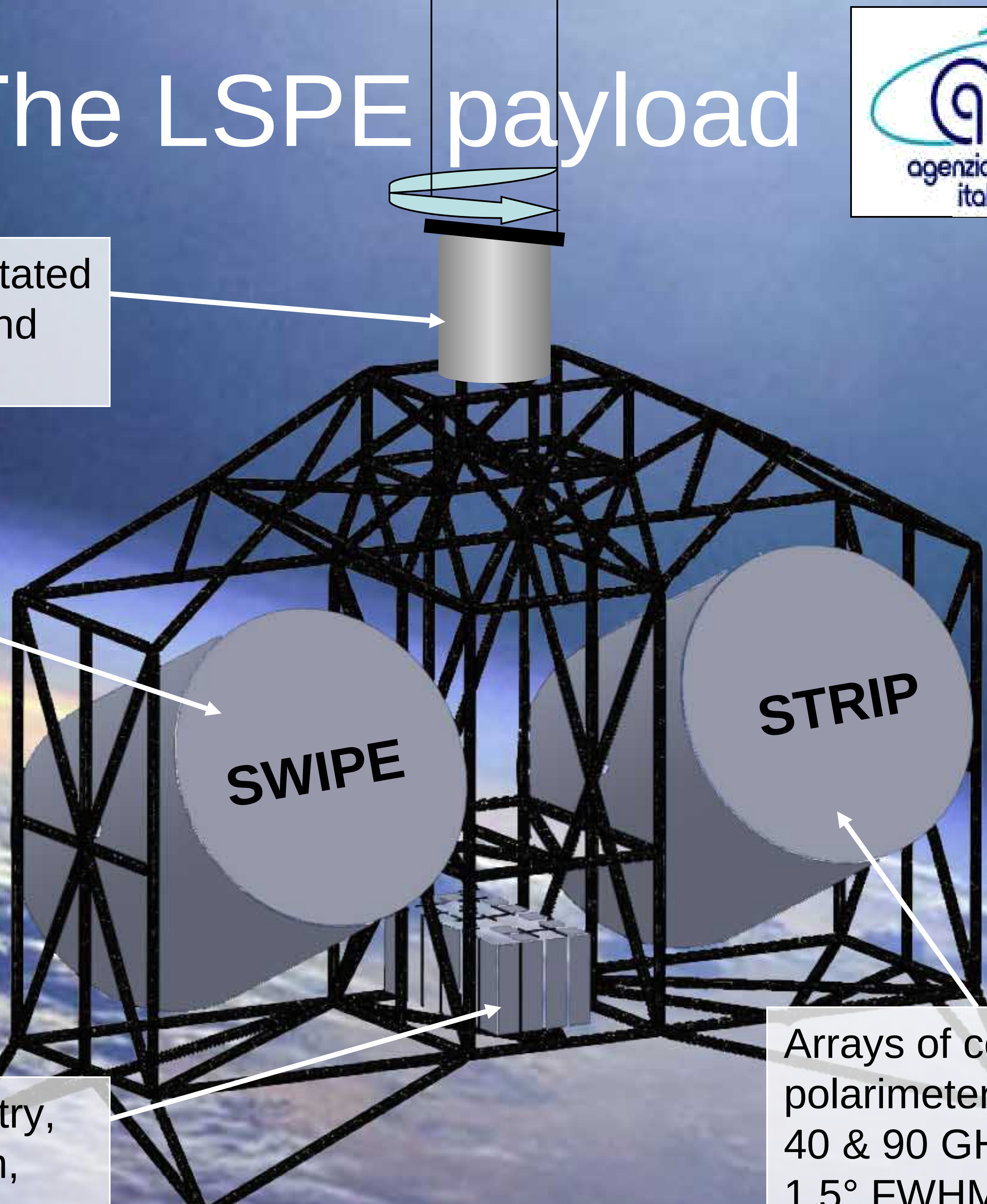

Arrays of coherent polarimeters at 40 & 90 GHz. 1.5° FWHM

Batteries (1GJ), telemetry, Attitude Control System, data storage

Mission profile

- The instrument will be flown at 38 km of altitude by a 800000m^3 balloon, at the end of 2014.
- Stratospheric balloons can be flown during the polar night despite of the low temperature of the air (see e.g. Archeops)
- The currently selected launch site is in the Svalbard islands (78° N), and the expected flight path will be a circle at approximately constant latitude.
- With recovery in Greenland, the flight can be 2-3 weeks long. This has been tested already in the summer.
- The site is easily reacheable (international airport) and large payloads have already been launched from there.

PEGASO circumpolar flight (2007) launched from Longyearbyen

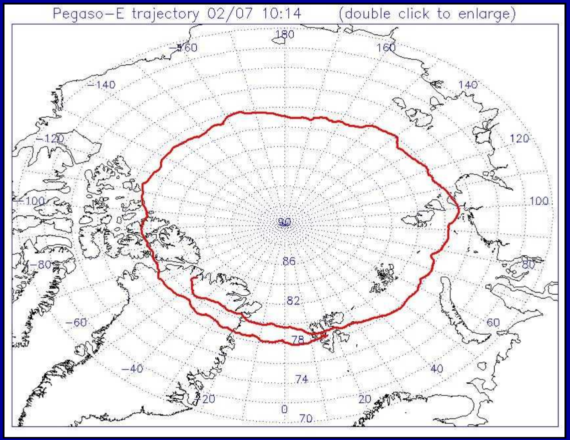

- The same thing can be done, with logistic complications, in Antarctica

Launch of the SORA experiment from the Longyearbyen airport (2009)

Sky Coverage

- The payload will just spin in azimuth during the flight.
- The telescopes of the two instruments will scan the sky at constant elevation. Performing a few elevation steps during the 2-3 weeks of the flight, more than 20% of the sky can be covered outside the galactic mask, with good cross-linking and significant integration time per pixel. (cfr. Farhang et al. astro-ph/1108.2043)

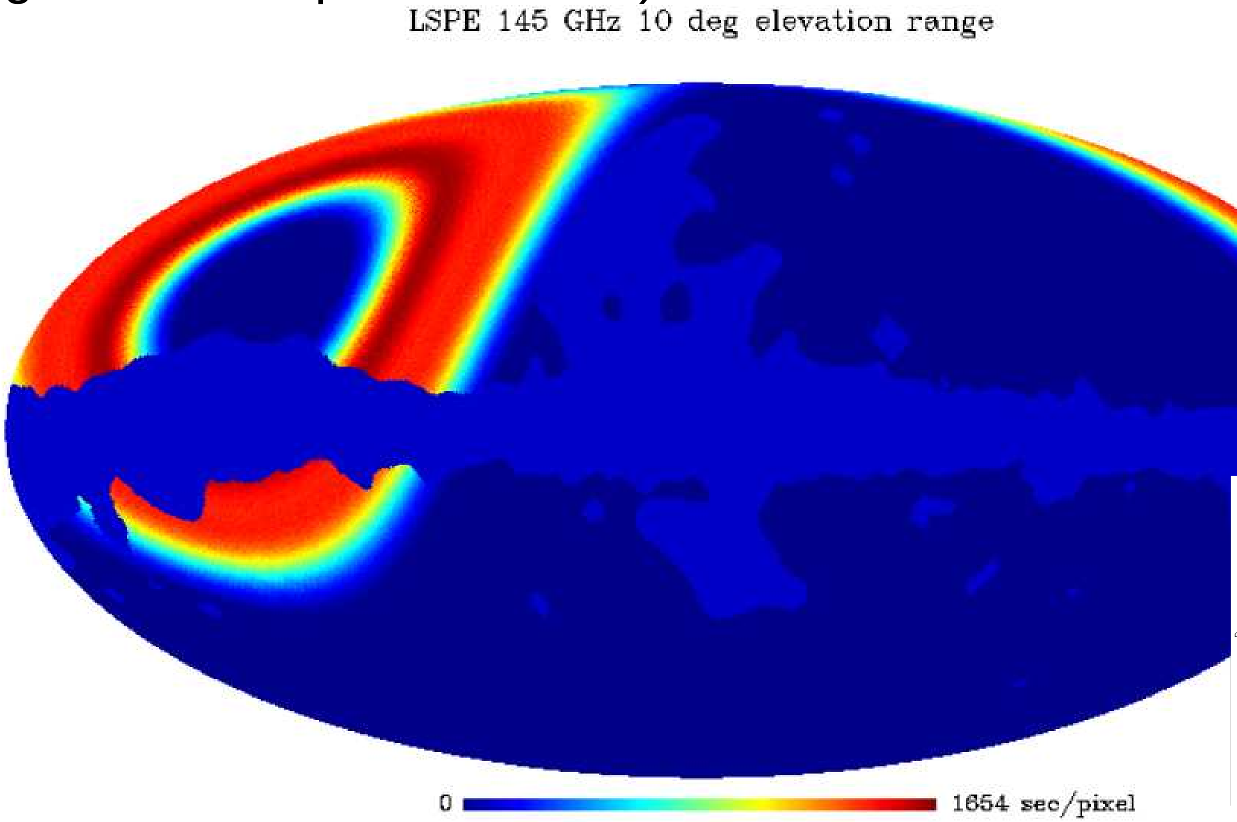

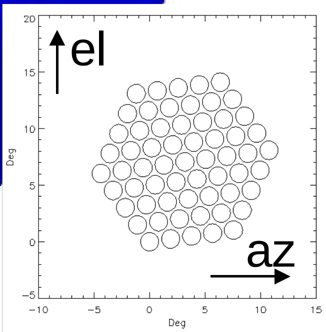

LSPE – ACS

- The payload spins at 2-3 rpm
- We use an azimuth pivot with torque motors similar to the ones used in BOOMERanG and Archeops (Pascale + Boscaleri AIP Conf. Proc. **616**, 56, 2001)
- The rotation speed is sensed by a set of 3 laser-gyors, driving the ACS control loop.
- The power required to spin the payload (about 100W) is due to the friction in the thrust bearings of the azimuth pivot and is provided by Lithium batteries.
- Absolute attitude is reconstructed by means of a fast star sensor similar to the one used in Archeops (Nati et al., Review of Scientific Instruments, **74**, 4169, 2003)

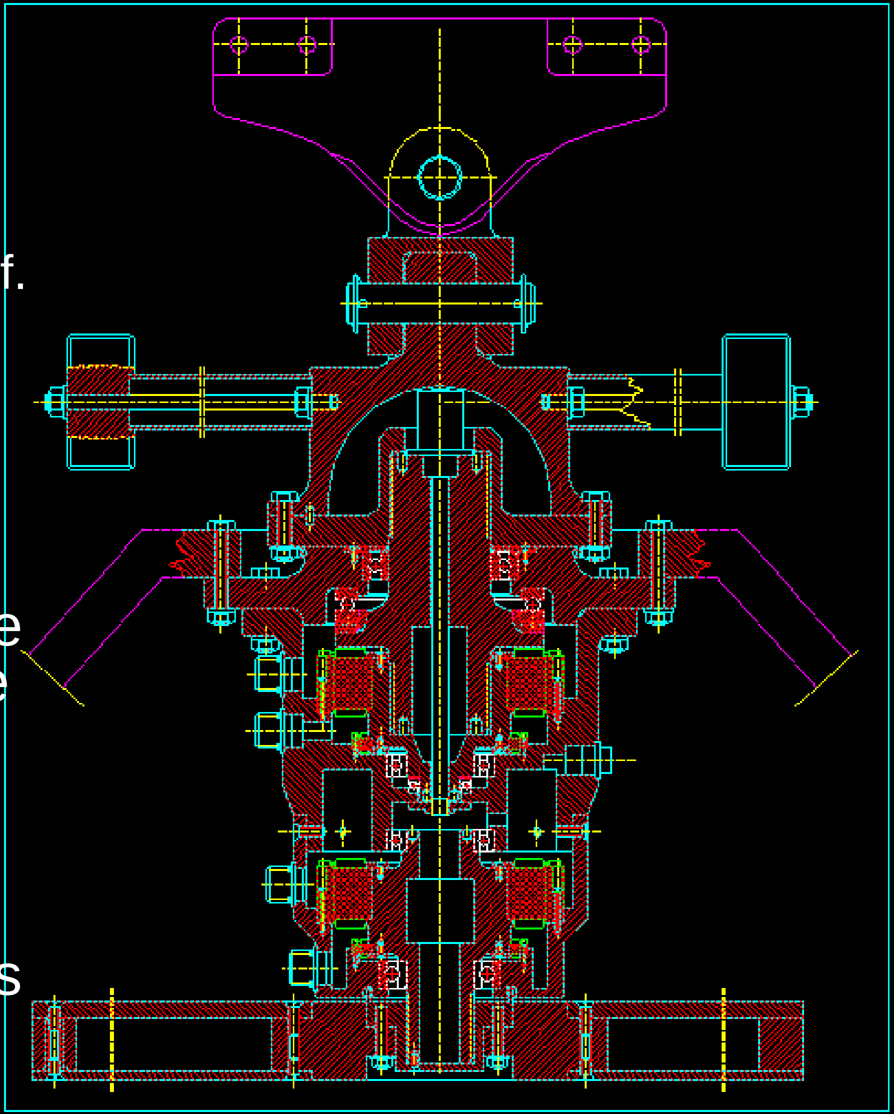

SWIPE

- The **S**hort **W**avelength **I**nstrument for the **P**olarization **E**xplorer
- Uses overmoded bolometers, trading angular resolution for sensitivity
- Sensitivity of photon-noise limited bolometers vs # of modes:

LSPE - SWIPE	eff =	0.25	
Bolometric	D lens =	0.4	m
Instrument	F =	0.8	m
N modes (geom) =	15	25	40
f (GHz)	90	145	220
λ (mm)	3.3	2.1	1.4
N det =	37	58	83
FWHM (deg) =	2.4	1.9	1.6
NET (µK/sqrt(Hz)) =	15	25	30
NET Focal Plane (µK/sqrt(Hz))=	**2.5**	**3.3**	**3.2**

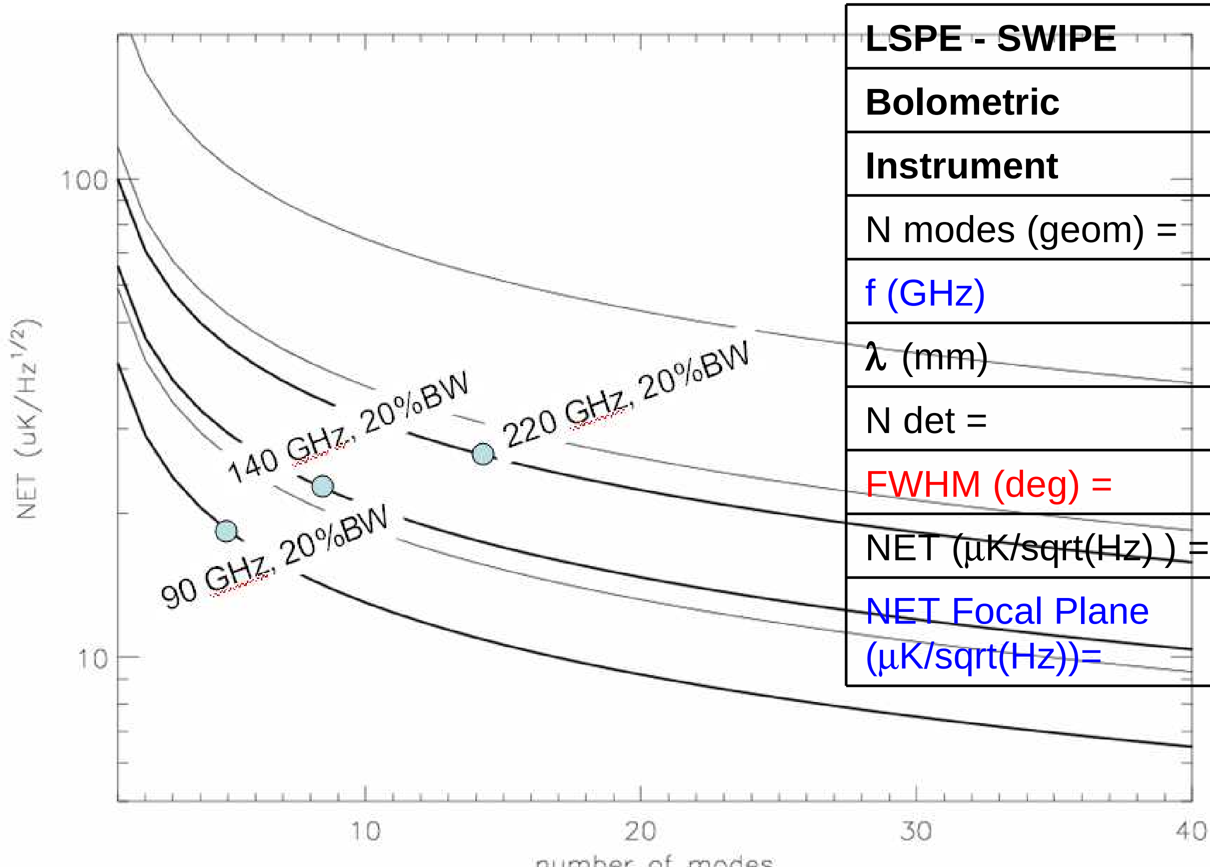

Number of modes actually coupling to the bolometer absorber

SWIPE

- Overmoded detectors are obtained coupling large area bolometer absorbers to Winston horns.
- Example of large-throughput spider-web bolometer (being developed in Italy, F. Gatti)

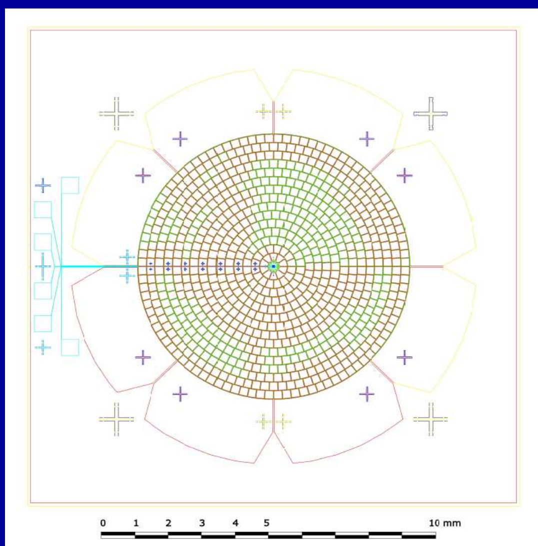

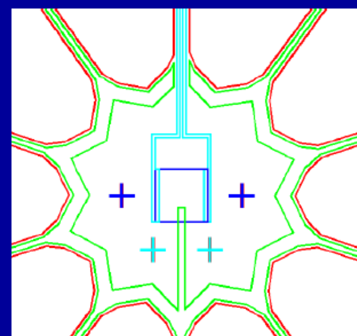

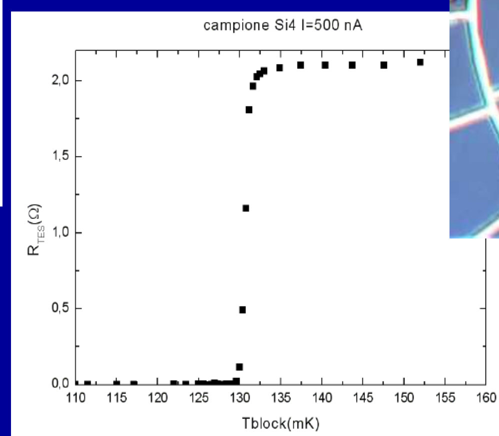

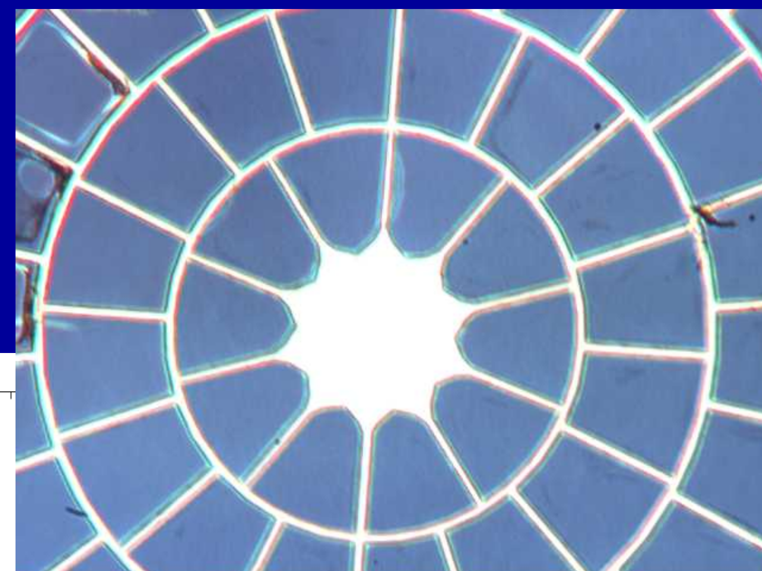

- SWIPE bolometers will be made also in Cambridge (Withington)

SWIPE

- Overmoded detectors are obtained coupling large area bolometer absorbers to Winston horns.

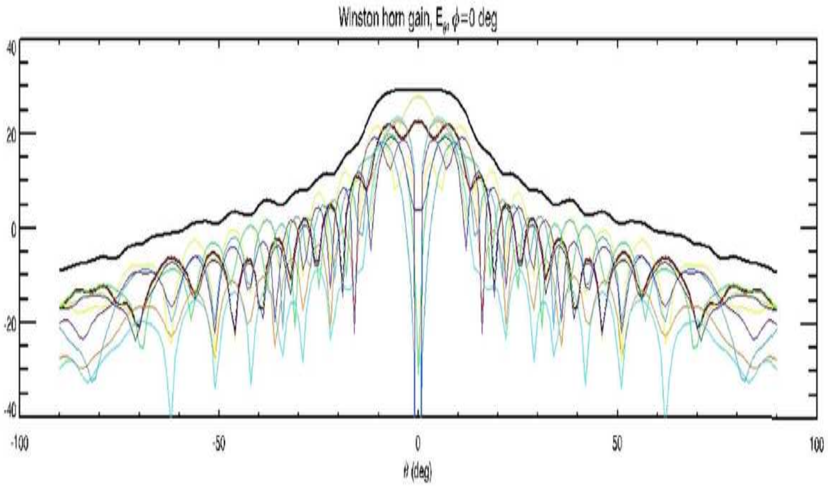

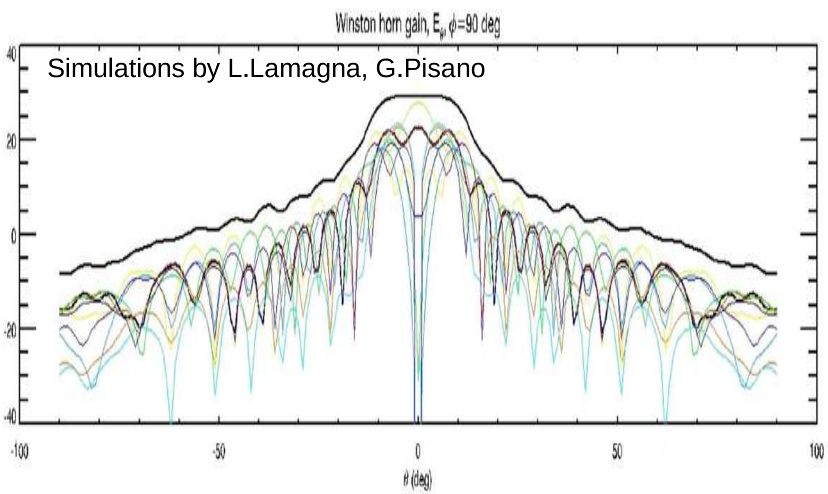

Simulations confirm that about half of the modes collected by the Winston horn actually couple to the bolometer absorber
(in single-polarization detectors).

SWIPE

- Polarimetry is implemented with a classical Stokes configuration.

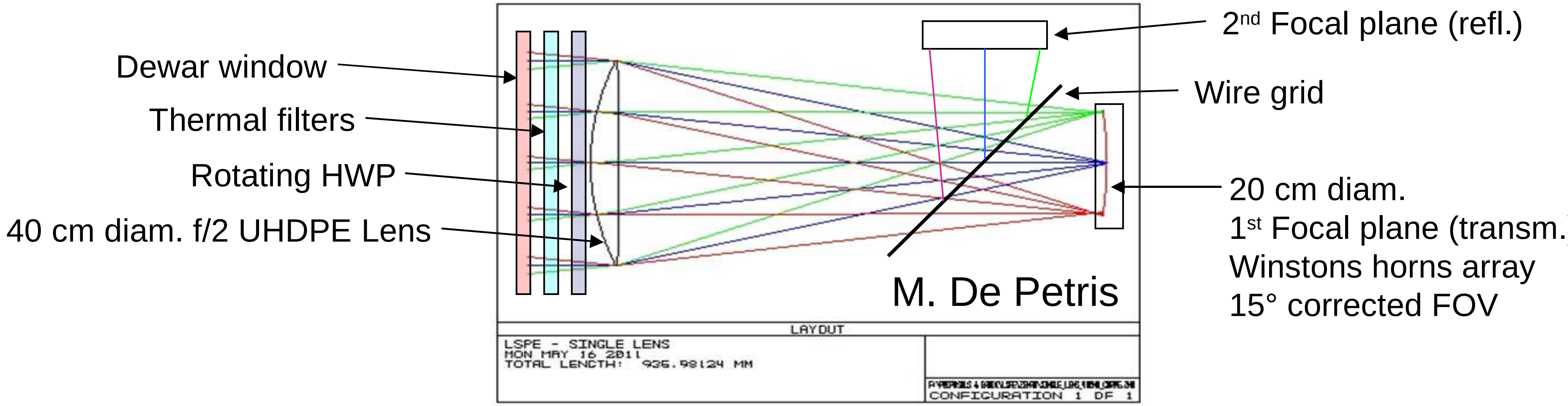

- The first optical element is a large diameter (50 cm TBC) HWP, obtained by means of diectric-embedded metal meshes (G. Pisano et al. Applied Optics, **47**, 6251, 2008, and follow-ups)

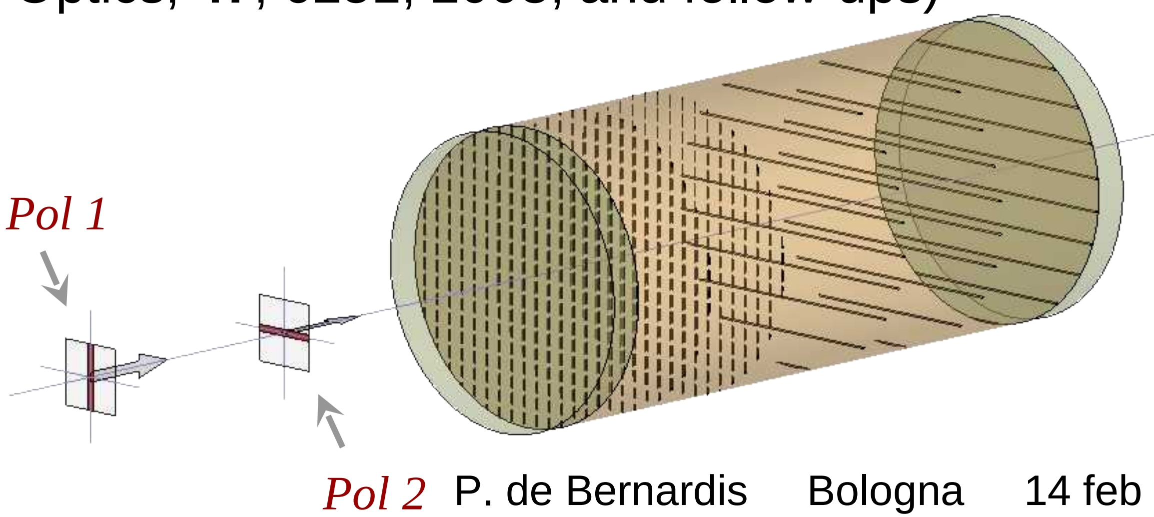

LSPE
Large Scale Polarization Explorer

SWIPE

agenzia spaziale italiana

LSPE-SAF: OPTICS REQUIREMENTS

Entrance Pupil Diameter	(mm)	400		
Effective Focal Length	(mm)	800		
f-number		2		
Focal Plane Diameter	(mm)	200		
Image Object Space	(deg)	14,3		
Focal plane scale	('/mm)	4,3		
Focal Plane Surface		curved		
Optics Symmetry		cilindrical		
Spectral Range	(GHz)	90	140	220
waves	(mm)	3,33	2,14	1,36
Angular Resolution	(arcmin)	28,6	18,4	11,7
number of modes		20	20	20
throughput (N lambda^2)	(cm^2 sr)	2,22	0,92	0,37
FWHM	(deg)	1,68	1,08	0,69
Strehl Ratio		> 95%		
Strehl Ratio variation along fov		< 1%		
Beam ellipticity		1%		
Cross Polarization		1%		
Instrumental Polarization		<1%		

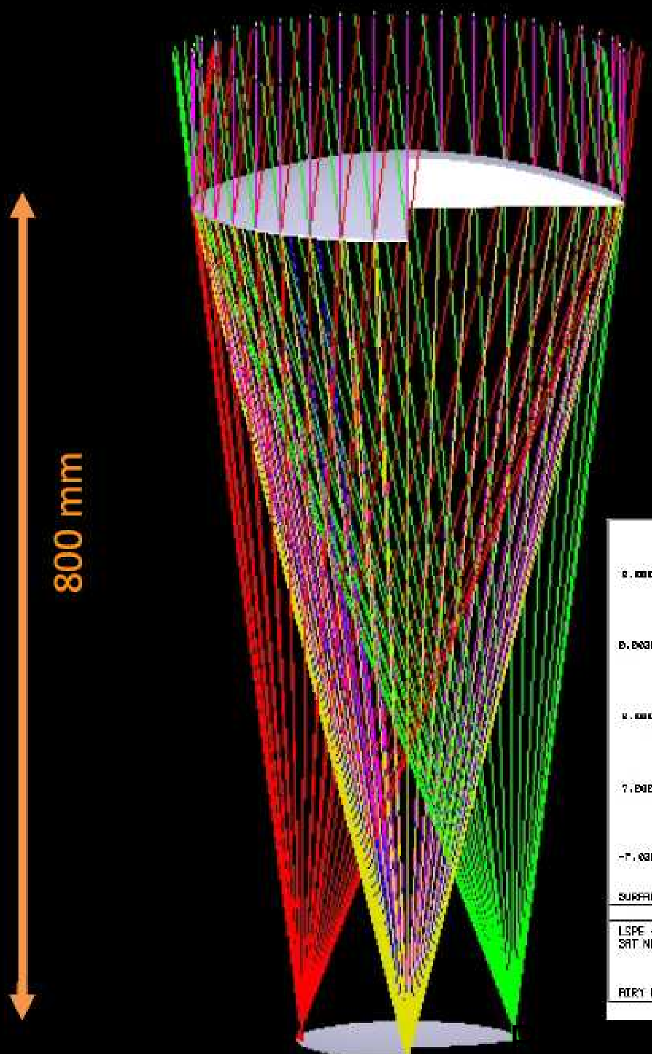

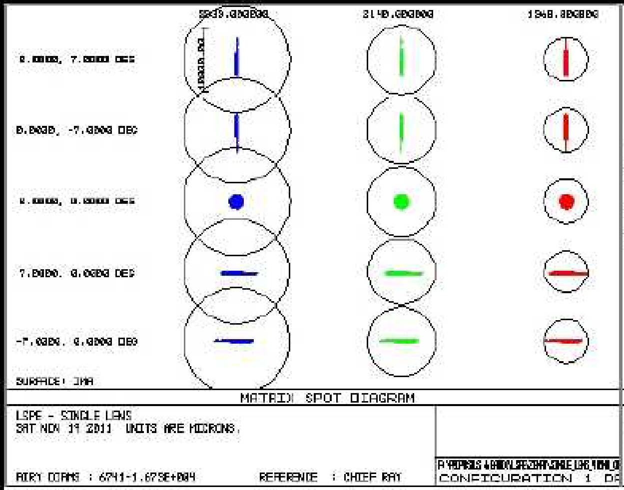

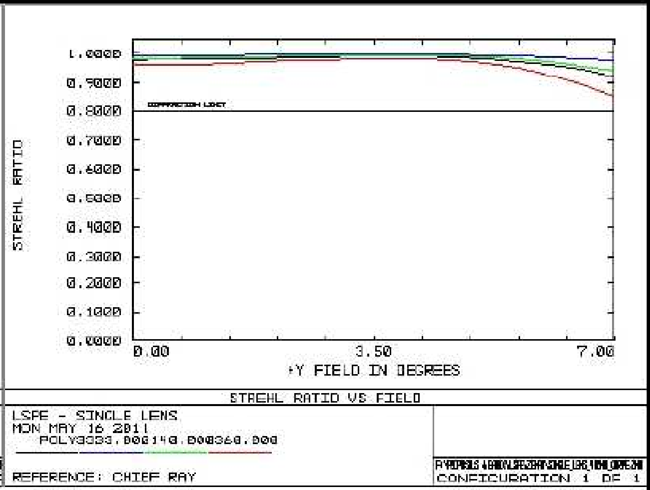

SWIPE

Custom cryostat (S. Masi)

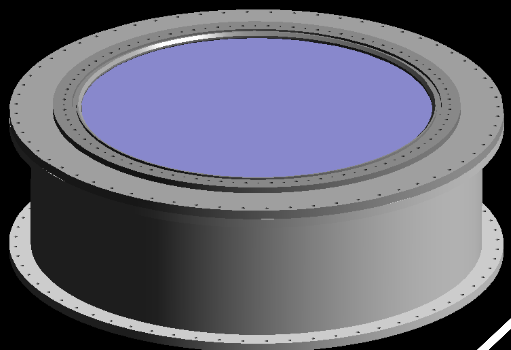

Plastazote window

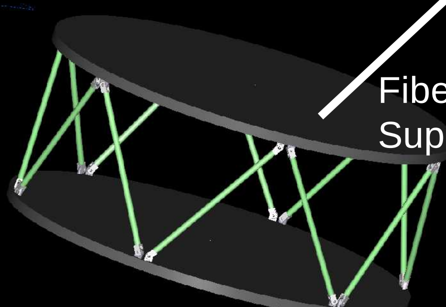

Fiberglass struts
Support system

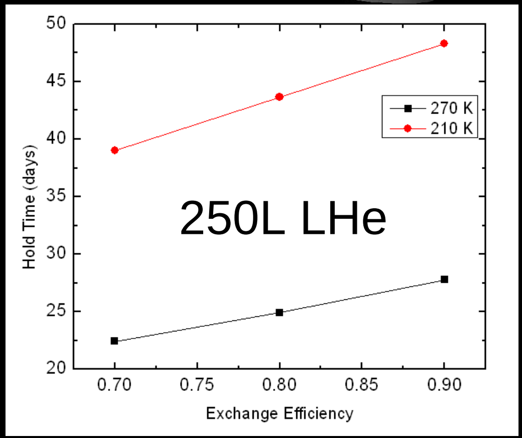

Arrays 90
& 220

Array 140

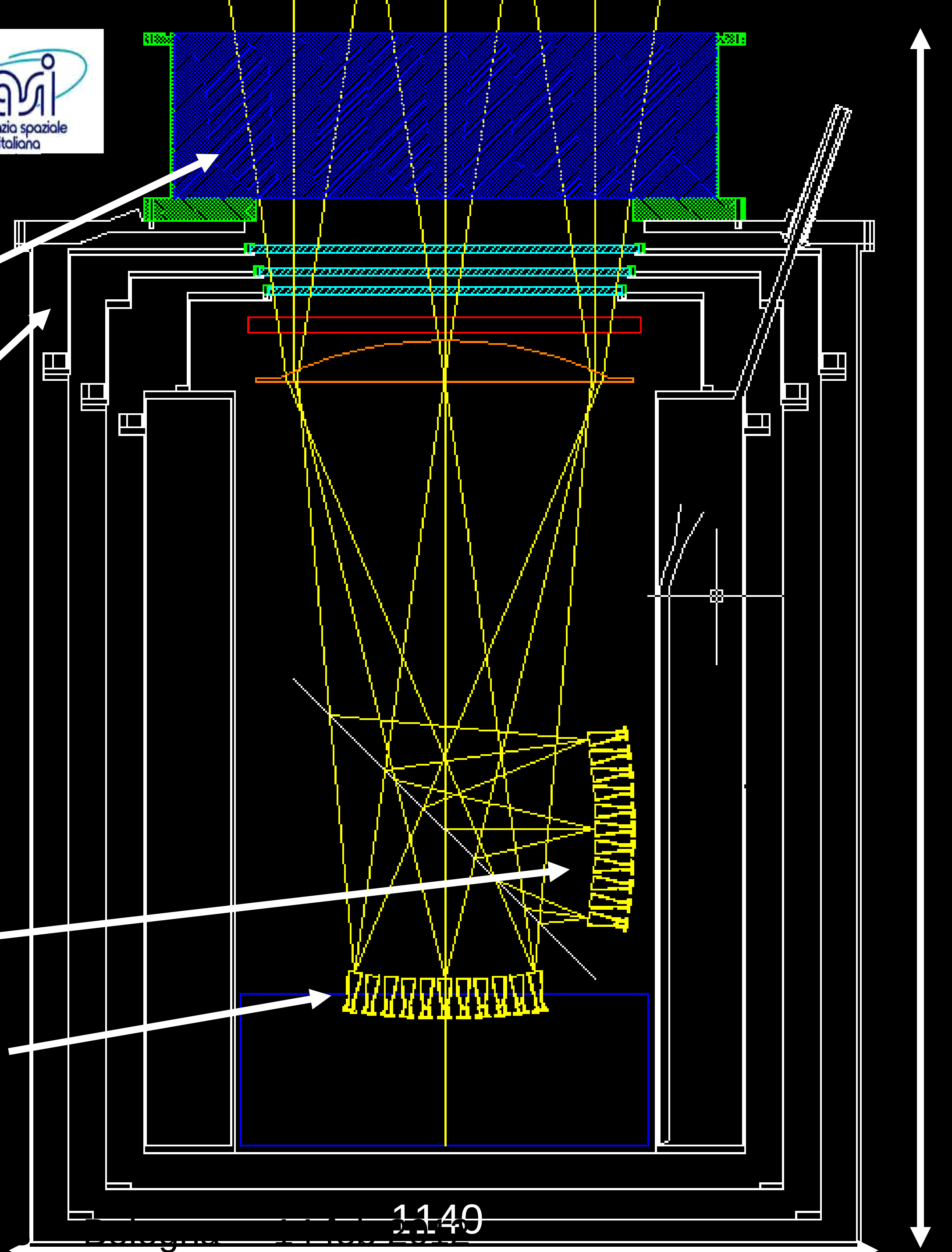

SWIPE

- The HWP will be rotated in steps using a low-friction cryogenic mechanism based on thrust bearings, similar to the one we have developed for PILOT (Salatino et al. A&A 528, A138, 2011).
- 11.25° step, 1 step/min, < 10mW
- Precision position readout with optical fibers & pinholes

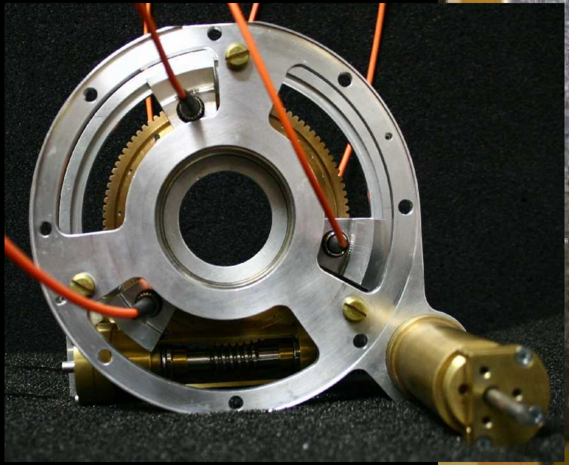

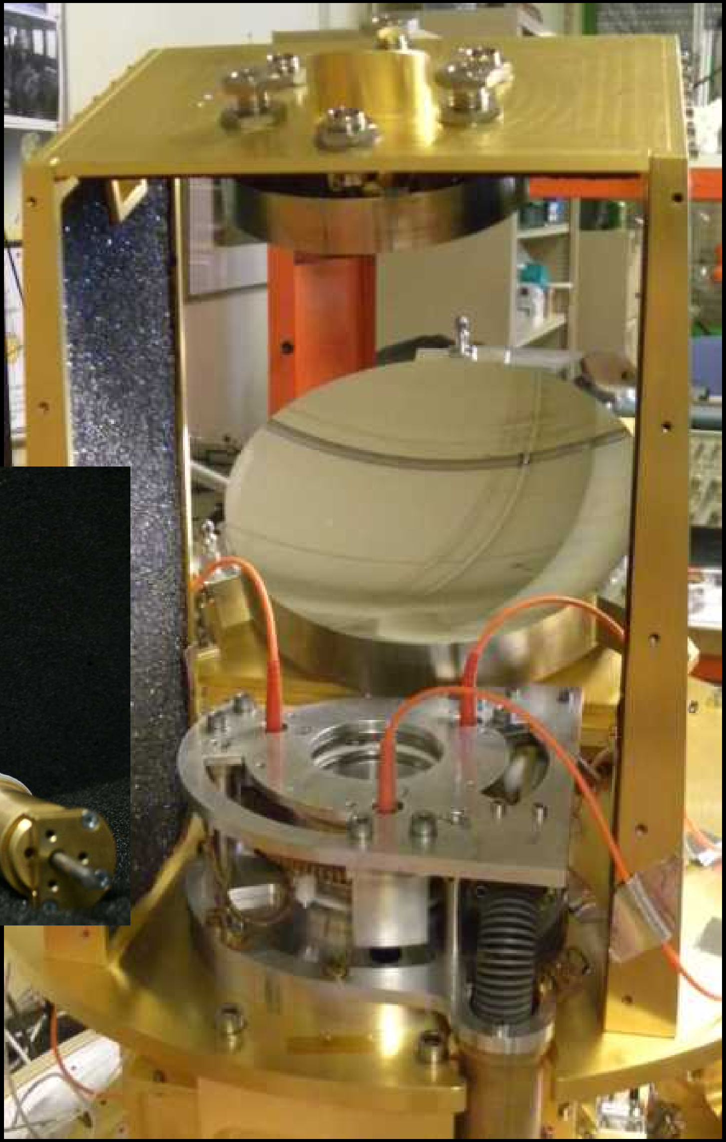

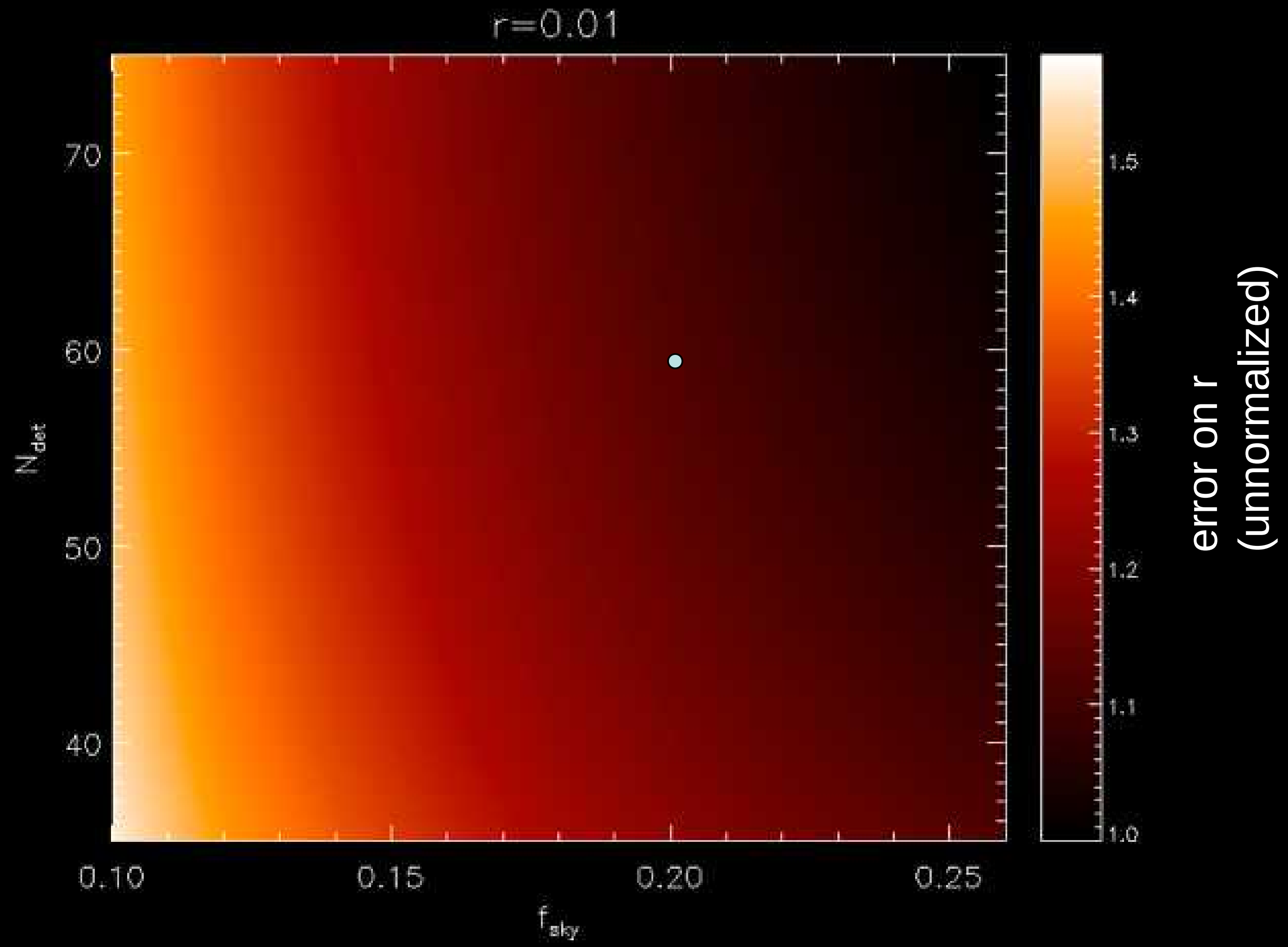

r=0.01
70
60
50
40
N_{det}
0.10
0.15
0.20
0.25
f_{sky}
1.5
1.4
1.3
1.2
1.1
1.0
error on r
(unnormalized)

SWIPE

- Simulations show that a step/integrate approach with 11.25° per step, 1 step/min and a gondola spinning at 3 rpm is already very effective in removing 1/f and drifts.
- Assuming drifts are negligible, the white-noise sensitivity of SWIPE is compared to the HFI in the table below:

	PLANCK – HFI (full sky)						LSPE – SWIPE (20%)		
Frequency (GHz)	100	143	217	353	545	857	90	145	220
FWHM Resolution (arcmin)	9	7	6	5	5	5	144	114	96
Sky coverage (%)	100	100	100	100	100	100	20	20	20
Obs Time (months)	30	30	30	30	30	30	0.467	0.467	0.467
Bandwidth (%)	33	33	33	33	33	33	25	25	25
N_det (polarized)	8	8	8	8	0	0	37	58	83
Channel NET (uK s^1/2)	25	31	45	140	//	//	2.47	3.25	3.21
Integration/beam (s)	33	20	15	10	-	-	660	415	225
Delta Q(U) (uK) on LSPE beams	**0.27**	**0.42**	**0.84**	**2.6**	**-**	**-**	**0.10**	**0.16**	**0.21**
	Improvement factor with respect to Planck-HFI (2° pixels)						**2.8**	**2.7**	**3.9**

STRIP

- The **STR**atospheric **I**talian **P**olarimeter uses coherent polarimeters working at 40 and 90 GHz, with a target sensitivity twice better than Planck LFI
- The main target is the polarized foreground (synchrotron), studied by means of 49 polarimeters in Q band. This is mandatory for an effective component separation, to remove foreground contamination from the cosmological channels (90 & 140 GHz from SWIPE).
- The 9 polarimeters in W band performs the same measurements as the bolometric W-band channel, using a completely independent technique. This provides the opportunity for a direct comparison, very efficient in detecting systematic effects.
- The required angular resolution (1.5°) is obtained by means of a 1.5m diameter telescope, focusing on an array of corrugated feedhorns, followed by high efficiency pseudo-correlation polarimeters (similar to the QUIET ones, see K. A. Cleary, Proc. SPIE 7741, 77412H, 2010).

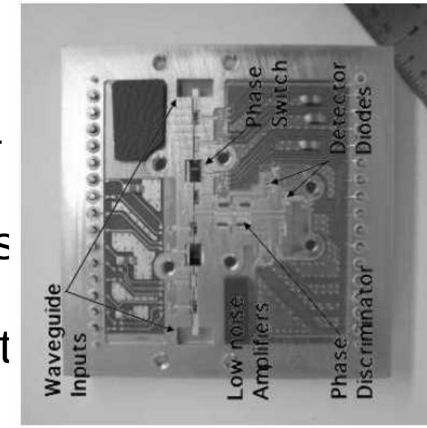

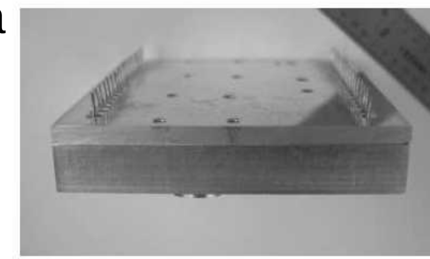

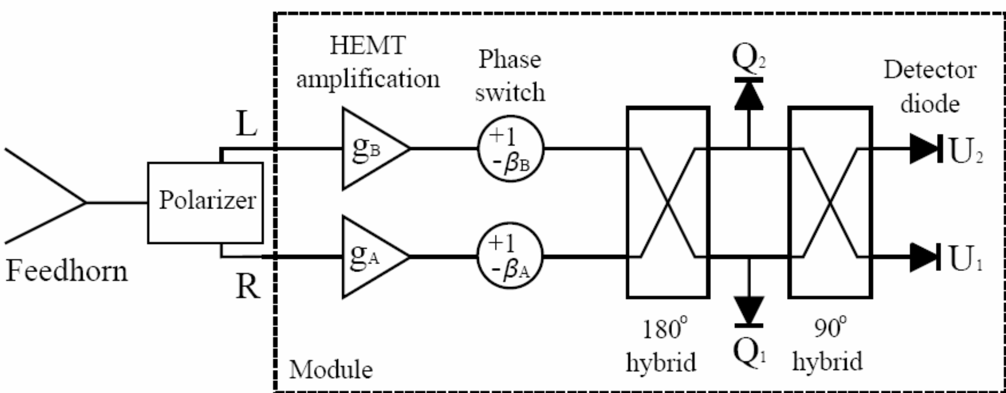

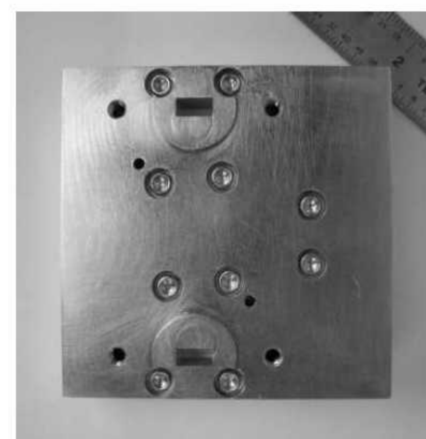

STRIP

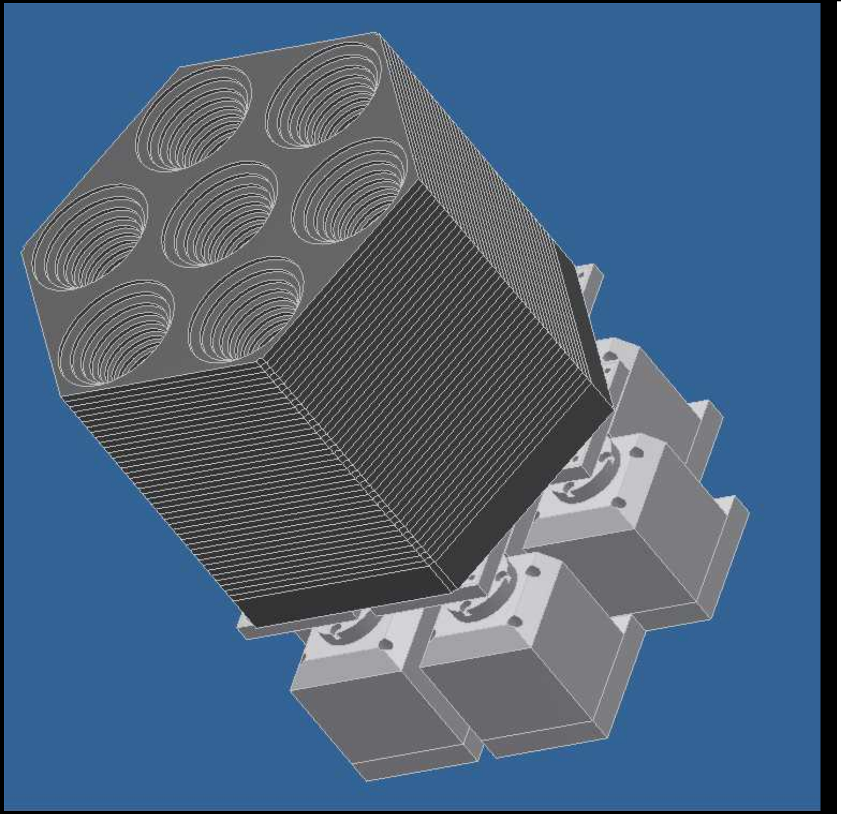

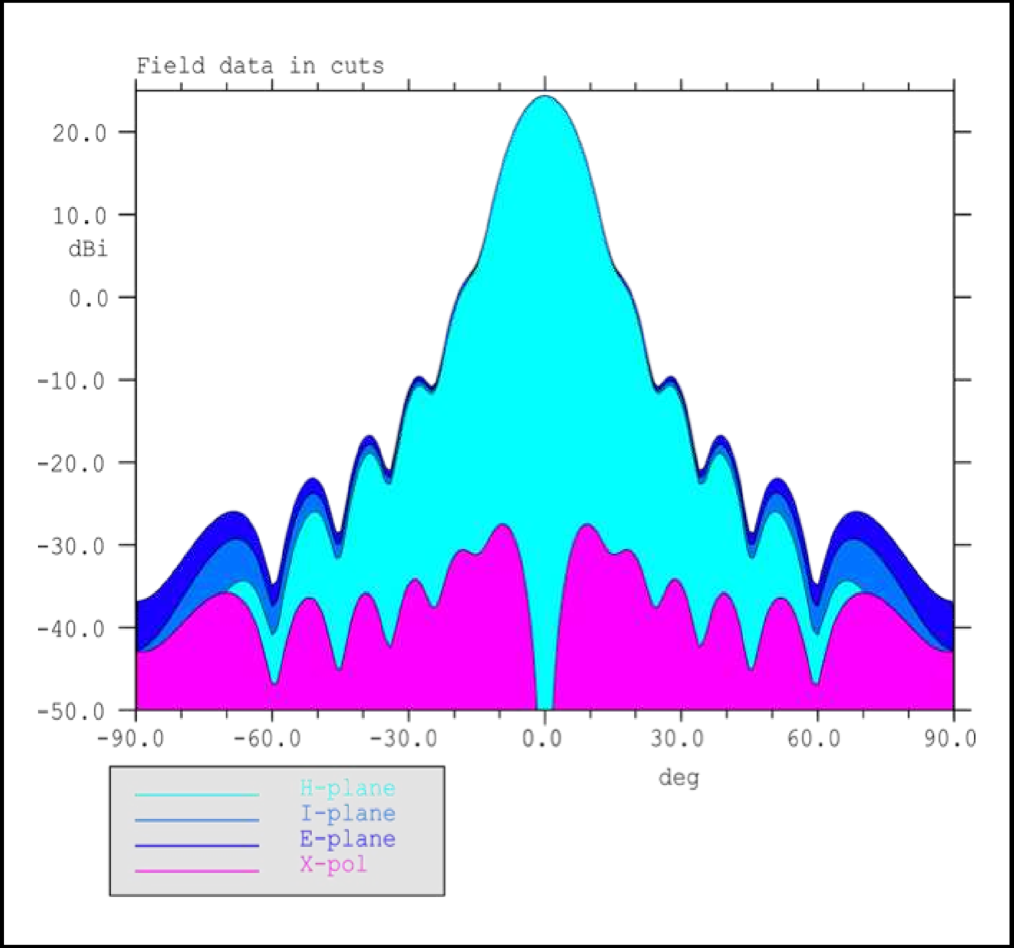

The corrugated feedhorns arrays are produced using the platelets technology (see e.g. Del Torto et al. JNST 6, 6009, 2011).

STRIP

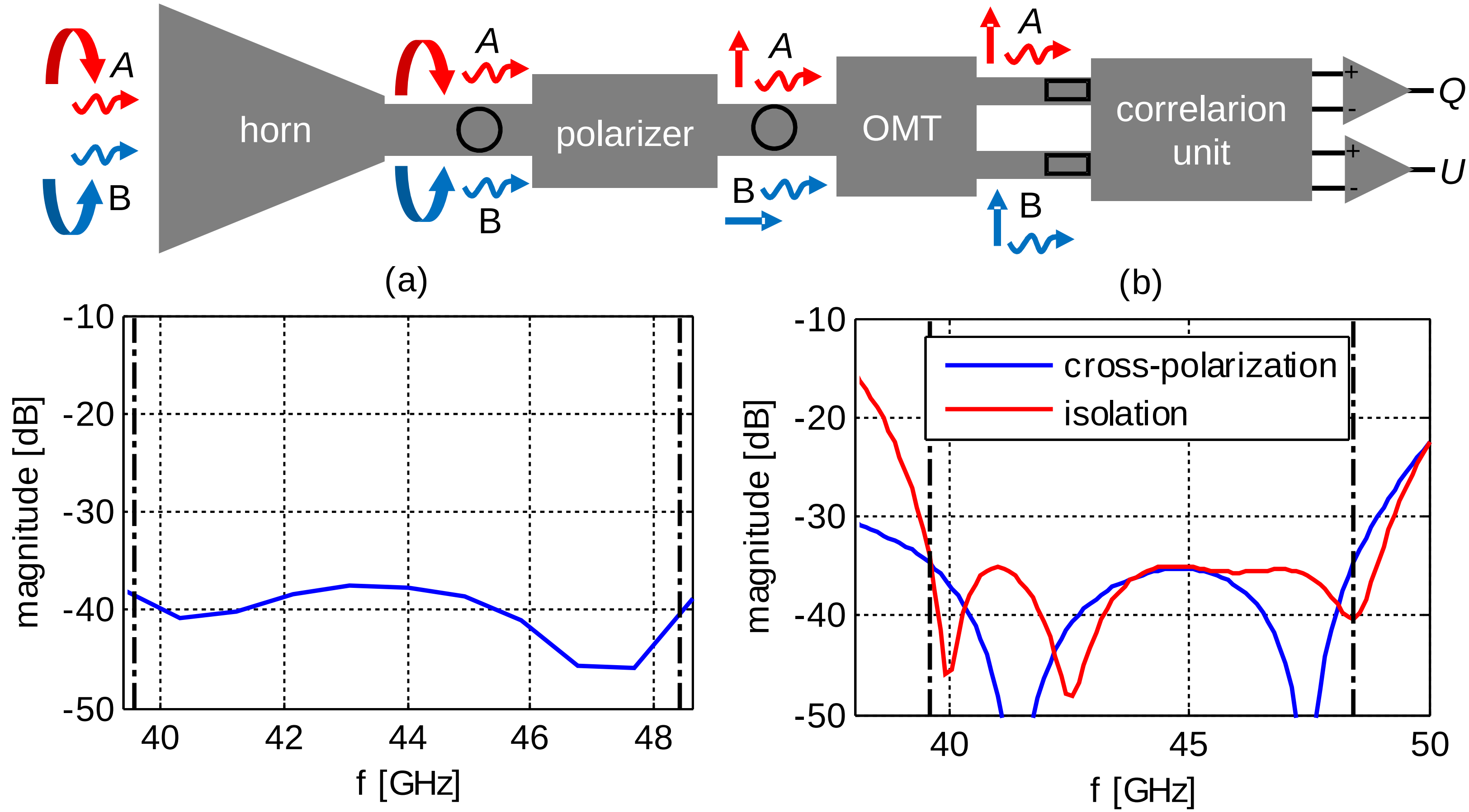

- High efficiency, wide band, polarizers and OMTs have been custom designed for this application at IEIIT

STRIP

- The polarimeters are cooled at the optimal operation temperature by cold He gas, evaporating from a large (500L) He cryostat (G. Morgante)

Stage	4K	20K	100K	Comments
Radiative (mW)	6,38	259,06	6156,87	*MLI 30 layers, 15 layers/cm*
Conductive (mW)	2,05	493,89	3052,94	*Piping in SS, Struts in G10, Wires in PhBronze (all harness in Flexi Cu with 20-30 cm thermal breaks)*
Active (mW)	832,00	1845,00	0,00	*On 4K stage heater dissipation is added on top of the parasitics load to maintain massflow, on the 20K stage the polarimeters dissipation plus active temperature control (0,2W average)*
Total (mW)	840,42	2597,95	9209,80	*no margin*
with margin	1092,55	3377,34	11972,74	*30% margin has been considered here*

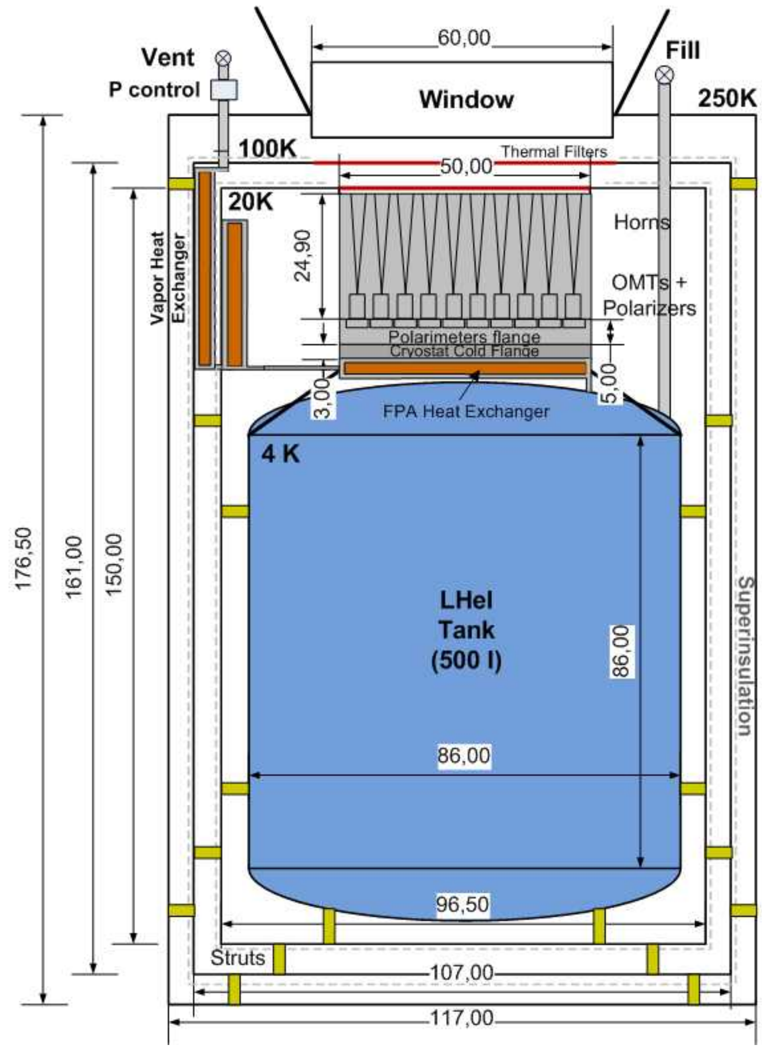

LSPE

Our target is r = 0.03, 3σ.

Expected performance of LSPE in constraining cosmological parameters, compared to Planck and SPIDER
(simulation by L. Pagano)

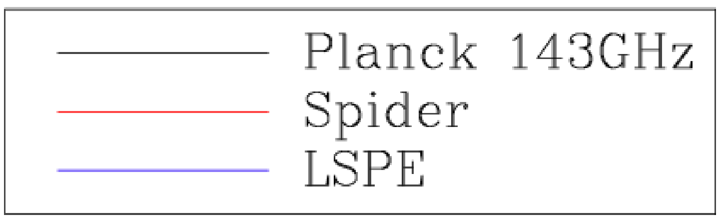

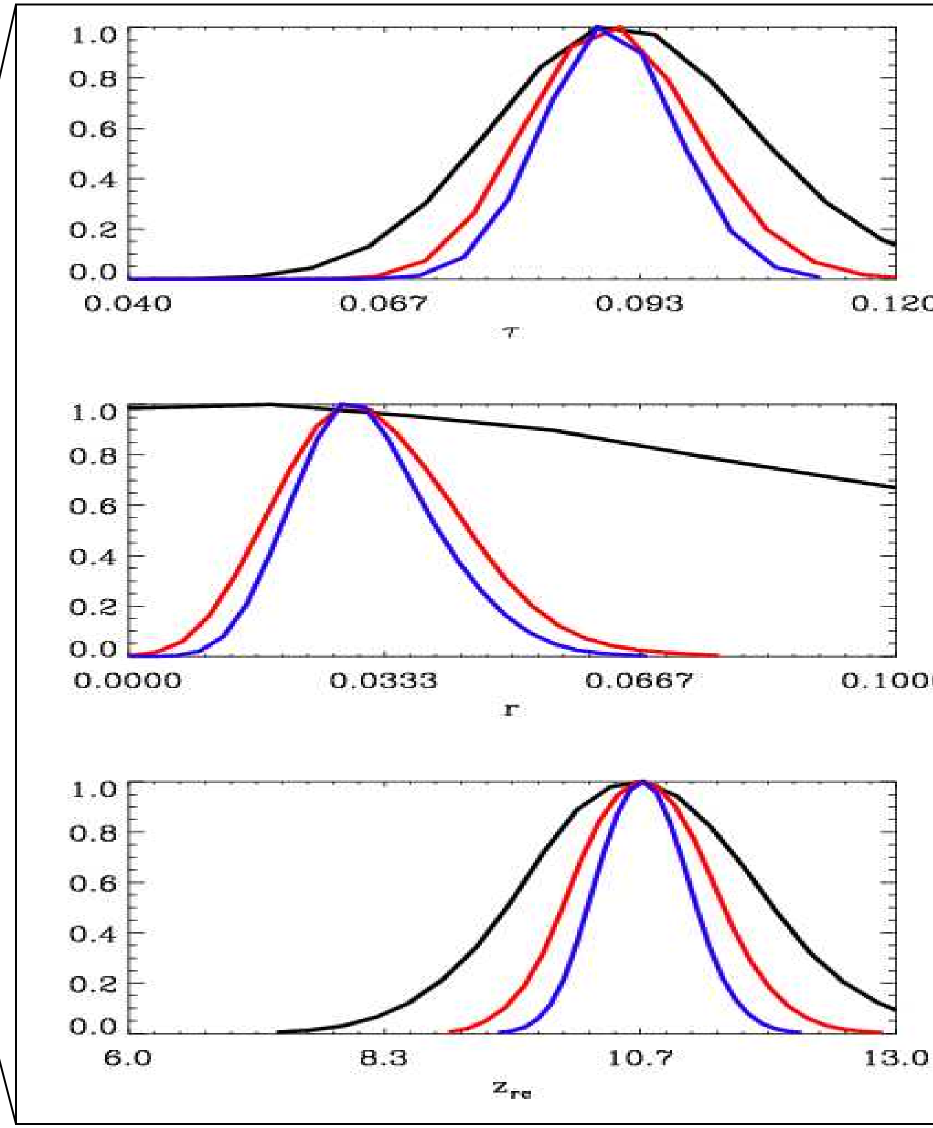

On the paper, a very competitive instrument

Certainly independent and using different methodology

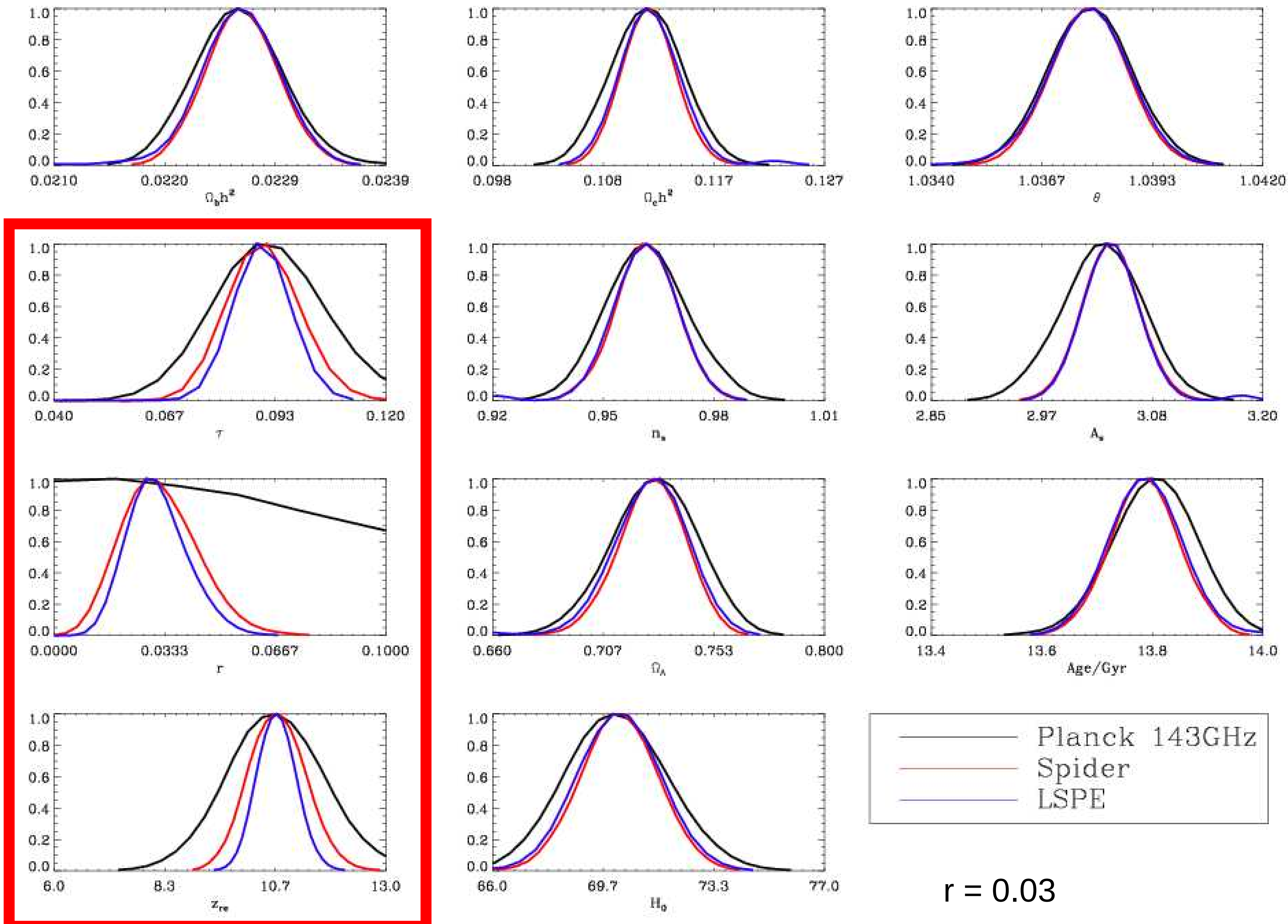

$\Omega_b h^2$
$\Omega_c h^2$
θ
τ
n_s
A_s
r
Ω_Λ
Age/Gyr
z_{re}
H_0
Planck 143GHz
Spider
LSPE

r = 0.03

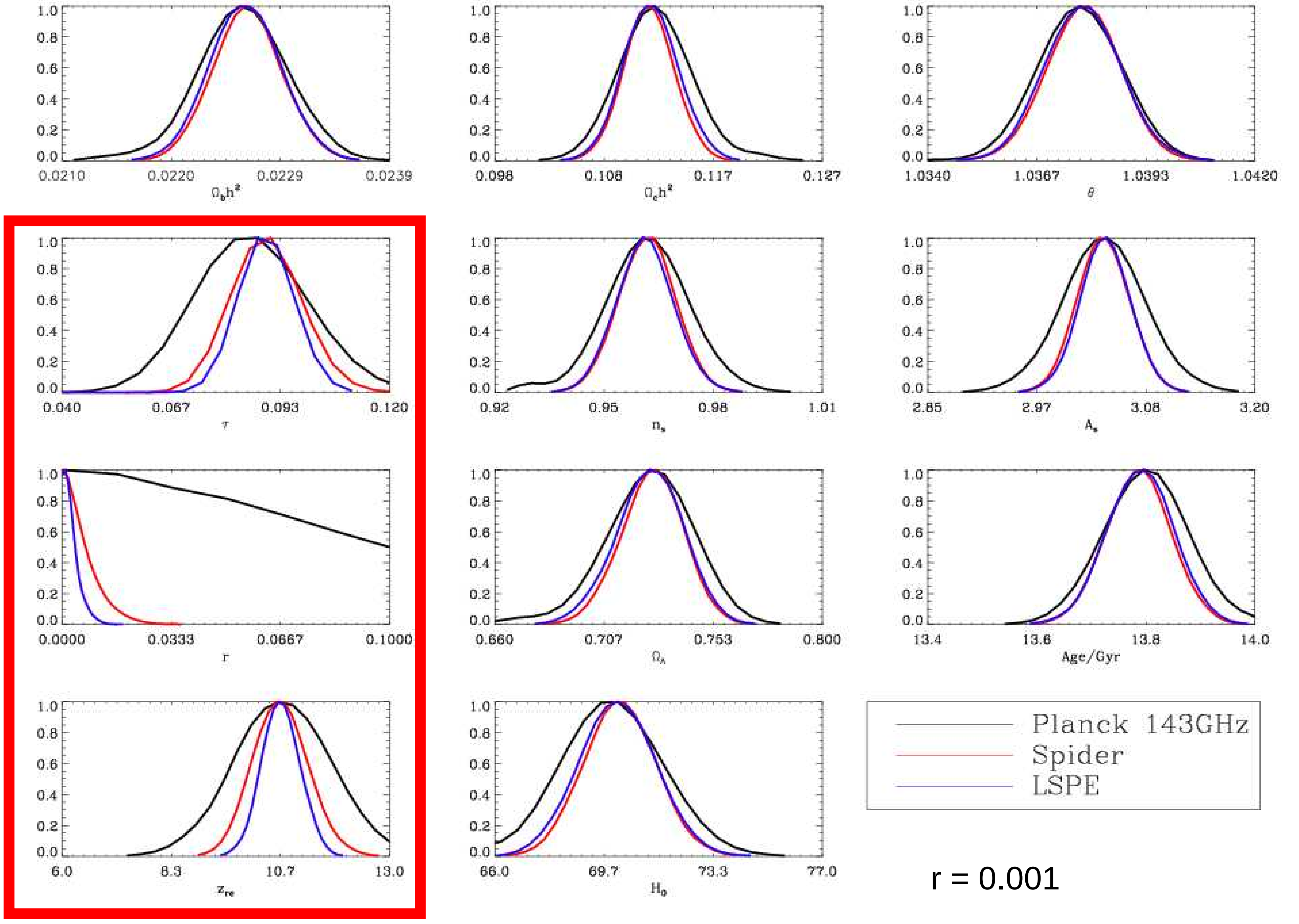

Planck 143GHz
Spider
LSPE
r = 0.001

LSPE schedule

Still a long way to go …

event	date
KO	Apr. 29, 2011
PDR	Dec 20, 2011
CDR	Apr. 30, 2012
IHDR	Oct. 29, 2012
TRR	Aug. 29, 2013
FAR	Jan. 29, 2014
Flight	End of 2014

A Pathfinder for LSPE

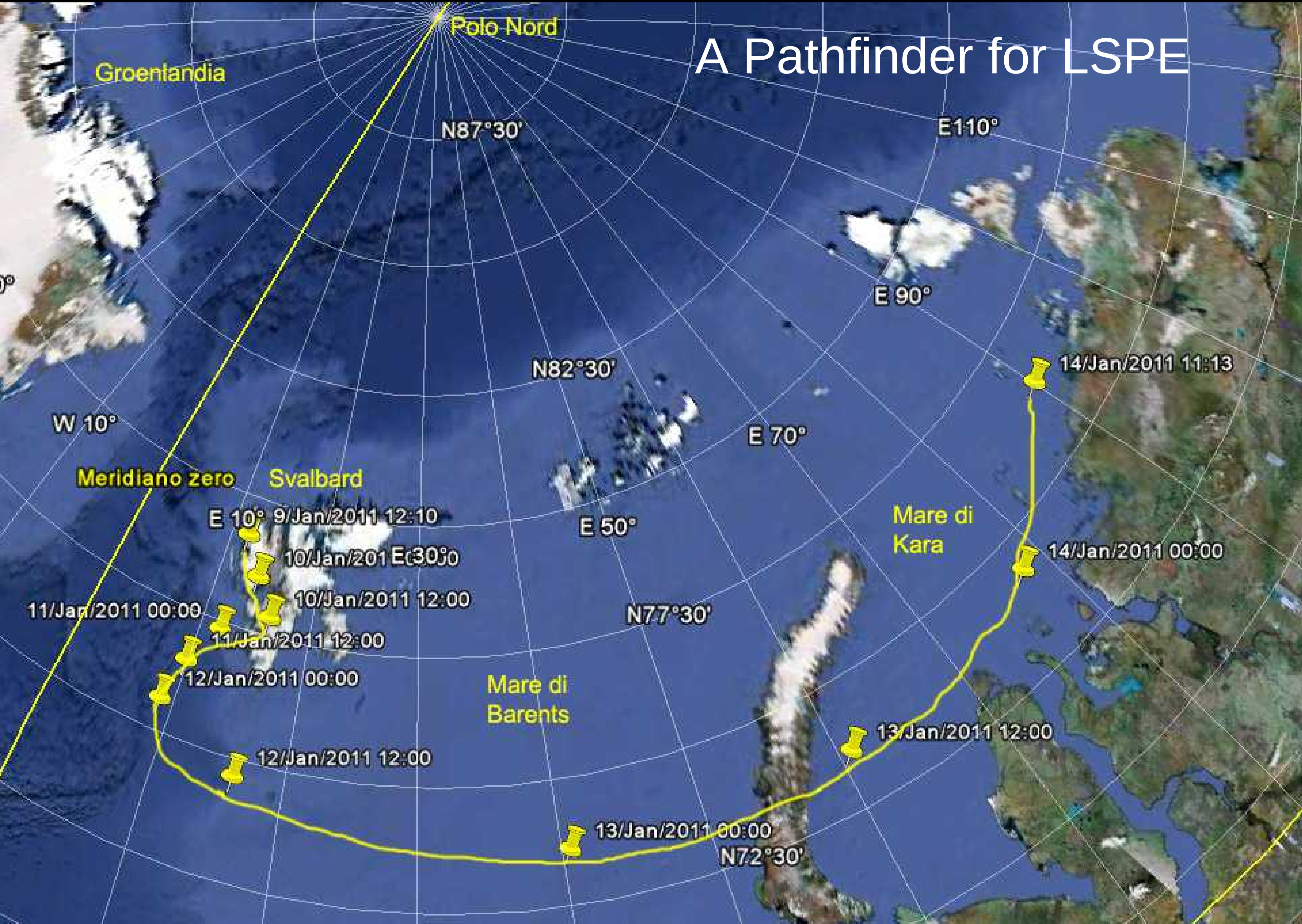

And now let’s dream …

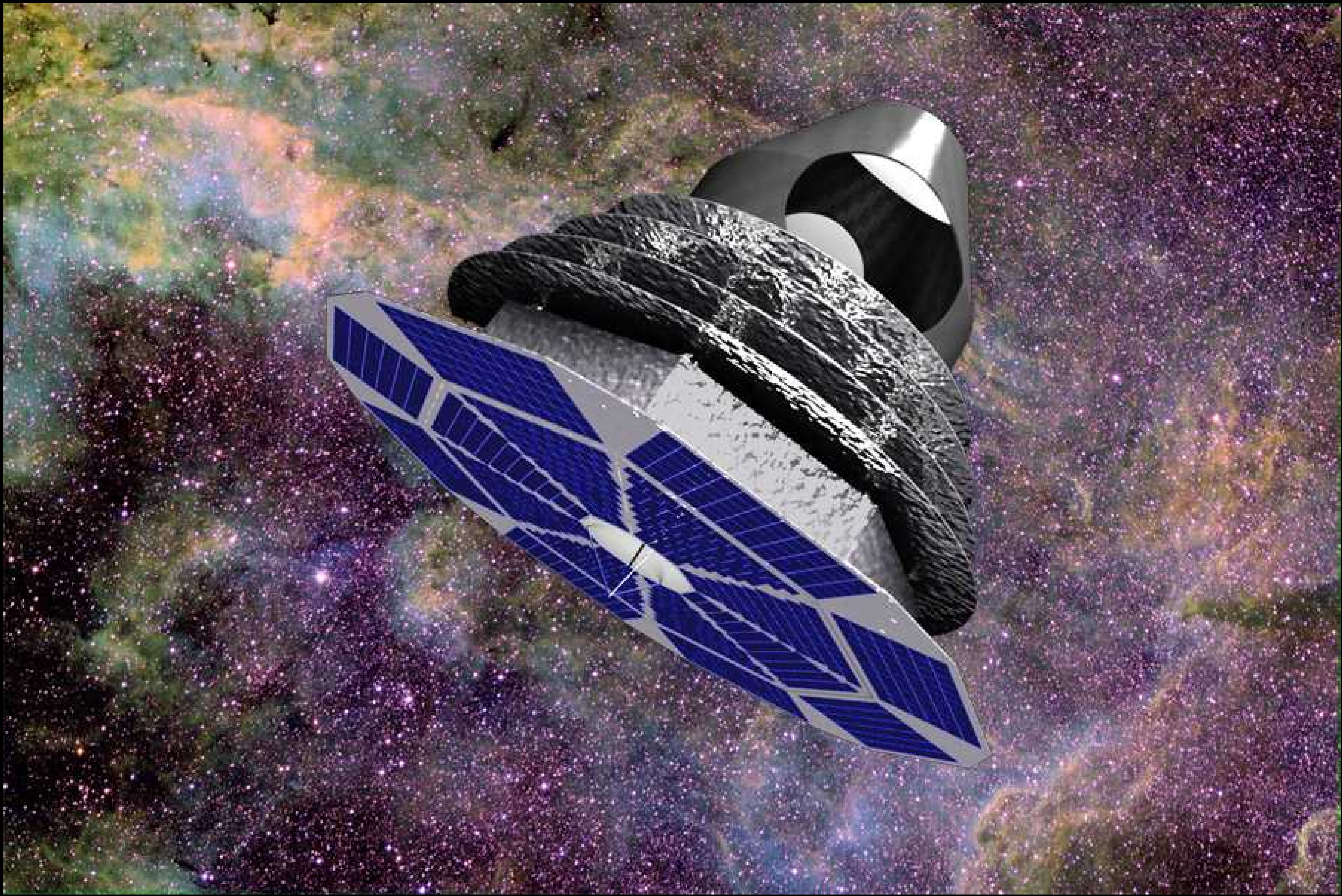

COrE: www.core-mission.org ESA-M3 (2020)

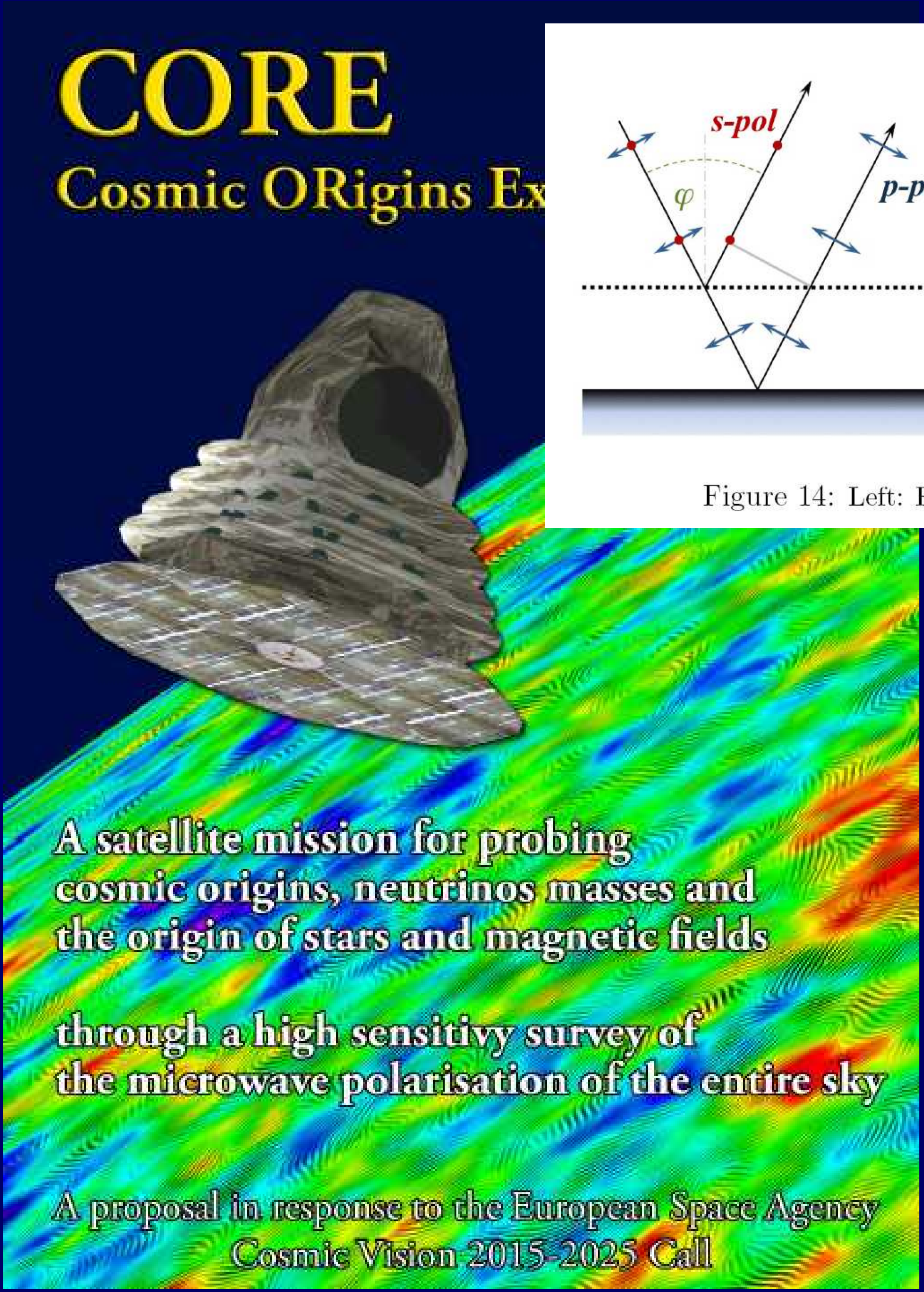

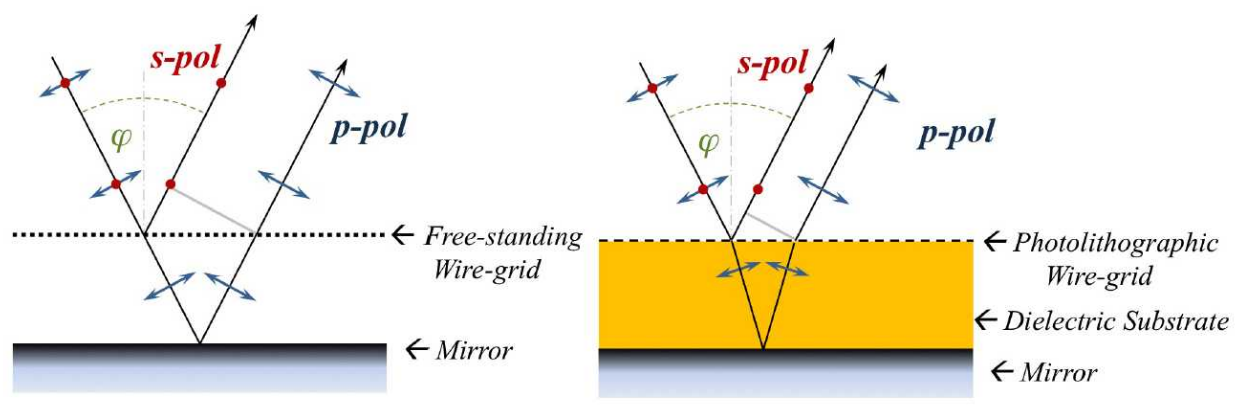

Figure 14: Left: Free-standing RHWP. Right: Dielectric substrate RHWP

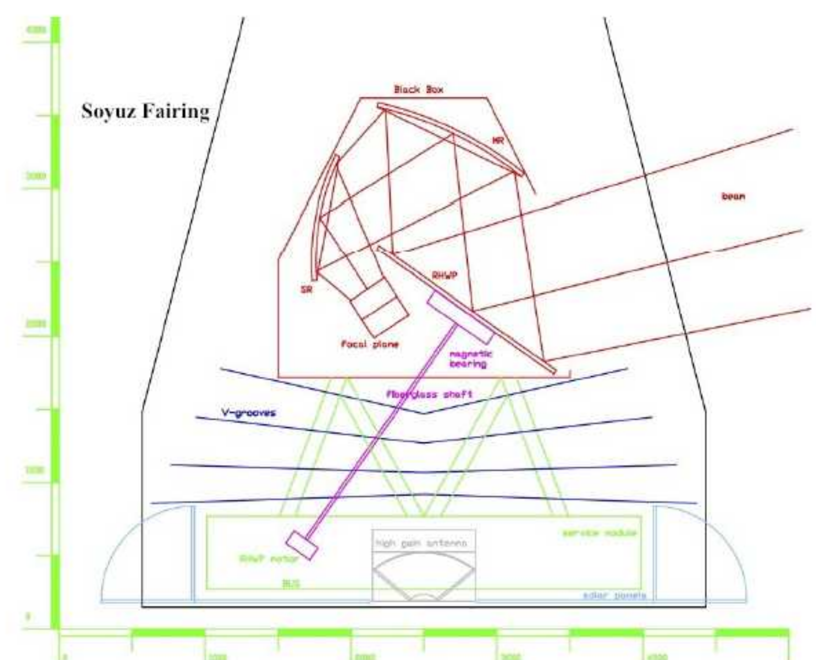

Figure 10: Fairing accommodation of *COrE*.

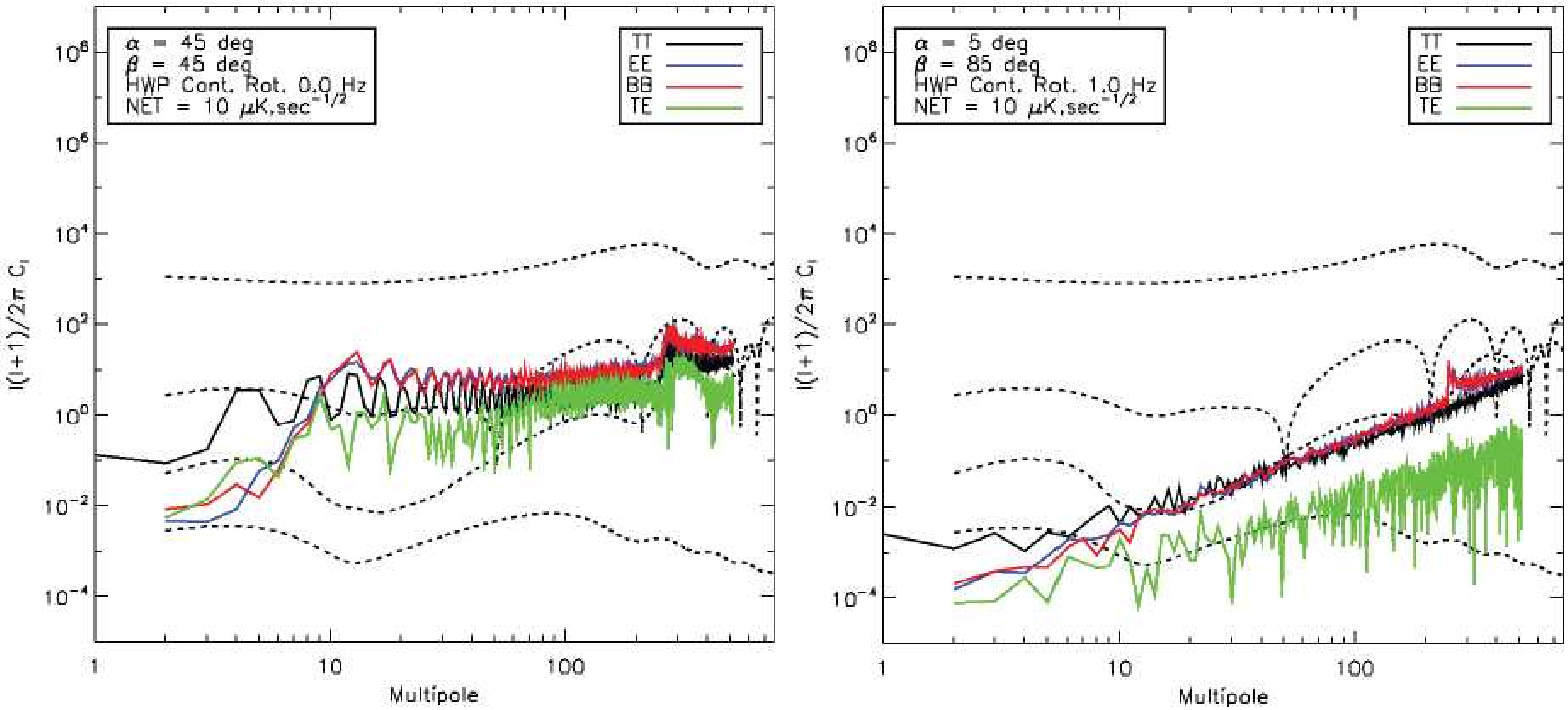

Figure 12: Angular power spectra of the $1/f$ noise timelines: Previous B-Pol proposal without HWP (left), Planck and continuously rotating HWP at 1Hz (right).

Table 2: *COrE* performances - assuming a 50% value for detection chain efficiency.

Central Freq. (GHz)	$\Delta\nu$ (GHz)	$N_{detectors}$	FWHM (arcmin)	Unpol. sensitivity (μK.arcmin)	Q & U sensitivity (μK.arcmin)
45	15	64	23.3	5.2	9.0
75	15	300	14	2.7	4.7
105	15	400	10	2.7	4.6
135	15	550	7.8	2.6	4.5
165	15	750	6.4	2.6	4.6
195	15	1150	5.4	2.6	4.5
225	15	1800	4.7	2.6	4.5
255	15	575	4.1	6.0	10.4
285	15	375	3.7	10.0	17
315	15	100	3.3	26.6	46
375	15	64	2.8	67.8	117
435	15	64	2.4	147.6	255
555	195	64	1.9	218	589
675	195	64	1.6	1268	3420
795	195	64	1.3	7744	20881

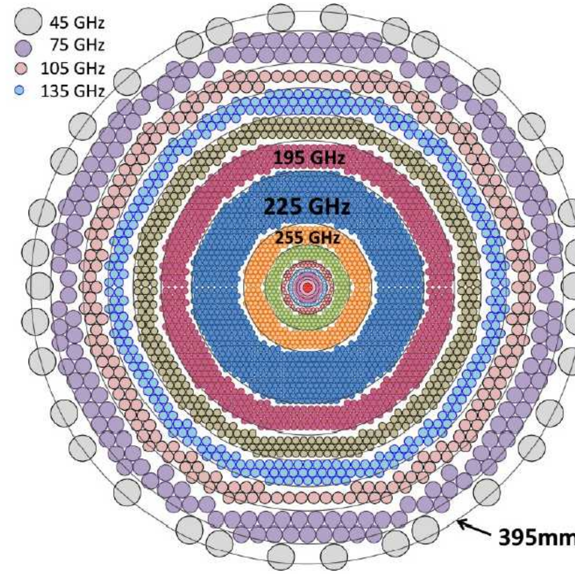

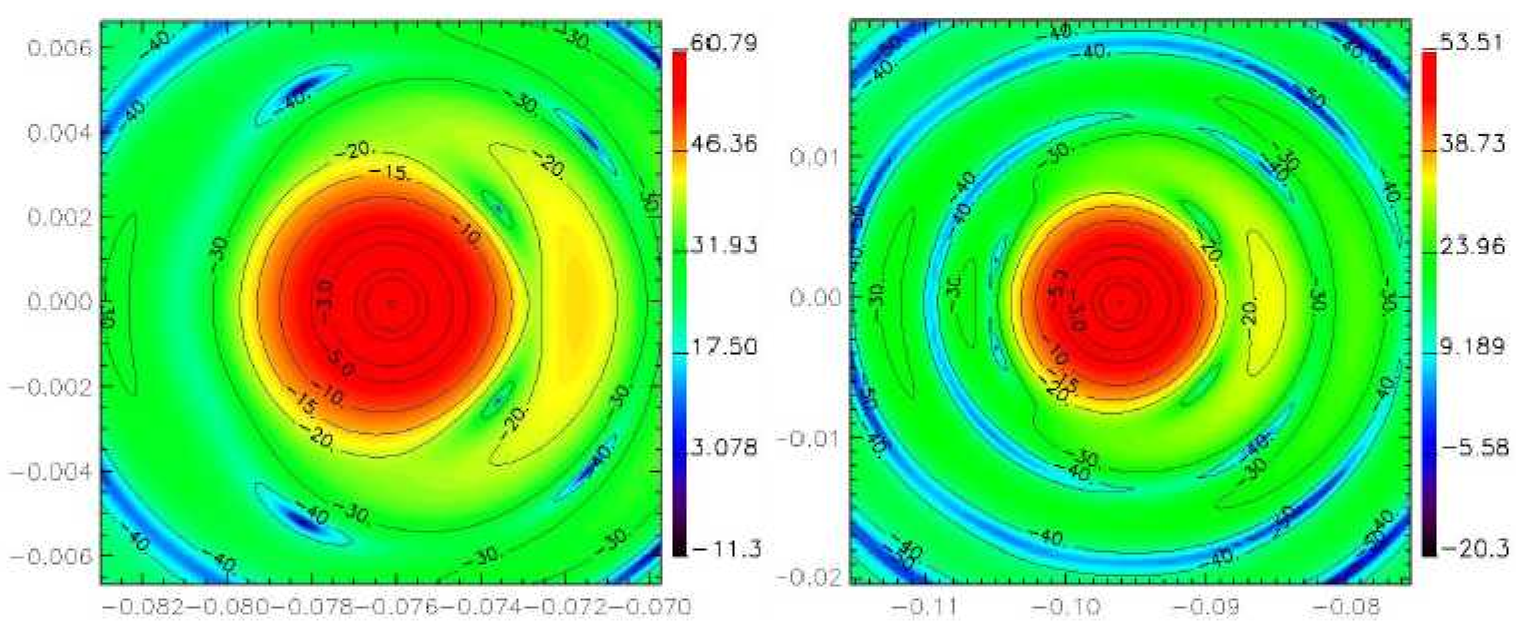

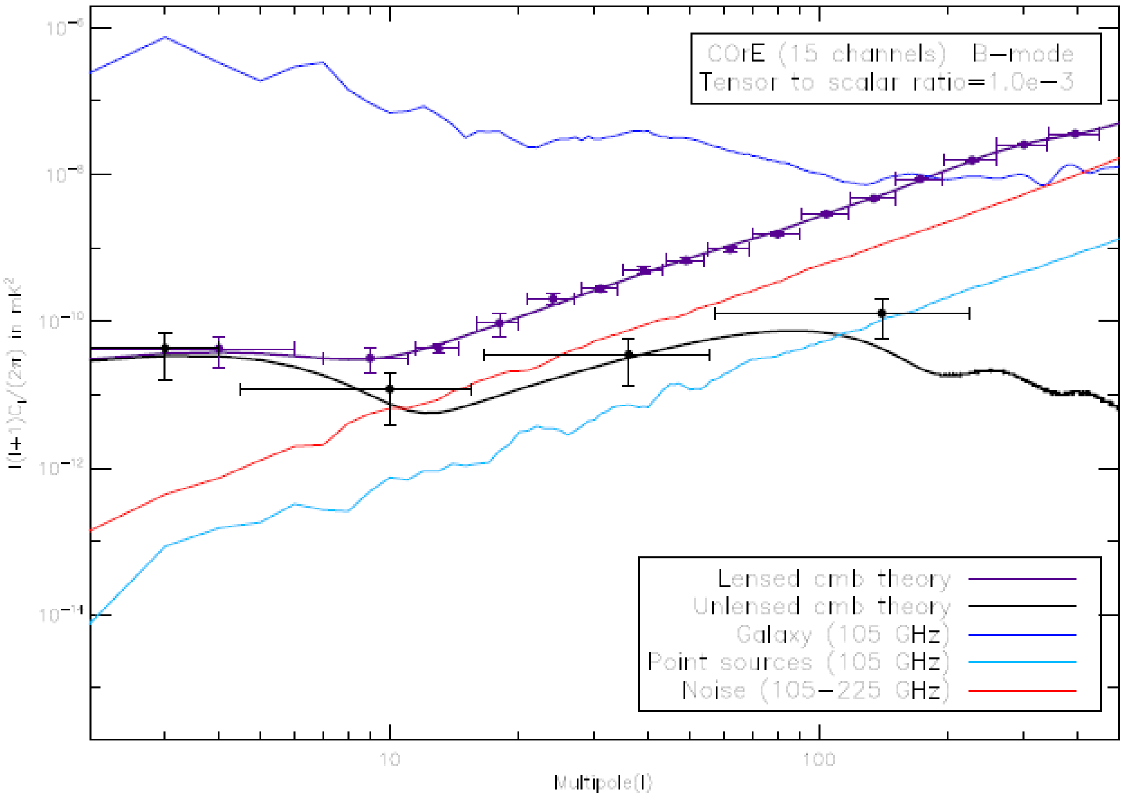

Figure 9: Component separation exercise for B mode detection assuming $(T/S) = 10^{-3}$. The solid black curve shows the predicted blackbody B mode power spectrum, which is a combination of the tensor B modes (black curve) and a gravitational lensing background (not shown) making primordial E modes appear as B modes in part. The upper solid blue curve shows the contribution of diffuse galactic emission in one of the "cleaner" channels (here 105 GHz). The red curve indicates the instrument noise that would be obtained combining five CMB channels, an the light blue curve indicates contamination by point sources after the brightest ones ($S > 100\,\mathrm{mJy}$ at 20GHz and $S > 500\,\mathrm{mJy}$ at 100 microns) have been cut out. The purple data points indicate the recovered raw primordial spectrum measurements, as compared to the theoretical spectrum (purple line). The black points result after the gravitational lensing contribution has been removed, leaving only the recovered tensor contribution. Here a galactic cut with a conservative $f_{sky} \simeq 0.50$ has been used.

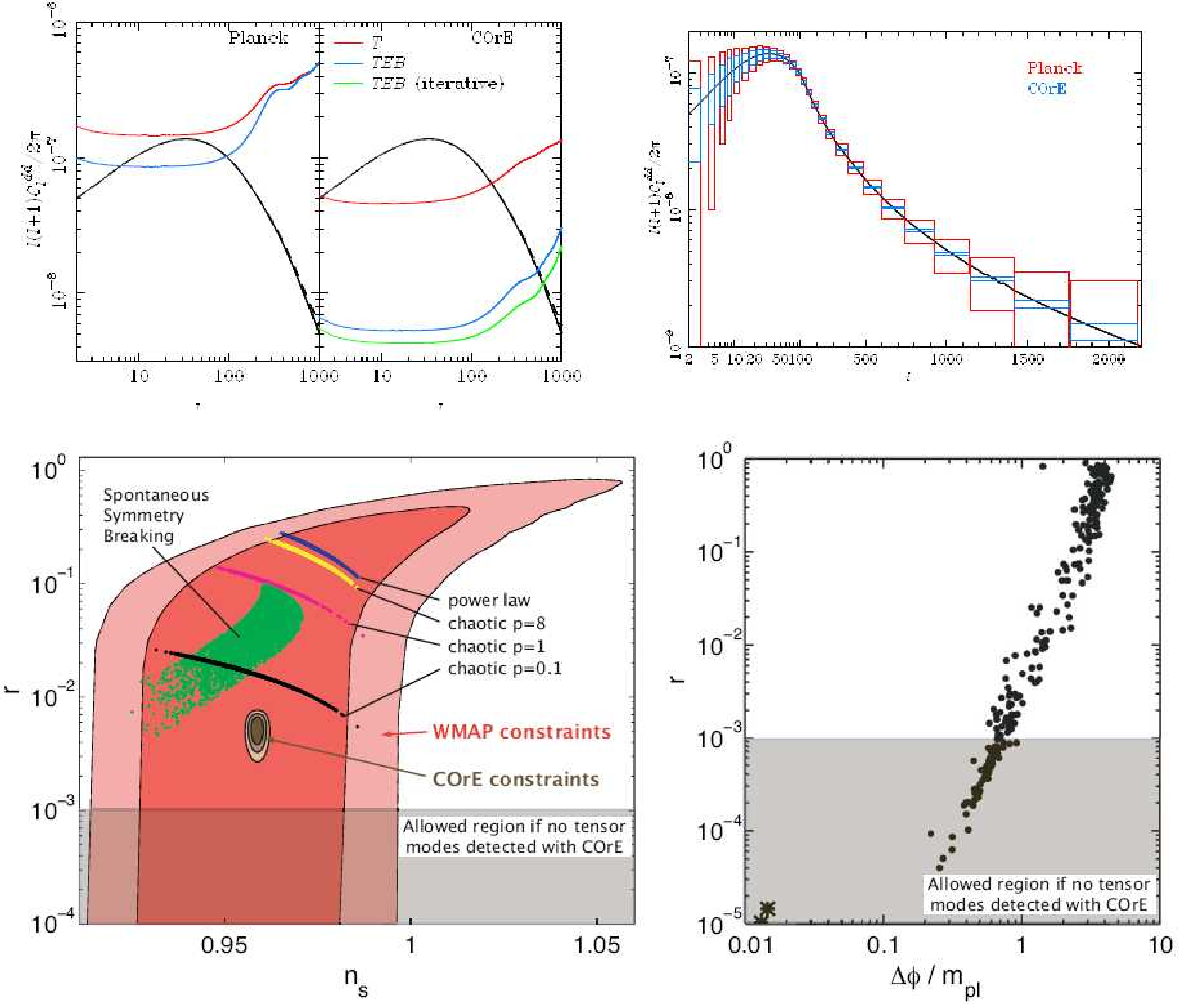

Planck
COrE
T
TEB
TEB (iterative)
$\ell(\ell+1)C_\ell^{dd}/2\pi$
10
100
1000
Planck
COrE
ℓ
Spontaneous Symmetry Breaking
power law
chaotic p=8
chaotic p=1
chaotic p=0.1
WMAP constraints
COrE constraints
Allowed region if no tensor modes detected with COrE
r
n_s
0.95
1
1.05
$\Delta\phi$ / m_{pl}
0.01
0.1
1
10

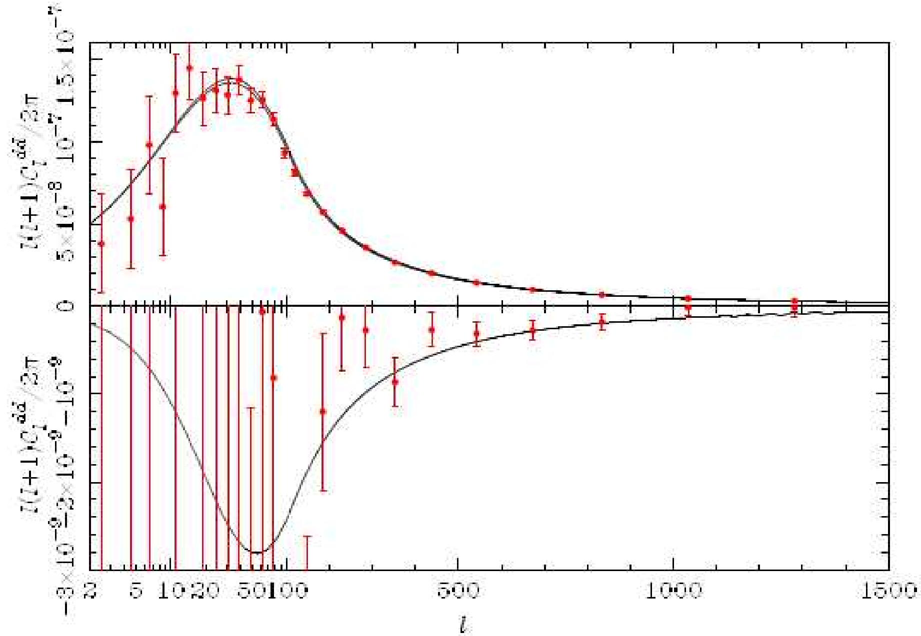

Figure 5: Simulated deflection power spectrum from *COrE* assuming an inverted hierarchy of neutrino masses with the minimum total mass allowed by oscillation data ($m_1 \approx m_2 = 0.05\,\mathrm{eV}$ and $m_3 = 0\,\mathrm{eV}$). In the upper panel, the solid lines are the theory power spectrum for this scenario (lower) and for three massless neutrinos (upper). The difference between these spectra is plotted in the lower panel illustrating how *COrE* can distinguish these scenarios from C_l^{dd} in the range $l > 200$.

- If neutrinos have hierarchical masses, *COrE* will bound the lightest mass to $m_1 < 0.034\,\mathrm{eV}$ (normal) and $m_3 < 0.045\,\mathrm{eV}$ (inverted) at 95% confidence.
- The minimal-mass inverted hierarchy could be distinguished from a scenario with three massless neutrinos at the 3σ level.
- If neutrino masses are degenerate, *COrE* will measure the total mass to $0.03\,\mathrm{eV}$ (1σ error). For comparison, the error expected from the Planck nominal mission (including lensing) is $0.10\,\mathrm{eV}$.

Precision measurements of the CMB:

The Sunyaev-Zeldovich Effect

Hot Plasma in Clusters of galaxies

visibile ← **Coma cluster** → X-rays

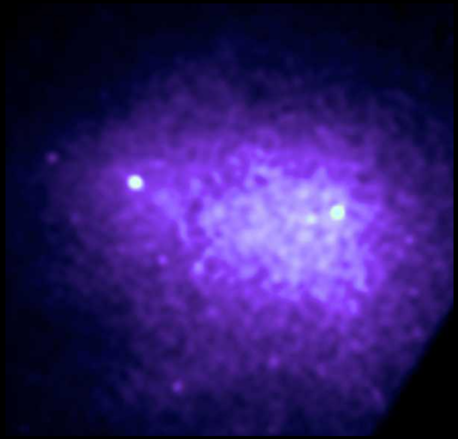

- X-ray measurements show that there is a hot (>10^7K) ionized and diluted gas filling the intracluster volume between galaxies.
- The baryonic mass of this gas can be more than the baryonic mass in the galaxies of the cluster.

Sunyaev-Zeldovich Effect

- Inverse Compton Effect for CMB photons against electrons in the hot gas of clusters
- Cluster optical depth: $\tau = n\sigma\mathbf{l}$ where $\mathbf{l}$ = a few Mpc = 10^{25} cm, $n < 10^{-3}$ cm^{-3} , σ = 6.65×10^{-25} cm^2
- So $\tau = n\sigma\mathbf{l} = 0.01$: there is a 1% likelihood that a CMB photon crossing the cluster is scattered by an electron
- $E_{electron} >> E_{photon}$, so the electron transfers part of his energy to the photon. To first order, the energy gain of the photon is

- The resulting CMB temperature anisotropy is

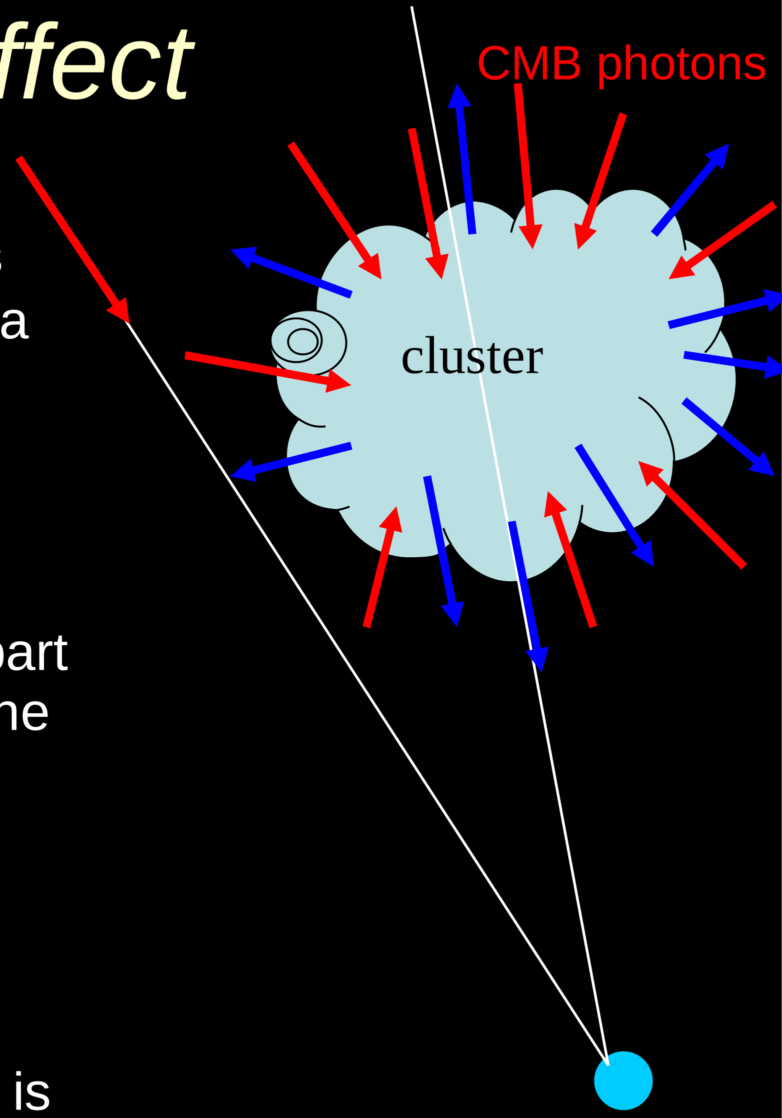

Sunyaev R., Zeldovich Y.B., 1972, Comm. Astrophys. Space Phys., 4, 173

Birkinshaw M., 1999, Physics Reports, 310, 97-195

The Sunyaev-Zeldovich Effect

- The S-Z Effect does not depend on the distance (redshift) of the cluster, and depends linearly on the density of the gas
- X-ray flux decreases significantly with distance and gas density (depends on the square of the density).

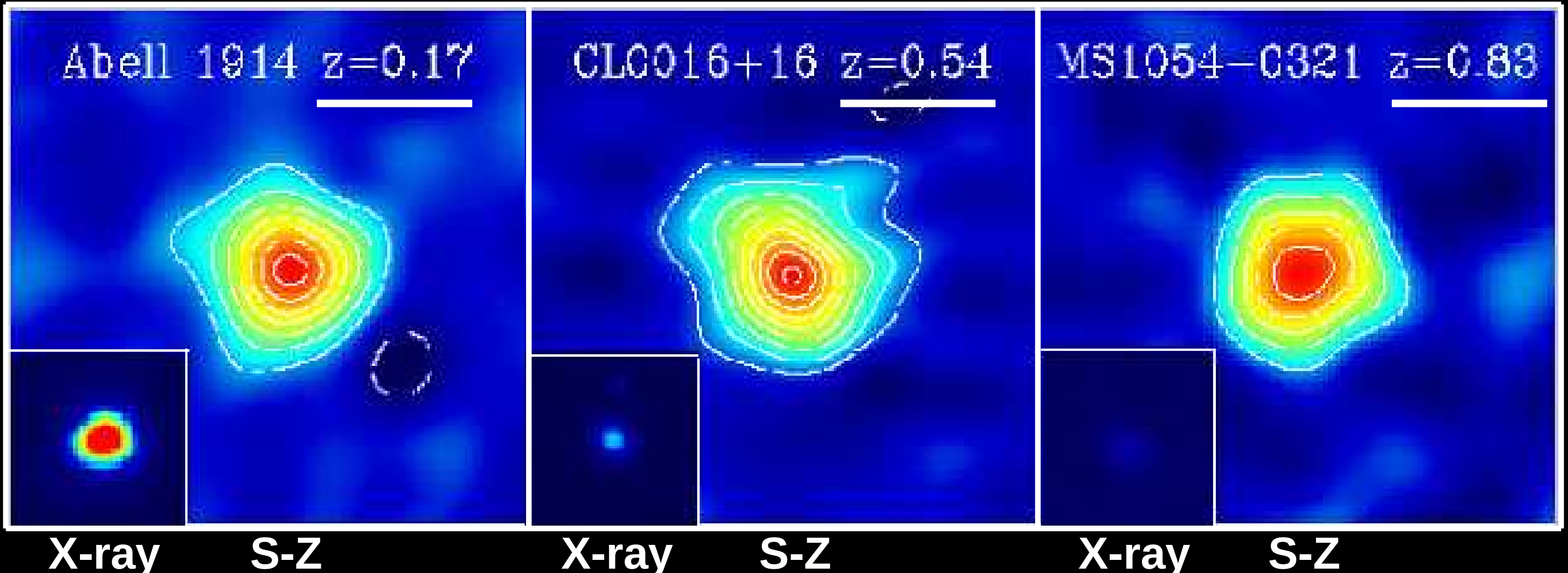

Sunyaev-Zeldovich Effect

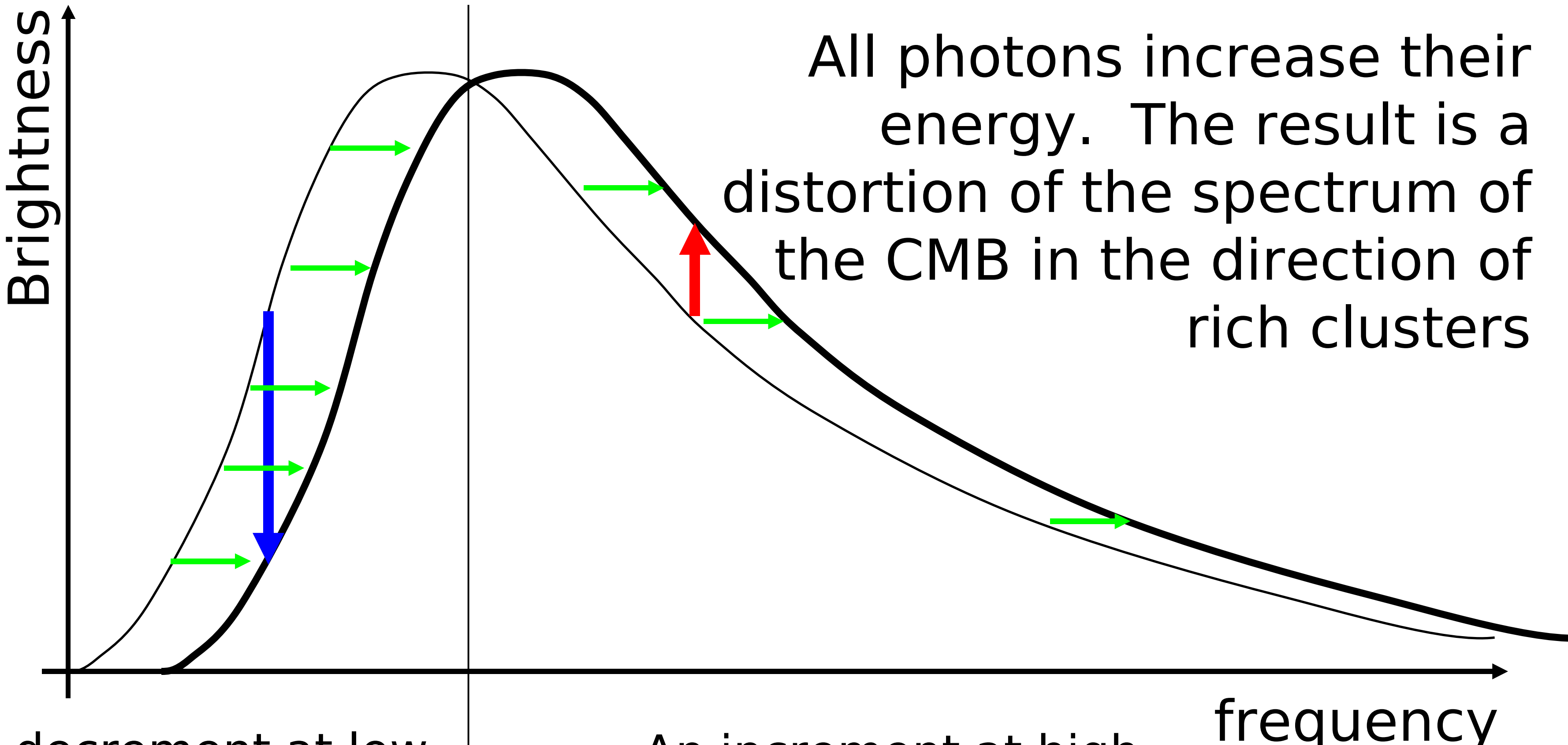

All photons increase their energy. The result is a distortion of the spectrum of the CMB in the direction of rich clusters

A decrement at low frequencies
(<217GHz)

An increment at high frequencies
(> 217GHz)

Kinematic S-Z

- In addition, if the cluster has a peculiar velocity (deviation from Hubble's flow) the scatterers are moving, and the scattered radiation undergoes a Doppler effect:

$$\frac{\Delta T}{T} = \tau \frac{\mathrm{v}}{\mathrm{c}}$$

- This has the same spectrum as CMB anisotropy

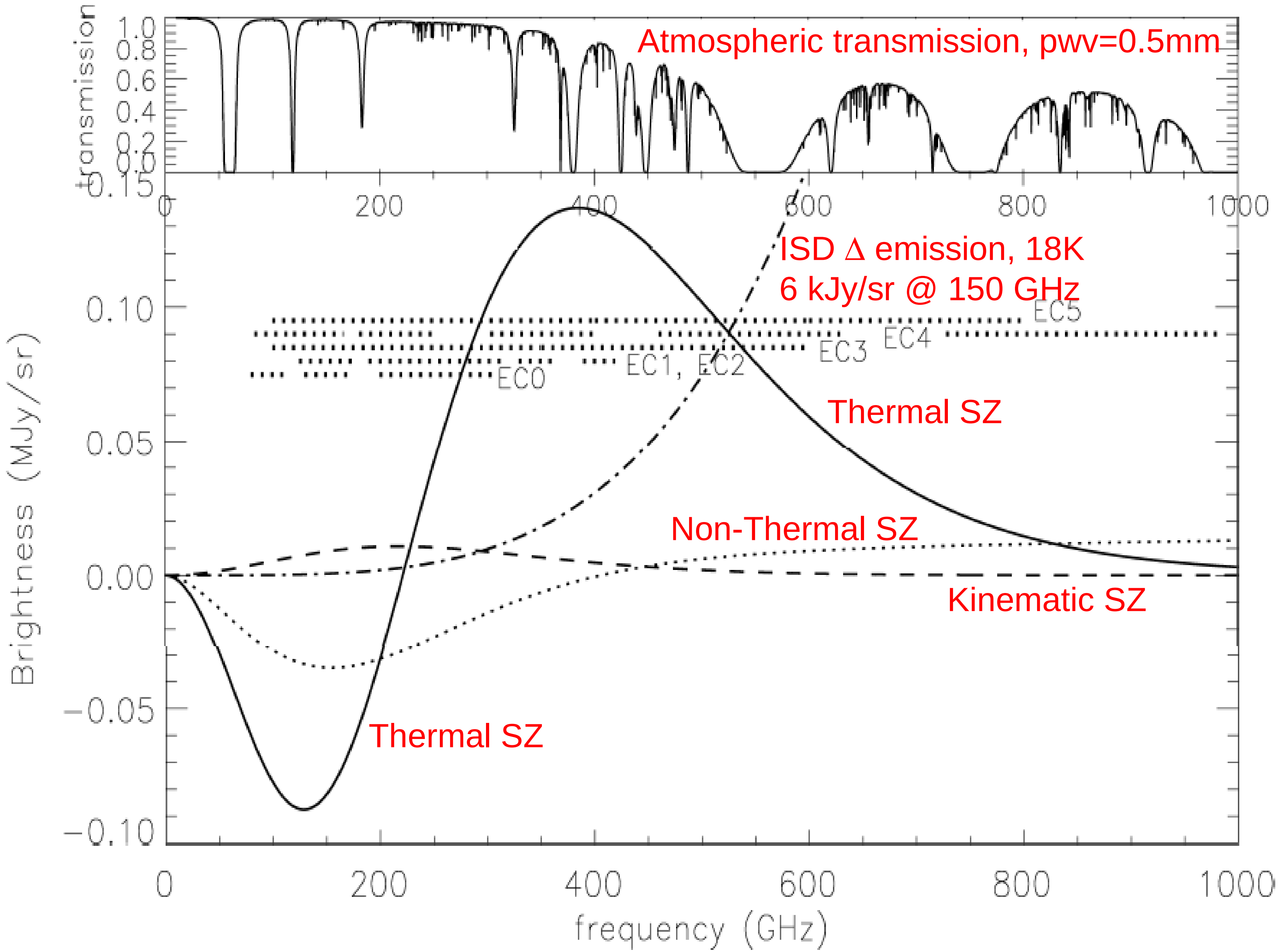

Atmospheric transmission, pwv=0.5mm
transmission
1.0
0.8
0.6
0.4
0.2
0.0
0.15
0.10
0.05
0.00
−0.05
−0.10
Brightness (MJy/sr)
0
200
400
600
800
1000
frequency (GHz)
ISD Δ emission, 18K
6 kJy/sr @ 150 GHz
EC0
EC1, EC2
EC3
EC4
EC5
Thermal SZ
Non-Thermal SZ
Kinematic SZ
Thermal SZ

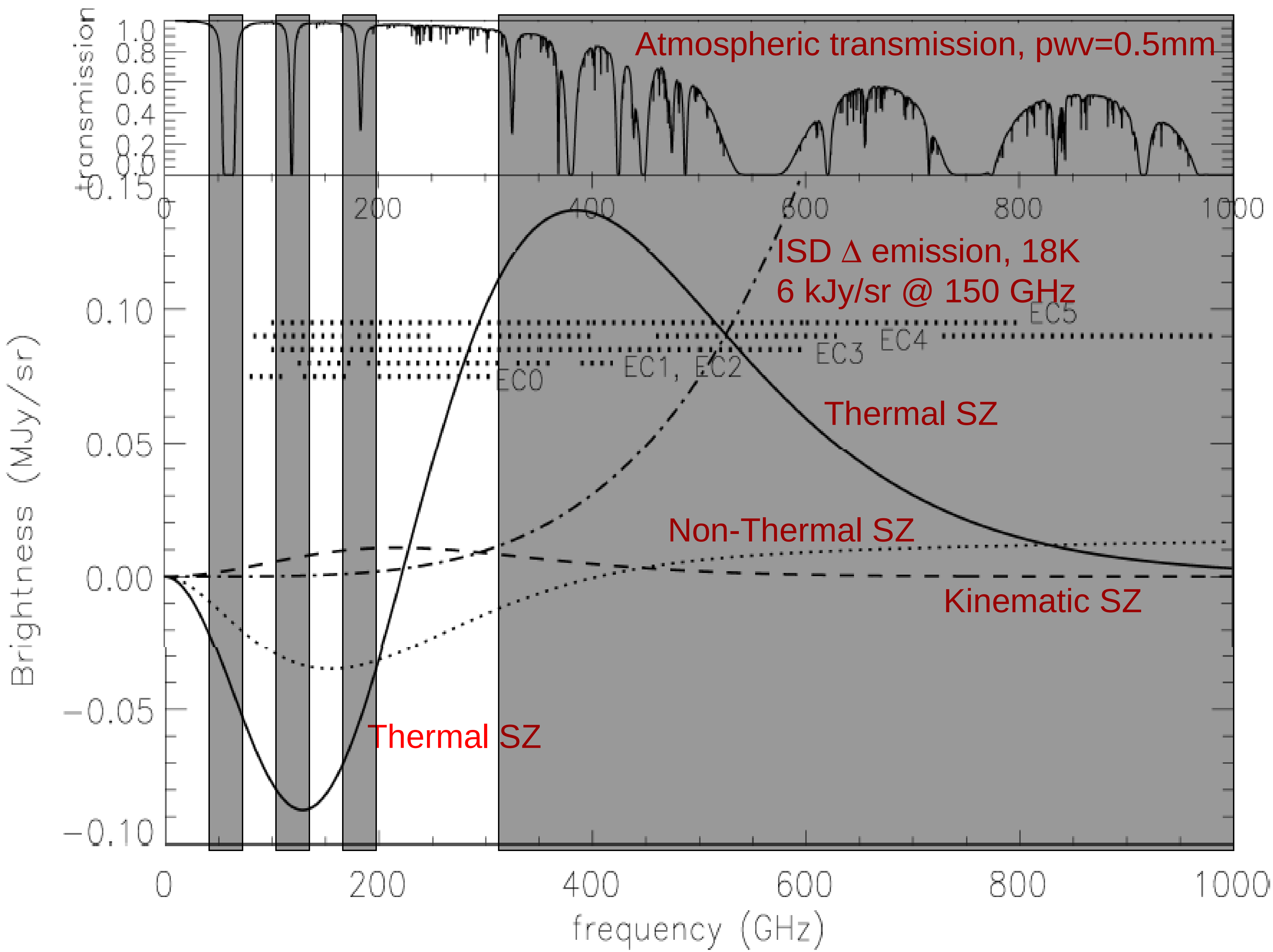

Atmospheric transmission, pwv=0.5mm
transmission
1.0
0.8
0.6
0.4
0.2
0.0
0.15
0.10
0.05
0.00
−0.05
−0.10
Brightness (MJy/sr)
ISD Δ emission, 18K
6 kJy/sr @ 150 GHz
EC0
EC1, EC2
EC3
EC4
EC5
Thermal SZ
Non-Thermal SZ
Kinematic SZ
Thermal SZ
0
200
400
600
800
1000
frequency (GHz)

Large Cluster (Coma-Like)

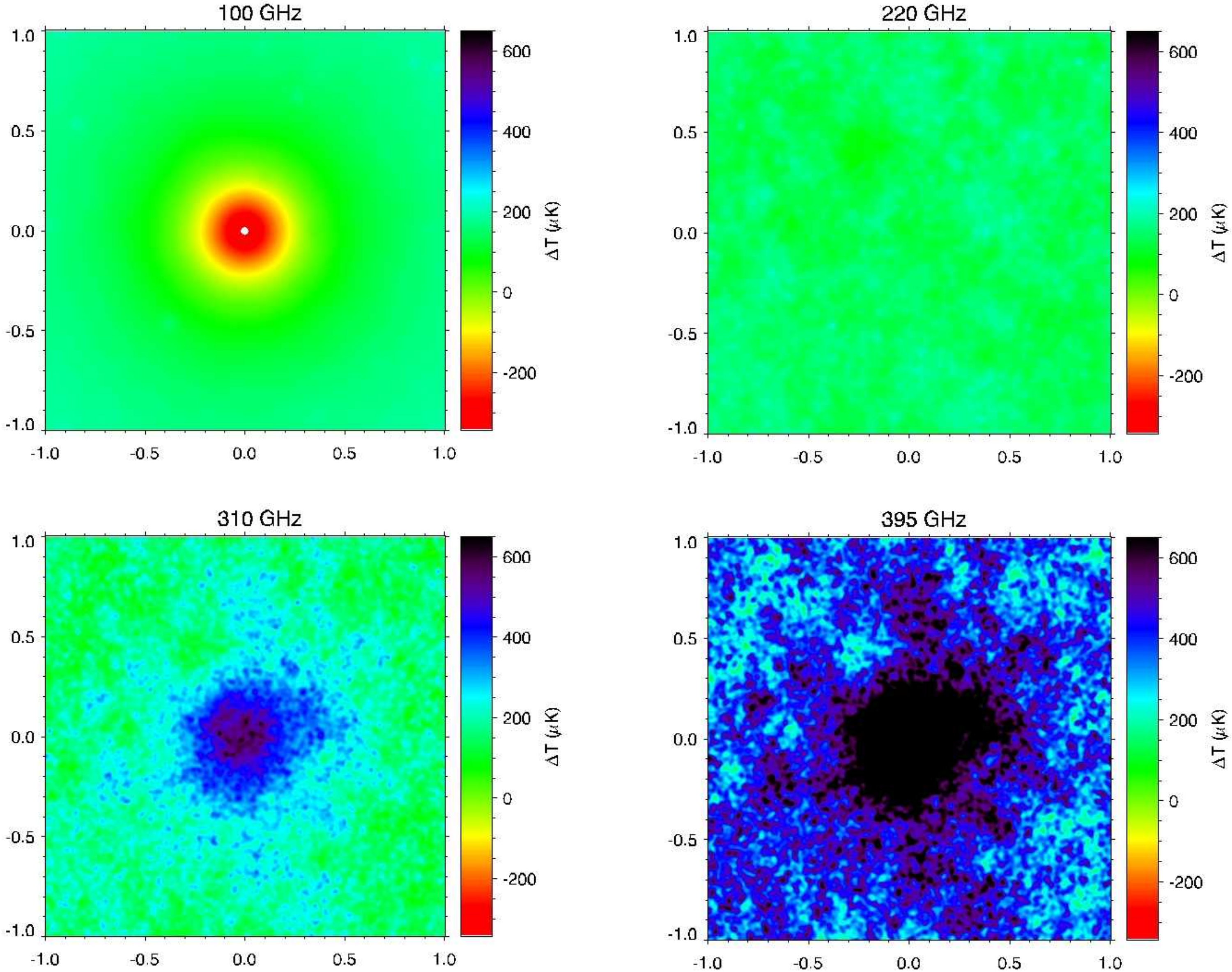

Simulated observation of a rich cluster, with a 3m telescope.

Components: SZ, CMB anisotropy, extragalactic sources

Small Cluster (1.2’ core)

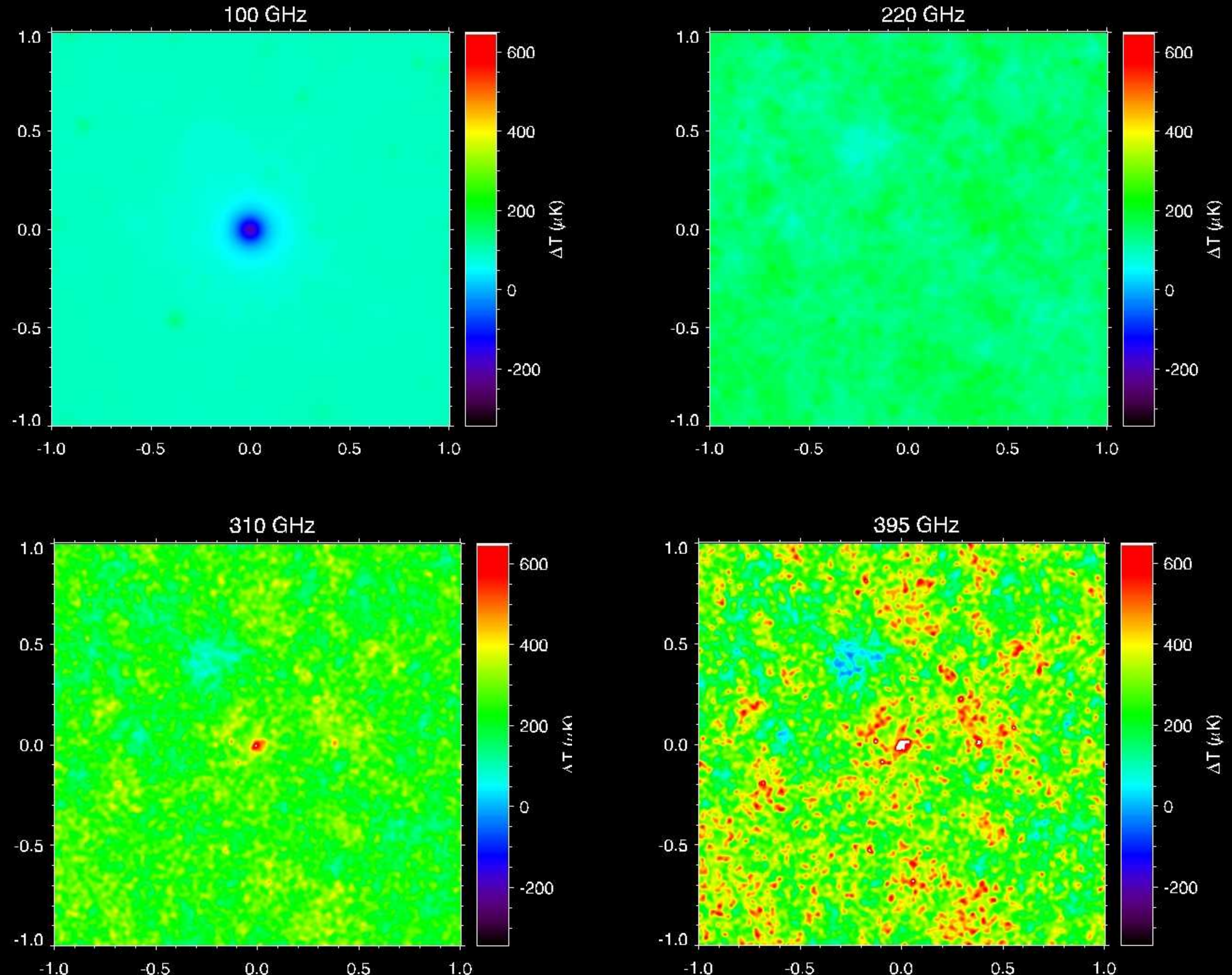

Simulated observation of a rich cluster, with a 3m telescope.

Components: SZ, CMB anisotropy, extragalactic sources

Dynamically Relaxed Clusters

X-ray
Images
(Chandra)

D = 1 GLy 3.5 GLy 6.7 GLy

0.4’ FWHM beam (λ = 1.1 mm D = 12000 mm)

0.5’ FWHM beam (λ = 1.4 mm D = 12000 mm)

0.7’ FWHM beam (λ = 2.0 mm D = 12000 mm)

Not all clusters are dynamically relaxed and well beheaved, like the ones above.
So we need large telescopes to study the internal structure,
and/or spectroscopic observations to detect non-thermal effects.

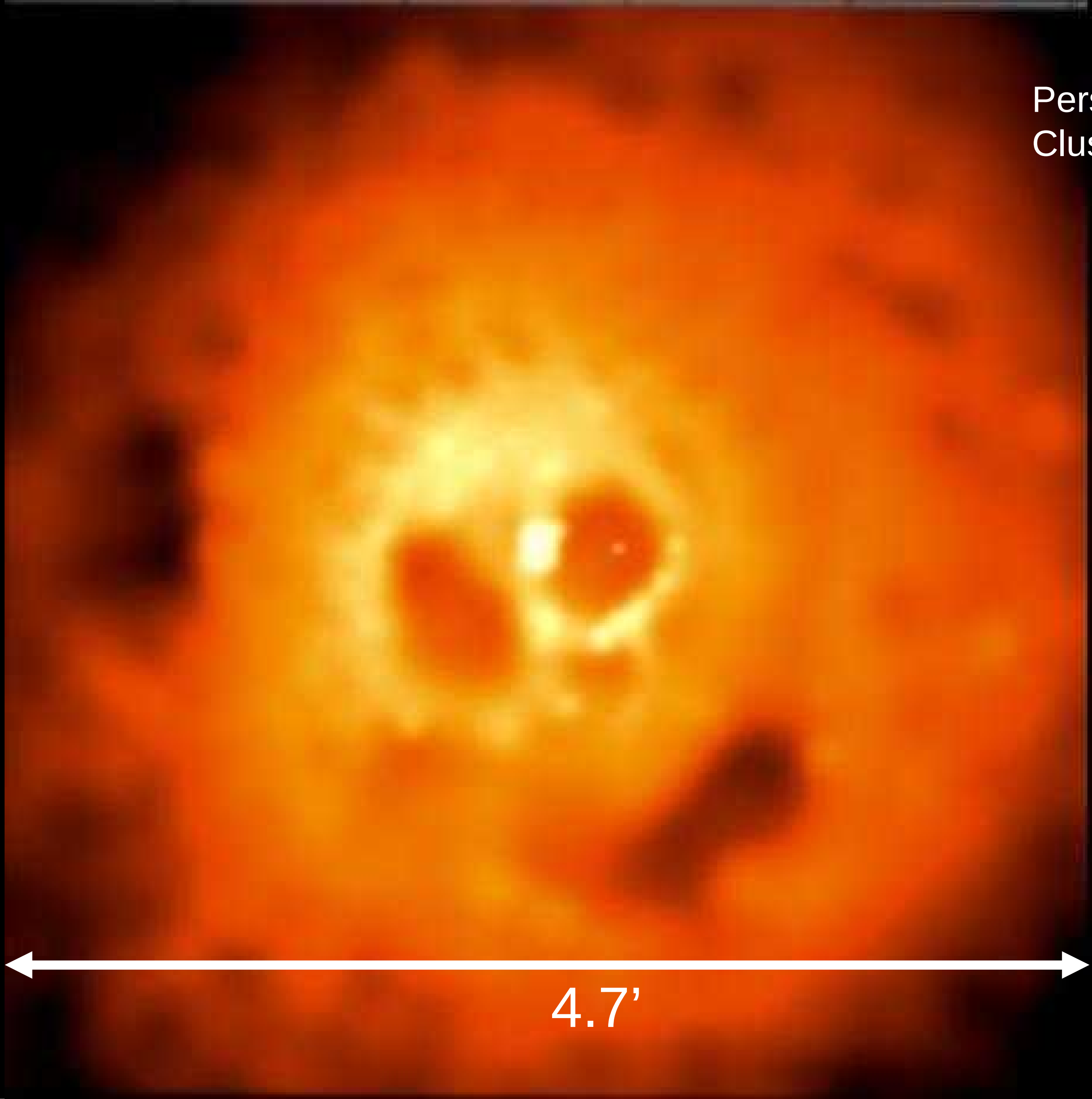
Perseus
Cluster
4.7’

large telescopes (10m class)

….

and large arrays

of detectors (1000 or more)

Atacama Cosmology telescope (ACT)
APEX – SZ
South Pole Telescope

2003

The South Pole Telescope

SPT

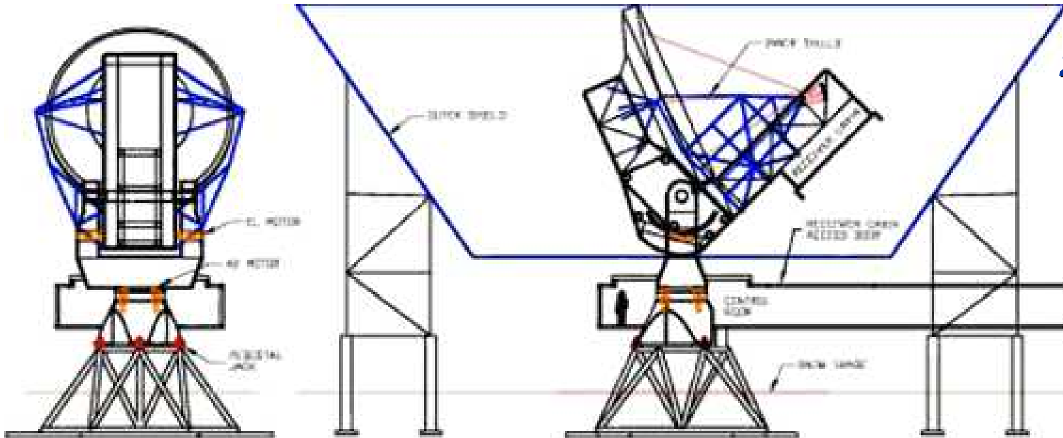

2006

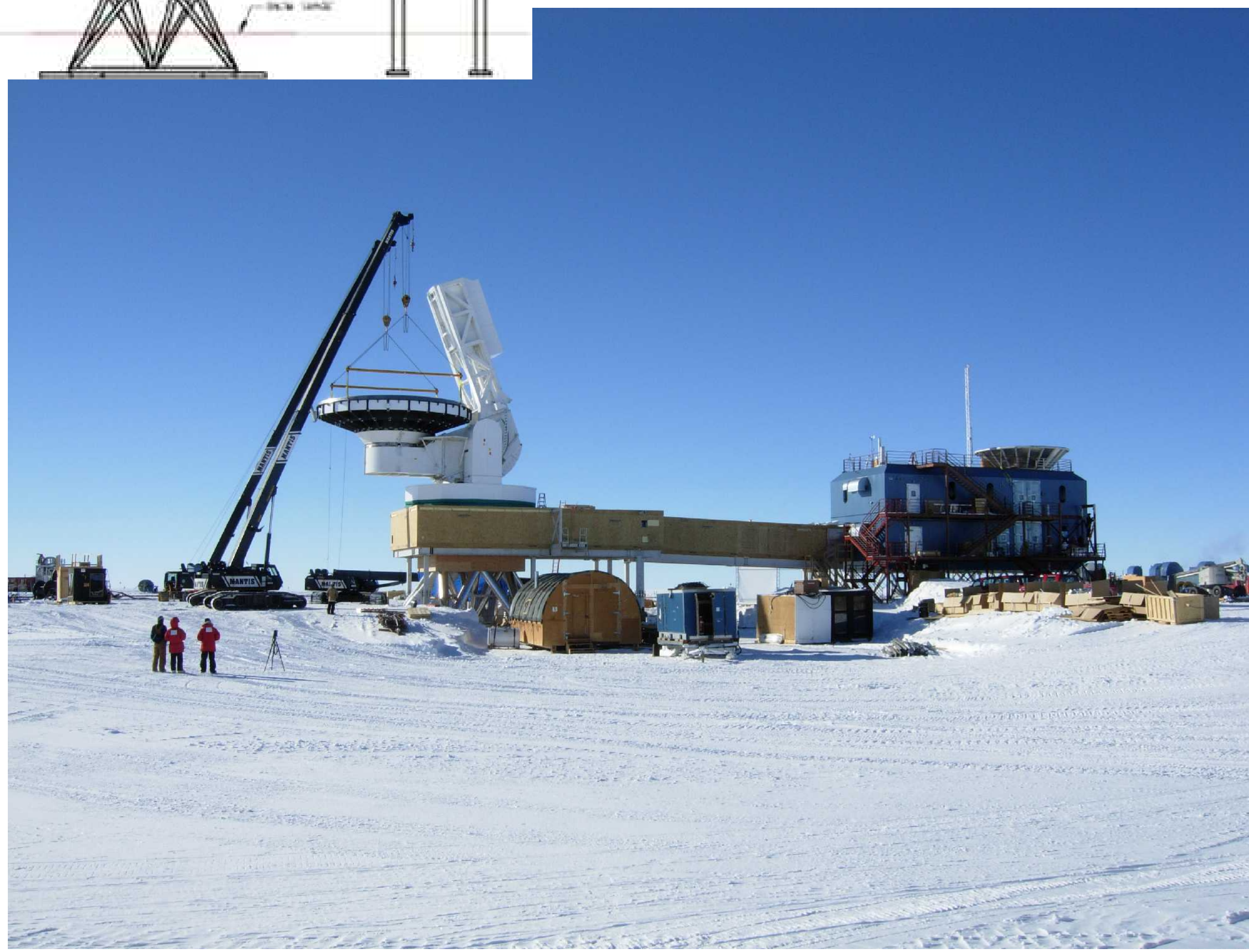

"The South Pole Telescope", Proc. SPIE, Vol. 5498, p 11-29, 2004 - astro-ph/0411122

2007: first light


Now

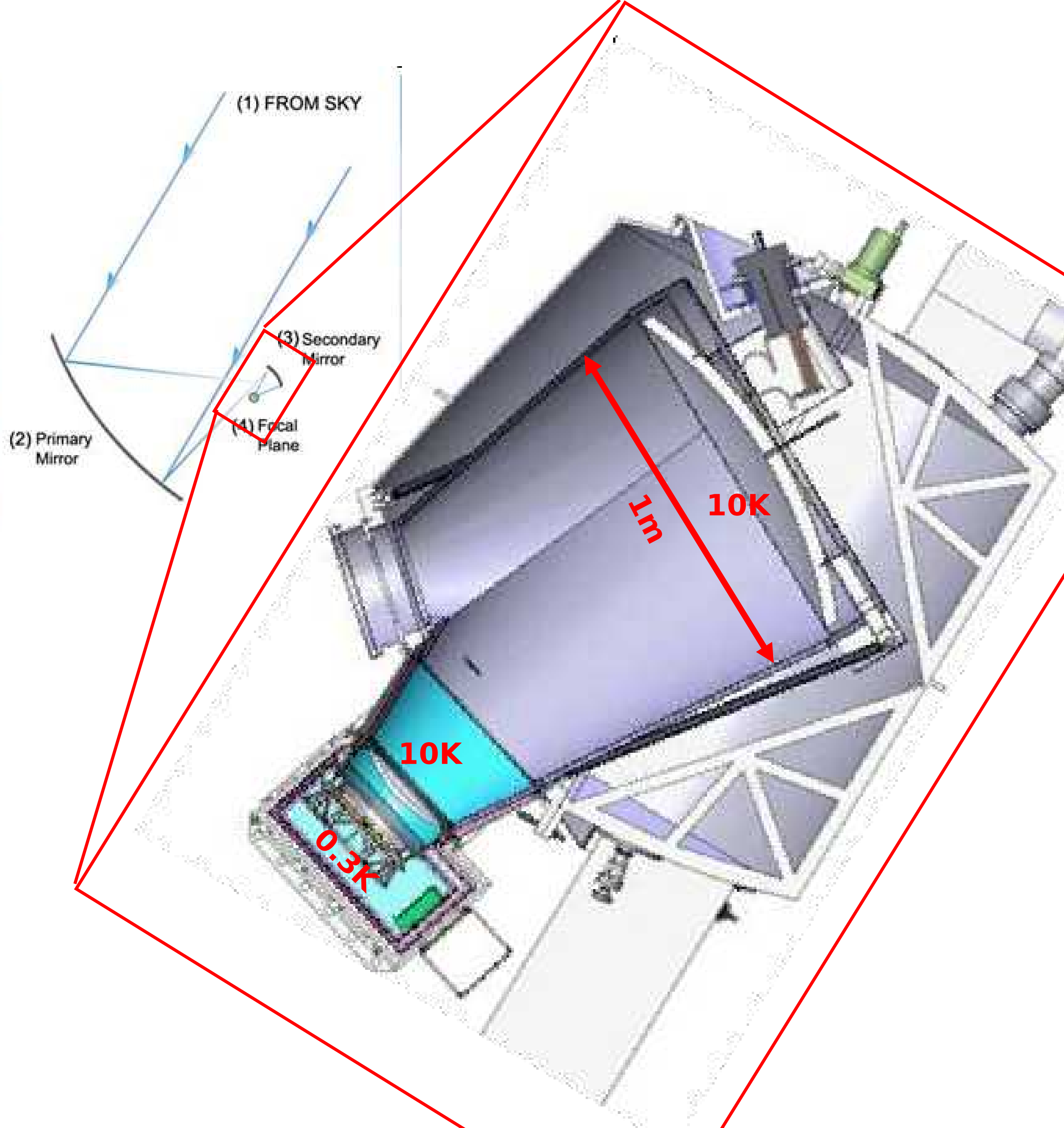
(1) FROM SKY
(3) Secondary Mirror
(2) Primary Mirror
(4) Focal Plane
1m
10K
10K
0.3K

Optics Cryostat + Receiver

Receiver Array

180 mm = 1 degree diameter (on sky)

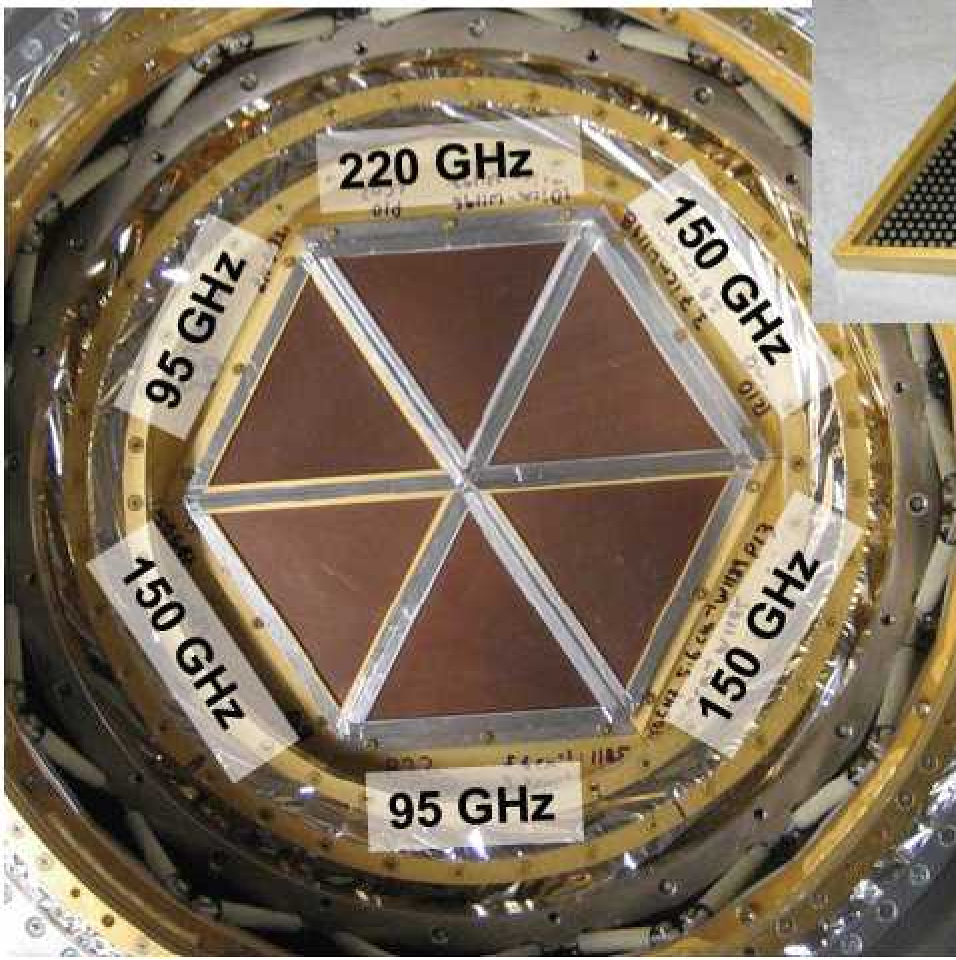

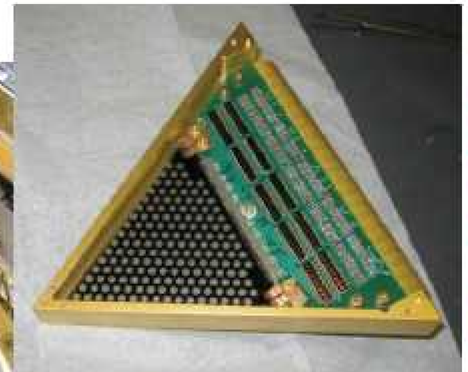

- 6 wedges * 160 bolometers per wedge = 960 channels
- 8 bolometers read out by a single SQUID using frequency-domain multiplexing
- Three bands: 90 GHz, 150 GHz, 220 GHz

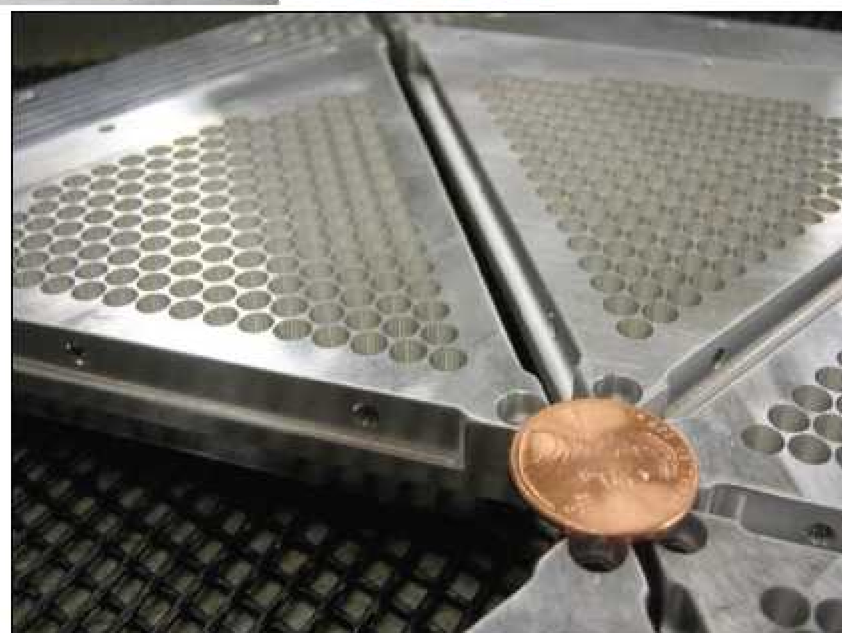

Bolometers

Suspended gold spiderweb bolometer read out with a TES and frequency domain multiplexing (like an AM radio)

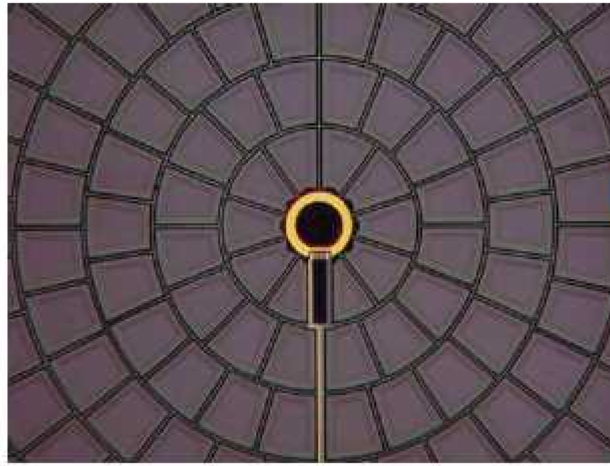

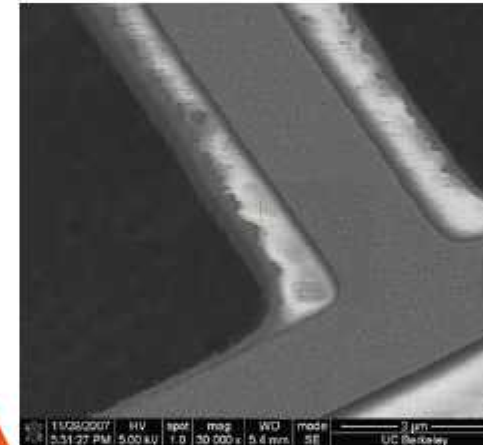

Al/Ti TES
Tc ~ 600mK

Six 160 pixel wedges are the heart of the SPT camera

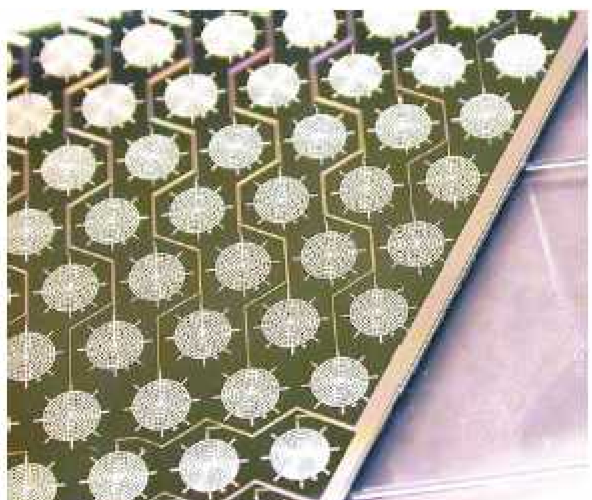

30 µm
TES detector

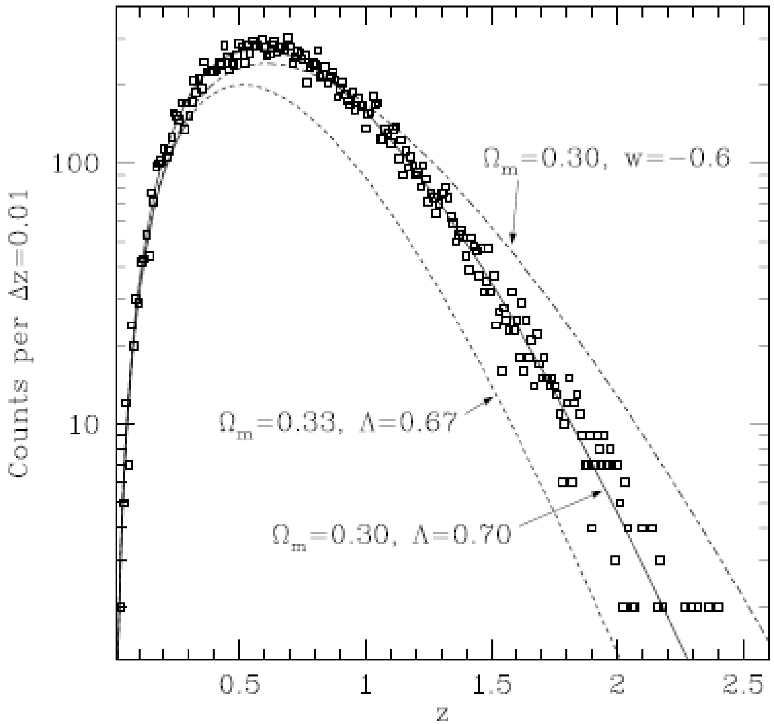

Figure 11. An illustration of the effect of cosmology on the expected number of SZE detected galaxy clusters as a function of redshift. The data points are appropriate for a 4000 square degree SPT survey with idealized sensitivity. The data points and the line passing through them were generated assuming a canonical $\Omega_M = 0.3$, $\Omega_\Lambda = 0.7, \sigma_8 = 1$ cosmology. The other two lines show the large effect in the expected cluster counts due to slight changes in the cosmology. The value of σ_8 was adjusted to give the same normalization for the local cluster abundance in each model. The bottom curve is for a model with more matter and correspondingly less dark energy. The top curve at shows the effect of only a change in the equation of state of the dark energy in the canonical model. (Figure courtesy of G. Holder)

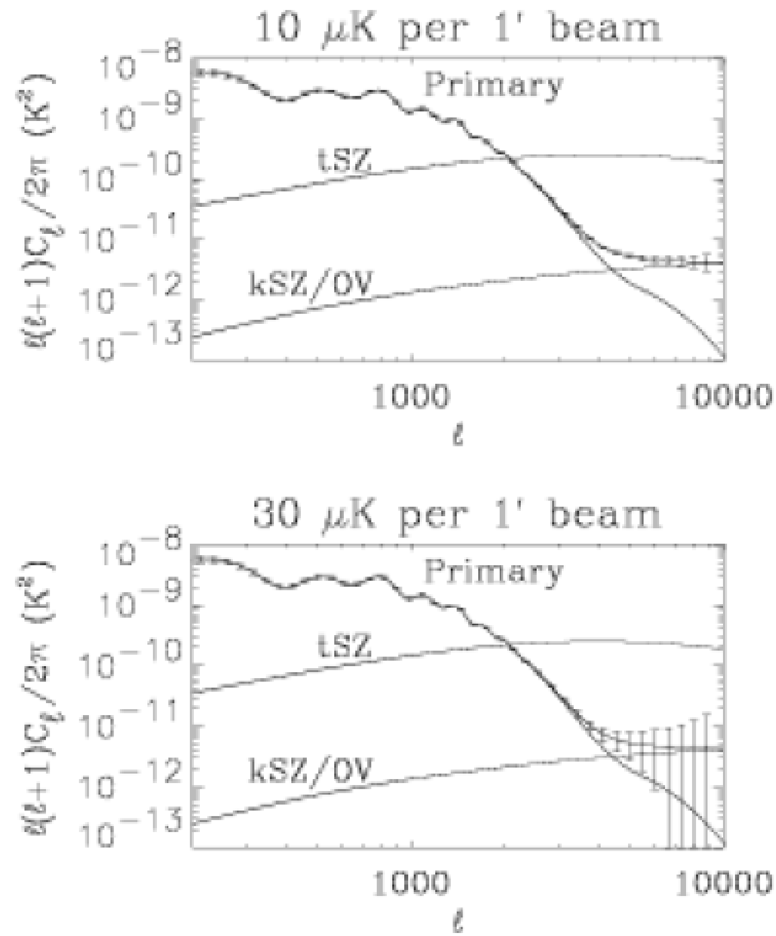

Figure 12. An illustration of the potential of the SPT to measure fine-scale CMB anisotropy. The two panels show statistical errors on the high-ℓ CMB power spectrum from 500 deg^2 of sky measured at two different levels of noise per 1′ beam. Both panels assume perfect subtraction of the thermal SZE signal and other astrophysical contaminants; achieving the required accuracy in this subtraction will be a significant challenge. (Spectra courtesy of W. Hu.)

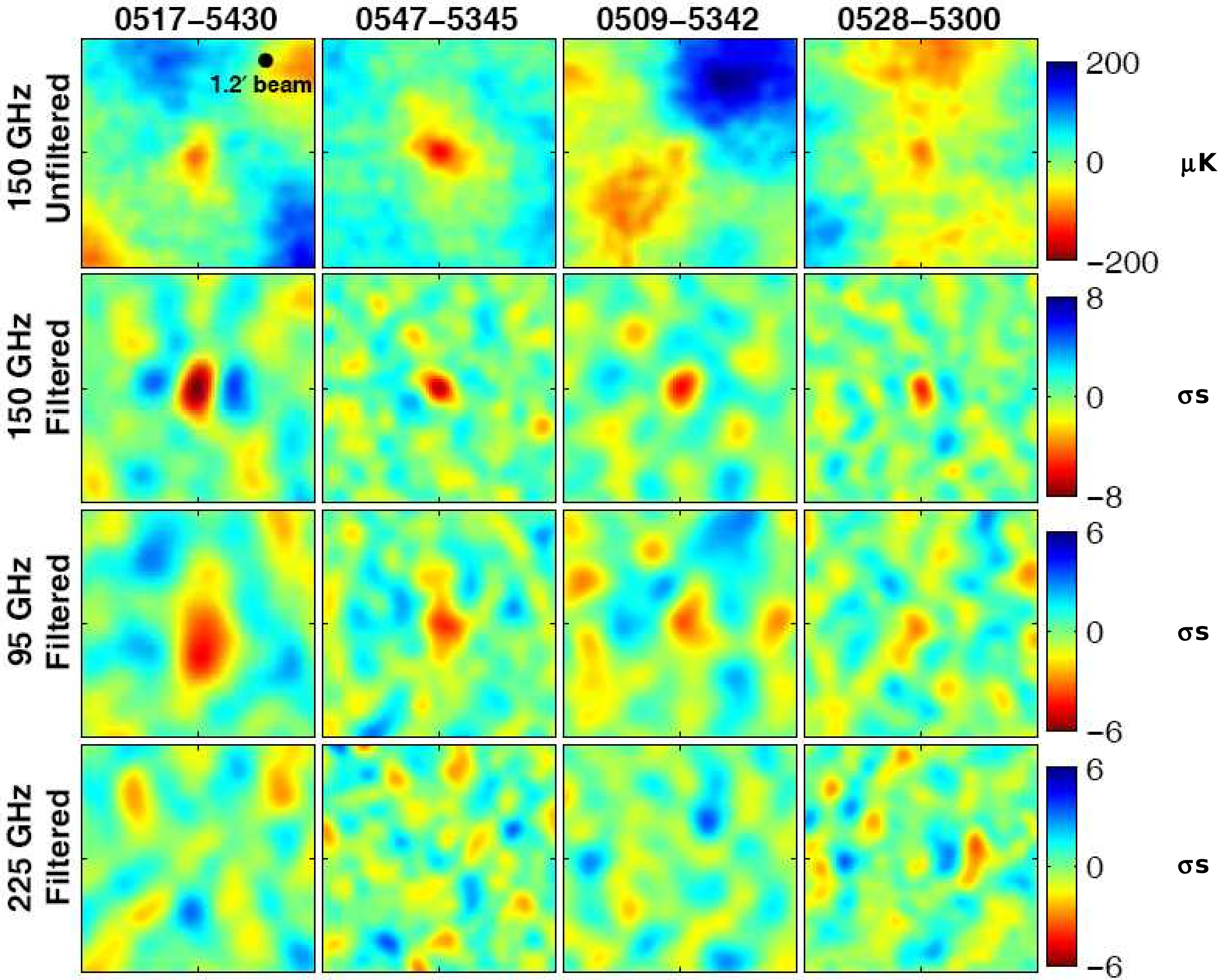

Galaxy clusters discovered with a Sunyaev-Zel'dovich effect survey - astro-ph/0810.1578

APEX 12m telescope
Atacama (ALMA site)

2 G. Siringo et al.: The Large APEX

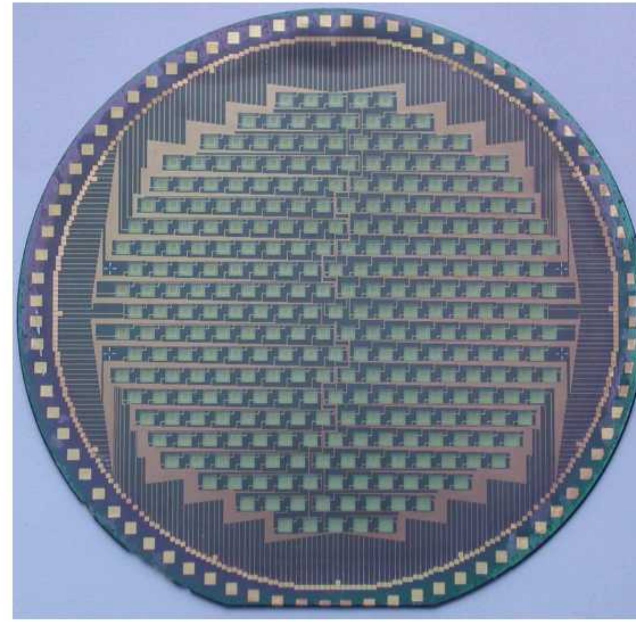

Fig. 1. Wiring side of a naked LABOCA array. Each light-green square is a bolometer.

295 bolometers LABOCA (345 GHz) Bonn

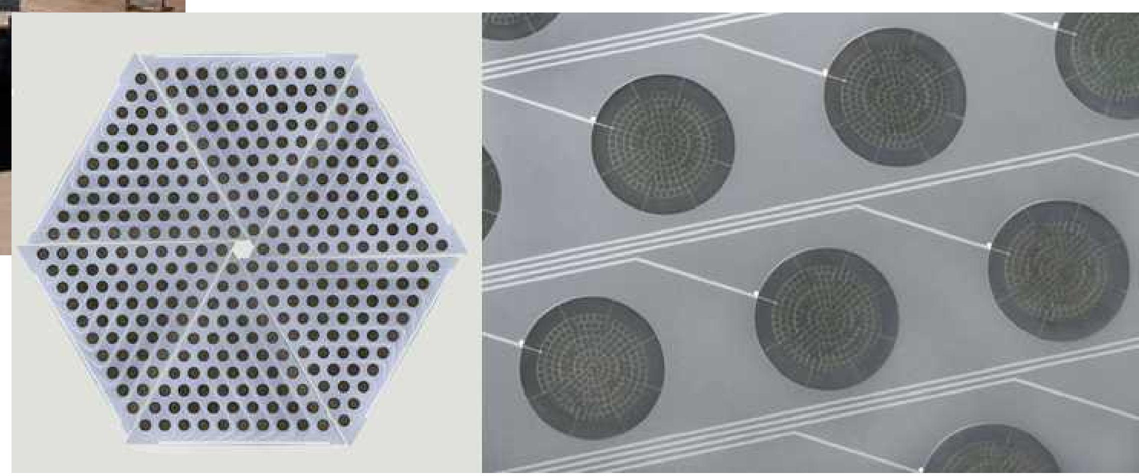

330 bolometers APEX-SZ (150 GHz) Berkeley

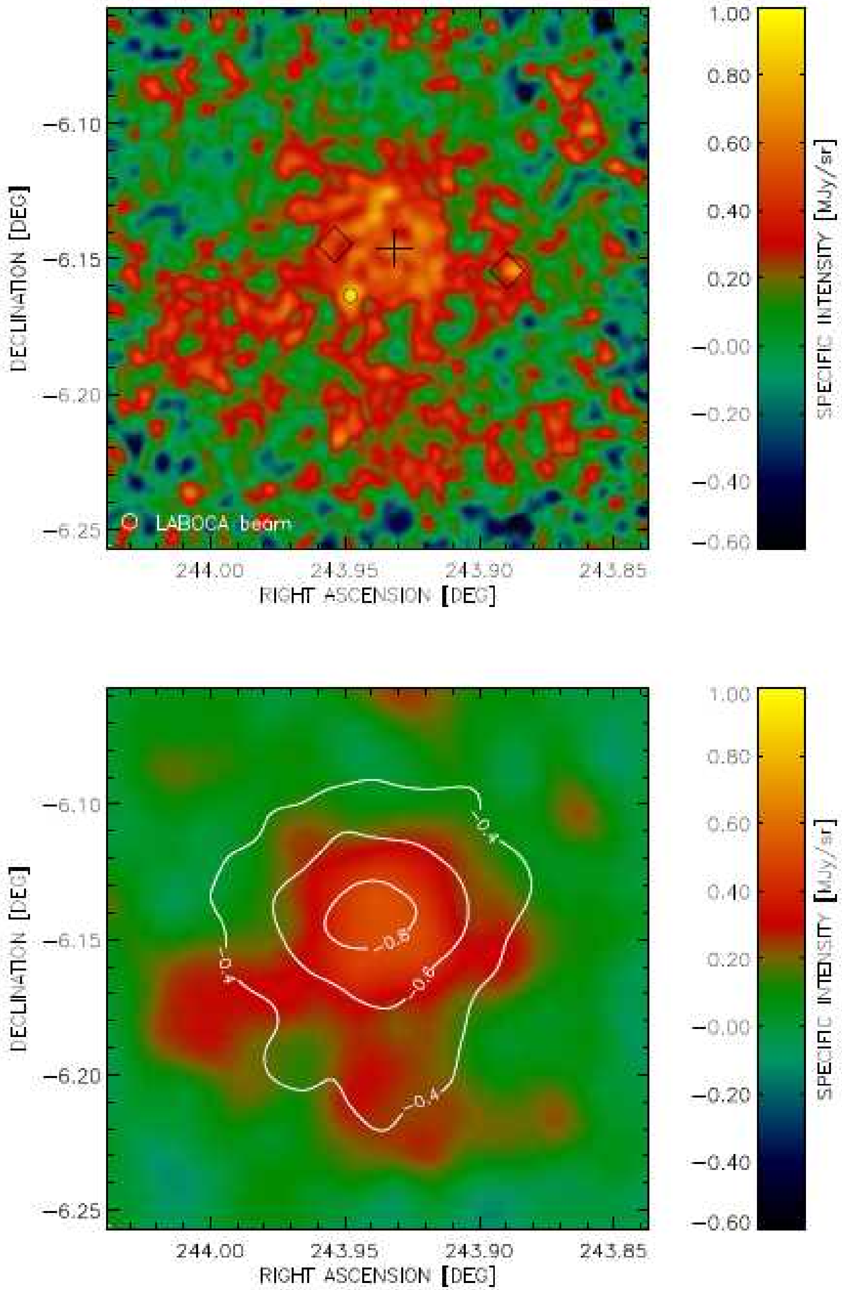

Fig. 2. *Top:* Final 345 GHz LABOCA map of Abell 2163, smoothed with the 19.5″ beam. The cross marks the position of a bright flat-spectrum radio source (Cooray et al. 1998). The diamonds mark the positions of two BCGs (Maurogordato et al. 2008). The circle marks the position of the bright point source found in the present data. *Bottom:* LABOCA map smoothed to the APEX-SZ resolution of 1 arcminute. The bright point source described in the text has been removed. The APEX-SZ 150 GHz map is shown as contours.

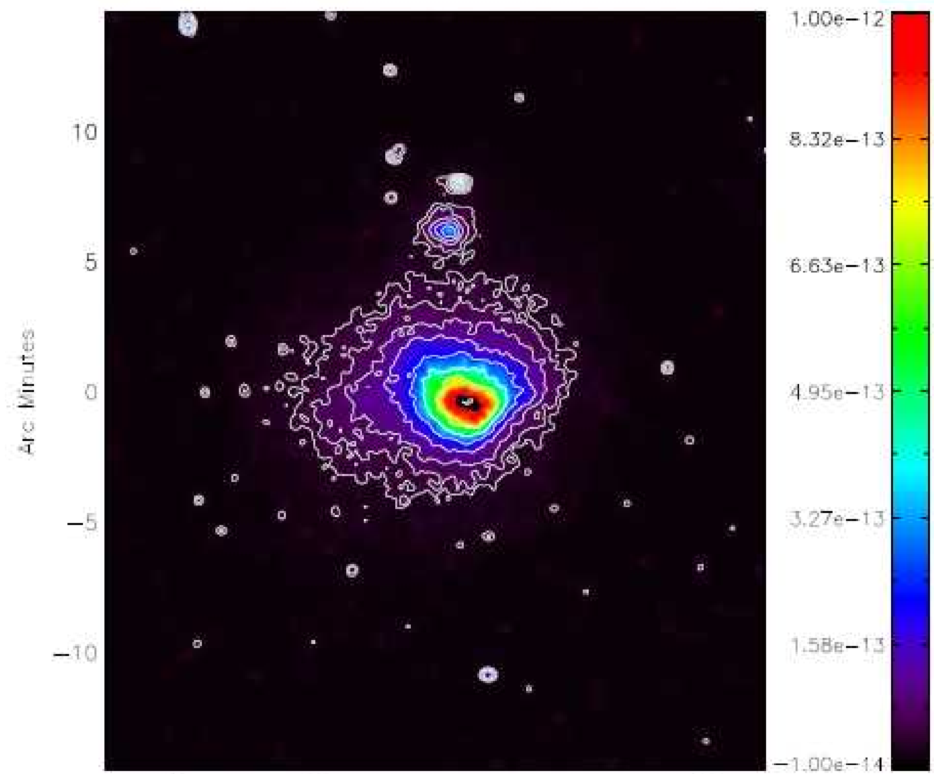

Fig. 3. Smoothed, background subtracted, X-ray map of Abell 2163 in the [0.5-2] keV band (see text for details). Logarithmically spaced contours highlight the large dynamical range of the cluster emission. The unit of the color scale is erg $s^{-1}cm^{-2}arcmin^{-2}$.

ACT : Atacama Cosmology Telescope

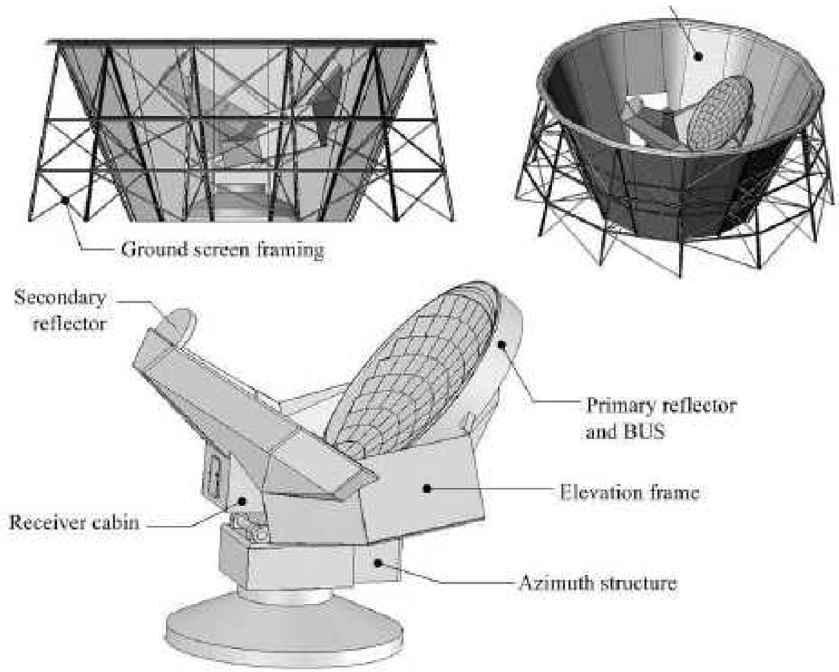

Fig. 1. The ACT telescope. The mechanical design has a low profile; the surrounding ground screen completely shields the telescope from ground emission. The screen also acts as a weather shield. An additional ground screen (not shown) mounted on the telescope hides the secondary and half the primary from the vantage point of the lower diagram. This inner ground screen is aluminum painted white to reduce solar heating. The primary mirror is $\sim$7 m in diameter including its surrounding guard ring. "BUS" refers to the mirror's

Astro-ph/0907.0461

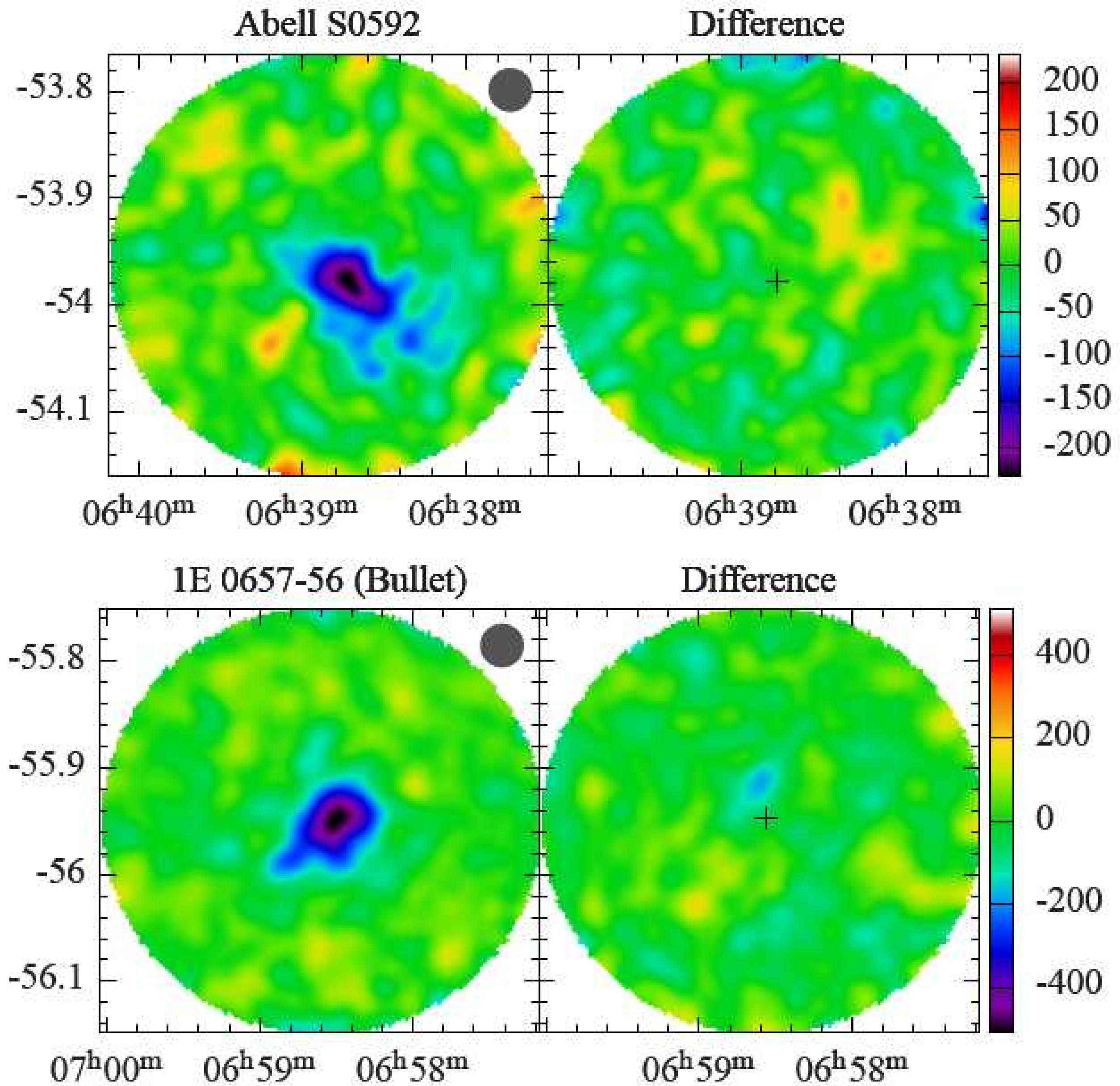

Detections during regular ACT survey , with 3 to 11 minutes of observation (!)

TABLE 2
SELECTION OF SZ CLUSTERS DETECTED BY ACT

ACT Descriptor	Catalog Name	J2000 Coordinates[a]		rms[b] [μK]	$t_{\rm int}$[c] [min]	$SNR\ (\theta)$[d]	ΔT_{SZ}[e] [μK]	$10^{10} \times Y(\theta)$[f]		
		RA	Dec.					$\theta \leq 2'$ (± 0.2)	$\theta \leq 4'$ (± 0.6)	$\theta \leq 6'$ (± 1.2)
Previously Detected										
ACT-CL J0245–5301	Abell S0295	$02^h45^m28^s$	$-53°01'36''$	44	10.1	15.2 (6.8′)	–250	0.89	2.36	3.91
ACT-CL J0330–5228	Abell 3128 (NE)	$03^h30^m50^s$	$-52°28'38''$	49	10.3	12.8 (4.3′)	–260	0.94	2.69	4.34
ACT-CL J0509–5345	SPT-CL 0509–5342	$05^h09^m20^s$	$-53°45'00''$	47	10.1	7.7 (5.2′)	–70	0.33	1.07	1.50
ACT-CL J0516–5432	Abell S0520	$05^h16^m31^s$	$-54°32'42''$	55	6.8	4.2 (4.1′)	–110	0.19	-0.11	-0.55
ACT-CL J0546–5346	SPT-CL 0547–5345	$05^h46^m35^s$	$-53°46'04''$	46	9.5	13.9 (5.8′)	–250	0.91	2.36	3.67
ACT-CL J0638–5358	Abell S0592	$06^h38^m46^s$	$-53°58'40''$	55	7.5	8.1 (3.1′)	–230	0.70	1.40	2.07
ACT-CL J0645–5413	Abell 3404	$06^h45^m29^s$	$-54°13'52''$	59	9.3	2.8 (2.0′)	–120	0.12	-0.18	-0.69
ACT-CL J0658–5556	1E 0657–56 (Bullet)	$06^h58^m33^s$	$-55°56'49''$	80	3.4	12.1 (2.7′)	–510	1.60	2.95	3.56
Previously Undetected										
ACT-CL J0329–5226	—	$03^h29^m27^s$	$-52°26'26''$	50	11.3	14.8 (7.9′)	–230	0.71	1.91	3.30
ACT-CL J0447–5107	—	$04^h47^m50^s$	$-51°07'09''$	57	7.9	13.4 (7.4′)	–250	0.75	2.60	4.02

[a] Position of the deepest point in 2′ FWHM Gaussian smoothed map, except for ACT-CL J0509–5345 which has a position which gives a maximal SNR (see text).[b] Map rms measured outside a 6′ mask and reported for a one square arcminute area.[c] Integration time, defined as the approximate total time (in minutes) that the telescope was pointed in the map region.[d] Maximum signal-to-noise ratio (Eq. 29) and the radius θ at which it was obtained.[e] Cluster depth, as measured in a 2′ FWHM Gaussian smoothed map at the listed coordinates; intended as a guide to the magnitude of the decrement.[f] See Eq. 32 and following discussion.

Planck is a very ambitious experiment.

It carries a complex CMB experiment (the state of the art, a few years ago) all the way to L2,

improving the sensitivity wrt WMAP by at least a factor 10,

extending the frequency coverage towards high frequencies by a factor about 10

All-sky Sunyaev-Zeldovich clusters

- Planck multiband observations of SZ clusters (ESZ) over the full sky: 189 high quality cluster candidates detected

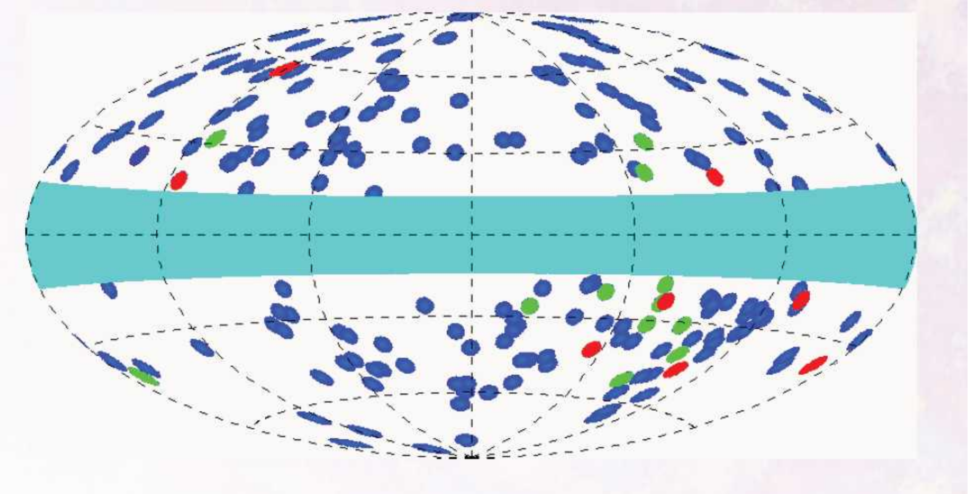

Fig.2 Distribution of ESZ clusters and candidate clusters on the sky (Galactic projection).

Known clusters	169
X-ray only	30
Optical Only	5
NEDSimbad only	1
X-ray + Optical	128
X-ray + SZ	1
SZ + Optical	1
X-ray + Optical + SZ	3
New Planck Clusters	20
XMM confirmed	11
AMI confirmed	1
Candidate new clusters	8

Discovered by Planck

- The clusters in the ESZ sample are mostly at moderate redshifts lying between z=0.01 and z=0.55, with 86% of them below z=0.3. The ESZ-cluster masses span over a decade from 0.9 to 15 × 10^{14} M_{sol}, i.e. up to the highest masses.

Clusters : Planck collaboration: astro-ph/1101:2024

All-sky Sunyaev-Zeldovich clusters

- SZ emission is extracted from multifrequency maps by filtering (matching multifrequency filter) and components separation.

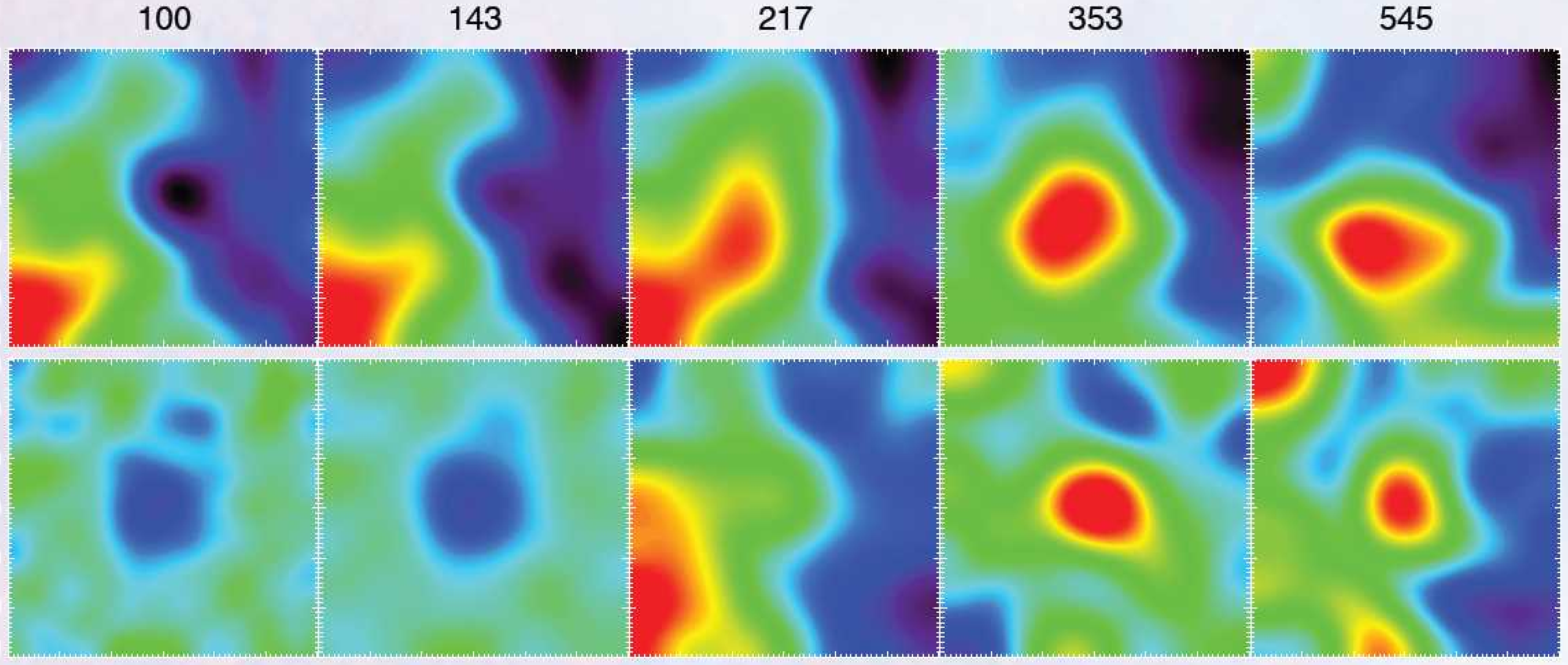

Fig. 3 *Planck* observation of A2256 (S/N~29). The upper panel shows the raw (1°x1°) maps at 100, 143, 217, 353, and 545GHz. The lower panel shows the corresponding cleaned maps.

- Candidates are then validated comparing to Planck sources lists and other datasets (X-ray, optical, NED, etc.)

All-sky Sunyaev-Zeldovich clusters

- Thanks to its all-sky coverage, *Planck* has a unique capability to detect the rarest and most massive clusters in the exponential tail of the mass function.
-
- As a matter of fact, two of the newly-discovered clusters in the ESZ and confirmed by XMM-Newton have estimated total masses larger than $10^{15}M_{sun}$.

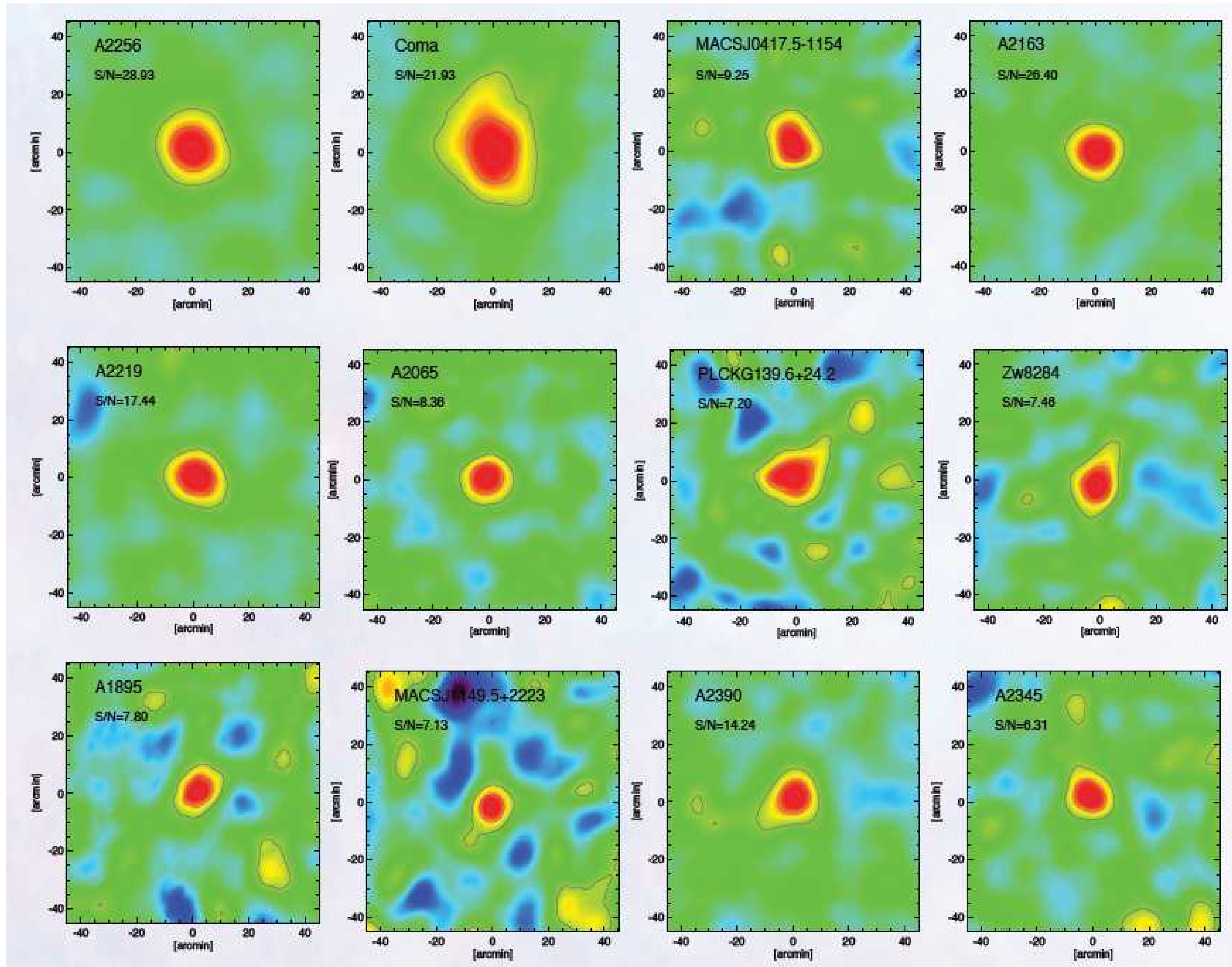

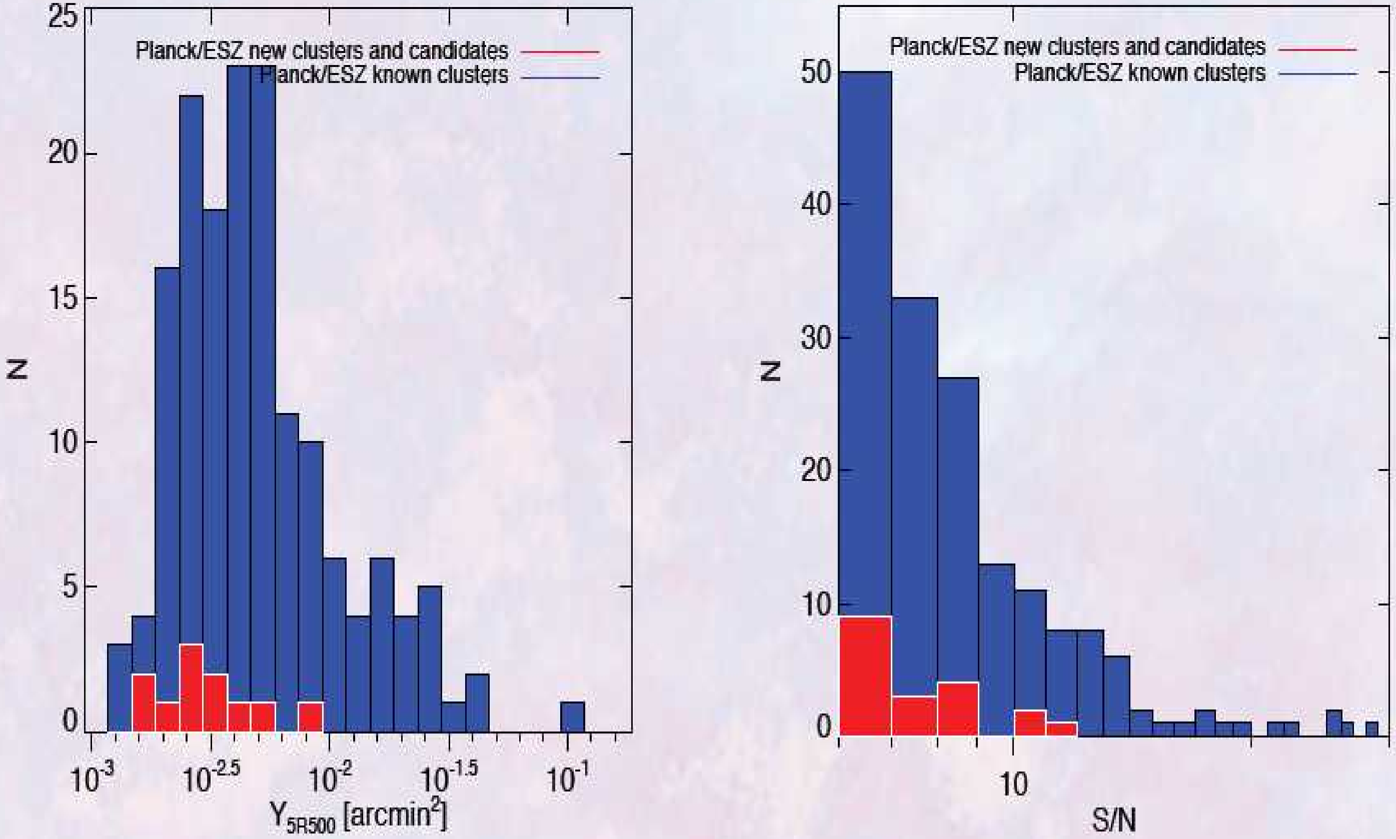

Fig.4 Distribution of the S/N and integrated Compton parameter values for the ESZ clusters and candidate new clusters

All-sky Sunyaev-Zeldovich clusters

Multiple Systems

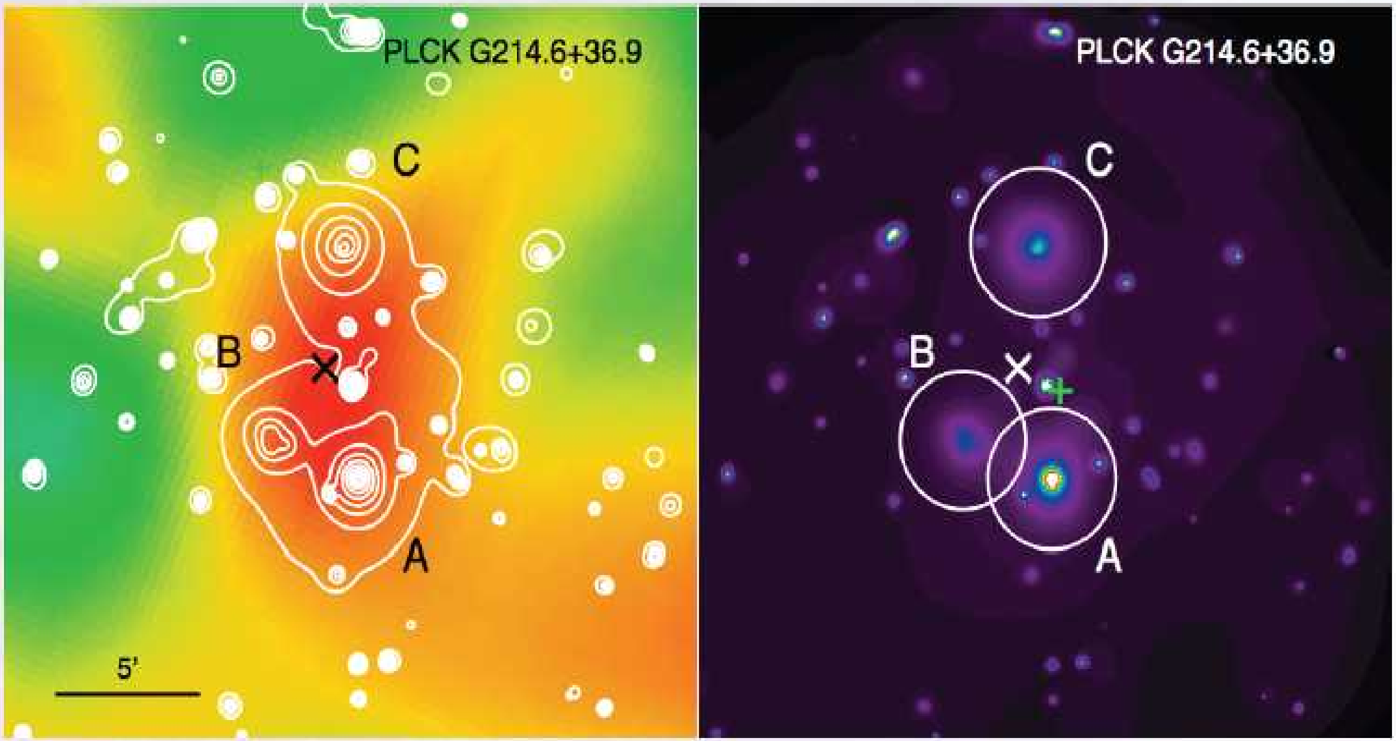

Example of the triple system PLCK G214.6+37.0. *Planck* Y_{SZ} *map (left)* with contours from the *XMM-Newton* wavelet filtered [0.3 – 2] keV image (right) overlaid in white. Extended components found in the *XMM-Newton* image are marked with letters. The circles in each *XMM-Newton* image denote the estimated R_{500} radius for each component.

OLIMPO : an update

S. Masi, P.A.R. Ade, E. Battistelli, A. Boscaleri, P. Camus, S. Colafrancesco, A. Coppolecchia, A. Cruciani, G. D'Addabbo, G. D'Alessandro, P. de Bernardis, S. De Gregori, G. Di Stefano, M. De Petris, M. Gervasi, K. Irwin, L. Lamagna, P. Marchegiani, P. Mauskopf,, L. Nati, F. Nati, R. Puddu, G. Romeo, A. Schillaci, C. Tucker, D. Yvon, A. Wuensche, M. Zannoni.

Dipartimento di Fisica, Università La Sapienza, Roma
Department of Physics and Astronomy, University of Cardiff, UK
IFAC-CNR, Firenze, Italy
Institut Neel, Grenoble, France
Istituto Nazionale di Geofisica, Roma, Italy
Osservatorio Astronomico di Roma, INAF, Italy
Dipartimento di Fisica, Università di Milano Bicocca, Italy
NIST Boulder CO. USA
CEA Saclay, France
INPE Brasil

The OLIMPO experiment is a mm-wave balloon-borne telescope, optimized for high-frequency measurements of the Sunyaev-Zeldovich effect. The instrument uses four bolometer arrays, for simultaneous observations at 150, 210, 350, 480 GHz, coupled to a 2.6 m diameter Cassegrain telescope, achieving a resolution of 4,3,2,2 arcmin FWHM respectively.

OLIMPO is a polar long-duration flight launched from Svalbard islands. The current observation plan includes deep integrations on a selected sample of 40 clusters, plus a wide blind survey of an empty sky area.

*We have recently upgraded the instrument adding **spectroscopic capabilities** within the 4 bands above, and discuss here the scientific potential of this innovative configuration.*

- In fig. 1 we show the OLIMPO balloon payload (Masi et al. 2008), with solar panels, ground shield and sun shield removed.
- Note the tiltable 2.6m primary mirror and the lightweigth secondary.
- Pointing is obtained rotating the payload around an azimuth pivot and changing the elevation of the inner frame, including the telescope, the FTS and the detector’s cryostat
- The total mass of the payload is 1.5 tons.

The Payload

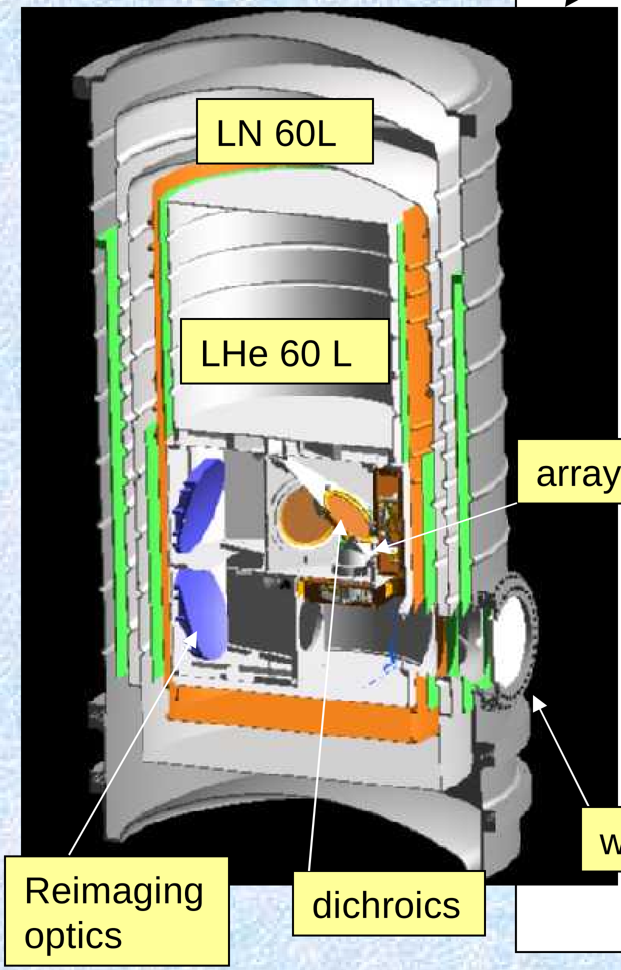
LN 60L
LHe 60 L
arrays
window
Reimaging optics
dichroics

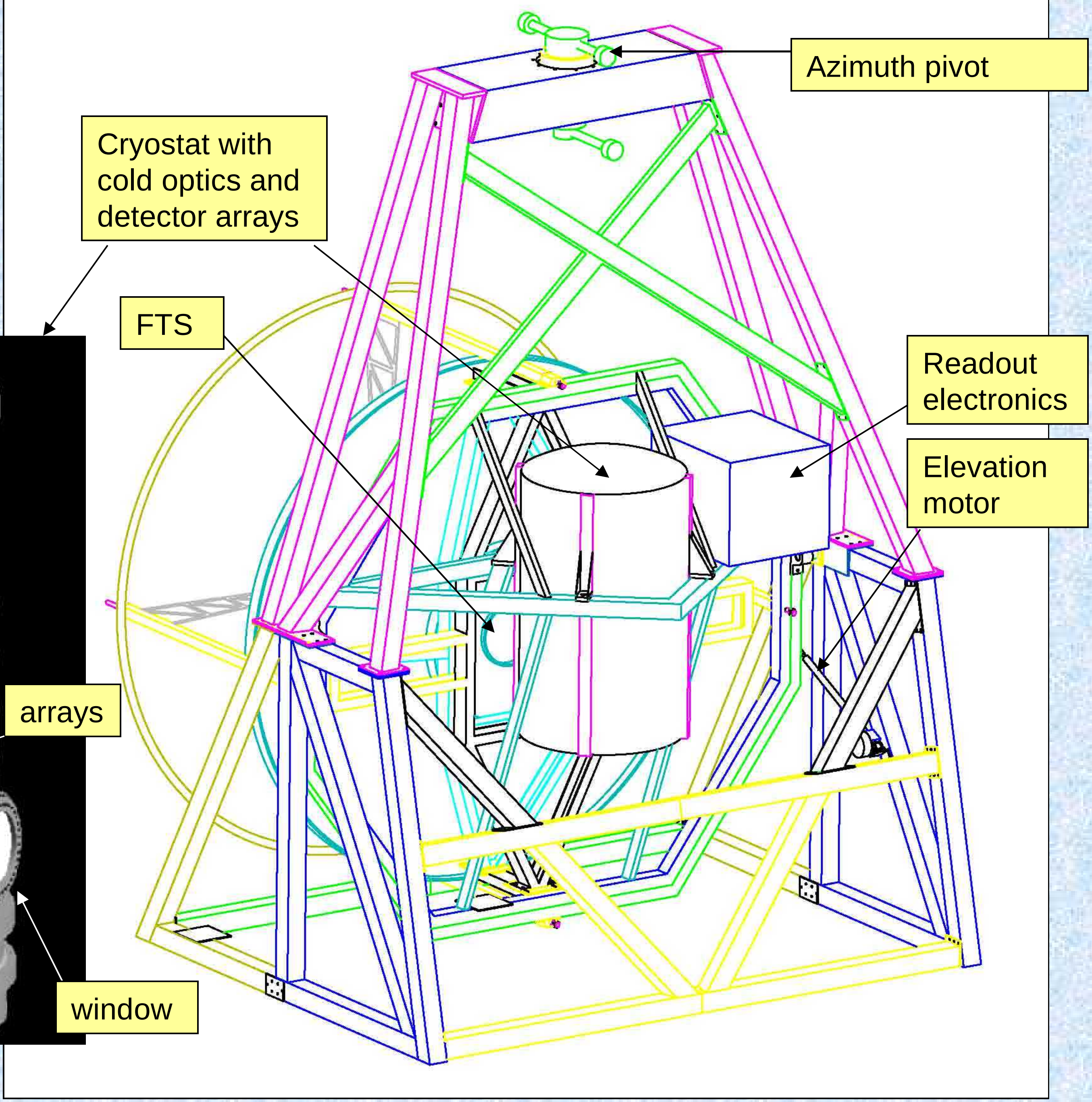
Cryostat with cold optics and detector arrays
FTS
Azimuth pivot
Readout electronics
Elevation motor

Low frequency arrays (TES)

- **Buffer: Si_3N_4**
- **Thermistor: Ti (60nm) + Au (10/20 nm)**
- **Absorber/heater: spiderweb T (10 nm) + Au (5 nm), filling fact 5%**
- **NET150GHz=145 μK√s**
- **NET220GHz=275 μK√s**
- **Univ. Of Cardiff (Mauskopf)**

High frequency arrays

- NbxSi1-x (x=0.085)
- SiN 3x3 mm2
- Palladium absorber
- NET340GHz=430 μK√s
- NET450GHz=4300 μK√s
- Inst. Neel Grenoble (Camus)

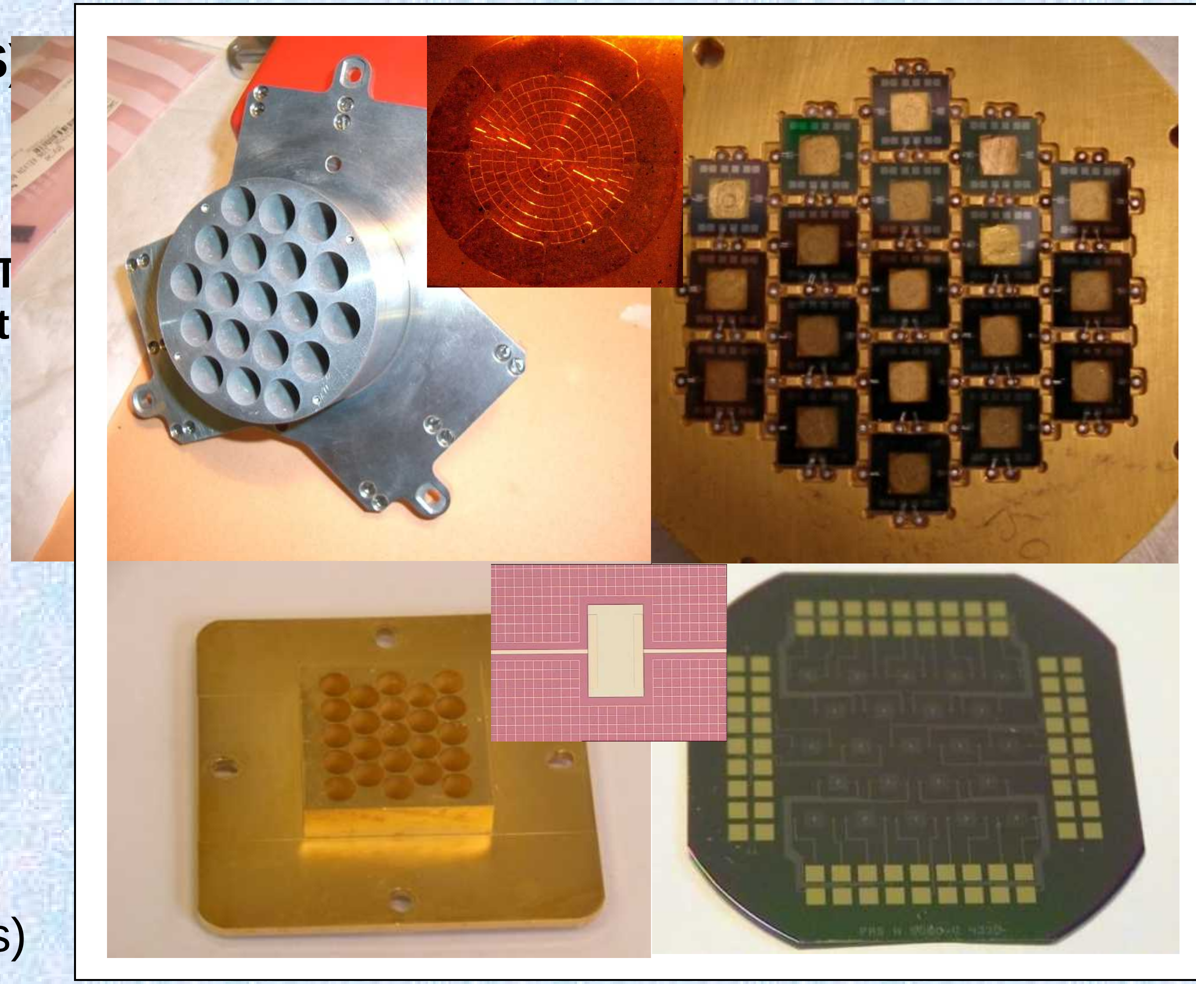

Filters Stacks (Ade, Tucker, Cardiff)

Bol.	ν_{eff} [GHz]	$\Delta\nu_{FWHM}$ [GHz]	Res. [‘]
19	148.4	21.5	4.2
19	215.4	20.6	2.9
23	347.7	33.1	1.8
23	482.9	54.2	1.8

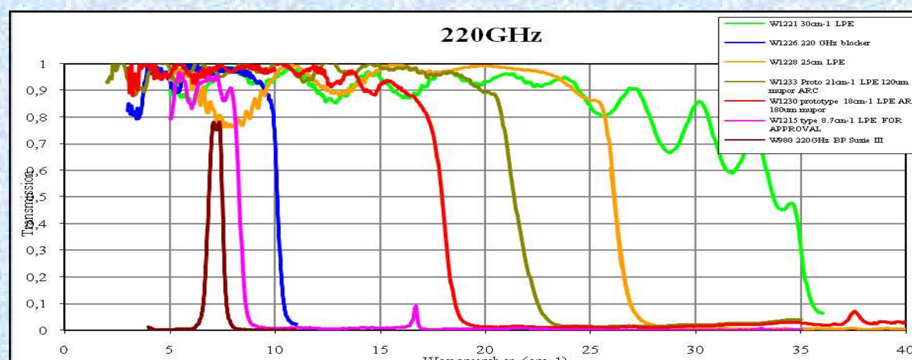

The spectroscopic instrument

- SZ studies can benefit significantly from spectroscopic measurements, which are required to break degeneracies between the parameters describing cluster and foreground emissions along the line of sight (see below).
- In 2008 we have studied for ASI a spectroscopic SZ space-mission (SAGACE, see de Bernardis et al. 2010).
- As a pathfinder, we are building a plug-in **D**ifferential **FTS** for OLIMPO.
- The **DFTS** configuration offers
  - an imaging spectrometer with very high throughput,
  - wide spectral coverage,
  - medium to high spectral resolution,
  - rejection of common-mode signals, like instrument emission and most of the ground pickup.
- The main problem is the high radiative background on the bolometers, which is solved splitting the observed frequency range in several bands with independent detector arrays. In the case of OLIMPO, this was already implemented in the 4-bands photometer.

The instrument is based on a double Martin Pupplett Interferometer configuration to avoid the loss of half of the signal.

A wedge mirror splits the sky image in two halves I_A and I_B, used as input signals for both inputs of the two FTS's.

outgoing fields :

Olimpo Telescope

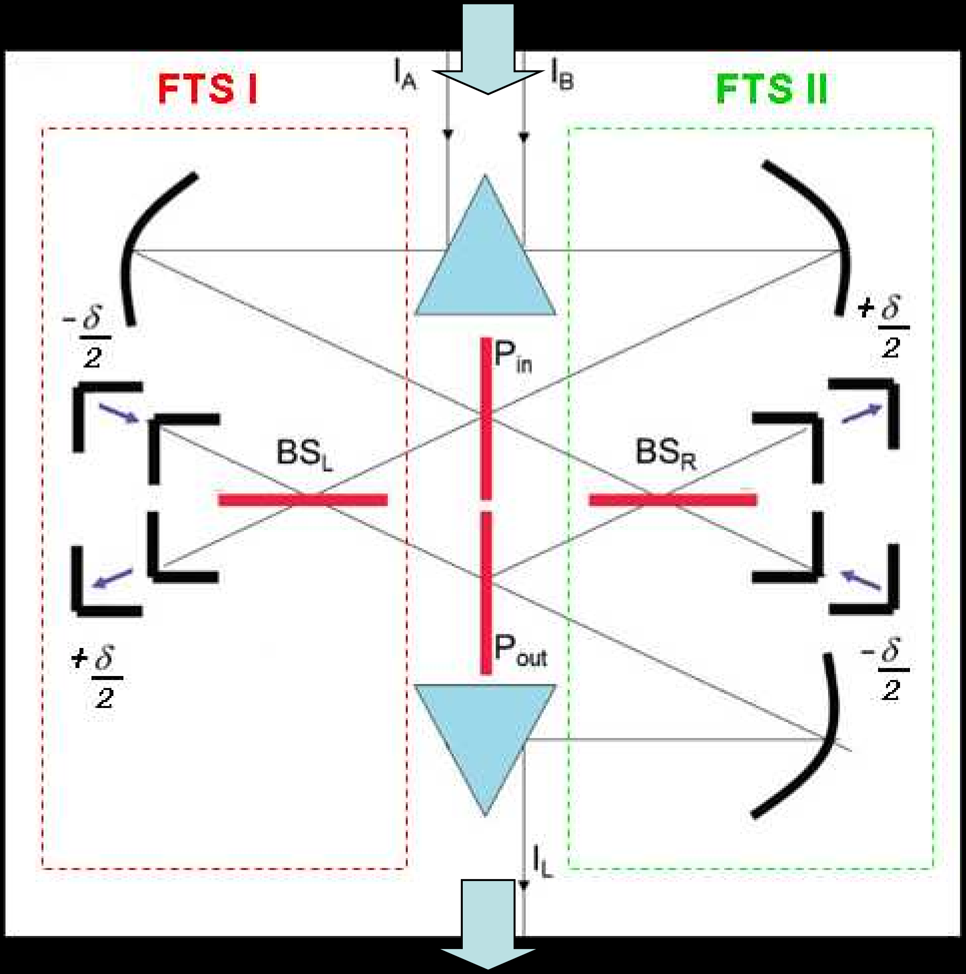

Olimpo Cryostat

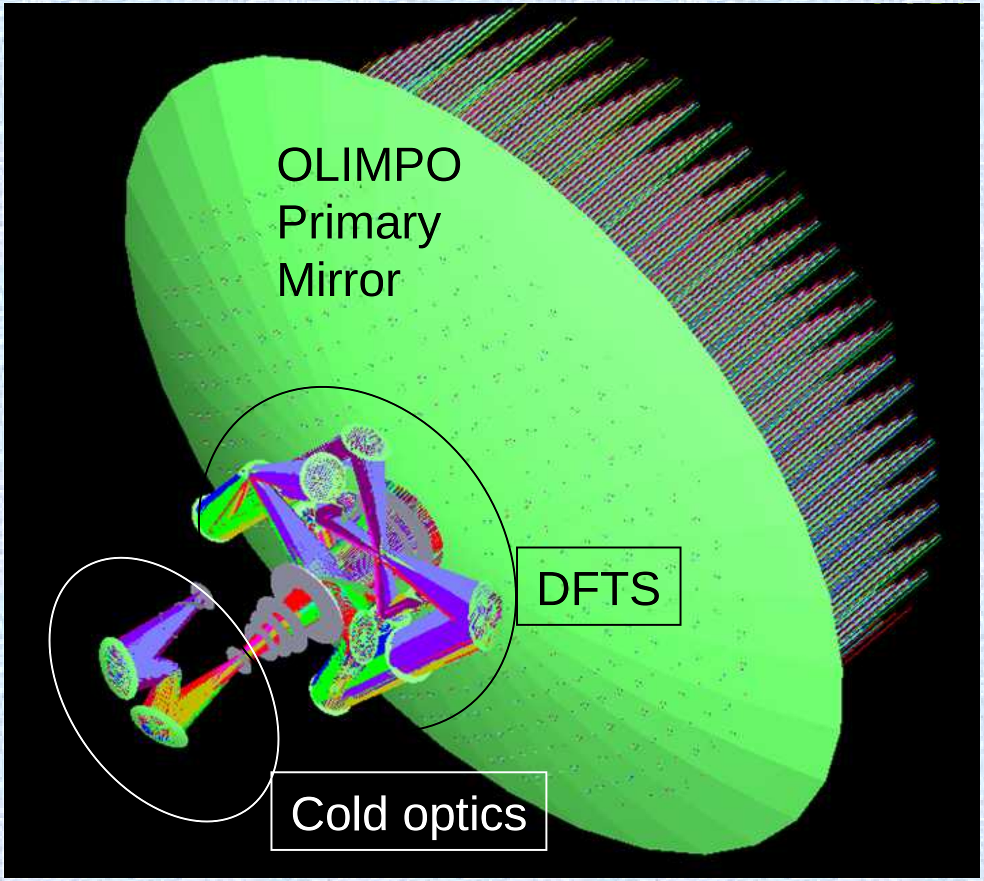

Global design of the optical system

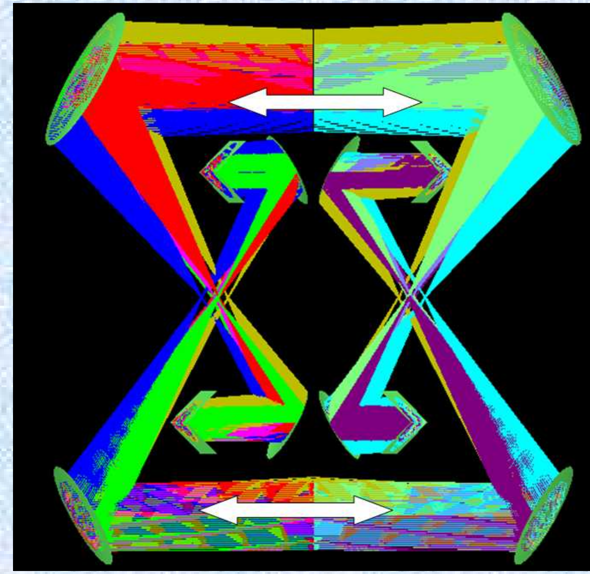
Optical layout of the doublel Martin-Puplett FTS

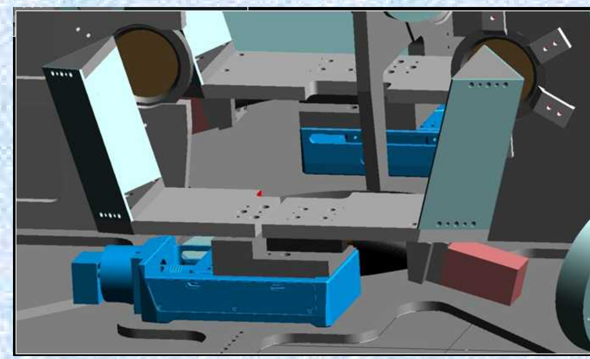
Mechanical arrangement of the translation stages

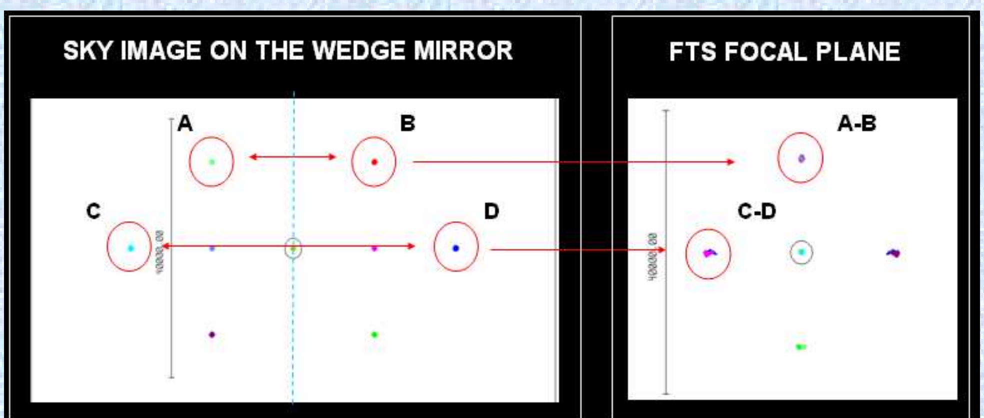

Differential field of view

The OLIMPO Martin-Puplett Differential Fourier Transform Spectrometer

Simulated OLIMPO measurement of a cluster l.o.s. with

τ_{th}=0.005,
T_e=10 keV,
τ_{nonth}=0.0001,
v_{pec}=500 km/s,
I_{dust}=6kJy/sr@150GHz

The data with the error bars are simulated observations from a single pixel of the OLIMPO-FTS, for an integration time of 3 hours. The two lines through the data points represent the input theory (thin) and the best fit for the plotted data realization (thick). The other thin lines represent thermal plus non-thermal SZE, and dust emission.

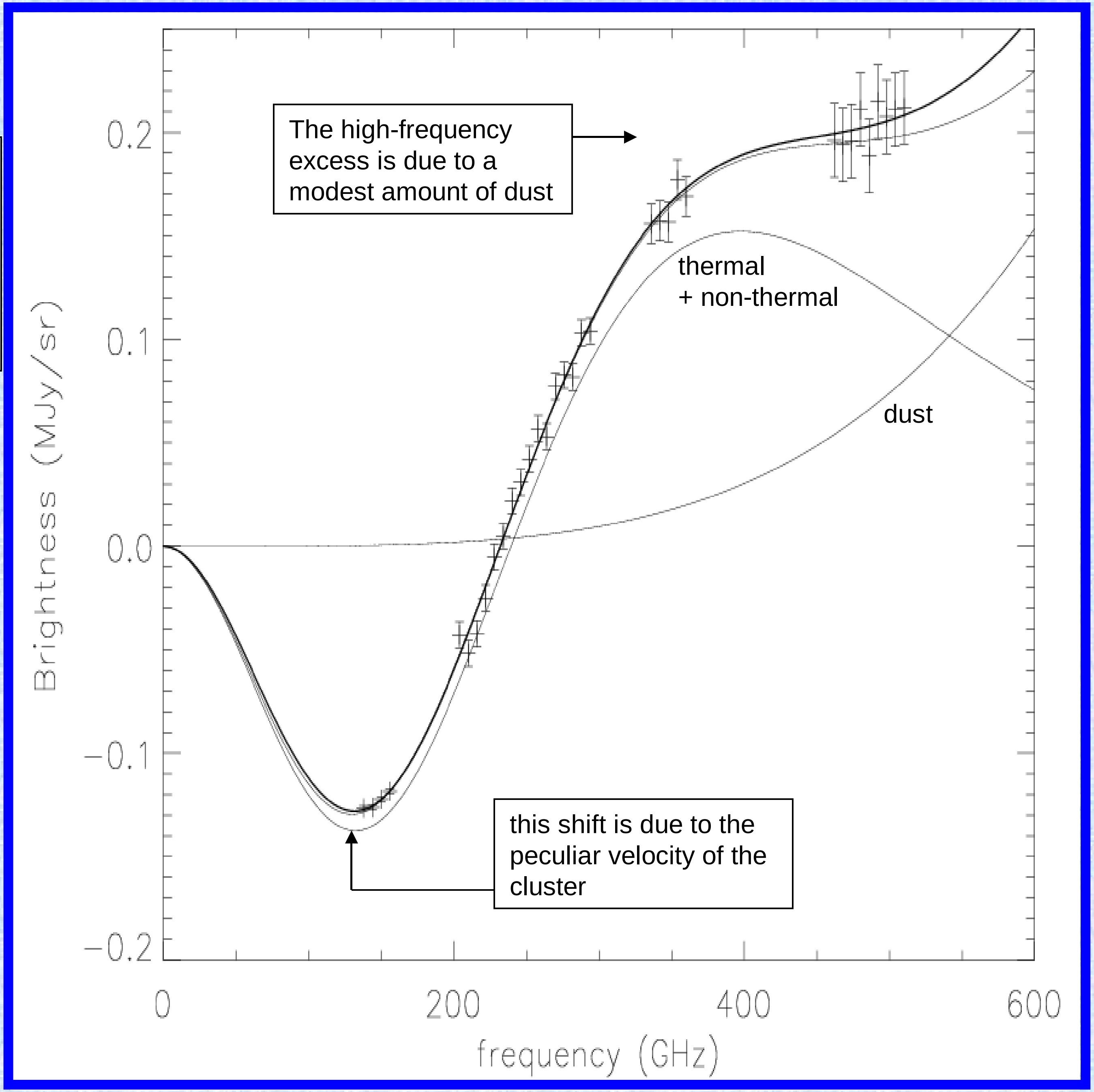

Parameters Determination

- In the presence of peculiar velocities, non-thermal populations (from AGNs in the cluster), and foreground dust, there are simply *too many free parameters* to be determined with the observation of a few frequency bands, like in ground-based measurements.
- We have carried out detailed simulations of OLIMPO observations in the spectroscopic configuration with an extended 200-300 GHz band.
- The spectroscopic configuration has superior performance in converging to the correct estimate of thermal optical depth and dust parameters, while the photometric configuration, *in the absence of priors*, tends to converge to biased estimates of the parameters. See de Bernardis et al. A&A **583**, A86 (2012).

Input parameters	OLIMPO FTS 3h integ. one detector	• No priors	• Prior T=(10$\pm$3) keV
τ_{th} =50x10^{-4}		τ_{th} =(63$\pm$27)10^{-4}	τ_{th} =(49$\pm$6)10^{-4}
T = 10 keV		T = (9.0$\pm$4.1) keV	T = (9.6$\pm$0.5)keV
τ_{non-th}=1x10^{-4}		τ_{non-th}=(14$\pm$9)10^{-5}	τ_{non-th}=(11$\pm$9)10^{-5}
ΔT_{CMB}=22μK		ΔT_{CMB}=(24$\pm$43)μK	ΔT_{CMB}=(22$\pm$43)μK
$\Delta I_{dust150}$=6 kJy/sr		$\Delta I_{dust150}$=(5.7$\pm$1.6)kJy/sr	$\Delta I_{dust150}$=(5.8$\pm$0.9)kJy/sr

Observation Program

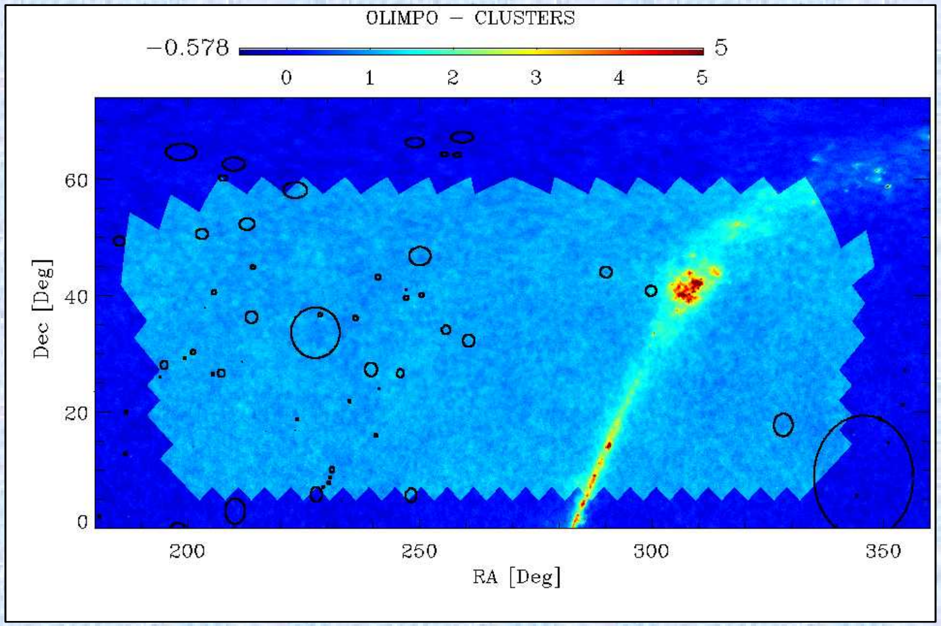

ind	ID	RA	Dec	TIME	frac	NAME
0	1	212.83	52.2	18000	1	3C295CLUSTER
1	40	194.95	27.98	3600	0	ABELL1656
2	43	203.13	50.51	3600	1	ABELL1758
3	44	205.48	26.37	3600	1	ABELL1775
4	45	207.25	26.59	3600	1	ABELL1795
5	48	216.72	16.68	18000	1	ABELL1913
6	49	223.18	16.75	11360.88	1.27	ABELL1983
7	50	223.63	18.63	18000	1	ABELL1991
8	51	223.21	58.05	5640.53	1.28	ABELL1995
9	53	227.56	33.53	18000	1	ABELL2034
10	54	229.19	7	3600	1	ABELL2052
11	55	230.76	8.64	3600	1	ABELL2063
12	56	234.95	21.77	3600	1	ABELL2107
13	57	236.25	36.06	18000	1	ABELL2124
14	58	239.57	27.23	3600	1	ABELL2142
15	59	240.57	15.9	3600	1	ABELL2147
16	61	247.04	40.91	18000	1	ABELL2197
17	62	247.15	39.52	3600	1	ABELL2199
18	63	248.19	5.58	3600	1	ABELL2204
19	65	250.09	46.69	3600	1	ABELL2219
20	66	255.68	34.05	7230	1.49	ABELL2244
21	69	260.62	32.15	18000	1	ABELL2261
22	70	290.19	43.96	3600	1	ABELL2319
23	71	328.39	17.67	3600	1	ABELL2390
24	98	241.24	23.92	13045.75	1.1	AWM4
25	100	299.87	40.73	18000	1	CYGNUSA
26	101	201.2	30.19	18000	1	GHO1322+3027
27	102	241.11	43.08	18000	1	GHO1602+4312
28	107	230.46	7.71	3600	1	MKW03S
29	120	228.61	36.61	18000	1	MS1512.4+3647
30	121	245.9	26.56	13147.05	1.1	MS1621.5+2640
31	128	201.15	13.93	18000	0	NGC5129GROUP
32	134	199.34	29.19	18000	1	RDCSJ1317+2911
33	143	231.17	9.96	18000	1	RXJ1524.6+0957
34	150	211.73	28.57	18000	1	WARPJ1406.9+2834
35	151	213.8	36.2	18000	1	WARPJ1415.1+3612
36	161	194.02	25.95	18000	0	[VMF98]128
37	162	203.74	37.84	18000	1	[VMF98]139
38	163	205.71	40.47	18000	1	[VMF98]148
39	164	214.12	44.78	18000	1	[VMF98]158
40	165	250.47	40.03	18000	1	[VMF98]184

- In a circumpolar summer long duration flight (>200h) we plan to observe 40 selected clusters and to perform a blind deep integration on a clean sky region
- We have optimized the observation plan distributing the integration time among the different targets according to their brightness and diurnal elevation.

Mission Profile

SORA LAUNCH:July 1st 2009 (1.5 ton)

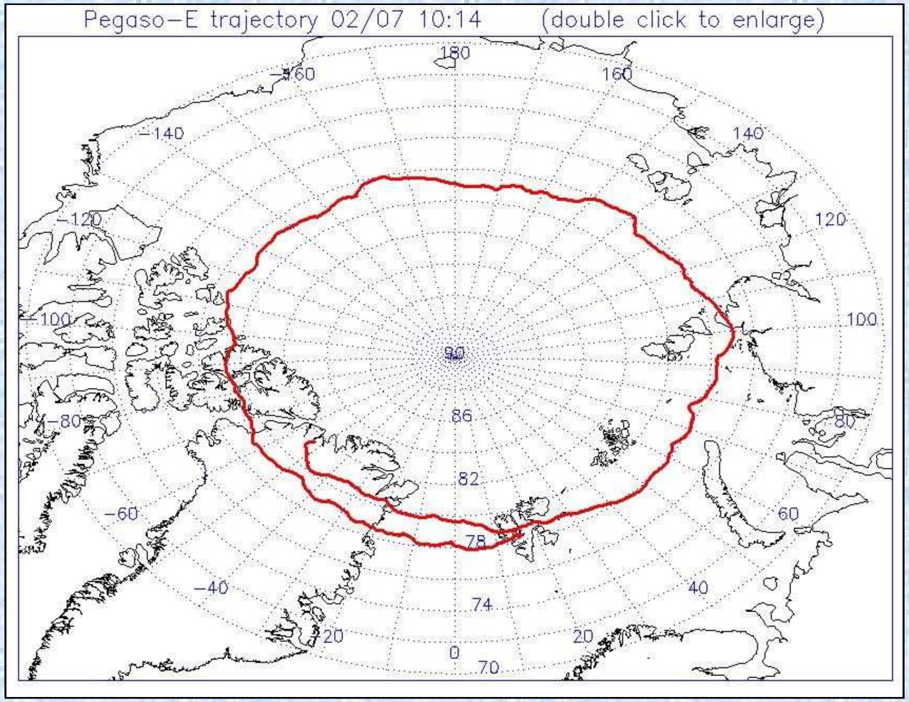

- We will use a long-duration circumpolar flight launched from Svalbard Islands (June 2013).
- We have tested these flights in collaboration with ASI, and demonstrared the feasibility of launching heavy payloads from the Longyearbyen airport, performing 2-3 weeks flights around the north pole during the Arctic summer.
- Backup-plan: Antarctica, 2014

And now let’s dream …

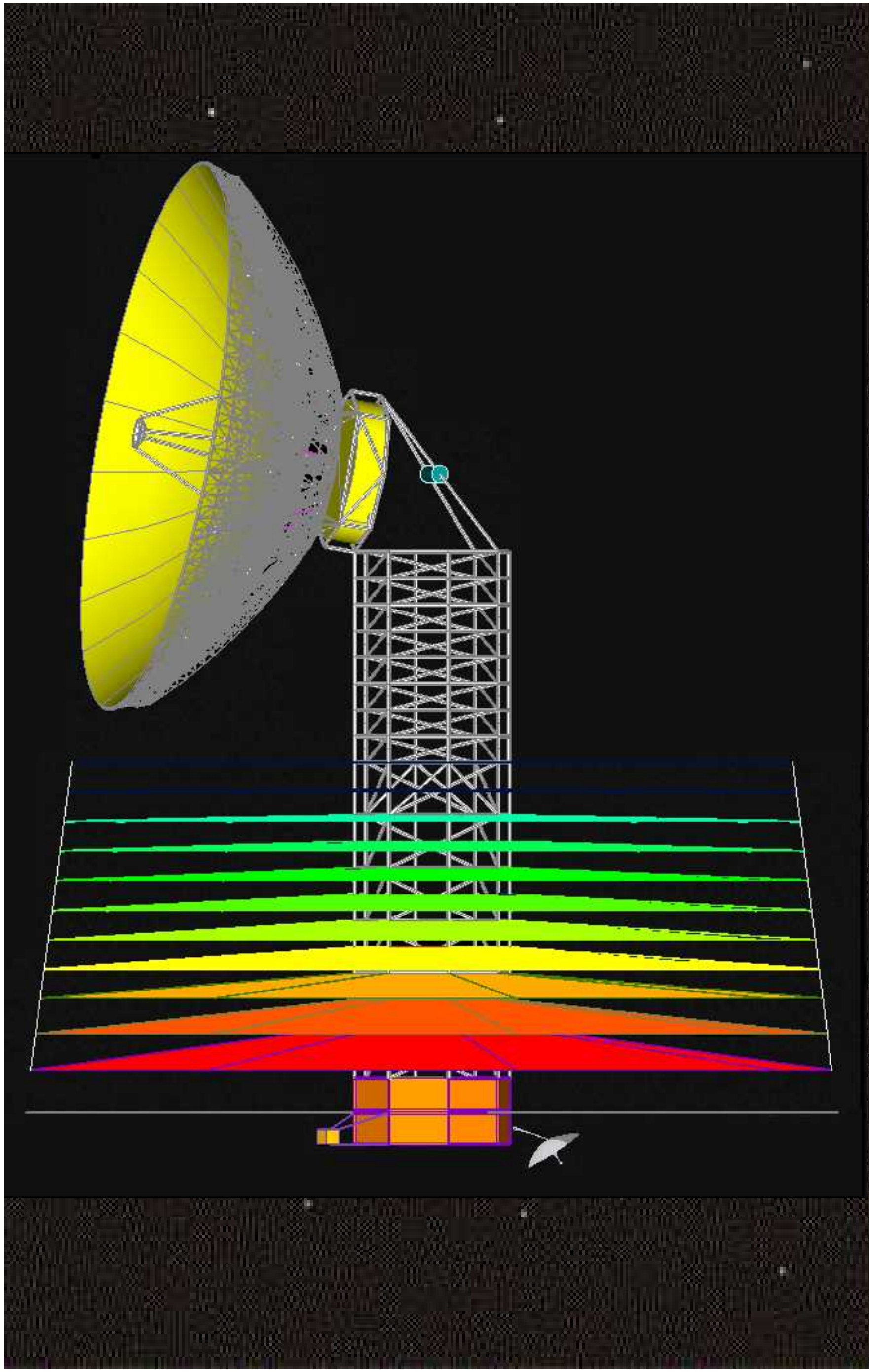

MILLIMETRON

antenna diameter 12 m

range of wavelength 0.01 - 20 mm

bolometric sensitivity
(wavelength 0. 3 mm, 1 h of integration)

$5 \cdot 10^{-9}$ Jy (sigma)

interferometry sensitivity
space-ground (ALMA)
(wavelength 0.5 mm, bandwidth 16 GHz
integration of 300 s)

10^{-4} Jy (sigma)

beam of the interferometer

10^{-9} arcsec

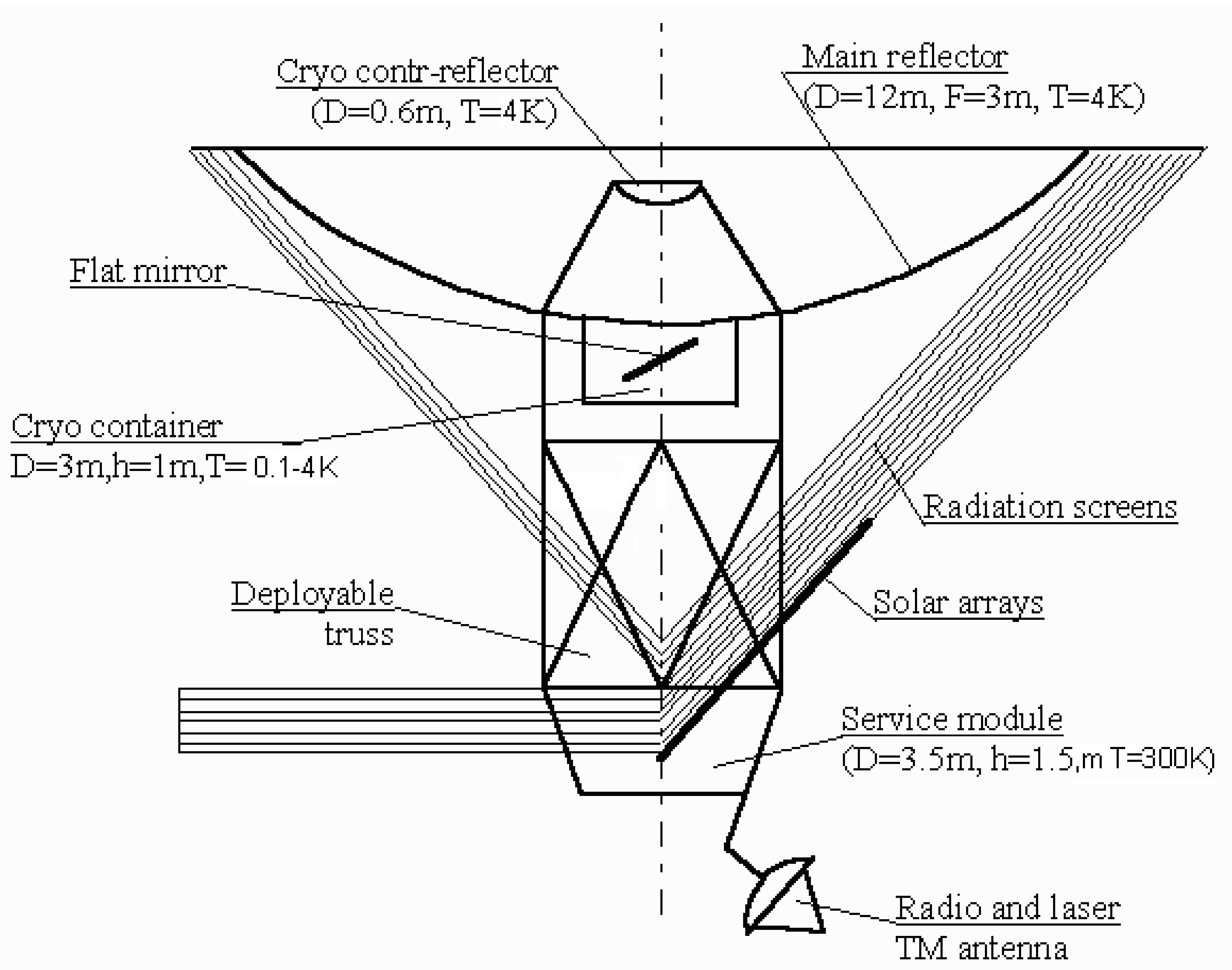

Cryo contr-reflector
(D=0.6m, T=4K)
Main reflector
(D=12m, F=3m, T=4K)
Flat mirror
Cryo container
D=3m,h=1m,T= 0.1-4K
Radiation screens
Solar arrays
Deployable
truss
Service module
(D=3.5m, h=1.5,m T=300K)
Radio and laser
TM antenna

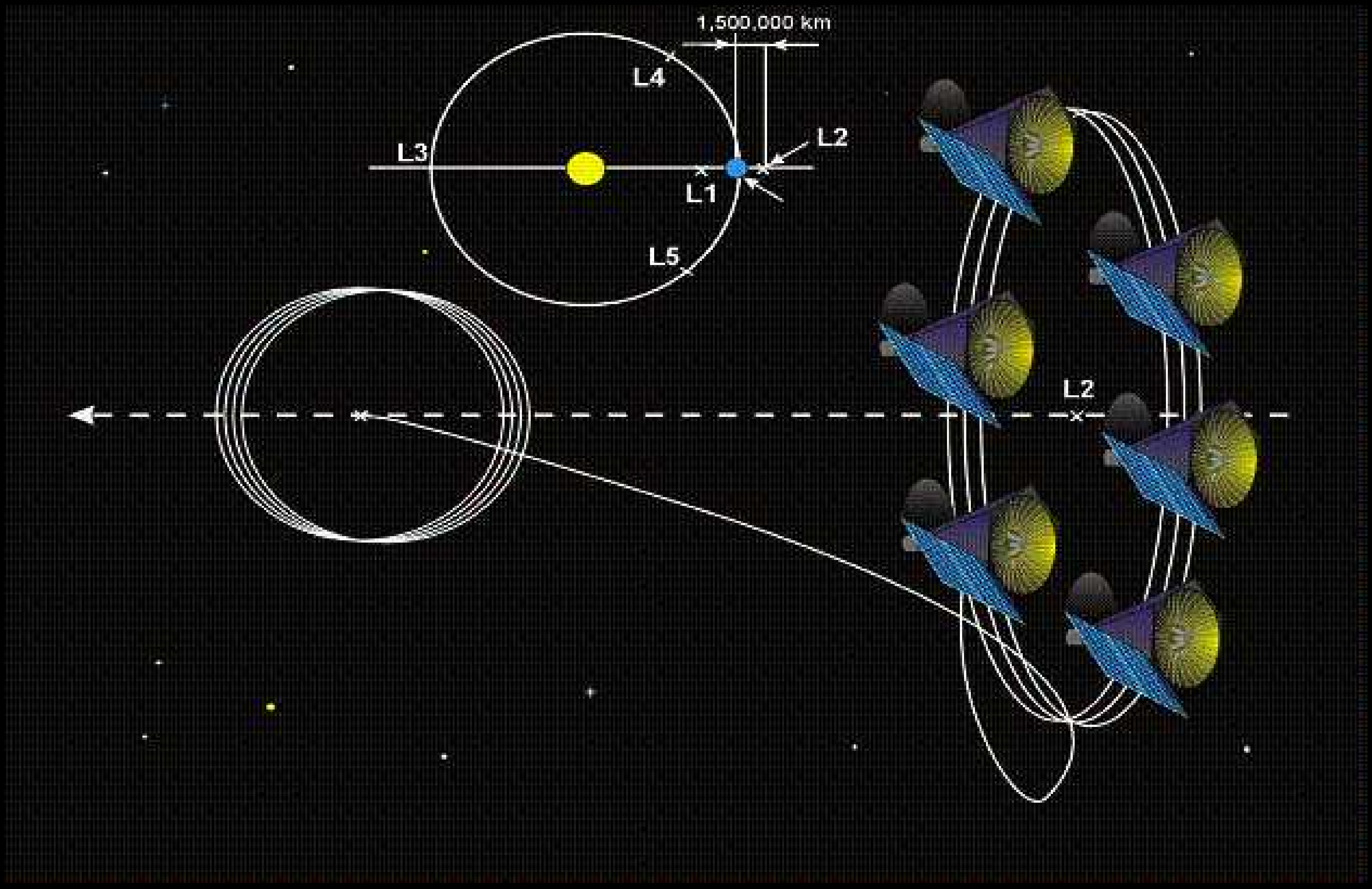

1,500,000 km
L4
L3
L2
L1
L5
L2

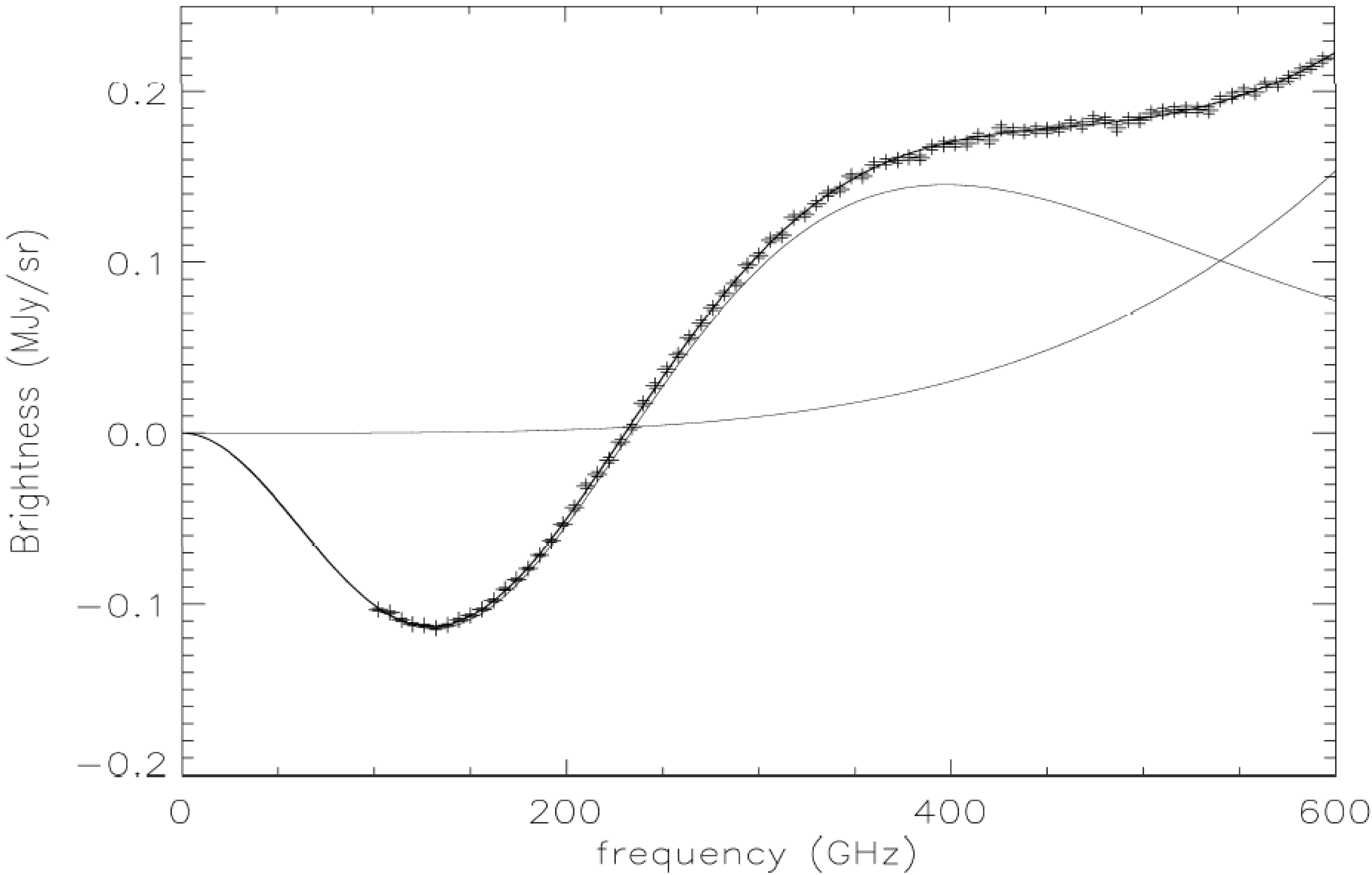

3 hours of observations of a rich cluster with a DFTS on Millimetron
Absolutely outstanding.

Parameter	input	best fit EC2 balloon - warm spec. prior $\sigma = 8$ keV	best fit EC2 balloon - warm spec. prior $\sigma = 3$ keV	best fit EC3 EO - cold spec. prior $\sigma = 8$ keV	best fit EC3 EO - cold spec. prior $\sigma = 3$ keV	best fit EC5 L2 - cold spec. prior $\sigma = 8$ keV	best fit EC5 L2 - cold spec. prior $\sigma = 3$ keV
$\tau_t \times 10^3$	5	5.0 ± 0.9	4.9 ± 0.8	5.8 ± 2.6	5.2 ± 0.6	5.1 ± 0.6	5.1 ± 0.5
$T(keV)$	8.5	8.4 ± 0.8	8.5 ± 0.1	7.7 ± 2.0	8.1 ± 0.8	8.5 ± 1.2	8.5 ± 1.0
$\Delta T_{CMB}(\mu K)$	22	20 ± 50	20 ± 50	23 ± 8	22 ± 8	22 ± 4	22 ± 4
$\Delta I_d(Jy/sr)$	600	570 ± 270	560 ± 270	590 ± 40	590 ± 40	600 ± 4	600 ± 4
$\tau_{nt} \times 10^3$	0.1	0.1 ± 0.1	0.1 ± 0.1	0.12 ± 0.03	0.11 ± 0.02	0.10 ± 0.01	0.10 ± 0.01
$p_1(511\ keV/c)$	2.75	2.6 ± 0.7	2.5 ± 0.7	2.5 ± 0.9	2.7 ± 1.1	3.0 ± 1.0	2.9 ± 0.9
$\langle \chi^2 \rangle / DOF$	-	34.9/34	34.9/34	77.8/78	78.0/78	110.0/110	110.1/110

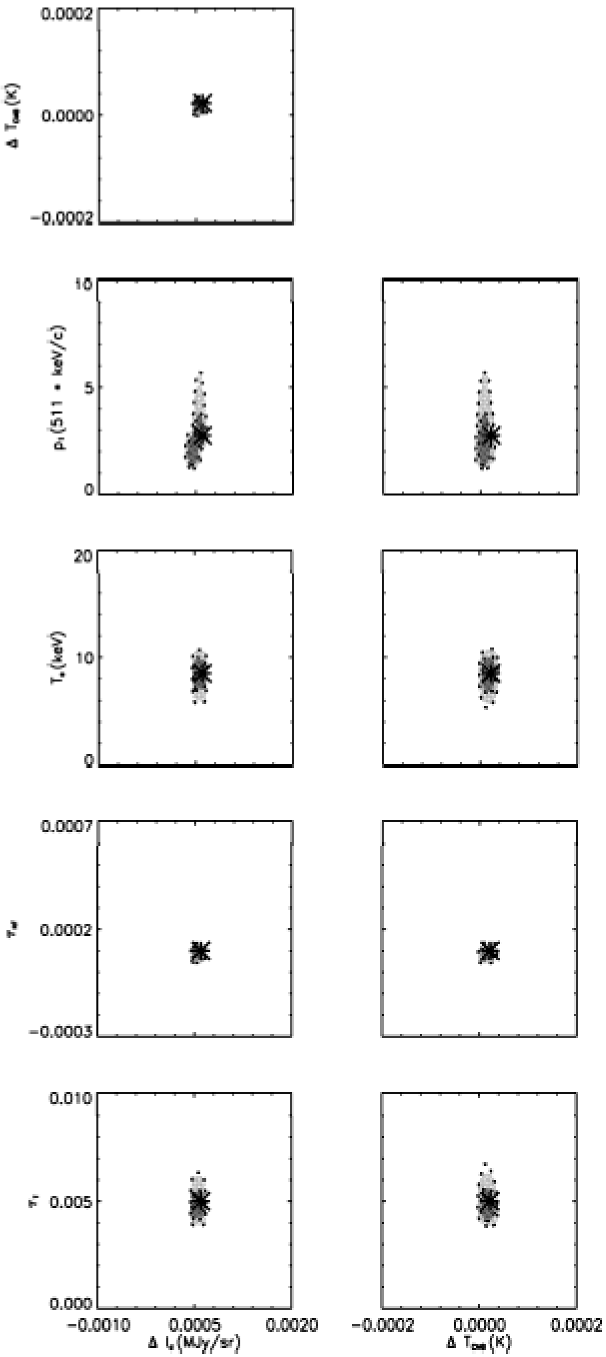

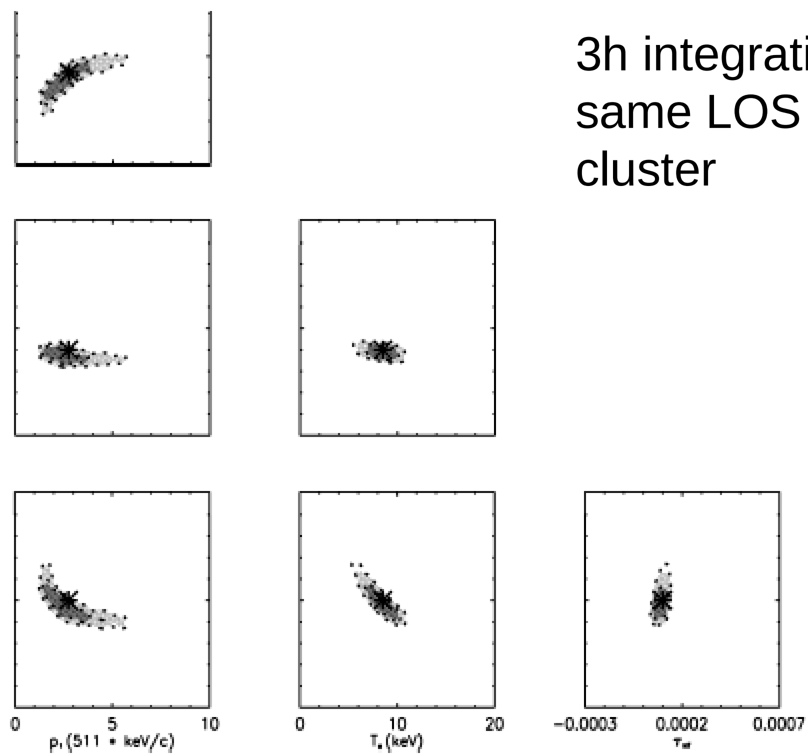

3h integration on the same LOS through a rich cluster

Stay tuned !